2013

Quantification of the environmental impact of titanium dioxide photocatalytic pavements for air pollution remediation

Heather Lee Dylla
Louisiana State University and Agricultural and Mechanical College

QUANTIFICATION OF THE ENVIRONMENTAL IMPACT OF TITANIUM DIOXIDE PHOTOCATALYTIC PAVEMENTS FOR AIR POLLUTION REMEDIATION

A Dissertation

Submitted to the Graduate Faculty of the
Louisiana State University and
Agricultural and Mechanical College
in partial fulfillment of the
requirements for the degree of
Doctorate of Philosophy

in

The Interdepartmental Program in Engineering Science

by
Heather Dylla
B.S., Bradley University, May 2006
M.S., Louisiana State University, August 2011
May 2013

ACKNOWLEDGEMENTS

This dissertation project would not have been possible without the support of many people. The author would first like to express her gratitude to her major professor, Dr. Marwa Hassan, for the opportunity she provided in conducting this research. In addition, her support, guidance, enthusiasm, and encouragement were invaluable throughout the journey. The author is also grateful for the assistance and knowledge provided by the supervisory committee members Dr. Louis Thibodeaux, Dr. Kelly Rusch, Dr. Louay Mohammad, Dr. Ayman Okeil and Dr. Vincent Wilson. Furthermore, the author would like to extend her gratitude to the Department of Construction Management and Industrial Engineering, the Marathon Engineering Diversity Graduate Fellowship Program and the LSU Office of Strategic Initiatives for financial assistance. In addition, she is grateful for assistance with sample preparation from the Louisiana Department of Transportation Research Center (LTRC) and guidance in ambient air monitoring from Earle Wright.

A special thanks is also given to her colleague and good friend James Gilford III for his moral support and advice as well as all her other colleagues including but not limited to David Osborn, Angel Lence, and Conor Farly, and undergraduate student Breanna Lee, for laboratory assistance. In addition, she was fortunate to have had the opportunity complete part of her studies abroad at the Interdisciplinary Lab of Electrochemistry and Ceramics at the Universidade Federal de Sao Carlos, Brasil, where she developed furture collaborations and more importantly lifelong friendships. Lastly, a special thanks is given to her friends and family who have consistently supported and encouraged her throughout this journey.

TABLE OF CONTENTS

ABSTRACT

Photocatalytic concrete pavements are a promising technology for mobile source air pollution remediation, however before widespread application of this technology is realized many unanswered questions remain regarding its overall environmental impact. In response to these questions, the goal of this study was to increase the understanding of the environmental impact of photocatalytic concrete pavement highways. To achieve this goal, the objectives of this study were to (A) construct a model that evaluates the nitrogen oxides (NO_x) reduction from photocatalytic pavements, (B) quantify the nitrates released from the photocatalytic degradation of NO_x, and (C) identify and characterize pathways for TiO_2 nanoparticle exposure.

To achieve objective A, a field study was conducted to evaluate the NO_x reduction. Results showed evidence of minimal photocatalytic reductions with large variability due to many unknown and known parameters. As a result, this study also investigated the use of laboratory results to better understand the significance of the NO_x reduction through the creation of a theoretical mass balance Lavoisier box model. Laboratory results indicated that the nitrogen monoxide (NO) oxidation rate is reaction rate mass transfer controlled following the Langmuir-Hinshelwood (L-H) model. A parametric study was completed to evaluate the L-H constants under different environmental conditions and statistical model was created to describe the NO oxidation rate. Incorporating the resulting NO oxidation rate into a Lavoisier box model the mass transfer mechanisms were compared and objective A was achieved. Objectives B and C of the project deal with evaluating potential unintended consequences resulting from implementation of photocatalytic concretes. To complete objective B, nitrates and TiO_2 nanoparticles released to water were quantified. Lastly, TiO_2 nanoparticles released to the air during construction activities were quantified and characterized to achieve objective C.

CHAPTER 1
INTRODUCTION

Air pollution has become a major concern of society, as air quality in large cities has been correlated with serious health hazards. Negative health effects, from long and short-term vehicle pollution exposure, are associated with living, working, and going to school in roadway microenvironments. The hypothesis, that traffic-related pollution is associated with health hazards such as respiratory symptoms, has been supported by research in Europe and the US (Kim et al. 2004, McConnell et al. 2010). Children and the elderly are especially vulnerable. Studies have shown that children have substantial deficits in lung growth and higher risk of asthma when living or attending school near major roadways (Gauderman et al. 2007, McConnell et al. 2010). Other negative impacts include: respiratory effects (asthma, bronchitis), cardiovascular effects, premature mortality, cancer, and adverse birth outcomes and developmental effects (Baldauf et al. 2009). In addition, these pollutants may travel long distances, to produce secondary pollutants, such as acid rain or ground-level ozone (EPA 2010).

Mobile emissions are the primary source of pollution in roadway microenvironments. Mobile emissions contribute to 29% of the volatile organic compounds (VOCs), 35% of the nitrogen oxides (NO_x), and 58% of the carbon monoxide (CO) pollution in the US (Kuhns et al. 2004). In cities, mobile emissions contribution is even higher, due to increased traffic volumes and urban development, which respectively increases pollution and inhibits pollution dispersion. This results in high ground level concentrations, in large populated areas (Baldauf et al. 2008, Thoma et al. 2008, Chen et al. 2008, Berkowicz et al. 2006). For example, in 2007, it was estimated by the American Housing Survey that more than 45 million people live within 300 feet of an airport, railroad, or major highway. According to the 2009 survey, this number is growing

and is disproportionate towards the lower income population (Baldauf et al. 2009, Vette 2010, U.S. Census Bureau 2009). As a result, mobile sources often create more harm on average compared to point sources (Fowlie et al. 2008).

Environmental regulation has been implemented to reduce the impacts of these pollutants, in efforts to protect public health and the environment. However, initial command and control methodologies have proven costly and ineffective (Proost and Dender 2001). The mobile nature of vehicle pollution makes it difficult to efficiently regulate. Current regulations are aimed at manufactures in the form of emission standards, which has allowed vehicles to become predominate in the modern lifestyle (Menz 2002). Even with cleaner vehicles available, the user ultimately decides the vehicle type used, how, when, and where it is used. Furthermore, the user currently has no incentive to drive cleaner emitting vehicles (Menz 2002). As a result, this has led to trends of increasing vehicle use, traffic congestion, and desire for larger cars, which offsets the rising stringent regulations (HEI 2010, Menz 2002, RITA 2011). Some researchers argue that this practice of continually reducing the emissions from vehicles through increased technology may not be enough. This has led some researchers to believe that current motor vehicle use worldwide is not sustainable over the long term (Menz 2002).

Even with catalytic converters reduction of NO_x emissions, NO_x after treatment will be required to meet the increasingly strict regulations (Maricq 2007). Controlling diesel engine emissions have been the main method employed to combat high pollution air quality concerns (Johnson 2006). Several methods have been investigated to reduce vehicle emissions such as lean NO_x traps and urea selected catalytic reduction (SCR). However, drawbacks exist with both techniques such as potential of producing secondary pollutants and thermal durability. In addition, specific drawbacks to lean NO_x traps are sulfur poisoning and additional energy use to

regenerate traps whereas SCRs drawbacks are potential of ammonia slip and nitrogen dioxide (NO_2) formation (Maricq 2007). As a result, they are still in their infancy stages (Maricq 2007).

In heterogeneous photocatalysis pollutants are decomposed to nonhazardous waste products with little energy requirements and little selectivity rather than just absorbing pollutants, common of traditional air purification methods, (Zhao and Yang 2003, Fujishima and Zhang 2006). Photocatalytic pavements reduce pollutants such as NO_x by 40% to 85% once pollutants are emitted in the air (Beeldens 2006). In addition, photocatalytic pavements have the advantage that they can be applied only to target areas such that they may be a cost effective air pollution abatement technique.

1.1 PROBLEM STATEMENT

Despite the potential benefits of photocatalytic pavements, widespread application has not been realized due to unanswered questions: 1. How significant is the NO_x reduction from photocatalytic pavement in roadway microenvironments? 2. Are nitrates released at harmful quantities potentially creating a water quality problem? 3. Are nanoparticles released during photocatalytic pavement life cycle?

1.2 OBJECTIVES

In response to these questions, the goal of this study was to better understand the environmental impact of photocatalytic concrete pavement highways. To achieve this goal, the objectives of this study are to (A) construct a model that evaluates the NO_x reduction from photocatalytic pavements, (B) quantify the nitrates released from the photocatalytic degradation of NO_x, and (C) identify and characterize pathways for TiO_2 nanoparticle exposure. Results of this project will quantify the significance of NO_x reduction of photocatalytic pavements, identify if any

tradeoff hazards exist from nitrates being released to water runoff, and quantify and characterize potential exposure routes of TiO_2 nanoparticles.

1.3 RESEARCH APPROACH

To achieve the aforementioned objectives, the research methodology proposed was divided into three integrated phases: Model Development, Potential Hazards to Water, and Potential Nanoparticle Exposure to Air. The outcomes of each phase are summarized in Figure 1.1 with the corresponding objective.

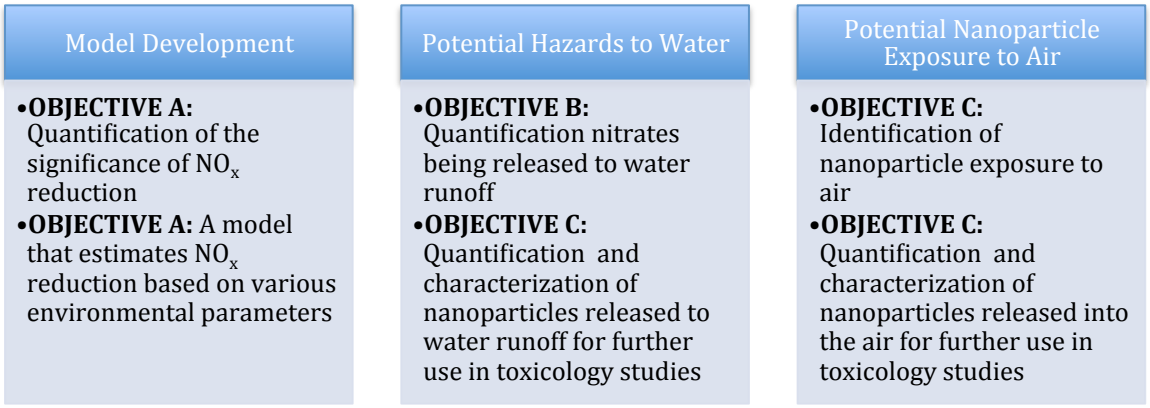

Figure 1.1 Project Phases and Expected Outcomes

The first phase, to develop a model that quantifies the significance of NO_x reduction from photocatalytic pavements under various environmental conditions, thus, achieving objective (a), is divided into four chapters, Chapters 3-6. Two model approaches were used; a statistical model, based on field study data and a mathematical model, based on the conservation of mass from laboratory experimental results.

In Chapter 3, results from a field study consisting of a ¼-mile concrete roadway sprayed with a photocatalytic coating in Baton Rouge, LA are presented. This was the first field installation of the spray TiO_2 photocatalytic pavement coating in the US. NO_x concentrations were monitored for both the coated and uncoated sections simultaneously for three weeks during

the spring season to directly measure photocatalytic degradation. Expanding on results from Chapter 3, Chapter 4 studies the impact of additional factors such as the vehicle activity and vehicle classification on the photocatalytic NO_x reduction due to photocatalytic pavements. A second field study was conducted with 22.3 m^2 of photocatalytic spray coated area and 22.3 m^2 of uncoated control area using a TiO_2 spray coat with improved durability. Similar to the first field study, the photocatalytic reduction of NO_x was evaluated by directly measuring NO_x reductions from the ambient air; however, to characterize the variability in traffic classification and activity between the two areas and its effects on interpreting NO_x reduction, a traffic study was also conducted for the photocatalytic and control areas.

Chapter 5 begins the work to develop the mathematical model, based on the conservation of mass and laboratory results. The first step was to model the photocatalytic degradation of nitrogen monoxide (NO) as a function of various environmental parameters. Since laboratory results indicated the NO oxidation rate was reaction mass transfer controlled, the Langmuir Hinshelwood (L-H) model was used. Due to noted possible durability issues with the spray coat photocatalytic pavements, the model was only created for the concrete samples with a photocatalytic mortar overlay. Using a plug flow photoreactor, the L-H reaction rate constant, k, and the adsorption equilibrium constant, Kd, were calculated at 5 different levels of relative humidity and 5 different levels of irradiance. A statistical model was created for both constants as a function of humidity and irradiance. Chapter 6 incorporates this statistical model into a Lavoisier mass balance model for roadway microenvironments to better understand the potential NO_x reductions in a real world setting. In doing so, the amount of NO reduced due to the photocatalytic pavement can be predicted under various environmental conditions and compared to other mass transfer mechanisms, thus achieving objective A. To demonstrate the model, the

percent of the mass transfer due to the photocatalytic reduction of NO was calculated for an area in Los Angeles, California.

The second phase, to assess the potential hazards released to water, is detailed in chapter 7. The first part of this chapter was to quantify how much nitrates are eluted into water, thus achieving part of objective B. Water samples were analyzed from photocatalytic concrete mortar overlay pavements and compared to water samples from concrete pavement controls before (baseline) and after photocatalytic oxidation of NO. The nitrates were quantified using the automated cadmium reduction test. The difference in nitrates eluted from pavement samples and the baseline is a result of the photodegradation of NO_x. In addition, the difference between the photocatalytic pavement samples and the concrete control samples is the potential added environmental impact of the photocatalytic pavement.

The second part of chapter 7 investigated whether engineered TiO_2 nanoparticles used in photocatalytic pavements will enter into water. For this study, water samples from soaking two different types of photocatalytic concrete pavements (photocatalytic mortar overlays and photocatalytic spray coats) were analyzed and compared to water samples from soaking a typical concrete pavement (control). These water samples were quantitatively analyzed with inductive coupled plasma atomic emission spectrometry (ICP-AES), thus achieving the remaining part of objective B.

Finally, the third phase to identify the potential for nanoparticle exposure of photocatalytic pavements during construction activities is described in Chapter 8. Nanoparticles released to the environment were quantified and characterized for further use in toxicology studies. In this study, the potential of exposure to synthetic nanoparticles released during construction activities for application of photocatalytic pavements was measured during

laboratory-simulated construction activities of photocatalytic mortar overlays and in an actual field application of photocatalytic spray coat. The scanning mobility particle sizer system (SMPS) measured the size distribution of nanoparticles released during laboratory and field activities. Since incidental nanoparticles are released during construction activities, nanoparticle emissions were compared to those from similar activities without nano-TiO_2, thus achieving objective C.

Chapter 9, the last chapter, consolidates the project results and also includes future recommendations and research ideas.

1.4 REFERENCES

Baldauf, R., Thoma, E., Hays, M., Shores, R., Kinsey, J., Gullett, B., Kimbrough, S., Isakov, V., Long, T., Snow, R., Khlystov, A., Weinstein, J., Chen, F., Seila, R., Olson, D., Gilmour, I., Cho, S., Watkins, N., Rowley, P., and Bang, J. (2008). "Traffic and meteorological impacts on near-road air quality: Summary of methods and trends from the Raleigh near-road study." Air & Waste Management Association, 58, 865-878.

Baldauf, R., Watkins, N., Heist, D., Bailey, C., Rowley, P., and Shores, R. (2009). "Near-road air quality monitoring: Factors affecting network design and interpretation of data." Air Qual Atmos Health, 2, 1-9.

Beeldens, A. (2006) "An environmental friendly solution for air purification and self-cleaning effect: the application of TiO_2 as photocatalyst in concrete." Belgian Road Research Centre. Proceedings of Transport Research Arena, Europe - TRA, Göteborg, Sweden, June, 2006.

Berkowicz, R. Hertel, Winther, M., and Ketzel, M. (2006). "Traffic pollution modeling and emission data" Environmental Modelling & Software, 21, 454-460.

Chen, H., Bai, S., Eisinger, D., Niemeier, D., and Claggett, M. (2008). "Modeling uncertainties and near-raod PM2.5: A comparison of CALINE4, CAL3QHC, and AERMOD." U.S. Federal Highway Administration, and U.C. Davis-Caltrans Air Quality Project.

Fowlie, M., Knittel, C.R., and Wolfram, C. (2008). "Sacred Cars? Optimal Regulation of Stationary and Non-Stationary Pollution Sources." National Bureau of Economic Research, (NBER). Working Paper No. 14504: 1-42.

Fujishima, A., and Zhang, X.. (2006). "Titanium dioxide photocatalysis: present situation and future approaches." Comptes Rendus Chimie. 9, 750-760.

Gauderman, W.J., Vora, H., McConnell, R., Berhane, K., Gilliland, F., Thomas, D., Lurmann, F., Avol, E., Kunzli, N., Jerrett, M., and Peters, J. (2007). "Effect of exposure to traffic on lung development from 10 to 18 years of age: a cohort study." Lancet, 369, 571-577.

Health Effects Institute (HEI). (2010). "Traffic-Related Air Pollution: A Critical Review of the Literature on Emissions, Exposure, and Health Effects." Special Report 17.

Johnson, T.V. (2006). "Diesel Emission Control in Review." SAE Technical Paper Series, 2006-01-0030, 1-18.

Kim, J.J., Smorodinsky, S., Lipsett, M., Singer, B. C., Hodgson, A.T., and Ostro, B. (2004). "Traffic-related air pollution near busy roads: the East Bay Children's Respiratory Health Study." American Journal Respiratory and Critical Care Medicine, 170, 520-536.

Kuhns, H.D., Mazzoleni, C., Moosmuller, H., Nikolic, D., Keislar, R.E., Barber, P.W., Li, Z., Etyemezian, V., and Watson, J.G. (2004). "Remote sensing of PM, NO, CO, HC emission factors for on-road gasoline and diesel engine vehicles in Las Vegas, NV." Science of the Total Environment, 322, 123-137.

Maricq, M.M. (2007). "Chemical characterization of particulate emissions from diesel engines: A review." Aerosol Science, 38, 1079-1118.

McConnell, R., Islam, T., Shankardass, K., Jerrett, M., Lurmann, F., Gilliland, F., Gauderman, J., Avol, E., Kuenzli, N.,Yao, L., Peters, J., and Berhane, K.. (2010). "Childhood Incident Asthma and Traffic-Related Air Pollution at Home and School." National Institute of Environmental Health Sciences, 1-33.

Menz, F.C. (2002). "The US experience with controlling motor vehicle pollution: lessons for China." International Journal Environment and Pollution, 18(1), 1-21.

Proost, S. and Dender, K.V. (2001). "The welfare impacts of alternative policies to address atmospheric pollution in urban road transport." Regional Science and Urban Economics, 31, 383-411.

Research and Innovative Technology Administration (RITA). (2011). "2011 National Transportation Statistics." United States Department of Transportation, <http://www.bts.gov/publications/national_transportation_statistics/> (June 7, 2011).

Thoma, E.D., Shores, R.C., Isakov, V., and Baldauf, R.W., (2008). "Characterization of near-road pollutant gradients using path-integrated optical remote sensing." Air & waste Management Association, 58, 879-890.

U.S. Census Bureau. (2009). American Housing Survey. <http://www.census.gov/hhes/www/housing/ahs/nationaldata.html> (June 7, 2011).

United States Environmental Protection Agency (EPA). (2010). Proposal to Revise the National Ambient Air Quality Standards for Ground-level Ozone, <http://www.epa.gov/ozonepollution/pdfs/20100106present.pdf> (July 2, 2010).

Vette A. (2010). "Near-Road Air Pollution." U.S. Environmental Protection Agency. Clean Air Research. <www.epa.gov/airscience> (June, 7 2007).

Zhao, J. and Yang, X. (2003). "Photocatalytic oxidation of indoor air purification: a literature review." Building and Environment, 38, 645-654.

CHAPTER 2
LITERATURE REVIEW

2.1 ENVIRONMENTAL PHOTOCATALYSIS BACKGROUND

Initial interest in environmental photocatalysis began in the 1970s, initiated by Fujishima and Honda's research in photoelectrochemical solar energy conversion (Fujishima and Honda 1972). Through biomimicy of plant photosynthesis, the researchers attempted to replicate the photo-induced redox reactions, by oxidizing water and reducing carbon dioxide, using a semiconductor irradiated by UV light (Fujishima and Zhang 2006). To accomplish this, the semiconductor is used as an electrode, which is connected to a counter electrode to generate electrical work while driving the redox chemical reactions (Fujishima and Honda 1972). Titanium dioxide (TiO_2) was the semiconductor chosen, due to a positive valence band edge that theoretically can oxidize water to oxygen (Fujishima et al. 2000). Fujishima and Honda found that when the surface was irradiated, a current was created such that oxidation occurred at the TiO_2 electrode and reduction at the counter electrode (Fujishima and Honda 1972). This proved that water could be decomposed into oxygen and hydrogen from solar irradiation, preferred since solar energy equates to roughly 5×10^{24} J per year (Cassar 2004).

The photoelectrochemistry concepts described were extended to research in heterogeneous photocatalysis applications by removing the external circuit (Fujishima and Zhang 2006). In 1977, Frank and Bard were two of the first to demonstrate this, by illustrating the decomposition of cyanide in water. Since then, increased interest in environmental photocatalysis was realized which caused TiO_2 to be applied to glass, tile, paper, and pavements for self-cleaning materials, water purification, air purification, sterilization, and oil spill remediation. From these studies, it has been shown that organic and inorganic compounds can be completely decomposed and that the TiO_2 surface has the ability to self-regenerate (Fujishima

and Zhang 2006). Therefore, rather than an adsorption of pollutants that is common to traditional air purification methods, heterogeneous photocatalysis can decompose pollutants to nonhazardous waste products with little energy requirements (Zhao and Yang 2003).

2.1.1 Heterogeneous Photocatalysis Mechanism

Heterogeneous photocatalysis requires a semiconductor photocatalyst in contact with a liquid or gas reaction medium. There are many semiconductors available for heterogeneous photocatalysis, such as CdS, ZnS, SnO_2, WO_3, SiO_2, ZrO_2, ZnO, Nb_2O_3, Fe_2O_3, $SrTiO_3$, and TiO_2 (Fujishima et al. 2000, Li et al. 2001, Zhao and Yang 2003). The photocatalytic ability of each is determined by the respective band gap, whereas the photocatalytic efficiency is impacted by crystal type, particle size, and any crystal modifications (Zhao and Yang 2003).

TiO_2, is the most popular semiconductor used for heterogeneous photocatalysis (Fujishima et al. 2000). Titanium dioxide has three crystal arrangements: anatase, rutile, and brookite (Husken et al. 2009). Of the three, anatase exhibits the highest photoactive efficiencies (Zhao and Yang 2003). Its excellent photocatalytic properties, such as highly oxidizing, photogenerated holes that produce hydroxyl radicals, as well as photogenerated electrons that produce superoxides from dioxygen, play an important role in photocatalytic reactions (Fujishima et al. 2000). Additional characteristics of TiO_2 that make it ideal for heterogeneous photocatalytic applications are its near transparency (especially useful in windows and glass), high stability in presence of aqueous electrolyte solutions, superhydrophilicity, relative cheapness, and commercial availability (Cassar 2004, Fujishima and Zhang 2006, Diamanti et al. 2008, Toma et al. 2009).

When TiO_2 is exposed to energy, from photons, that exceed the band gap energy of 3.2 eV, an electron is expelled from the valence band to the conduction band, leaving a hole behind

(Zhao and Yang 2003, Fujishima et al. 2000). For TiO_2, this process is initiated by energy from a UV light wavelength determined by the electromagnetic radiation, *hv*, where *h* is Planck's constant and *v* is the frequency of light. The production of electron-hole pairs, called excitons, results in redox or oxidation chemical reactions (Fujishima et al. 2000, Zhao and Yang 2003, Hunger et al. 2008). In the presence of water, these oxidizing holes, h^+, and photogenerated electrons, e^-, create hydroxyl radicals and superoxides respectively, shown in Equations 2.1 and 2.2 (Fujishima et al. 2000).

$$OH^- + h^+ \rightarrow OH^* \quad (2.1)$$

$$O_2 + e^- \rightarrow O_2^- \quad (2.2)$$

The resulting hydroxyl radicals and superoxides are key for oxidation or reduction reactions allowing for degradation of pollutants. For example in the degradation of nitrogen oxide (NO), the hydroxyl radicals oxidize NO to water-soluble nitrates, as shown in Equations 2.3 and 2.4 below (Beeldens 2008):

$$NO + OH^* \xrightarrow{T_iO_2} NO_2 + H^* \quad (2.3)$$

$$NO_2 + OH^* \xrightarrow{T_iO_2} NO_3 + H^* \quad (2.4)$$

This complete process is illustrated as follows in Figure 2.1.

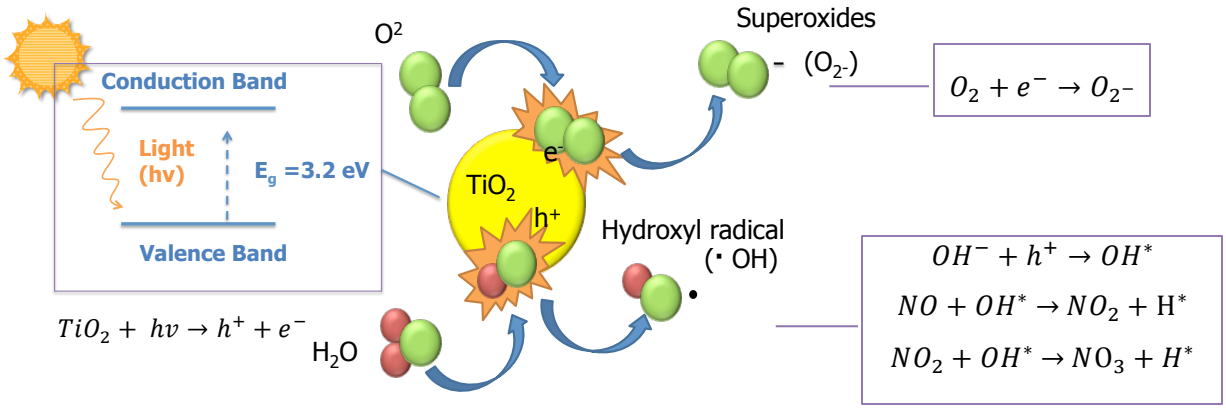

Figure 2.1 Photocatalytic Process (modified from Nano 2000)

2.1.2 Photocatalytic Reaction Kinetics

Photocatalytic reactions are a heterogeneous reaction, such that the reaction occurs at the interfacial surface of a solid-gas or solid-liquid. The reaction follows a series of several steps (Figure 2.2). Diffusion, the first step, is rarely the mass transfer-limiting step, unless if diffusion occurs through a solution. The following three steps, surface adsorption, reaction and product desorption are difficult to differentiate, as these steps occur simultaneously. Thus, these three steps are considered together as a single reaction rate, which is often the mass transfer-limiting step (Valsaraj 2009).

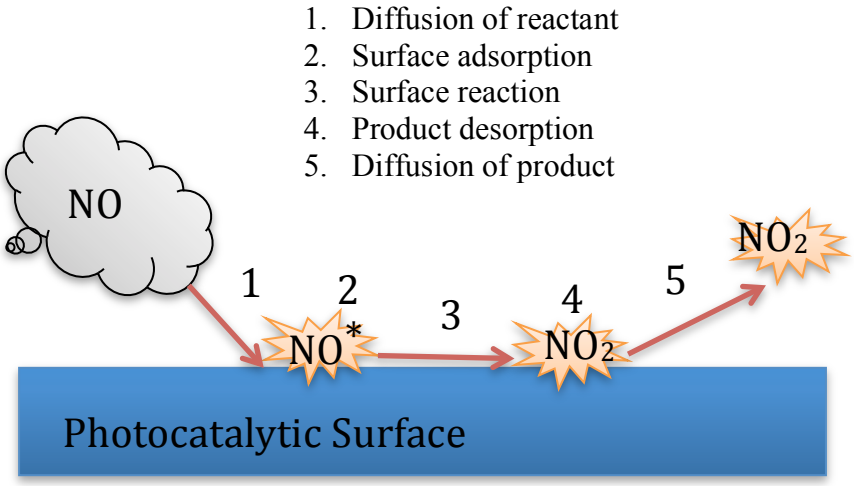

Figure 2.2 Heterogeneous Surface Reaction Schematic for NO (modified from Valsaraj 2009)

For heterogeneous reactions, the reaction rate typically follows the Langmuir-Hinshelwood (L-H) model:

$$r = \frac{kKdC}{1+KdC} \quad (2.5)$$

Where k is the L-H reaction rate constant (mg/m^{3}s); Kd is the L-H adsorption equilibrium constant (m^3/mg) for the given pollutant, and C is the concentration of the pollutant as a gas (Hunger 2010).

Hence, the conversion rate, r, is dependent upon the surface adsorption, or surface concentration of the pollutant. When more than one pollutant exists, competition between the two pollutants for adsorption exists. In this case, the reaction rate in Equation 2.5 is modified for two pollutants (A and B) as follows:

$$r_A = \frac{kK_AC_A}{1+K_AC_A+K_BC_B} \quad (2.6)$$

2.1.3 TiO_2 Production

Titanium dioxide commercial production is well developed due to its use as a whitener in paint and more recent use in the cosmetic industry for sun protection. Typically, rutile phase TiO_2 particles between 250 nm to 1 μm in diameter are produced for pigments while anatase particles between 1 and 100 nm are produced for sun protection (Grubb and Bakshi 2010).

There are two well-developed production processes that exist: the Chloride Process (the main process used in the United States) and the Sulfate Process (the main process used in Europe) (Grant et al. 2004, Grubb and Bakshi 2010). The sulfate process was the first developed process and was the sole process up to the 1950s. This process involves a reaction of sulfuric acid with the titanium feedstocks, typically ilmenite ore. In the 1940s DuPont started to develop and commercialize the chloride process such that various grades of ores could be used (Dobson et al. 1994). Despite this, initially, the chloride process also used ilmenite ore as the feedstock

due to limited rutile resources available during this time period. However, in the 1960s when sources of rutile were discovered in Australia, the feedstock was switched, simplifying the chemistry of the chloride process as well (Dobson et al. 1994). Today, natural occurring rutile TiO_2 deposits are ideal for the chloride processes and titanium-rich ilmenite (Fe TiO_3) ores are ideal for the sulfate process (Grubb and Bakshi 2010).

There are disadvantages and advantages to both production processes. The chloride process can only make rutile phase TiO_2 while the sulfate process can produce both phases (Grant et al. 2004). The waste produced during the sulfate process is making it become more unsustainable (Grant et al. 2004). As a result, a relatively new production process is the Altairnano hydrochloride process. This process also uses ilmenite ore however it is processed with hydrochloric acid instead of sulfuric acid (Grubb and Bakshi 2010).

Ilmenite can be found in many places around the world whereas naturally occurring rutile is becoming scarce (Grubb and Bakshi 2010, Grant et al. 2004). Due to the declining rutile sources, many manufacturers are using Ti slag in replacement (Grant et al. 2004). Ilmenite is most commonly mined in Australia, South Africa and Canada, and as a result, the majority of the world share of the TiO_2 produced in 1995 was in North America with growing productions in the Asia/Pacific (Grubb and Bakshi 2010, Grant et al. 2004).

In 2010 approximately 7.2 million tons of TiO_2 was produced, of which 0.7% of were nanoparticles. By 2015 the production of TiO_2 nanoparticles is expected to quadruple (Future Markets, Inc. 2011). The construction industry is the largest user of TiO_2 nanoparticles for uses in self-cleaning surfaces and air purification (ObservatoryNANO 2011). Italcementi Group has it own photocatalytic cement "TX Active" which has been applied to indoor surfaces and tunnel walls and has been applied in Italy (400,000 m^2), France, Belgium, Morocco and the United

States. Despite this, Japan is considered the global leader in both photocatalytic TiO_2 production and consumption and Europe is considered the second (ObservatoryNANO 2011).

2.2 PHOTOCATALYSIS PAVEMENTS

Titanium dioxide mediates heterogeneous photocatalysis, and therefore can be a self-cleaning material, possibly useful in environmental pollution remediation (Fujishima and Zhang 2006). For air purification, large surface areas in close contact to high pollution concentrations are ideal (Beeldens 2006). For this purpose, applications of TiO_2 were expanded to create photocatalytic pavements. The versatility, relatively low cost, and large-scale application possibilities of cement/concrete make it an important and popular substrate (Lackhoff et al 2003). In addition, some research shows synergetic effects have been exhibited when TiO_2 has been used with cementitious and various construction materials (Cassar 2004). As a result, concrete represents the primary pavement material investigated.

2.2.1 Background in Photocatalytic Concrete

TiO_2 was first introduced to cement materials used in buildings to retain the white color and aesthetic characteristics, thus creating a self-cleaning effect (Husken et al. 2009, Cassar et al. 2003). The discoloration, particularly on white concrete, is due to the accumulation of organic compounds. Initial studies of photocatalytic concretes were based on colorimetric tests. Exposing the surface with an organic dye such as rhodamine B, the colorimetric measurements monitored the reduction of pollution on the surface when exposed to UV irradiation (Cassar 2004).

Current research switches the focus from self-cleaning concrete to an evaluation of TiO_2 for air remediation techniques. Many chemicals have shown an ability to degrade from TiO_2 photocatalytic concrete substrates, such as NO_x, SO_x, NH_3, CO, as well as volatile organic

carbons, such as benzene, and toluene, organic chlorides, aldehydes, and polycondensated aromatics (Cassar 2005). The concrete matrix helps trap both, air pollutants and intermediate byproducts, thereby promoting a complete degradation of pollutants. As a result, the concern of intermediates released into the atmosphere is reduced (Sopyan et al. 1996, Lackoff et al 2003, Cassar 2004, Berdahl and Akbari 2008). In addition, research by Cassar has shown that cement exhibits small amounts of photocatalytic degradation without TiO_2 caused from the hydroxides in the cement matrix. Thus, when added to concrete mix designs, TiO_2 increases its natural photocatalytic ability to one that is even higher than the TiO_2 alone, suggesting a synergistic effect (Cassar 2004). Cassar attributes this synergy to both the high adsorption capacity of the concrete matrix aiding complete degradation, as well as concrete's natural photocatalytic ability, making concrete an ideal substrate for photocatalytic materials (Cassar 2004). As a result, applications of TiO_2 in concrete have spread to road sound barriers, sidewalks, and highway overlays for air remediation (Osburn 2008).

Field applications of TiO_2 photocatalysts pavements are already in progress in Japan and Europe and are recently initiated in the United States. Japan has applied TiO_2 coatings to roadways and sound barriers amongst various cities such as Osaka, Chiba, Chigasaki, Suitama and Shinatoshin, covering at least 50,000 m^2 of surface area, and claiming at least 0.5 to 1.5 $mmol/m^2$ reduction rates (Osburn 2008). Full-scale examples in Segrate, Italy, show photocatalytic durability lasted at least one year; however, longer duration tests are still in progress (Cassar 2004). Despite the availability of the studies, comparison between the experiments is challenging, due to the different variables, testing methods, and reporting methods (Osburn 2008).

2.2.2 Application Techniques for Photocatalytic Concrete Pavements

Several application methods have been investigated for photocatalytic concrete pavements. TiO_2 nanoparticles have been incorporated into concrete pavements by applying a photocatalytic concrete pavement overlay, spraying as a thin exterior film of suspended TiO_2 nanoparticles in a binding agent, or sprinkling TiO_2 nanoparticles on curing concrete (Hassan et al. 2009). Yet the spray application and sprinkle techniques have higher concentrations of TiO_2 exposed on the surface, leading to higher photocatalytic efficiencies, TiO_2 is most commonly incorporated into cement photocatalytic pavement overlays (Hassan et al. 2009, Chen and Li 2007). Researchers prefer photocatalytic overlays due to their higher durability (Diamanti et al. 2008, Beeldens 2008). When incorporated into the concrete cement mix, abrasion from traffic results in new TiO_2 particles to be exposed. Furthermore, the mechanical strength of the TiO_2 modified cement is increased, due to the pozzolanic activity of TiO_2 in hydrating cement and denser structure (Lackhoff et al. 2003, Watts and Cooper 2008, Beeldens 2008). Nonetheless, the spray coat application has the major advantages of being simpler and is potentially cheaper to apply to current concrete roadways.

2.2.2.1 Photocatalytic Mortar Overlays

The thickness of photocatalytic mortar overlays ranges from 0.3 to 8 mm (Beeldens 2008, Chen and Li 2007). TiO_2 nanoparticles are added directly to the cementitious mortar mix to produce the overlay. TiO_2 can be incorporated into mortar mixtures in two forms - as aqueous suspended nanoparticles, or as nanoparticle powders. Aqueous suspended particles are often smaller sizes, near 88 nm in diameter, thus increasing its photocatalytic activity. The aqueous nanoparticle solution can be incorporated into a mortar overlay, substituting for some of the water requirements (Diamanti et al. 2008). TiO_2 powder particles sizes are usually larger than suspended ones, ranging between 150-400 nm in diameter, thus slightly decreasing its

photocatalytic activity (Diamanti et al. 2008). However, when the sizes are mixed, there is a synergistic effect and the photocatalytic efficiencies are enhanced (Diamanti et al. 2008, Cassar et al. 2003). Research by Diamanti et al. (2008) suggested a mixture of 3% anatase powder and 2% anatase suspension versus cement weight as an optimized mix design (Diamanti et al. 2008). A similar effect can be achieved using a mixture of anatase (larger band gap) and rutile (smaller band gap) crystals (Zhao and Yang 2003). Optimum photocatalytic mixtures of anatase and rutile particles are already commercially available, the most famous being, Degussa P25, which uses a 20-30/70-80 rutile-anatase ratio (Strini et al. 2005, Zhao and Yang 2003).

TiO_2 is generally added as a percent of the cement weight. As expected, increasing TiO_2 concentrations increase photocatalytic pavement effectiveness. However, research shows that this relationship is not linearly dependent; instead, increases at lower concentrations, such as 1% to 3%, have a greater impact on the improved photooxidation activity, compared to increases at higher concentrations, such as 3% to 6% (Watts and Cooper 2008, Strini et al. 2005). The increased concentration not only impacts the photocatalytic efficiencies, but also corresponds to the additional material costs. Italcementi's product TX, utilizing TiO_2 as a photocatalyst, is known to add as much as 20% to the cost of cement (Berdahl and Akbari 2008). As a result, when adding TiO_2 to current bulk materials, such as cement to minimize the additional costs, concentrations between 1-5% nanoparticles to cement are ideal (Watts and Cooper 2008, Strini et al. 2005).

Additional significant variables include mix design factors, such as the water/cement ratio, size and type of aggregates, and cement aggregate ratio (Poon and Cheung 2007, Watts and Cooper 2008, Cassar et al. 2003). Not many experiments exist on optimization of the concrete mix design for photocatalytic degradation. Poon et al. investigated the impact of different

aggregates and cement aggregate ratios for the photocatalytic properties of concrete pavement blocks. Poon found that recycled aggregates had higher NO removal than sand, possibly due to the higher porosity. Similarly, more porous specimens can be achieved by eliminating fine aggregates below 300 μm. Consequently, removal of fine aggregates predominately increased the NO removal efficiency by at least 4% (Dylla et al. 2010[a], Poon and Cheung 2007). Furthermore, when glass was used as an aggregate, the photocatalytic properties were enhanced, due to the increased transmission of light. In addition, decreasing the cement content from a 1:2 cement aggregate ratio to a 1:3 ratio increased NO reduction efficiencies by 30% (Poon and Cheung 2007).

2.2.2.2 Spray Coat

The spray coat technique is becoming more popular due to its simple, versatile, and quick application, which can be applied to concrete or asphalt pavement substrates. TiO_2 nanoparticles are suspended in an aqueous base binder, which are sprayed on top of hardened pavement surfaces in two parts. The base coat is first applied as a primer in order to provide for a clean and durable surface. The base coat used by Hassan et al. 2011, has 2% by weight of anatase titanium dioxide (non photocatalytic grade) suspended particles. The top coat has also 2% titanium dioxide suspended nanorods that are about 6nm in diameter and of a photocatalytic grade. The primer and top coat are both applied by a spray gun using a cross hatch spray formation to ensure even coverage at the optimal application rate of 20 g/m^2 (Hassan et al. 2011). From current research, nitrogen dioxide reduction efficiencies were 25% with a 9 l/min flow for concrete substrates and as high as 53% for asphalt substrates with a 1.5 l/min flow (Hassan et al. 2009, Hassan et al. 2011).

2.2.3 Photocatalytic Pavement Durability

Few studies have investigated the photocatalytic pavement durability. The photocatalytic layer must be resistant to repeated traffic wear, abrasion, and delamination. Hassan et al. 2010 investigated the pavement durability, evaluating abrasion and wear. The loaded wheel test and rotary abrasion test were used to accelerate pavement wear and abrasion, respectively. The photocatalytic efficiencies were measured before and after, wear and abrasion, to identify any reduction in efficiencies. Scanning Electron Microscopy (SEM) and Energy Dispersive Spectroscopy (EDS) before and after the accelerated wear and abrasion were used to identify any significant loss of TiO_2, to understand the change in photocatalytic efficiencies (Hassan et al. 2010).

2.2.3.1 Resistance to Repeated Traffic Wear

To test the resistance to repeated traffic loadings, the Hamburg-type Loaded Wheel Tester (LWT) can be employed to simulate a repeated rolling load. The LWT employs a scaled dynamic wheel passing back and forth over the specimen at a load of 702N and frequency of 56 passes per minute. For each pass the progress of surface rutting is monitored and recorded. The test concludes after 20,000 cycles, in which the final deformation is recorded and failure is identified for 6 mm for asphalt substrates (LADOT 2000).

Yet this test is designed for asphalt pavements, Hassan et al. 2010 used this test by comparing the performance of a photocatalytic pavement to a concrete pavement for control. The photocatalytic concrete pavements measured rut depth after 20,000 passes was minimal (less than 1mm) and did not differ from the control sample. Thus the results concluded that the use of the coating did not appear to affect the wear resistance of the surface (Hassan et. al 2010). Similarly, with the exception of one sample, there was no negative impact to the photocatalytic

efficiencies. The SEM coupled with EDS results, confirmed a significant concentration of TiO_2 on the surface remained after wear (Hassan et. al 2010).

2.2.3.2 Resistance to Abrasion

To test the resistance to abrasion, the rotary abrasion (RA) test is used. Defined by ASTM C 944, the rotary abrasion test uses a cutter rotating at 200 rpm under a constant load of 98N for 2 minutes to wear the coating surface. The abrasion resistance is determined by measuring the loss of the sample weight in grams (ASTM C944).

Results from Hassan et al. 2009, which employed this test, concluded that mortar overlays are more susceptible to abrasion compared to the spray coating. The greater loss of weight, noted for the overlay samples, maybe associated with a loss of mortar, fines, and TiO_2 nanoparticles (Hassan et al. 2009). Despite this, the photocatalytic efficiencies of the mortar overlays remained constant before abrasion and after abrasion, whereas the spray application efficiencies significantly decreased. Similarly, the SEM coupled with EDS results illustrated similar relative concentrations of TiO_2 for the mortar overlay samples, confirming the theory that as abrasion occurs, more TiO_2 particles are exposed (Hassan et al. 2010). Meanwhile, the spray coat application SEM and EDS images illustrated a decrease in relative concentration of TiO_2, explaining the decrease in reduction efficiencies (Hassan et al. 2009).

2.2.3.3 Resistance to Delamination

To test the durability against delamination of the photocatalytic mortar overlay, the shear resistance is measured by means of a direct shear test. The direct shear test applies a normal load concurrent with a shear load, simulating traffic loads (Canestrari et al. 2005). The shear load – static, ramped, or repeated– is applied up to 31,000 N, while the deformation is recorded

(AASHTO T 320). Currently, there is no known research that has characterized photocatalytic mortar overlay pavements shear resistance.

2.2.4 Environmental Factors Impacts on Photocatalytic Pavements Efficiency

There are many environmental factors that affect the photooxidation efficiency. Understanding these relationships is progressive and often varies by photocatalytic material thus making comparisons difficult. Nevertheless, known environmental factors consist of pollutant types, pollutant competition, pollution concentrations, air velocity, relative humidity, UV light intensity, and photocatalytic degeneration and regeneration.

2.2.4.1 Pollutant Types

Many different pollutants threaten our society in both the indoor and outdoor environments. Emissions from vehicle combustion are nitrogen oxides (NO_x), sulfur dioxide (SO_2), carbon monoxide (CO), and volatile organic compounds (VOCs) threatening both human health and the environment. For example, NO_x and VOCs pollutants are precursors to smog, especially prevalent on hot, sunny days (Berdahl and Akbari 2008). Furthermore, NO_x and SO_2 are the leading causes of acid rain, which not only destroys the environment by killing and reducing the biodiversity of forests and lakes, but also degrades our buildings (Poon and Cheung 2007, Thoma et al. 2008). Outdoor air also impacts indoor environments. NO_x and VOCs are both associated with sick building syndrome (Liu et al. 2008).

The photodegradation rates of each pollutant vary due to different adsorption rates and reaction schemes. For example, VOCs such as benzene, toluene, ethylbenzene, and xylene collectively referred to as BTEX all showed various photo-steady-states and reaction rates (Ao et al. 2002). As a result, in research, there are continual attempts to describe the ability of titanium dioxide to degrade these pollutants through better understanding of the chemical kinetics.

Nitrogen Oxides

Nitrogen oxides are one of the most common pollutants researched for removal potentials. Nitrogen oxides have detrimental effects on the outdoor environment by promoting acid rain and effects on the indoor air quality, contributing to sick building syndrome. Further, roadway microenvironments contribute to 35% of NO_x emissions (Kuhns et al. 2004). For example, in Baton Rouge, NO_x emissions are typically 0.010 ppm. However the maximum can reach 0.152 ppm (DEQ 2006). Currently, EPA limits nitrogen dioxide to a 0.053 ppm recorded annual mean (EPA 2010[b]). This regulation is expected to get stricter in the near future (EPA 2010[b]).

The approved method of NO_x detection is chemiluminescence. Chemiluminescence occurs when light is emitted from a reaction, which in the case of NO_x is between NO and ozone. The amount of light emitted is proportional to the NO concentration. For nitrogen dioxide, an indirect approach is taken, since a catalytic converter must first reduce the nitrogen dioxide to nitric oxide in order to be measured. After catalytic conversion, the total NO measured corresponds to the NO_x concentration. Therefore, the nitrogen dioxide concentration is the difference between the total NO_x and the NO (EPA 1999, EPA 2007).

Titanium dioxide has the ability to remove NO_x, but the removal percentage differs due to many other known variables. For example, titanium dioxide, when added to mortar, can remove up to 92% of NO_x in 7 hours of exposure from a 300 W lamp. A similar mortar layer was applied to a full-scale road in Segrate, Italy, with vehicle traffic of 1200 units per hour. The photocatalytic mortar overlay application, on sunny days, resulted in a 50% reduction of NO_x concentration with stability of a year (Demeestere et al. 2008). Based on a summary of quantitative investigations published, a probable estimate of 200 m^3 of air per day of NO_x can be removed from photocatalytic oxidation (Berdahl and Akbari 2008).

The photooxidation of NO_x follows the reaction scheme (Yu 2003):

$$NO + {}^{1}/_{2}\, O_2 \rightarrow NO_2 \quad (2.7)$$

$$2NO_2 + {}^{1}/_{2}\, O_2 + H_2O \rightarrow 2HNO_3 \quad (2.8)$$

Since NO_2 is an intermediate of NO, NO is typically used to test the photocatalytic ability for simplicity purposes (Yu 2003). Furthermore, the photooxidation of studies incorporating NO_2 are challenging, due to its high instability. For example, there appears to be another reaction occurring between NO_2 and the concrete surface, possibly heterogeneous hydrolysis. As a result, the equilibrium concentrations changed when different percentages of NO_2 were incorporated into the NO_x gas mix, possibly due to this reaction. The amount of NO_2 disappearance from the equilibrium concentration was increased with decreasing flow rates. In fact, when the inlet stream was 70% NO_2, the majority of the NO_2 was scrubbed without requiring photocatalytic degradation (Dylla et al. 2011).

Few studies have mentioned the amount of nitrates being released to water, stating only that the amount released is 10 times inferior to the original pollutant level (PICADA 2001). The final product NO_3 is absorbed by concrete substrates, due to the alkalinity of concrete (Sleiman et al. 2009, Yu 2003). Furthermore it is theorized, but not confirmed, that the nitrates absorbed by the concrete react with the calcium hydrate $Ca(OH)_2$ in the concrete cement, neutralizing to $Ca(NO_3)_2$ and H_2O (Li and Qian 2009).

Sulfur Dioxide

Sulfur dioxide, another contributor to acid rain, has also been tested for photodegradation by TiO_2. Vehicle sources contribute up to 7% of the total SO_2 emissions (Zhan et al. 2009). Ambient concentrations typical of Baton Rouge are 0.004 ppb for sulfur dioxide, with maximums reaching 0.076 ppb (DEQ 2006). EPA limits for sulfur dioxide is 75 ppb, recorded

as a one-hour average (EPA 2010[a]). Sulfur dioxide is measured by the pulsed fluorescence SO_2 analyzer (EPA 1999). Studies have shown that adsorption rates of SO_2 are 1.6-5 times higher than NO adsorption. Despite the higher adsorption rates, the SO_2 removal efficiency is not as promising as NO removal. In theory, SO_2 interacts with an active metal oxide, forming sulfates and sulfites that are easily absorbed on the surface thus inhibiting the TiO_2 activation. This explains the higher adsorption rate and lower removal rates of SO_2, compared to NO (Toma et al. 2006).

Volatile Organic Compounds

Volatile organic compounds (VOCs) threaten human health by causing cancer and the environment by means of greenhouse gases that increase global warming (Ao et al. 2004). VOCs are classified by the World Health Organization (WHO) as all organic compounds with boiling points in the range of 50 to 260°C, excluding pesticides. VOCs are typically higher for indoor environments as compared to outdoor environments. However, outdoor air is considered a source for indoor VOC pollution. Although the largest source of VOC pollution is from building materials, vehicles are still responsible for 29% (Kuhns et al. 2004). For example, aromatic hydrocarbons including toluene, xylenes, ethylbenzene, trimethylbenzenes, and aliphatic hydrocarbons inclusive of octane, decane, and undecane are emitted from sources of gasoline and combustion (Wang et al. 2007). These petroleum derivatives are the most common VOCs found in both indoor and outdoor environments (Ao et al. 2004, Saarela et al. 2003). Typical ranges of individual indoor VOCs concentrations are between 5 $\mu g/m^3$ to 50 $\mu g/m^3$, which typically totals at concentrations higher than 50 $\mu g/m^3$. The pollutants can be measured by a solid phase microextraction or analytical gas chromatography and quantified by a mass selective detector (Saarela et al. 2003, Ao et al. 2004, Demeestere et al. 2008). According to a

summary published of quantitative investigations, a probable estimate of 60 m^3 of air per day of VOCs can be removed from photocatalytic oxidation (Berdahl and Akbari 2008).

For VOCs the reaction rates are dependent on pollutant type. Generally higher soluble compounds tend to have higher reaction rates. Thus, the ordering of conversion rates is as follows: alcohols and glycol ethers > aldehydes, ketones, and terpene hydrocarbons> aromatic and alkane hydrocarbons> halogenated aliphatic hydrocarbons (Berdahl and Akbari 2008). More specifically, the benzene, toluene, ethylbenzene, and o-xylene (BTEX) removal efficiencies are ranked in increasing oxidation rates as benzene, toluene, ethylbenzene, and o-xylene (Strini et al. 2005, Demeestere et al. 2008). Although, VOCs are known to fully oxidize, some less desirable intermediates may be exposed (Berdahl and Akbari 2008). As a result, kinetic studies are becoming increasingly important; not only to understand the reaction rates, but more importantly to understand the intermediate chemicals.

2.2.4.2 Chemical Interaction and Competition

As shown, different reaction schemes exist depending on the pollutant. This results in different rates of photocatalytic degradation. Many pollutants are known to be able to photo-oxidize; however, interaction and competition of other pollutants is yet to be understood. In the presence of other chemicals, simultaneous photocatalytic oxidation reactions may inhibit or promote the removal rates. Pollutants such as SO_2 and BTEX are known to inhibit degradation of other pollutants while NO can enhance degradation. Specifically, BTEX and SO_2 are known to inhibit degradation of formaldehyde, interfering with the formaldehyde degradation by decreasing the conversion by 10%. The SO_2, absorbed first into the TiO_2 surface, inhibits the adsorption of formaldehyde. Similarly, BTEX competed for adsorption with formaldehyde (Ao et al. 2004). BTEX also interferes with NO reduction (Ao et al. 2002). In contrary, NO_x enhances

photodegradation of various pollutants. For example, NO_x increased the formaldehyde photodegradation rates by 5% at lower humidity levels and as much as 25% at high humidity levels (Ao et al. 2004). When BTEX combined with NO_x photooxidation, the largest enhancement was in the pollutants with lower reaction rates, benzene and toluene (Ao et al. 2002). Theory suggests that the photodegradation of NO_x results in OH radicals, which can be employed for pollutant conversion (Equations 2.9 for NO degradation and 2.10 for NO_2 degradation) (Ao et al. 2004, Ao et al. 2002).

$$NO + 2HO_2 \bullet \rightarrow NO_2 + OH \bullet \quad (2.9)$$

$$NO_2 + NO + H_2O \rightarrow 2OH \bullet + 2NO \quad (2.10)$$

However, the more NO_2 added to the NO_x mix, the lower the NO_x reduction efficiencies are realized. Thus, as the NO_2/NO_x ratio increases, the NO_x reduction efficiencies decrease. Introducing a NO_x gas mixture with 75% NO_2, the NO_x reduction efficiencies drop 32% equivalent to a 56% reduction in total efficiency (Dylla et al. 2010[b]).

2.2.4.3 Concentration of Pollutants and Flow Rates

Research further supports that removal efficiency is a function of the quantity of pollutants and exposure periods. In research, flow rates varied from 1 L/min to 9 L/min (Poon and Cheung 2007, Beelden 2006, Yu 2003, Chen and Li 2007, Dylla et al. 2010[a]). For the TiO_2 on roof tiles, when longer periods of gas residence time with lower amounts of toluene gases are present, removal efficiencies increase, whereas with shorter periods and higher concentrations of toluene the efficiencies decrease (Demeestere et al. 2008). Similar results were concluded in experiments with indoor uses of TiO_2 photocatalytic oxidation of ethylene, formaldehyde, toluene, 1-butene, and BTEX (Zhao and Yang 2003, Demeestere et al. 2008, Sleiman et al. 2009, Ao et al. 2002). For example, an increase in flow rate decreased the removal efficiency of

toluene from 95% to 65% (Sleiman et al. 2009). This trend is also exhibited for photodegradation of outdoor concentrations of NO_x. As the flow rate increased the NO_x removal efficiency decreased linearly (Dylla et al. 2010[a]). However, when there are mixed gases present, there is interaction between the two factors. As a result, at slower flow rates there is less of a negative impact resulting from increasing NO_2/NO_x ratios (Dylla et al. 2010[b]).

A possible explanation is that an increase in flow decreases the residence time with the photocatalytic reactor, which can be calculated by the flow rate divided by the volume of the photoreactor. This equates to less time for the pollutants to be absorbed by the photocatalytic compound (Dylla et al. 2010[a]). In addition, an increase in pollutant concentration increases the mass transfer rate and accumulation of final products (Sleiman et al. 2009, Demeestere et al. 2008, Ao et al. 2002). An accumulation of oxidation products on the surface inhibits continuous adsorption of pollutants, potentially leading to deactivation of the photocatalysis (Ao et al. 2002).

Thus, research points to the main use of TiO_2 for small pollutant loads, similar to those found in indoor and outdoor air (Demeestere et al. 2008). For example, varying the concentration of NO and NO_x within typical the ambient levels, showed no significant impact on the NO_x reduction efficiencies. This indicates that at ambient levels of NO_x concentration the photocatalytic oxidation is not limited by the TiO_2 active sites and no competitive adsorption effect between the byproducts and NO_x occurs (Dylla et al. 2010[b]). Despite this, it is still important to locate photocatalytic surfaces near pollutants to ensure exposure (Beeldens 2006).

2.2.4.4 Relative Humidity

Water vapor has both negative and positive impacts, which is surprising, since water is a key source for hydroxyl radicals (Zhao and Yang 2003, Demeestere et al. 2008, Wang et al. 2007, Sleiman et al. 2009). As expected, the absence of water for some chemicals hinders the reaction

rates common in toluene, benzene and formaldehyde photocatalytic oxidation. Surprisingly, water can also inhibit photocatalytic oxidation rates. Researchers suggest one explanation is that water particles compete with the pollutant molecules absorbed (Demeestere et al. 2008, Wang et al. 2007, Sleiman et al. 2009). Another thought is that the water forms one or more layers of film, which prevents the pollutant from reaching the TiO_2 layer (Sleiman et al. 2009). Thus, too much water interferes with reaction rates, which sometimes results in optimum humidity conditions (Wang et al. 2007).

Optimal humidity conditions were identified for removal of formaldehyde. At lower humidity levels, not enough radicals are present and at high percentages, competition impacts the amount of pollutants absorbed. Researchers suggest that 55% relative humidity as optimal for removal of formaldehyde (Liu et al. 2008). Contrary, in another study formaldehyde did not exhibit an optimal humidity level; instead, the conversion decreased from 80% to 54%, when the humidity level increased 2100 to 22000 ppmv (Ao et al. 2004). Thus, there seems to be a discrepancy in findings as to whether or not an optimal relative humidity level exists (Liu et al. 2008, Sleiman et al. 2009). Furthermore, for the same humidity increase (2100 to 22000 ppmv), toluene removal efficiencies decreased from 72% to 19%, suggesting that the humidity level impact is also pollutant specific (Ao et al. 2004). For example, the optimum relative humidity for NO_x reduction is at 25% relative humidity compared to 55% exhibited for formaldehyde (Dylla et al. 2010[b], Liu et al. 2008). Whereas other pollutants, such as TCE and toluene, exhibit only negative impacts when water content increases (Zhao and Yang 2003, Sleiman et al. 2009). These discrepancies indicate that the impact of humidity is not easy to describe. Impacts may differ by pollutant type, concentration, and possible other experimental factors (Ao et al. 2002).

2.2.4.5 UV intensity and Wavelength

It is clear that TiO_2 needs light as an energy provider to function and degrade any pollutants. Several experiments show that with the absence of light, photodegradation does not take place (Liu et al. 2008, Anpo and Takeuchi 2003, Poon and Cheung 2007, Nonami et al. 2004, Zhao and Yang 2003). Changing the light source impacts the wavelength and the photon flux; where the wavelength is primarily responsible for the photocatalytic activity and the irradiance or photon flux impacts the rate of degradation. For TiO_2, wavelengths smaller than 400 nm are required for irradiation, which corresponds to the UV spectrum from the sun (Fujishima et al. 2000, Zhao and Yang 2003). TiO_2 can be doped or undoped to increase the spectrum of wavelengths available for irradiation (Hunger et al. 2008). Higher intensities result in more photons produced, thus higher photocatalytic oxidation rates (Fujishima et al. 2000, Zhao and Yang 2003). The relationship between UV light intensity versus photocatalytic oxidation rates is often a linear correlation. The rate of increase is dependent upon chemical pollutant. For example, when the irradiance changed from 0 to 1500 $\mu W/cm^2$ the effects were a linear impact, increasing the oxidation activity drastically for o-xylene and ethylbenzene and slightly for benzene and toluene (Strini et al. 2005). In addition, photocatalytic oxidation of TCE was enhanced from 0.08 x 10^{-6} to 0.25 x10^{-6} mol/s.g as the light intensities increased from 0.08 mw/cm^2 to 0.45 mw/cm^2 (Zhao and Yang 2003). The irradiance not only increases the activity rates, it impacts the intermediates formed. For example, more intermediates were formed using the germicidal lamps with higher intensities, when compared to lower intensities of black lamps (Zhao and Yang 2003).

2.2.4.6 Photocatalytic Degeneration and Regeneration

Another highly debated variable of photocatalysis is the possible degeneration of the photocatalytic properties also known as catalyst poisoning. This may present the need of a way

to restore the photocatalytic properties of TiO_2 (Nonami et al. 2004). Since TiO_2 is a catalyst and undergoes no change, it can theoretically be used indefinitely (Nonami et al. 2004). As a result, degeneration is caused by other factors such as interference of absorbed intermediates, and a decrease of catalytic surface from the buildup of dirt, scum, gum, oil, and grease, especially if used in outdoor environments (Zhao and Yang 2003, Yu 2003). Thus, removal of these absorbed products can induce regeneration of photooxidation efficiencies.

Degeneration can be caused by accumulation of pollutants degradation products, which may adsorb to the surface. Further, the alkalinity of concrete allows NO_3^-, the final photodegradation product of NO_x, to easily adsorb (Beeldens 2008). The adsorption of these products can compete with the adsorption of pollutants and is a function of the time and concentration of pollutant degraded (Sleiman et al. 2009, Yu 2003). For example, photodegradation of low concentrations of toluene showed no degeneration, measured over the 48 hours, whereas photodegradation of higher concentrations showed deactivation and even a slight, yellowish color change, due to the accumulation of the absorbed species (Sleiman et al. 2009, Demeestere et al. 2008).

In addition, degeneration is likely to occur from common roadway contaminants, dirt, de-icing salt, and motor oil. Research shows that these typical roadway contaminants had a strong negative impact on the photocatalytic NO_x removal efficiency. Yet, each contaminant had a strong negative impact, the magnitude of the impact is dependent on the soilure type. Oil had the largest negative impact, which could be a result from competition between photocatalytic active sites between oil and NO_x. In fact, oil has the potential to photodegrade as well; however, further research is required to measure degradation efficiencies of motor oils. Dirt and dust had lower impacts, which could be a result from blocking the UV light. Furthermore, the coverage

level increased the negative effects of the roadway contaminants. In addition, there was interaction between the effect of these contaminants and other environmental factors such as flow and humidity (Dylla et al. 2011). As a result, methods for regeneration are being investigated.

Regeneration theories include washing the surface with water simulating rain, blowing air, or surface burning (Beeldens 2008, Zhao and Yang 2003). Comparisons between the regeneration methods quickly eliminated air as a solution. For example, the TiO_2 on roof tiles, when flushed with clean air, had no change on the photocatalytic properties; however, simulating natural rain showed 42% regeneration (Demeestere et al. 2008). To test the water theory, Beeldens removed photocatalytic blocks field tests to test in the lab. The blocks removed for laboratory tests, were removed over several different time periods to represent different exposure levels. The photocatalytic efficiencies were recorded before washing the surface and after washing. The results showed that additional washing could play a significant role in improving the photocatalytic efficiencies to maintain durability (Beeldens 2008, Hunger et al. 2008). In addition, water washing is also improves the photocatalytic efficiencies for samples covered in soil and deicing salt (Dylla et al. 2011).

When tested in the outdoor environments, rainfall has shown an effect in regenerating the photocatalytic activities, similar to those of lab washing. As a result, some recommended that washing be completed at least every two months during the dry seasons (Yu 2002). However, water washing or rain has not been effective in exposure to adhesives and water insoluble contaminants. As a result, using a degreasing agent may be beneficial. Exposure to different contaminates is dependent on location, thus exposure to these contaminates can be controlled by locality (Yu 2003). Other proposed solutions from Zhao and Yang included burning the surface

or water washing to eliminate intermediates and restore the active sites on the catalyst surface (Zhao and Yang 2003). Despite the debate, one thing upon which research agrees is that the durability of the catalytic activity must be proven for widespread implantation and possible regeneration techniques, i.e.) applying water wash must be evaluated if degeneration occurs (Berdahl and Akbari 2008).

2.3 ENVIRONMENTAL IMPACT ASSESSMENTS OF PHOTOCATALYTIC PAVEMENTS

To properly assess the environmental impact of a material, all mediums for exposure and all facets of a product's lifecycle must be evaluated to avoid unintended consequences (Davis and Thomas 2006). Thus a common methodology used to assess material environmental impact, is life cycle assessment defined by the ISO 14040 standard. Life cycle assessment is a cradle to grave analysis used to understand and evaluate the impact of a product. The "cradle-to-grave" analysis provides a thorough understanding of the product impact, such that areas for improvement are identified (ISO 14040). Yet it is environmentally focused, other social and economic impacts can be analyzed in conjunction.

Despite the benefits, there are several problems and obstacles facings the LCA's use for construction materials. The main obstacle is the amount of time and cost required to conduct a proper LCA. Likewise, to build and update material impact database inventories, to simplify impact assessment process, is tedious, costly, and time consuming (Huang et al. 2009, Treloar et al. 2004, Nishioka et al. 2005). As a result, alternative methods were developed to simplify the procedure.

The second obstacle is that the impact assessment requires the hazard or toxicity of the material wastes is known, which is often not known in the case of nanoparticles (Nishioka et al. 2005, Stern and McNeil 2008). The toxicity of nanoparticles is dependent on several

characteristics; particle size, surface area, metals/impurities, surface charge, morphology, crystallinity, and solubility in biological fluids, some of which are even difficult to measure (Isaacs 2009). In addition, unfortunately there is also an absence of exposure data for current nanomaterial containing products. This is widely reported as a significant research gap by nanoparticle toxicologists (Stern and McNeil 2008). Consequently, toxicology data for nanoparticles is still in its infancy. Therefore, there is limited understanding of the possible risks and consequences from using manufactured nanoparticles, required for the environmental impact assessment. Despite this, LCA is still acceptable to evaluate the environmental impact of nanocomposites. However, a comprehensive environmental assessment (CEA) is recommended to accompany the LCA results, identifying identify possible exposure pathways, methods to mitigate exposure, and potential exposure concentrations of a selected stressor (Curran 2009).

2.3.1 Life Cycle Assessment

There are four phases defined by the ISO 14040 standard: the goal and scope definition, the inventory phase, impact assessment phase and the interpretation phase (ISO 14040).

1. **Goal and scope definition**

   The goal and scope phase defines the boundary and level of detail necessary for the inventory phase. This includes the definition of the product under study, functional unit, system boundaries, allocation procedure, and LCI impact categories. When defining consideration to data requirements, availability, quality, and limitations should be noted. All assumptions made should also be noted. The functional unit is required to define what is being studied for comparison studies (ISO 14040).

   The system boundary defines what unit processes are included. It is recommended that all unit processes that are expected to impact the environment should

be included. Minor impacts can be ignored to reduce time and cost to study. Additional considerations of the system boundaries are the goals, application, data, and resources available for the study. It is important to clearly note the boundaries and any assumptions made because of their relationship to the result's degree of confidence (ISO 14040).

2. Inventory

The inventory phase collects data necessary to evaluate the material environmental impact throughout its life cycle. Inventory must be collected for the functional unit considering all of the processes defined within the scope of the system boundaries in order to estimate the consumption of resources and quantities of waste and emissions (Hassan 2009). Processes to consider are raw material acquisition, inputs and outputs from manufacturing, transportation, production and operation fuel use, maintenance, end of life options, and emissions to air, water, or soil (Huang et al. 2009, ISO 14040). Allocation of the data must also include any energy recovered through reuse and recycling procedures. Specifically related to pavement infrastructures, the usage lifespan has significant impacts on social, environmental, and economic factors, from congestion, pollution, and safety characteristics (Kendall et al. 2008). Furthermore, these characteristics interact. For example, added congestion can equate to increased pollution, which can be modeled by vehicle emission models such as MOBILE 6.2 in combination with traffic flow models (Zhang et a. 2008).

The inventory is not limited to environmental impacts, impacts such as noise, heat and odor, or cost can also be included (ISO 14040, Haas et al. 2006). Cost is most commonly analyzed using the Life Cycle Cost Analysis (LCCA). LCCA measures the economic benefits to compare competing alternative investments. It uses principles of

engineering economics such as present worth methods, which are already common to the pavement industry. Researchers in pavement LCCA are encouraging alternative methods such as rate-of-return or cost-effectiveness formulation for medium to long term paving projects (Haas et al. 2006).

3. Impact Assessment, LCIA (ISO 14044)

The life cycle impact assessment (LCIA) phase assesses the significance of the environmental impact for the product. The LCIA steps are: (1) select impact categories, (2) assign and classify inventory results, (3) calculate category indicator, (4) assign optional weight categories to calculate an overall assessment rating and analyze results. Normalization adjusts the calculation to the magnitude of the category to a relative reference value. By dividing the resulting indicator by its corresponding reference value, magnitude is transformed to a relative probable impact (ISO 14044). This provides a better understanding of the relative significance of the impact, rather than just indicating the total mass quantities of each pollutant released (Nishioka et al. 2005).

4. Interpretation

The final results provide a relative potential impact per functional unit; however, it is important to note that the results are not the actual impact. Thus, the results can be misleading; exposure in a densely populated area would have a greater health impact, which is not considered in the LCIA (Nishioka et al. 2005). In addition, there are uncertainties in the impact results that are difficult to quantify (Pennington et al. 2004). Some uncertainties are the prediction of the service life, expected maintenance, and disposal (Huang et al. 2009). Despite this, the results identify areas where the environmental impact is high and potential process improvements can be made.

Sensitivity analysis can be used to evaluate areas with high uncertainty. Understanding the environmental impacts of several products for a defined function, allows additional information to support consumer or users decisions (Treloar et al. 2004).

2.3.2 Simplifications of Environmental Impact Assessments

Tools have been developed to simplify the complexity of LCA procedures. Such examples are Building for Environmental and Economic Sustainability (BEES) developed by the EPA, PaLATE, the input-output method and hybrid LCAs (Horvath 2003, Kendall et al. 2008, Treloar et al. 2004). BEES is a database of different materials life cycle emissions and the associated impact on ten different categories. Yet simple to use, it is limited to conventional building materials (Kendall et al. 2008). PaLATE is a similar database program specifically for pavement materials. It proved useful for comparisons of rehabilitation projects (Horvath 2003). The input-output method uses linkages from national economic tables, which can be related to industry pollution records (Treloar et al. 2004). Yet these systems are fast and easy, case-specific data is unavailable. Hybrid LCA resolves these issues, by integrating the more reliable LCA data for important nodes with the simple input-output models used for less important nodes (Treloar et al. 2004).

2.3.3 Comprehensive Environmental Assessments

For materials where there is high uncertainty regarding the risks involved, a life cycle-risk assessment approach is used, known as "comprehensive environmental assessment" (CEA). CEA integrates life cycle approaches with risk assessments, such that potential exposures along the life cycle are identified for a given stressor (Curran 2009). Risk assessments seek to understand if a potential hazard exists, whether there will be exposure, and if there are methods to minimize exposure (Curran 2009). Thus, the objective of the CEA is all embracing,

attempting to answer many of the unresolved questions for nanoparticle toxicology (Curran 2009):

- Will there be exposure?
- Are some nanomaterials more likely to be exposed?
- How will they be exposed?
- At what concentrations will they be exposed?
- Are they hazardous?
- Are there methods to mitigate exposure or can they be controlled?

CEA is not a replacement for the LCA or an extension. While the LCA provides a quantitative impact assessment, the CEA is fundamentally qualitative. There are five different facets that make up the basic structure of a CEA studies: life cycle stages, environmental pathways, transport and transformation, exposure (biota and human), and effects. The first facet is the life cycle stage, which identifies all stages of a product's life cycle. For each stage, there is a potential that the stressor may be released over several environmental pathways – water, soil, air, and food chain. Thus, the second facet, environmental pathways, identifies emissions of the stressor to each of these environmental mediums. Once emitted to the medium, the stressor undergoes transport and transformation processes, identified by the transport and transformation facet. These transformation processes can produce secondary contaminants, which should not be neglected. The transportation process, determines the fate of the particles and thus the exposure potential, leading to the fourth facet, exposure (biota/human). Finally, the last facet, effects, attempts to describe the risks to the ecosystem and human health (Davis 2007). If possible, the effects are also described quantitatively relating the dose and toxic potency to potential exposure studies. However, due to the limited data availability, the quantitative risk characterization is

still in its infancy (Davis 2007, Davis and Thomas 2006). Still the results provided pertinent information to guide research needs.

2.3.3.1 TiO_2 Nanoparticle Potential for Hazard

Risks of nanoparticles are difficult to study, requiring a comprehensive research approach involving exposure assessments, toxicological studies and life cycle analysis (Sahu and Biswas 2010). TiO_2 nanoparticles in the environment have the potential to be ecotoxic and have negative biochemistry impacts. The toxicity of nanoparticles not only depends on the particle type and concentration but also on the physical characteristics of the nanoparticle such as size, surface area (Lovern et al. 2007). In addition to the individual nanoparticle toxicity, nanoparticles can facilitate in transferring of other known toxins. Specific to TiO_2 nanoparticles, the environmental risks are complicated by its photocatalytic ability. For example, TiO_2 nanoparticles can oxidize compounds to forms that are more bioavailable.

Initial toxicity studies of TiO_2 nanoparticles on rodents have shown that inhalation of nano- TiO_2 can cause pulmonary inflammation in rats and mice (Long et al. 2007, Zhu et al. 2010). Initial aquatic TiO_2 toxicity studies have shown toxicity at 2.0 ppm for Daphnia magna and 50% mortality at 5.5 ppm. Furthermore, the toxicity to Daphnia magna increases with UV-exposure and exposure duration (Hunde-Rinke and Simmons 2006, Zhu et al 2010). In longer exposure durations, the nano- TiO_2 accumulates in the body of Daphnia magna potentially decreasing the number of offspring at low concentrations of 0.2 mg/L, and higher mortality of Daphnia Magna at concentrations 1 and 5 mg/L (Zhu et al, 2010). As for algae (Desmodesmu subspicatus), the growth was impacted at concentrations as low as 12.5 mg/L and 50% mortality at 44 mg/L (Hund-Rinke and Simmons 2006). In fact, research has shown that the negative toxicity to algae is not a result of the light shading effect (the absorption of light from the opaque

nanoparticles aqueous suspension) but from aggregates formed, that entrapped the algal cells, thus, reducing the light available (Aruoja et al. 2009). Furthermore, under UV light nano- TiO_2 generates hydroxyl radicals, which aid to decomposition, of organic matter including algae (Aruoja et al. 2009). This reaction is well documented in decomposition studies of algae, bacteria, and nitrogen oxides (Aruoja et al. 2009, Fujishima et al. 2006).

Much is unknown about the influence of TiO_2 on the biochemistry of contaminants or nutrients, however, many risks have been identified. Nanoparticles can absorb or adsorb contaminants or nutrients facilitating the plant uptake of these contaminants or nutrients. This can have negative or positive impacts either accelerating nutrient transfer or introducing toxins (Nowack and Bucheli 2007). In addition, the photocatalytic oxidation reactions can transfer compounds to more bioavailable forms. For example, arsenic-III is oxidized to the more bioavailable form, arsenic-V, thus, increasing the arsenic uptake in aquatic fish such as carp (Luo et al. 2010). Similarly, TiO_2 photocatalytic oxidation reactions could resuspend nutrients and contaminants that had been recently absorbed into the organic matter making them more bioavailable (Luo et al. 2010). It was shown that under dark conditions, the release of phosphorous from the sediment is retarded and instead is absorbed to the TiO_2 nanoparticle's large surface area. Meanwhile under UV irradiation, the photodegradation of organic matter and photochemical transformation of iron enhanced the resuspension of the phosphorous from the sediment (Luo et al. 2010).

2.3.3.2 TiO_2 Nanoparticle Potential for Exposure

As photocatalytic technology advances, the release of TiO_2 nanoparticles into the environment is inevitable. With widespread use of photocatalytic materials and large scale manufacturing, TiO_2 nanoparticles will be introduced to the environment at new quantities and qualities (Wiesner[b] et

al. 2009). The exposure of these particles into the environment will be throughout the life cycle of the photocatalytic material including manufacturing, use, and disposal, all of which influences its overall impact on the environment and humans (Wiesner[a] et al. 2009, Meyer et al. 2009, Reijnders 2009).

The amount of these particles and to which medium is largely dependent on the engineered matrices in which they are incorporated (Wiesner[a] et al. 2009). For example, naturally dispersed nanoparticles are more likely to have greater potential for mobility than nanofillers for composite materials that require break down of the matrix to release particles (Meyer et al. 2009). In order to assess the risks of nanoparticles and characterize the hazards, an understanding the potential for exposure is essential (Stern and McNeil 2008). The challenge of obtaining nanoparticle exposure data is that nanoparticles are ubiquitous, formed naturally, incidentally or artificially. They are found in the atmosphere, oceans, soil, and on or in living organisms (Wiesner[b] et al. 2009, Guzman et al. 2006). The differences between the three types of occurring nanoparticles are blurred and it is questionable whether the types are distinguishable from another (Wiesner[b] et al. 2009).

Natural Nanoparticles

Natural nanoparticles are the building blocks and thus have been in existence since the beginning of life; however, their role is not quite understood (Wiesner[a] et al. 2009). Natural sources of TiO_2 are primarily from minerals such as Rutile (TiO_2) and Ilmenite ($FeTiO_3$) found as accessory minerals in plutonic and metamorphic rocks or as detrital minerals in beach sands (Kaegi et al. 2008). Furthermore, natural TiO_2 can be found in river water at the nanoscale (Wigginton et al. 2007). Over the years, ecosystems have adapted to "cohabitate" with these nanoparticles; however, many details are still unknown, such as what are environmental sinks, what is the mass

present in each environmental sink and what are the controlling environmental parameters determining these spatial and temporal distributions (Wiesner[b] et al. 2009).

Incidental Nanoparticles

Incidental nanoparticles are an unintended result of anthropogenic or natural sources. Anthropogenic sources include combustion exhaust (Brouwer et al. 2009), welding (Brouwer et al. 2004), and tire abrasion (Gustafsson et al. 2008, Dahl et al. 2006) whereas natural sources are nanoparticles generated in forest fires (Stern and McNeil 2008). As a result, incidental nanoparticles emerged after the industrial revolution from the increased combustion emissions in the atmosphere (Guzman et al. 2006). Near roadway microenvironments with heavy traffic, nanoparticle concentrations range from 5,000 to 3,000,000 particles/cm^3 (Stern and McNeil 2008). From tire abrasion alone, concentrations of incidental nanoparticles released are as high as 39 $\mu g/m^3$ at 70 km/hour (Gustafsson et al. 2008).

Artificial Nanoparticles

Artificial nanoparticles are manufactured nanoparticles engineered for various consumer products (Guzman et al. 2006, Stern and McNeil 2008). Currently, TiO_2 nanoparticles released are mostly manufactured for use in cosmetics, paints, coatings, and self-cleaning materials (Meyer et al. 2009). In fact, TiO_2 nanoparticles are of the highest concentration of engineered nanoparticles detected in Europe and the United States sludge-treated soil or sediment, or wastewater effluent, reflecting the worldwide production volume (Gottschalk et al. 2009). Furthermore, the amount of predicted TiO_2 nanoparticle concentrations released is expected to increase exponentially (Gottschalk et al. 2009).

2.4 PHOTOCATALYTIC PAVEMENTS ENVIRONMENTAL IMPACT TO AIR

The environmental wastes to air of photocatalytic pavements are identified during material production and construction, however; during the use of photocatalytic pavements there are many benefits that are difficult to quantify due to the numerous environmental impacts. As a result, current LCA studies assume an average photocatalytic reduction rate per pollutant when quantifying the potential benefits (Hassan 2009). In addition, knowledge of the exposure potential of TiO_2 nanoparticles to air is also limited with most research in the area of occupational exposure during nanoparticle synthesis.

2.4.1 Quantifying Benefits from Photocatalytic Pavements

Quantifying the potential benefits realized is essential but difficult. With focus on NO_x reduction, lab-simulations are the most common studies used to measure and compare the photocatalytic efficiencies of various materials. Lab experiments were first conducted to develop relationships of variables and determine feasibility of photooxidation. Since photocatalysis is a relatively new technology, standards did not exist until recently. As a result, lab experiments use a variety of setups. It was not until recently that standards, created in Japan, were adapted as ISOs.

Field tests and pilot tests have been conducted to validate the feasibility of application techniques, however analysis and conclusions are challenging (Beeldens 2006, Berdahl and Akbari 2008, Maggos et al. 2008). Field tests are expensive and difficult, due to the large area and the number of significant parameters that must be tested (i.e. sunlight exposure, wind, humidity, temperature, and pollution concentrations) (Berdahl and Akbari 2008, Maggos et al. 2008). Despite the challenge, field tests are important, as lab results typically overestimate the photocatalytic capabilities, by not properly representing the harsh environmental conditions (Maggos et al. 2008). Demonstration of the technology in real world environmental conditions is

essential. Furthermore, with these results, models may be used to translate lab efficiencies to field efficiencies such that these numerical simulations supplement additional field studies (Hunger et al. 2010, Beeldens 2008, Berdahl and Akbari 2008).

2.4.1.1 Measuring Photocatalytic Efficiencies from Lab Simulations

Until recently there has not been a standard available for measuring photocatalytic efficiencies. Consequently, photocatalytic oxidation experiments resulted in a variety of experimental setups (Beelden 2006, Hunger et al. 2008, Strini et al. 2005). Through grouping the experimental setups by calculation techniques, two developed methods are found to evaluate photocatalyst activity; each requires a slightly different experimental setup schematic. The first setup, being the most common and easiest, is the single-pass or open flow-through reactor. The photocatalytic activity is measured by its reduction efficiency, calculated by the decrease in concentration between the outlet and the inlet of the reactor as shown in Equation 2.11:

$$\eta = \frac{C_{in} - C_{out}}{C_{in}} \tag{2.11}$$

where, η is photocatalytic reduction efficiency, C_{in} is the inlet concentration, and C_{out} is the outlet concentration.

To avoid errors from material adsorption, the inlet concentration is often replaced with the equilibrium concentration before irradiation. This change is shown in Equation 2.12:

$$\eta = \frac{C_o^* - C^*}{C_o^*} \tag{2.12}$$

where, η is photocatalytic reduction efficiency, C_o^* is the initial equilibrium concentration (lights off) and C^* is the equilibrium concentration (lights on).

The advantage of this method is that a single pass of gas can flow at various concentrations. However, disadvantages to this method are the a) resulting errors at low

concentration levels due to the small difference, b) adsorption of pollutants on the reactor, and c) pollutant concentration over the substrate is not uniform (Strini et al. 2005). An example of the single-pass open flow reactor experiment setup is drawn in Figure 2.3 below, a diagram of the experimental setup used by Yu 2003.

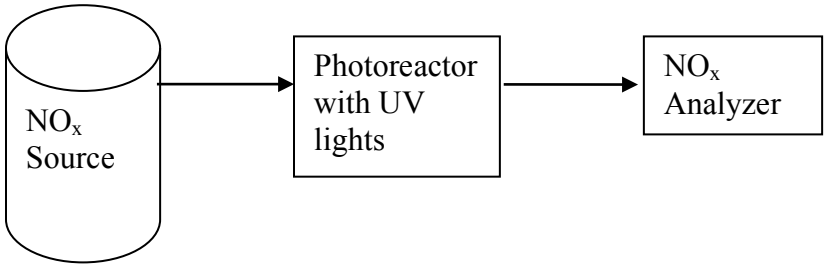

Figure 2.3 Single Pass Test Schematic (modified from Yu 2003).

The second, more complex approach uses recirculation, often referred to as the static method. The static method uses a closed circuit of air circulation to measure the abatement of NO_x over time (Strini et al. 2005, Hunger et al. 2008). This experimental setup follows the schematic shown in Figure 2.3 below. Unlike the single-pass open flow reactor setup, the recirculation setup evaluates the photodegradation half-life (Zorn et al. 2000). Regardless of the experimental setup, the photocatalytic byproducts may also be measured for verification of degradation results (Strini et al 2005).

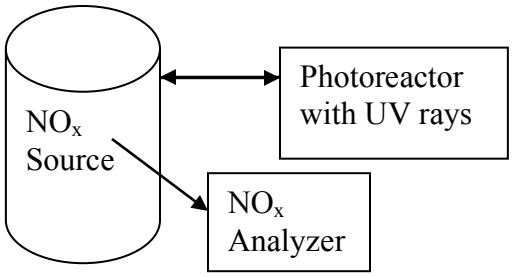

Figure 2.4 Recirculation Test Schematic (modified from Zorn et al. 2000)

Equipment

Both experimental setups require the following equipment: pollutant source, photoreactor, and pollutant analyzer. For the open, flow-through reactor, the pollutant source is usually a compressed gas cylinder of the particular pollutant compound of interest (Poon and Cheung 2007, Yu 2003). Since the pollutant is of such high concentrations compared to normal ambient concentrations, the pollutant is mixed with zero air, or air free of pollutants, for dilution. Mass flow controllers are used to control both the desired outlet concentration and flow rate to the photoreactor. Often a calibrator is used for this purpose. The photoreactor houses the substrate in a controlled environment for the reaction to occur. Then the analyzer measures the outlet stream from the controlled environment of the photoreactor. Humidifiers are also incorporated into the above schematics to test the impact of humidity (Hunger et al. 2008).

Photoreactor

The photoreactor is an enclosed environment housing the photocatalytic substrate. It has an inlet and outlet for sampling ports to monitor the pollution concentration. Typically, chambers are made of stainless steel or Pyrex glass with a rubber sealant to protect against pollution adsorption and leakage (Poon and Cheung 2007, Beeldens 2006, Hunger et al. 2008). However, in efforts to reduce costs, wooden photoreactors lined with aluminum foil have also been effective (Chen and Li 2007). Choosing materials compatible with the pollutant gas is essential, since many pollutants are highly reactive (EPA 1999). The size of the photoreactors ranged from as little of 1 mL to as large as 100 L volume capacity, where the space time, τ, is calculated as follows (Noguchi et al. 1998, Beeldens 2006, Queffeulou et al 2010):

$$\tau = \frac{V}{Q} \qquad (2.13)$$

Where V is the volume of air space in photoreactor and Q is the flow rate.

Smaller photoreactors were most likely to be made of glass cylinders or Pyrex tubing, whereas the larger photoreactors used a metal container (Noguchi et al. 1998, Beeldens 2006). The light source can either be inside or outside of the photoreactor, often dependent upon the photoreactor size. Light sources outside the photoreactor have the advantage of being able to modify the distance, such that the irradiance can be varied. In these setups, it is important to have a UV transparent glass top to allow passage of the UV rays (Nimlos et al. 1996, Noguchi et al. 1998, Piera et al. 2002, Kim and Hong 2002, Hunger et al. 2008). Light sources inside the photoreactor often heat the photoreactor. To mitigate the heat gains, fans were often used for cooling (Hunger et al. 2008).

Light Source

Since the reaction is dependent on the wavelength of the light, the light source chosen is important. Light sources vary from mercury lamps, germicidal lamps, solar lamps, UV-A lamps and metal halides, all with differently corresponding wavelengths. Fluorescent lamps typically have wavelengths of 420-650 nm with three irradiance peaks at 460, 560, and 600 nm, whereas UV-A emits wavelengths within 300-400 nm with a maximum irradiance peak at 345 nm (Hunger et al. 2008). It is recommended that fluorescent lamps be used for doped particles while UV-A sources (i.e. fluorescent black lights) for undoped particles (Hunger et al. 2008, Beeldens 2006). With phosphor coatings, black lights emit only UV-A light, while the harmful, short-wave UV-B and UV-C lights are absorbed (Fujishima and Zhang 2006). Maximum wavelengths emitted for black lights are generally smaller, near 355 nm (Yu 2003). The wavelength required for TiO_2 irradiation is between 300 to 365 nm, thus UV-A sources are recommended. The sun emits 1-2 mW/cm^2 in wavelengths below 350-400 nm (Zhao and Yang 2003). Therefore, the recommended irradiance is near 1 mW/cm^2, which can be measured by a UV-A radiometer

(Zhao and Yang 2003, Kim and Hong 2002, Piera et al. 2002, Sopyan et al. 1996, Hunger et al. 2008). To eliminate heat from lights, fans can be used for additional cooling or the distance between the lights and the photoreactor can be increased to decrease the heating effect (Hunger et al. 2008).

Humidity Controller

The humidity may be controlled in many ways. For simplicity, many experiments used the natural, room relative humidity. Meanwhile, to increase the humidity, air is passed through either a water bath or a humidifier (Dalton et al. 2002, Sleiman et al. 2009). A humidity sensor is placed in the photoreactor to note and record the relative humidity (Sleiman et al. 2009).

Gas Analyzer

The gas analyzer is determinant on pollutant type and concentration. The sampling intervals can either be continuous or discrete, depending on the gas analysis techniques available. For NO_x portable analyzers are available for continuous concentration monitoring at ambient air conditions (Yu 2003). The approved technique for EPA standards in NO_x ambient air testing is chemiluminescence (EPA 1999).

Testing Standards for Performance of Photocatalytic Materials

More current research follows the experimental setup standards first defined by the Japanese, the JIS TR Z 0018 "Photocatalytic materials-Air purification test procedure" standards. The creation of the JIS TR Z 0018 is the first part of many standards to be developed for testing photocatalytic products. The Japanese standard was adapted for the ISO TC 206/SC N, "Fine ceramics (advanced ceramics, advanced technical ceramics) – Test method for air purification performance of photocatalytic materials – Part 1: Removal of nitric oxide" (Beeldens 2006, JIS

2004). The method is meant to be reproducible for a variety of materials, such as building materials and road construction materials (JIS 2004).

The standard specifies a procedure for evaluating the photocatalytic performance in removal of nitrogen oxides, yet photocatalytic oxidation can occur for a variety of pollutants such as dyes, organics, and inorganics. NO is regarded as the ideal model pollutant for determination of guidelines and testing standards. This is because dyes tend to exhibit limited decomposition without catalysts. VOCs are more resistant to UV degradation, decomposing to CO_2 and H_2O. VOCs are the ideal model pollutant for indoor situations; however, for outside applications -especially in concrete- the value of degradation measured can be inflated, due to the naturally occurring carbonation of concrete. In addition, VOCs often represent toxic chemicals, which are difficult to handle (Hunger et al. 2008).

The experimental setup following the JIS and ISO standards is the single pass flow-through method, previously described and illustrated in Figure 2.2 (Beeldens 2008). The photoreactor size is determined such that it is 3 times the length of the sample and at least 5 mm of air space is provided above the sample. To avoid turbulence in the airflow, the test specimen should be centered in the photoreactor. Fluorescent lamps with wavelengths between 300-400 nm and xenon lamps with optical filters to block the lower radiation are acceptable light sources. The light source shall be placed outside of the photoreactor at an adjustable distance to obtain an irradiance of $10W/m^2$ measured by a UV-A photometer. Therefore, the window must not absorb light longer than 300 nm, thus quartz or borosilicate glass is recommended. A chemiluminescent NO_x analyzer measures the concentration of the pollutant. Proper calibration steps must be followed in accordance to the specified standards (JIS 2004).

The test piece shall be pretreated and stored in an airtight container if testing does not immediately proceed. The pretreatment process entails irradiation of the test piece with UV light for at least five hours to remove any organic matter using an irradiance of $10W/m^2$ or higher. Then the material is washed in purified water for more than two hours and air dried at room temperature, until a constant weight is achieved (JIS 2004).

To begin the NO_x removal test, the specimen first shall be exposed to pollutants under dark conditions for at least 30 minutes to determine the adsorption rate. The flow rate of the inlet gases shall be 3 L/min with a 1.0-ppm concentration of NO at 50% humidity and room temperature. The second stage, with the light source on, may start as soon as the outlet concentration equals the inlet concentration. The NO and NO_2 concentrations shall be continuously monitored for at least five hours under irradiation. After five hours, photoirradiation may be stopped and the gas, supply is changed to the zero-calibrated gas until the concentration of NO_x is zero (JIS 2004).

Since NO_x removal results primarily in nitrate ion and nitrite ion, washing with water is the suggested removal technique to restore the photocatalytic efficiencies. After elution, the recovery from washing is calculated. To wash the sample, the material is immersed in purified water for one hour and the volume is recorded. The procedure is repeated, using a new sample of purified water of the same volume as the first. The samples of the water after washing waken quantify the concentration of nitrates and the amount of NO_x eluted from the test piece (JIS 2004).

After the test, the net amount of NO_x (mol) removed is calculated. The net amount of NO_x removed is the summation of the total NO adsorbed and the amount of NO removed, minus any NO_2 that is formed and the amount desorbed. All of these can be calculated from a typical

graph of concentration versus experiment time. Equation details for each amount are provided in the JIS standards. Standard equations, a diagram of the equipment setup, and a typical graph are provided by the standards as well (JIS 2004).

2.4.1.2 Measuring Photocatalytic Pavement Efficiencies from Field Studies

To measure the pollution reduction of NO_x continuously in the field often presents a challenge, due to a large number of influencing parameters, time, and costs. As a result, researchers have attempted to simplify field tests by employing indirect techniques to measure photocatalytic degradation or controlling some of the variables. However, according to Hunger et al. 2010, none of the current field studies demonstrated a reduction in pollution exclusively resulting from the photocatalytic pavement layer (Hunger et al. 2010).

Indirect Measurements of Photodegradation in Field Studies

For example, indirect techniques can be used to measure the photocatalytic degradation of NO_x by measuring the NO_3^- deposited on the surface. Nitrates, water-soluble, are washed from the surface with water and measured similar to the JIS procedure (Beeldens 2008). The amount of degradation can be indirectly calculated using the amount of NO_3^- collected using the stoichiometry given the following equations:

$$NO + \bullet OH \xrightarrow{hv,TiO_2} NO_2 + H^+ \quad (2.14)$$

$$NO_2 + \bullet OH \xrightarrow{hv,TiO_2} NO_3^- + H^+ \quad (2.15)$$

Nevertheless, results recorded in the field were difficult to develop any photocatalytic reduction relationships due to the numerous impacting factors (i.e. traffic activity, wind, light, and humidity making it comparison difficult) (Beeldens 2008).

Controlling Variables in Order to Measure Photodegradation in Field Studies

In efforts to control environmental factors, artificial street canyons were developed and tested in a France field study. One set of panels was treated with a photocatalytic mortar, which was compared to the control set with no coating. The difference, between the coated and control average concentrations, was used to calculate the photocatalytic degradation of NO_x (Maggos et al. 2008). In this experiment, the gas source emissions -SO_2, CO, CO_2, VOCs and NO_x- and flow were controlled and measured. The results concluded that NO_x could be reduced ranging from 36% to 82% dependent upon the pollution emissions, wind direction, and wind speed (Maggos et al. 2008).

Assessing Degeneration and Durability of Photocatalytic Coating in Field Studies

To test the durability of photocatalytic pavements under field conditions, a pilot study in Antwerp, France used removable blocks. This allowed the blocks to be removed over several different time periods. Since photocatalytic efficiencies can be reduced from traffic induced abrasion, wear, and absorbed contaminants, the photocatalytic efficiencies were recorded before and after washing the surface with water (Beeldens 2008). Thus, the degeneration of photocatalytic efficiencies from adsorbed compounds is distinguished from degeneration from the traffic induced abrasion and wear of the photocatalytic layer. The degeneration of the photocatalytic efficiencies from adsorbed compounds is the difference of photocatalytic efficiencies before and after washing the adsorbed compounds from the surface. The photocatalytic degeneration from traffic induced abrasion and wear is the difference of the photocatalytic efficiencies after washing over time. Results suggest that after one year of testing the degeneration of the photocatalytic efficiency, from traffic induced abrasion and wear, is 20% (Beeldens 2008).

2.4.2.3 Photocatalytic Pavement Model Approaches

Few models exist to describe the performance of photocatalytic pavement materials reduction of NO_x. Currently, only reaction kinetic models have been used to describe photocatalytic mortar pavements reaction rate, using the Langmuir-Hinshelwood (L-H) model. Environmental factors impacting the photocatalytic reaction rate, including relative humidity, temperature, and flow are incorporated into the model using regression studies (Bengtsson and Castellote 2010).

For example, using Equation 2.5, the reaction rates for NO photodegradation is described as follows:

$$r_{NO} = \frac{k*KdC_{NO}}{1+KdC_{NO}} \quad (2.16)$$

where,

k = L-H reaction rate constant;
Kd = the L-H adsorption equilibrium constant; and
C_{NO} = the concentration of NO.

To solve for the L-H reaction rate constant and the L-H adsorption equilibrium constant, lab experiments are used. For a single pass experimental setup, assuming plug flow in the photoreactor, the mass balance can be written as such:

$$r_{NO} = -v_{air} * \frac{dC_{NO}}{dx} = \frac{k*KdC_{NO}}{1+KdC_{NO}} \quad (2.17)$$

where,

v_{air} = gas velocity; and
$\frac{dC}{dx}$ = rate of change of concentration per horizontal distance.

Integrating the mass balance, Equation 2.17, over the length of the photoreactor with the following boundary conditions shown in Equation 2.18, results in the following linear equation (Equation 2.19).

$$C_{NO} = C_{NO,in} \tag{2.18}$$

$$\frac{\ln\left(\frac{C_{NO,in}}{C_{NO,out}}\right)}{C_{NO,in}-C_{NO,out}} = \frac{kKd\left(\frac{V}{Q}\right)}{C_{NO,in}-C_{NO,out}} - Kd \tag{2.19}$$

where,

$C_{NO,in}$ = inlet concentration;
$C_{NO,out}$ = outlet concentration;
Q = flow rate;
V = volume of the photoreactor; and
L = Length of the photoreactor.

Thus, from linear regression analysis, k and Kd can be observed from the graph of ln(Cin/Cout)/(Cin-Cout) versus 1/(Cin-Cout). Where Kd is the y-intercept and k is Q/mKdV, where m is the slope of the line. Further, the linear relationship of integral rate law analysis is evidence that the reaction is a gas-solid reaction following the L-H mechanism, rather than a gas-phase reaction (Sleiman et al. 2009).

To account for the impact of humidity, competition between the two pollutants for adsorption exists, thus the equation takes the form as Equation 2.20 previously noted (Hunger et al. 2010).

$$r_{NO} = \frac{kK_{NO}C_{NO}}{1+K_{NO}C_{NO}+K_{H2O}C_{H2O}} \tag{2.20}$$

Despite knowledge of this relationship, researchers found that the results did not follow this model. Instead, statistic regression techniques were used to incorporate the impact of relative

humidity more adequately (Hunger et al. 2010, Bengtsson and Castellote 2010). In doing so, a parametric study of photocatalytic mortars illustrated that the relative humidity impacts both the L-H reaction rate and L-H adsorption equilibrium constant. As the humidity increases, there is a significant reduction in the L-H reaction rate, whereas the L-H adsorption equilibrium constant increases to an optimum at 40% relative humidity before it decreases. Similarly, the irradiance and temperature are also incorporated into the model using regression. The irradiance was found to only impact the L-H reaction rate whereas the temperature was found to impact both the L-H adsorption constant and reaction rate. Using multifactorial regression, all of the environmental parameters were incorporated into one model to predict pavement photocatalytic NO oxidation reaction rate (Bengtsson and Castellote 2010).

This final model is valid when the reaction is the limiting transfer mode, which is the case for high flow and high concentrations (Sleiman et al. 2009, Salvado-estivill et al. 2007, Taghipour and Mohseni 2005). In the case that it is mass transfer limiting, the NO mass balance would be as follows:

$$-\dot{m} = \frac{-ShD}{2h} C_{No} \tag{2.21}$$

where,

Sh = Sherwood's number the ratio of convective to diffusive mass transfer;
D = Diffusion coefficient of NO in air (estimated by kinematic viscosity of air $\nu = 1.51 * 10^{-5}$ m^2/s); and
h = height of the air flow over the photocatalytic surface.

By integrating over the photoreactor, using the same boundary conditions previously defined (Equation 2.18), the percent NO_x reduced is as follows:

$$1 - \frac{C_{NO,out}}{C_{NO,in}} = 1 - e^{\frac{-ShDL}{2v_{air}h^2}} \tag{2.22}$$

To understand the significance of the photocatalytic reduction, the reaction rate may be incorporated into air pollution dispersion models for roadway microenvironments. Despite this, to the author's knowledge, no such model exists. Rather, the only known model developed incorporated a deposition flux to describe the reaction rate into 3-D computational fluid dynamics model. Further, this model simulated the photocatalytic degradation of NO_x for a pilot street cannon containing TiO_2-mortar panels rather than photocatalytic pavements. This model used numerical modeling techniques using MIMO, an analytical microscale model, specific to air motion near building structures (Ehrhard et al 2000). Numerical solutions of Reynolds Average Navier-Stokes (RANS) equations for atmospheric fluid are used to simulate air concentrations per time and location (San et al. 2004). The conservation of mass, momentum, energy and passive pollutants are numerically solved using the finite volume discretization method. The photocatalytic degradation of NO_x was simplified and incorporated into the model using a "deposition" module to approximate removal flux, F_d as follows (Moussiopoulos et al. 2008):

$$F_d = U_{dep} * C_{wall\ average} \tag{2.23}$$

Where U_{dep} is deposition velocity (m/s) is a material property calculated from lab experiments, and $C_{wall\ average}$ is the average concentration of NO_x on the wall. Comparison between the simulated results and field results concluded that this model adequately described the photocatalytic NO_x reduction (Moussiopoulos et al. 2008). However, the U_{dep}, typically not used to describe the photocatalytic degradation rate, does not incorporate environmental factors that influence the reaction rate such as humidity, irradiance, and temperature determined by kinetic models.

Extensive research has been conducted on TiO_2 photocatalytic reactor models, which have incorporated reaction kinetic modeling with pollutant dispersion models such as

computational fluid dynamics (Duran et al. 2011, Salvado-Estivill et al. 2007). These models were useful to predict the concentration of pollutants and understand the significance of various transport mechanism when the reactor design is modified (Sharma et al. 2004). Despite this, incorporating reaction kinetic models into roadway dispersion models for photocatalytic pavements is limited.

There are several roadway microenvironments pollution dispersion models such as Gaussian plume dispersion model, computational fluid dynamics (CFD), atmospheric box model, and statistical models such as source apportionment (Lin and Yu 2008). Dispersions models are described as either, Lagrangian or Eulerian depending on the frame of reference of the transport equations. The Eulerian models relate the transport to coordinates working from a fixed grid while Lagrangian models follow a volume or parcel of air moving downwind, modeling the pollutant as it moves (Sharma et al. 2004). A brief description of these models and the associated advantages and disadvantages are presented in Table 2.1.

Table 2.1 Comparison of Air Dispersion Models

Model	Description	Advantages	Disadvantages
Gaussian Plume Dispersion Models	Models dispersion by bell-shaped normal standard distribution	Well developed, software available	Does not include reaction, unsuitable for urban conditions
Computational Fluid Dynamic Models	Models dispersion by fluid flow	Detailed, 3D fluid simulations, suitable for urban environments	Long processing time, requires expert knowledge, difficult to include reactions, uncertainties still exist
Statistical Models	Models concentration from receptor specific parameters	Simple, does not require expert knowledge,	Requires a large amount of historical data, receptor specific
Box Models	Models dispersion by mass balance	Simple for complex reactions	Assumes well mixed

For transportation pollution modeling Gaussian plume models are the most common (Bhatt 2005). The Gaussian plume model assumes that the dispersion is modeled as a bell-shape normal standard distribution, which is a function of the horizontal and vertical dispersion parameters (Lin and Yu 2008). The model is initially for a single puff point source, however, it is modified for continuous sources, by a summation of a series of single puffs, and for line and area sources. For traffic pollution, the Gaussian line source model is used to predict pollutant concentrations for identified receptors. The most prominent models created for traffic pollution modeling is the CALINE series developed by the California department of transportation. There are several versions available including CAL3QHC, CALINE3, and the latest, CALINE4 (Chen et al. 2008). Input requirements included, traffic volume, emission factors, roadway geometry, wind speed and direction, ambient air temperature, mixing height, atmospheric stability class, and receptor coordinate (Benson 1984). Carbon dioxide, nitrogen dioxide, and particulate matter all can be modeled, however NO_2 analysis requires additional inputs and reaction calculations (Chen et al. 2008, Benson 1984). Further background behind this model is described elsewhere (Benson 1984, Bhatt 2005).

Computational fluid dynamics is a physical approach to model pollutant dispersion, predominantly used to understand the flow through complex systems (Sharma et al. 2004, Vardoulakis et al. 2003). For this reason, they are primarily used for modeling pollutant dispersion in street canyons of urban areas (Vardoulakis et al. 2003). Since they do not include photochemical reactions, simplified photochemical algorithms must be combined with CFD models. In addition, the computational power required to solve the fluid equations limit this modeling technique to micro-scale studies (Holmes and Morawska 2006, Vardoulakis et al. 2003). However, with improving technology, CFD techniques are becoming more popular, since

they provide detailed flow and concentration profiles for complex urban areas (Vardoulakis et al. 2003). ARIA Local, MISKAM, and MIMO are CFD models developed for local transportation air pollution modeling (Moussiopoulos et al. 2008, Holmes and Morawksa 2006). It is still uncertain the applicability and accuracy of results of CFD models for vehicular pollution dispersion models (Sharma et al. 2004).

One drawback to the Gaussian plume models and to some extent CFD models is that generally chemical and physical mechanisms are neglected or difficult to implement. To include more detailed chemical reaction schemes, box models are advantageous. Based on the fundamental theory of mass conservation for a defined a volume, various transport and transformation mechanisms are simple to incorporate into the model (Lin and Yu 2008, Holmes and Morawska 2006). The defined volume (the box) is typically assumed as a well-mixed uniform concentration (Holmes and Morawska 2006). This is the major drawback to box models; thus, they are not as effective for point sources or local environmental studies. Despite this, they are particularly effective for modeling area pollution sources and effective to identify the significant transport and transformation mechanism (Holmes and Morawska 2006, Cheng et al. 2006). STREET-SRI, AURORA, and CPB are box models developed for transportation air pollution modeling (Cheng et al. 2006).

Statistical approaches include regression, multi-regression, and artificial neural networks. Estimates are calculated by the statistical relationship to various factors collected at a particular receptor (Sharma et al. 2004). Source apportionment models, which attempt to identify different sources contribution to the pollution at a particular receptor, use many of these statistical methods such as principal component analysis (PCA) and multilinear regression (Vallius et al. 2008). These models are important to identify sources contribution to human exposure for air

pollution policy and regulation to mitigate associated risks (Zeng et al. 2010). These models are easy to use but they are receptors or location specific, require large amounts of historical data, and do not identify the significance of various physical and chemical processes (Sharma et al. 2004).

2.4.3 Nanoparticles Released to Air

Yet, nanoscale TiO_2 is one of the most manufactured and greatest used of all nanoparticles, few studies have shown the release of nano- TiO_2 into the natural environment (Kaegi et al. 2008). Uses of TiO_2 for photocatalytic cements for both building façades and pavements have the potential of releasing TiO_2 due to abrasion. For example, a durability study on TiO_2 photocatalytic pavements illustrate the potential of TiO_2 particle loss due to abrasion from repeated traffic (Hassan et al. 2010). Yet this has not been quantified for photocatalytic pavements, it has been quantified for photocatalytic coatings on wood, polymers, and tiles. Using a scanning mobility particle sizer (SMPS), this study concluded that tiles had the highest potential to release nano- TiO_2, 22 particles/cm^3 to air, thus concentration increased with exposure to UV-light (Hsu and Chein 2007). Additional studies demonstrate TiO_2 nanoparticles are potentially released during synthesis (Methner et al. 2010[b]).

Currently, no known standard exists for measuring nanoparticles emissions to air. Various methodologies on studying potential exposure pathways have been proposed. The most comprehensive is the Nanotechnology Emission Assessment Technique (NEAT) developed by the National Institute for Occupational Safety and Health (NIOSH) for aerosol nanoparticle exposure studies (Methner[a] et al. 2010). In summary, most investigations advise nanoparticles to be characterized by particle size, surface area, particle count, elemental composition, and surface morphology (Methner[a] et al. 2010, Brouwer et al. 2009). In order to account for natural and

incidental nanoparticles, background concentrations are first quantified. While, nanoparticles released are shown if there is an increase of nanoparticles compared to background concentrations resulting from various activities (Methner[a] et al. 2010, Brouwer et al. 2009).

In the case of aerosolized nanomaterials, the scanning mobility particle sizer (SMPS) can provide real-time, on-line nanoparticles size distributions. Real-time size measurements can be made from 2.5-1000 nm. The SMPS system includes an electrostatic classifier, a differential mobility analyzer (DMA), and a condensation particle counter (CPC) (Sahu and Biswas 2010). The electrostatic classifier combined with the differential mobility analyzer collects, and separates the particles by size before the sample is passed through the particle counter to give the size distribution. Recent studies employing SMPS equipment have been used by many disciplines to characterize incidental nanoparticles from processes including combustion or welding (Brouwer et al. 2004) and to characterize nanoparticles released during synthesis/manufacturing (Sahu and Biswas 2010, Methner[b] et al. 2010), or nanocomposite abrasion (Hsu 2007). The nanoparticle sizes recorded can be used to calculate particle surface areas (Methner et al. 2010[a]).

For nanoparticle counting, both the condensation particle counter and the optical particle counter are recommended by NEAT to obtain accurate readings spanning the whole nanoparticle size ranges. The optical condensation particle counters provide precise counts of particles between 300 nm to 25 microns for various bin sizes (TSI 2010). For sizes smaller than 300 nm, the particles are no longer detectable by optical scattering methodologies. Therefore, the condensation particle counter is used in which a fluid, applied to the nanoparticles, grows them to optical detectable sizes for real time counts (TSI 2010). As a result, NEAT recommends that for nanoparticles less than 300 nm the condensation particle counter is used whereas for particles

greater than 1 micron the optical particle counter (TSI 2010, Methner [a] et al. 2010). For particles between 300 nm and 1 micron NEAT recommends the use of both methods (Methner [a] et al. 2010). In addition to NIOSH studies, this equipment have been used for studies related to nanoparticle fate and transport, vehicle and combustion emissions, tire pavement abrasion emissions (Dahl et al. 2006), surface coating sanding (Gohler et al. 2010), and nanoparticle synthesis (Methner[a] et al. 2010).

Lastly, for morphology and shape characterization, nanoparticles must be collected for offline analysis. To do this an electrostatic precipitator nanoparticle sampler can be used. This ensures high collection efficiencies for various substrates such as TEM grids, or SEM substrates (Dahl et al. 2006, Brouwer et al. 2009, Methner[a] et al. 2010). For more controlled particles size assurance, this equipment may be coupled downstream from an electrostatic classifier that filters samples by defined sizes between 2 nm to 1,000 nm (TSI 2010). Otherwise care needs to be taken to ensure grids are not overloaded (Methner[a] et al. 2010).

2.5 ENVIRONMENTAL IMPACT TO WATER

The environmental wastes to water from production and construction operations of photocatalytic pavements are well known. For example, during synthesis of TiO_2 water discharges wastes such as chlorine and heavy metals (Battelle Columbus and Lockheed-Martin Environmental 1996, Hassan 2009). In fact, there are many LCA studies on TiO_2 synthesis, including a study specific to TiO_2 nanoparticles (Grubb and Bakshi 2010). However, during the use of photocatalytic pavements there are many benefits and disadvantages that are difficult to quantify. For example, TiO_2 in water can degrade can naphthalene and 4-chlorophenol (Pramauro et al. 1998, Watts and Cooper 2008). Furthermore, potential trade-offs include the adverse environmental impact from photodegradation intermediates and products, or TiO_2

nanoparticles released to the environment through water and transported to other mediums such as soil.

2.5.1 Nitrate Analysis

For the photodegradation of NO_x, nitrate is the product. Excess nitrate in the environment may cause eutrophication. Few studies have mentioned the amount of nitrates being released to water only stating that the amount released is 10 times inferior to the original pollutant level (PICADA 2001). One study shows that between 70-97% of the theoretical nitrates are removed from glass substrates after being immersed in deionized water for one hour (Martinez et al. 2011). However, it is theorized but not confirmed that the nitrates, HNO_3, react with the calcium hydrate $Ca(OH)_2$ in the concrete cement to neutralize to $Ca(NO_3)_2$ and H_2O (Li and Qian 2009).

2.5.2 Nanoparticles in Water

Currently, no studies exist illustrating the exposure potential of TiO_2 particles released to water from photocatalytic pavements. However, one study by Kaegi et al. 2008, illustrated the release of synthetic TiO_2 nanoparticles, 3.5×10^8 particles/L, from exterior paint applications to the aquatic environments. This study was the first that showed significant amounts of manufactured TiO_2 released into the aquatic systems. TiO_2 was released first as agglomerates in direct façade storm water runoff and was disaggregated as it reached the inlet of the urban runoff storm water systems. Researchers suggest that it is plausible that the organic matrix was either dissolved or degraded during its transport (Kaegi et al., 2009).

To identify nanoparticles released to water, offline sampling is most common. Water samples can be collected and particles filtered by size for TEM with EDX, SEM with EDX, inductive coupled plasma atomic emission spectrometry (ICP-AES) and mass spectrometry (ICP-MS). TEM with EDX can identify elemental composition as well as characterize the size.

SEM can characterize the morphology (Kaegi et al., 2009). For quantitative concentration results, ICP-MS can be used to measure mass concentration for metals at ppt concentrations whereas ICP-AES higher concentrations in ppb ranges.

2.6 ENVIRONMENTAL IMPACT TO SOIL

The environmental wastes to soil from photocatalytic pavements production and construction are also available in the previously mentioned LCA studies. However, during the use of photocatalytic pavements TiO_2 nanoparticles in may be released to the soil.

2.6.1 Nanoparticles in Soils

Currently, no studies exist illustrating the exposure potential of TiO_2 particles released to the soil from photocatalytic pavements. Due to low quantities and their tendency to aggregate, nanoparticles in soil are difficult to characterize. Efforts to separate and isolate nanoparticles in soil includes, wetting-drying and freezing-thawing, prolonged shaking, ultrasonication, centrifugation, cross-flow filtration, and chemical pretreatment. If separated, nanoparticles can be characterized by conventional offline analytical methods such as scanning electron microscopy, TEM, EDS, and X-ray diffraction. For qualitative results, nanoparticles can be suspended in water for ICP-AES (Theng and Yuan 2008).

2.7 REFERENCES

AASHTO T 320, "Determining the Permanent Shear Strain and Stiffness of Asphalt Mixtures Using the Superpave Shear Tester (SST)." American Association of State and Highway Transportation Officials, Washington D.C.

Anpo, M., and Takeuchi, M. (2003). "The design and development of highly reactive titanium oxide photocatalysts operating under visible light irradiation." Journal of Catalysis, 216, 505-516.

Ao, C.H., Lee, S.C., Yu, J.Z., and Xu, J.H. (2004). "Photodegradation of formaldehyde by photocatalyst TiO_2: Dffects on the presences of NO, SO_2 and VOCs." Applied Catalysis B: Environmental, 54, 41-50.

Ao, C.H., Lee, S.C., Mak, C.L., and Chan, L.Y. (2002). “Photodegradation of volatile organic compounds (VOCs).” Applied Catalysis B: Environmental, 42, 119-129.

Aruoja, V., Dubourguier, H.-C., Kasemets, K. and Kahru, A. (2009). "Toxicity of nanoparticles of CuO, ZnO and TiO_2 to microalgae Pseudokirchneriella subcapitata." Science of the Total Environment, 407(4), 1461-1468.

ASTM Standard C944, (2005) "Test Method for Abrasion Resistance of Concrete or Mortar Surfaces by the Rotating-Cutter Method." ASTM International, West Conshohocken, PA.

Baldauf, R., Thoma, E., Hays, M., Shores, R., Kinsey, J., Gullett, B., Kimbrough, S., Isakov, V., Long, T., Snow, R., Khlystov, A., Weinstein, J., Chen, F., Seila, R., Olson, D., Gilmour, I., Cho, S., Watkins, N., Rowley, P., and Bang, J. (2008). “Traffic and meteorological impacts on near-road air quality: Summary of methods and trends from the Raleigh near-road study.” Air & Waste Management Association, 58, 865-878.

Baldauf, R., Watkins, N., Heist, D., Bailey, C., Rowley, P., and Shores, R. (2009). “Near-road air quality monitoring: Factors affecting network design and interpretation of data.” Air Qual Atmos Health, 2, 1-9.

Ballari, M.M., Hunger, M., Husken, G., and Brouwers, H.J.H.. (2010). “NO_x photocatalytic degradation employing concrete pavement containing titanium dioxide.” Applied Catalysis B: Environmental, 95, 245-254.

Battelle Columbus and Lockheed-Martin Environmental (1996). “Life cycle assessment for chemical agent resistant coatings.” EPA 68-C4-0020, 1-254.

Beeldens, A. (2006) “An environmental friendly solution for air purification and self-cleaning effect: the application of TiO_2 as photocatalyst in concrete.” Belgian Road Research Centre. Proceedings of Transport Research Arena, Europe - TRA, Göteborg, Sweden, June, 2006.

Beeldens, A. (2008). “Air purification by pavement blocks: final results of the research at the BRRC.” Transport Research Arena Europe, Ljubljana.

Bengtsson, N. and Castellote, M. (2010). “Photocatalytic activity for NO degradation by construction materials: parametric study and multivariable correlations.” Journal of Advance Oxidation Technologies, 13(3), 341-349.

Benson, P. (1984). “CALINE4 – A dispersion model for predicting air pollutant concentrations near roadways.” 57328-604167. Office of Transportation Laboratory, California Department of Transportation, Sacramento, CA.

Berdahl, P. and Akbari, H. (2008). Evaluation of Titanium Dioxide as a Photocatalyst for Removing Air Pollutants. California Energy Commission, PIER Energy-Related Environmental Research Program. CEC-500-2007-112.

Berkowicz, R. Hertel, Winther, M., and Ketzel, M. (2006). "Traffic pollution modeling and emission data" Environmental Modelling & Software, 21, 454-460.

Bhatt, H. (2005). Determination of Safe Buffer Width of Roadway to Protect Human Health from Harmful NO_x Exposure. Master Thesis, University of Texas at Arlington.

Brouwer, D. (2010). "Exposure to manufactured nanoparticles in different workplaces." Toxicology, 269, 120-127.

Brouwer, D. Duuren-Stuurman, B., Berges, M., Jankowska, E., Bard, and Mark, D. (2009). "From workplace air measurement results toward estimates of exposure? Development of a strategy to assess exposure to manufactured nano-objects." Journal Nanoparticle Research, 11, 1867-1881.

Brouwer, D.H., Gijsbers, J.H.J, and Lurvink, M.W.M., (2004). "Personal exposure to ultrafine particles in the workplace: Exploring sampling techniques and strategies." Annals of Occupational Hygiene, 48(5), 439-453.

Canestrari, F., Ferrotti, G., Partl, M.N. and Santagata, E. (2005). "Advanced testing and characterization of interlayer shear resistance." Transportation Research Record. NO. 1929, 69-78.

Cassar, L. (2004). "Photocatalysis of cementitious materials: clean buildings and clean air", MRS Bulletin, May 2004, 1-4.

Cassar, L. (2005). "Nanotechnology and photocatalysis in cementitious materials." NICOM'2. Bilbao, 1-7.

Cassar, L.; Pepe, C.; Tognon, G.; Guerrini, G.L.; Amadelli, R. (2003). "White cement for architectural concrete, possessing photocatalytic properties." 11th Congress on the Chemistry of Cement, Durban.

Chen, D. H. and Li, K., (2007). Photocatalytic Coating on Road Pavements/Structures for NO_x Abatement. 26 January 2007. Texas Air Research Center, Lamar University, Beaumont, TX

Chen, H., Bai, S., Eisinger, D., Niemeier, D., and Claggett, M. (2008). "Modeling uncertainties and near-raod PM2.5: A comparison of CALINE4, CAL3QHC, and AERMOD." U.S. Federal Highway Administration, and U.C. Davis-Caltrans Air Quality Project.

Cheng, S., Li, J., Feng, B., Jin, Y. and Hao, R. (2006). "A Gaussian-box modeling approach for urban air quality management in a northern chinese city—I. model development." Water Air Soil Pollution, 178, 37-57.

Curran, M.A. (2009). "The opportunities and pitfalls of applying life cycle thinking to nanoproducts and nanomaterials." Nanotechnology and Life Cycle Analysis Workshop, Chicago, IL., Nov. 4-5, 2009. <http://www.uic.edu/orgs/nanolcaworkshop/speakers.html> (June 7, 2011).

Curran, M.A. (2006). "Life cycle assessment: Principles and practice." EPA/600/R-06/060. National Risk Management Research Laboratory, Cincinnati, OH, 1-78.

Dahl, A., Gharibi, A., Swietlicki, E., Gudmundsson, A., Bohgard, M., Ljungman, A., Blomqvist, G., and Gustafsson, M. (2006). "Traffic-generated emissions of ultrafine particles from pavement-tire interface." Atmospheric Environment, 40, 1314-1323.

Dalton, J.S., Janes, P.A., Jones, N.G., Nicholson, J.A., Hallam, K.R. and Allen, G.C. (2002). "Photocatalytic oxidation of NO_x gases using TiO_2: a surface spectroscopic approach." Environmental Pollution, 120, 415-422.

Davis, M.J. (2007). "How to assess the risks of nanotechnology: Learning from past experience." Journal of Nanoscience and Nanotechnology, 7, 402-409.

Davis, M.J. and Thomas, V.M. (2006). "Systematic approach to evaluating trade-offs among fuel options: The lessons of MTBE" Annals of the New York Academy of Science, 1076, 498-515.

Demeestere, K., Dewulf, J., De Witte, B., Beeldens, A. and Van Langenhove, H. (2008). "Heterogeneous photocatalytic removal of toluene from air on building materials enriched with TiO_2". Building and Environment, 43(4), 406-414.

Diamanti, M.V., Ormellese, M. and Pedeferri, M. (2008). "Characterization of photocatalytic and superhydrophilic properties of mortars containing titanium dioxide." Cement and Concrete Research, 38, 1349-1353.

Dobson, D.C., Shepherd, W.G., and Stoner, R.D. (1994). "Strategic Capacity Preemption: DuPont (Titanium Dioxide) (1980)" The Antitrust Revolution: The Role of Economics, Kwoka, J.E. Jr. and White, L.J., Harper Collins, New York, 157-188.

Duran, E.J., Mohseni, M., and Taghipour, F. (2011). "Design improvement of immobilized photocatalytic reactors using a CFD-Taguchi combined method." Industrial and Engineering Chemistry Research, 50, 824-831.

Dylla, H., Hassan, M. M., Mohammad, L., and Rupnow T. (2011). "Effects of Roadway Contaminants on Titanium Dioxide Photodegradation of NO_x." Journal of the Transportation Research Record, 2240, 22-29.

Dylla[a], H., Hassan, M. M., Mohammad, L., Rupnow T., and Wright, E. (2010). "Evaluation of the Environmental Effectiveness of Titanium Dioxide Photocatalyst coating for concrete pavements." Journal of the Transportation Research Record, 2164, 46-51.

Dylla[b], H., Hassan, M., Schmitt, M., Rupnow, T. and Mohammad, L. (2010). "Laboratory investigation of mixed nitrogen dioxide (NO_2) and nitrogen oxide (NO) gasses on titanium dioxide photocatalytic efficiency in concrete pavements." Journal of Materials in Civil Engineering, 23(7) 1087-1093.

Ehrhard, J., Khatib, I.A., Winkler, C., Kunz, R, Moussiopoulos, N., and Ernst, G. (2000). "The microscale model MIMO: development and assessment." Journal of Wind Engineering and Industrial Aerodynamic, 85, 163-176.

Fowlie, M., Knittel, C.R., and Wolfram, C. (2008). "Sacred Cars? Optimal Regulation of Stationary and Non-Stationary Pollution Sources." National Bureau of Economic Research, (NBER). Working Paper No. 14504: 1-42.

Fujishima, A., and Honda, K. (1972). "Electrochemical Photolysis of Water at a Semiconductor Electrode." Nature, 238, 37-38.

Fujishima, A., Rao, Tata N. and Tryk, D. A. (2000). "Titanium dioxide photocatalysis." Journal of Photochemistry and Photobiology C: Photochemistry Reviews, 1, 1-21.

Fujishima, A., and Zhang, X.. (2006). "Titanium dioxide photocatalysis: present situation and future approaches." Comptes Rendus Chimie. 9, 750-760.

Future Markets, INC. (2011). The World Market for Nanoparticle Titanium Dioxide. 1-67.

Gauderman, W.J., Vora, H., McConnell, R., Berhane, K., Gilliland, F., Thomas, D., Lurmann, F., Avol, E., Kunzli, N., Jerrett, M., and Peters, J. (2007). "Effect of exposure to traffic on lung development from 10 to 18 years of age: a cohort study." Lancet, 369, 571-577.

Gloria, T.P, Lippiatt, B.C. and Cooper, J. (2007). "Life cycle impact assessment weights to support environmentally preferable purchasing in the United States." Environmental Science and Technology, 41, 7551-7557

Gohler, D., Stintz, M. Hillemann, L. and Vorbau, M. (2010). "Characterization of nanoparticle release from surface coatings by the simulation of a sanding process." Annals of Occupational Hygiene, 1-10.

Gottschalk, F., Sonderer, T., Scholz, R.W., and Nowack, B. (2009). "Modeled Environmental Concentrations of Engineered Nanomaterials (TiO_2, ZnO, Ag, CNT, Fullerenes) for Different Regions." Environmental Science & Technology, 43(24), 9216-9222.

Grant, S., Freer, A.A., Winfield, J.M., Gray, C., Overton, T.L., and Lennon, D. (2004). "An undergraduate teaching exercise that explores contemporary issues in the manufacture of titanium dioxide on the industrial scale." The Royal Society of Chemistry, 6, 25-32.

Grubb, G.F, and Bakshi, B.R. (2010). "Life cycle of titanium dioxide nanoparticle production." Journal of Industrial Ecology, 15(1), 81-95. SAS INPUTs

Gustafsson, M., Blomqvist, G, Gudmundsson, A., Dahl, A., Swietlicki, E., Bohgard, M., Lindbom, J., and Ljungman, A. (2008). “Properties and toxicological effects of particles from the interaction between tyres, road pavement and winter traction material.” Science of the Total Environment, 393, 226-240.

Guzman, K. A., Taylor, M. R., and Banfield, J.F. (2006). "Environmental Risks of Nanotechnology: National Nanotechnology Initiative Funding, 2000−2004." Environmental Science & Technology, 40(5), 1401-1407.

Haas, R., Tighe, S., and Falls, L. (2006). “Determining Return on Long-Life Pavement Investments.” Transportation Research Record: Journal of the Transportation Research Board, 1974(-1), 10-17.

Hassan, M.M. (2009). “Life-Cycle Assessment of Warm-Mix Asphalt: Environmental and Economic Perspectives.” Transportation Research Board 88th Annual Meeting, (CD-ROM), Transporation Research Board, Washington, D.C.

Hassan, M.M., H. Dylla, Mohammad, L.N. and T. Rupnow. (2009). “Effect of Application Methods on the Effectiveness of Titanium Dioxide as a Photocatalyst Compound to Concrete Pavement.” 89th Transportation Research Board Annual Meeting, 10-0963.

Hassan, M.M., Dylla, H., Mohammad, L., and Rupnow T. (2010). “Evaluation of the durability of titanium dioxide photocatalyst coating for concrete pavement.” Journal of Construction and Building Material, 28(8), 1456-1461.

Hassan, M.M., Mohammad, L.N., Dylla, H., Cooper, S.B. III, Mokhtar, A., Asadi, S. (2011). “A breakthrough concept in the preparation of highly-sustainable photocatalytic warm asphalt mixtures.” Proceedings of 2011 NSF Engineering Research and Innovation Conference, Atlanta, Georgia, 1-6.

Health Effects Institute (HEI). (2010). “Traffic-Related Air Pollution: A Critical Review of the Literature on Emissions, Exposure, and Health Effects.” Special Report 17.

Holmes, N.S. and Morawska, L. (2006). “A review of dispersion modeling and its application to the dispersion of particles: An overview of different dispersion models available.” Atmospheric Environment, 40, 5902-5928.

Horvath, A., (2003). Life-Cycle Environmental and Economic Assessment of Using Recycled Materials for Asphalt Pavements. University of California-Berkeley: Berkeley.

Hsu, L.Y., and Chein, H-M. (2007). “Evaluation of nanoparticle emission for TiO_2 nanopowder coating materials.” Nanoparticles and Occupational Health, 9, 157-163.

Huang, Y., R. Bird, and Heidrich, O. (2009). “Development of a life cycle assessment tool for construction and maintenance of asphalt pavements.” Journal of Cleaner Production, 17(2), 283-296.

Hund-Rinke, K. and Simon, M. (2006). "Ecotoxic Effect of Photocatalytic Active Nanoparticles (TiO_2) on Algae and Daphnids (8 pp)." Environmental Science and Pollution Research, 13(4), 225-232.

Hunger, M., Husken, G., and Brouwers, J. (2010). "Photocatalytic degradation of air pollutants – From modeling to large scale application." Cement and Concrete Research, 40, 313-320.

Hunger, M., Husken, G., and Brouwers, J. (2008). "Photocatalysis applied to concrete products, Part 1: Principles and test procedure." Materials Science, ZKG International. 61, 77-85.

Husken, G., Hunger, M., and Brouwers, H.J.H. (2009). "Experimental study of photocatalytic concrete products for air purification." Building and Environment, 44, 2463-2474.

Isaacs, J. (2009). "Considerations for LCA of Nanotechnologies" Presented at Nanotechnology and Life Cycle Analysis Workshop, Nov. 5-6, 2009, Chicago, IL.

International Organization of Standardization, (ISO). (2006). "Environmental management-Life cycle assessment-Principles and framework." ISO 14040:2006. ISO.

International Organization of Standardization, (ISO). (2006). "Environmental management-Life cycle assessment-Principles and framework." ISO 14044:2006. ISO.

Japanese Industrial Standard (JIS). (2004). "Fine ceramics (advanced ceramics, advanced technical ceramics) – Test method for air purification performance of photocatalytic materials- Part 1: Removal of nitric oxide", JIS R 1701-1,1-9.

Johnson, T.V. (2006). "Diesel Emission Control in Review." SAE Technical Paper Series, 2006-01-0030, 1-18.

Kaegi, R., Ulrich, A., Sinnet, B., Vonbank, R., Wichser, A., Zuleeg, S., Simmier, H., Brunner, S., Vonmont, H., Burkhardt, M., and Boller, M. (2008). "Synthetic TiO_2 nanoparticle emission from exterior facades into the aquatic environment." Environmental Pollution 156(2), 233-239.

Kendall, A., Keoleian, G. and Lepech, M. (2008). "Materials design for sustainability through life cycle modeling of engineered cementitious composites." Materials and Structures, 41(6), 1117-1131.

Kim, S.B. and Hong, C.S. (2002). "Kinetic study for photocatalytic degradation of volatile organic compounds in air using thin film TiO_2 photocatalyst." Applied Catalysis B: Environmental, 35, 305-315.

Kim, J.J., Smorodinsky, S., Lipsett, M., Singer, B. C., Hodgson, A.T., and Ostro, B. (2004). "Traffic-related air pollution near busy roads: the East Bay Children's Respiratory Health Study." American Journal Respiratory and Critical Care Medicine, 170, 520-536.

Kuhns, H.D., Mazzoleni, C., Moosmuller, H., Nikolic, D., Keislar, R.E., Barber, P.W., Li, Z., Etyemezian, V., and Watson, J.G. (2004). "Remote sensing of PM, NO, CO, HC emission factors for on-road gasoline and diesel engine vehicles in Las Vegas, NV." Science of the Total Environment, 322, 123-137.

Lackhoff, M., Prieto, X., Nestle, N., Dehn, F. and Niessner, R. (2003). "Photocatalytic activity of semiconductor-modified cement—influence of semiconductor type and cement ageing." Applied Catalysis B: Environmental, 43, 205-216.

Louisiana Department of Environmental Quality (DEQ). (2006). "Ambient Air Data Sets." Ambient Air Monitoring Data and Reports, <http://www.deq.louisiana.gov/portal/DIVISIONS/Assessment/AirFieldServices/AmbientAirMonitoringProgram/AmbientAirMonitoringDataandReports.aspx> (March 6, 2011).

Louisiana State Department of Transportation (LADOT). (2000). Louisiana Standard Specifications for Roads and Bridges. State of Louisiana, Department of Transportation and Development, Baton Rouge.

Li, L. and Qian, C. (2009). "A lab study of photo-catalytic oxidation and removal of nitrogen oxides in vehicular emissions and its fieldwork on Nanjin No.3 bridge of Yangtze River." Journal of Pavement Resource Technology, 2(5), 218-222.

Li, X.Z., Li, F.B., Yang, C.L., and Ge, W.K. (2001). "Photocatalytic activity of WOx- TiO_2 under visible light irradiation." Journal of Photochemistry and Photobiology A: Chemistry, 141, 209-217.

Lin, J. and Yu, D. (2008). "Traffic-related air quality assessment for open road tolling highway facility." Journal of Environmental Management, 88, 962-969.

Liu, T., Li, F., Li, X. (2008). "TiO_2 hydrosols with high activity for photocatalytic degradation of formaldehyde in a gaseous phase." Journal of Hazardous Material, 152, 347-355.

Long, T. C., N. Saleh, Tilton, R.D., Lowry, G.V., and Veronesi, B. (2006). "Titanium Dioxide (P25) Produces Reactive Oxygen Species in Immortalized Brain Microglia (BV2): Implications for Nanoparticle Neurotoxicity." Environmental Science & Technology, 40(14), 4346-4352.

Lovern, S. B., Strickler, J. R. and Klaper, R. (2007). "Behavioral and physiological changes in Daphnia magna when exposed to nanoparticle suspensions (Titanium Dioxide, Nano-C60, and C60HxC70Hx)." Environmental Science & Technology, 41(12), 4465-4470.

Luo, Z., Wang, Z., Li, Q., Pan, Q., and Yan, C. (2010). "Effects of titania nanoparticles on phosphorus fractions and its release in resuspended sediments under UV irradiation." Journal of Hazardous Materials, 174(1-3), 477-483.

Maggos, T., Plassais, A., Bartzis, J.G., Vasilakos, C, Moussiopoulos, A. and Bonafous, L. (2008). "Photocatalytic degradation of NO_x in a pilot street canyon configuration using TiO_2-mortar panels." Environmental Monitoring Assessment, 136, 35-44.

Maricq, M.M. (2007). "Chemical characterization of particulate emissions from diesel engines: A review." Aerosol Science, 38, 1079-1118.

Martinez, T., Bertron, A. Ringot, E., and Escadeillas, G. (2011). "Degradation of NO using photocatalytic coatings applied to different substrates." Building and Environment, 46, 1808-1816.

McConnell, R., Islam, T., Shankardass, K., Jerrett, M., Lurmann, F., Gilliland, F., Gauderman, J., Avol, E., Kuenzli, N.,Yao, L., Peters, J., and Berhane, K.. (2010). "Childhood Incident Asthma and Traffic-Related Air Pollution at Home and School." National Institute of Environmental Health Sciences, 1-33.

Methner[b], M., L. Hodson, A. Dames, and C. Geraci. (2010). "Nanoparticle emission assessment technique (NEAT) for the identification and measurement of potential inhalation exposure to engineered nanomaterials --Part b: Results from 12 field studies." Journal of Occupational and Environmental Hygiene, 7, 163-176.

Methner[a], M., L. Hodson, Dames, A., and Geraci, C. (2010). "Nanoparticle emission assessment technique (NEAT) for the identification and measurement of potential inhalation exposure to engineered nanomaterials--Part A." Journal of Occupational & Environmental Hygiene, 7(3), 127-132.

Menz, F.C. (2002). "The US experience with controlling motor vehicle pollution: lessons for China." International Journal Environment and Pollution, 18(1), 1-21.

Meyer, D. E., M. A. Curran, and Gonzalez, M.A. (2009). "An Examination of Existing Data for the Industrial Manufacture and Use of Nanocomponents and Their Role in the Life Cycle Impact of Nanoproducts." Environmental Science & Technology 43(5), 1256-1263.

Moussiopoulos, N., Barmpas, P., Ossanlis, P. and Bartiz, J. (2008). "Comparison of Numerical and Experimental Results for the Evaluation of the Depollution Effectiveness of Photocatalytic Coverings in Street Canyons." Environmental Modeling and Assessment, 13(3) 357-368.

Nano (2000). "Major Products: TiO_2." <http://www.nanoin.com> (March 6, 2011).

Nimlos, M.R., Wolfrum, E.J., Brewer, M.L., Fennell, J.A. and Bintner, G. (1996). "Gas-Phase Heterogeneous Photocatalytic Oxidation Ethanol: Pathways and Modeling." Environmental Science and Technology, 30, 9-12.

Nishioka, Y., Levy, J.I., Norris, G.A., Wilson, A., Bennett, D.H., and Spengler, J.D., (2005). "A risk-based approach to health impact assessment for Input-Output analysis, Part 1: Methodology." The International Journal of Life Cycle Assessment, 10(3), 193-199.

Noguchi, T., Fujishima, A., Sawunyama, P., and Hashimoto, K. (1998). "Photocatalytic Degradation of Gaseous Formaldehyde Using TiO_2 Film" Environmental Science and Technology, 32, 3831-3833.

Nonami, T.; Hase, H.; Funakoshi, K, (2004). "Apatite-coated titanium dioxide photocatalyst for air purification." Catalysis Today, 96, 113-118.

Nowack, B. and Bucheli, T. D. (2007). "Occurrence, behavior and effects of nanoparticles in the environment." Environmental Pollution, 150(1), 5-22.

ObservatoryNANO. (2011). "Applications of Photocatalysis", Chemistry and Materials, Briefing No. 10, February 2011, 1-4.

Osburn, L (2008). "A literature review on the application of titanium dioxide reactive surfaces on urban infrastructure for depolluting and self-cleaning applications." Built Environment CSIR.

Pennington, D.W., Potting, J., Finnveden, G., Lindeijer, E., Jolliet, O., and Rebitzer, G. (2004). "Life cycle assessment Part 2: Current impact assessment practice." Environment International, 30(5), 721-739.

Photocatalytic Innovated Coverings Applications for Depollution Assessment (PICADA). (2001). "Guideline for end-users." GROWTH Project GRD1-2001-40449, <http://www.picada-project.com> (June 7, 2011).

Piera, E., Ayllon, J.A., Domenech, X., and Peral, J. (2002). "TiO_2 deactivation during gas-phase photocatalytic oxidation of ethanol" Catalysis Today, 76, 259-270.

Poon, C.S., and Cheung, E. (2007). "NO removal efficiency of photocatalytic paving blocks prepared with recycled materials." Construction and Building Materials, 21, 1746-1753.

Pramauro, E. Prevot, A.B., Vincenti, M., and Gamberini, R. (1998). "Photocatalytic degradation of naphthalene in aqueous TiO_2 dispersions: Effect of nonionic surfactants" Chemosphere, 36(7), 1523-1542.

Panayotou, T. (1994). "Economic Instruments for Environmental Management and Sustainable Development." United Nations Environmental Programme, Nairobi, Feb. 23-24, 1995. Environmental Economic Series Paper

Proost, S. and Dender, K.V. (2001). "The welfare impacts of alternative policies to address atmospheric pollution in urban road transport." Regional Science and Urban Economics, 31, 383-411.

Queffeulou, A., Geron, L., and Schaer, E., “Prediction of photocatalytic air purifier apparatus performances with a CFD approach using experimentally determined kinetic parameters.” 65, 5067-5074.

Reijnders, L. (2009). “The release of TiO_2 and SiO_2 nanoparticles from nanocomposites.” Polymer Degradation and Stability, 94, 873-876.

Research and Innovative Technology Administration (RITA). (2011). “2011 National Transportation Statistics.” United States Department of Transportation, <http://www.bts.gov/publications/national_transportation_statistics/> (June 7, 2011).

Ribeiro, C., Vila, C., Stroppa, D., Mastelaro, V., Bettini, J., Longo, E., and Leite, E. (2007). "Anisotropic Growth of Oxide Nanocrystals: Insights into the Rutile TiO_2 Phase." Journal Physical Chemistry C, 111, 5871-5875.

Saarela, K., Tirkkonen, T., Laine-Ylikjoki, J., Jurvelin, J., Nieuwenhuijsen, M.J., and Jantunen, M. (2003). “Exposure of population and microenvironmental distributions of volatile organic compound concentrations in the EXPOLIS study.” Atmospheric Environment, 37, 5563-5575.

Sahu, M and Biswas, P. (2010). “Size distributions of aerosols in an indoor environment with engineered nanoparticle synthesis reactors operating under different scenarios.” Journal Nanoparticle Research, 12, 1055-1064.

Salvado-Estivill, I., Hargreaves, D.M. and Puma, G.L., (2007). “Evaluation of the intrinsic photocatalytic oxidation kinetics of indoor air pollutants.” Environmental Science and Technology, 41, 2028-2035.

San, J.R., Perez, J.L., and Gonzalez, R.M. (2004). “Preliminary experiments with a street numerical model (MIMO) nested with MM5-CMAQ: Madrid City application.” Air Pollution XII, Rhodes, 14, 591-599.

Sharma, N., Chaudhry, K.K., and Chalapati Rao, C.V. (2004). “Vehicular pollution prediction modeling: A review of highway dispersion models.” Transport Reviews, 24(4), 409-435.

Shi, J.P. and Harrison, R.M. (1997). “Regression modeling of hourly NO_x and NO_2 concentrations in urban air in London.” Atmospheric Environment, 31(24), 4081-4094.

Sleiman, M., Conchon, P., Ferronato, C., and Chovelon, J.M. (2009). “Photocatalytic oxidation of toluene at indoor air levels (ppbv): Towards a better assessment of conversion, reaction intermediates and mineralization.” Applied Catalysis B: Environmental, 86(3-4), 159-165.

Sopyan, I., Watanabe, M., Murasawa, S., Hashimoto, K. and Fujishima, A.. (1996). “An efficient TiO_2 thin-film photocatalyst: photocatalytic properties in gas-phase acetaldehyde degradation.” Journal of Photochemistry and Photobiology A: Chemistry, 98, 79-86.

Stern, S.T. and McNeil, S.E. (2008). “Nanotechnology safety concerns revisited.” Toxicological Sciences, 101(1), 4-21.

Strini, A.; Cassese, S.; and Schiavi, L. (2005). “Measurement of benzene, toluene, ethylbenzene and o-xylene, gas phase photodegradation by titanium dioxide dispersed in cementitious materials using a mixed flow reactor.” Applied Catalysis B: Environmental, 61, 90-97.

Taghipour, F., and Mohseni, M. (2005). “CFD simulation of UV photocatalytic reactors for air treatment.”AIChE Journal, 51(11), 3039-3047.

Theng, B.K.G. and Yuan, G. (2008). “Nanoparticles in the soil environment.” Elements, 4, 395-399.

Thibodeaux, L.J. and Mackay, D. (2011). “Dry Gaseous Deposition,” Handbook of chemical mass transport in the environment. CRC Press, Boca Raton, FL. 144-147.

Thoma, E.D., Shores, R.C., Isakov, V., and Baldauf, R.W., (2008). “Characterization of near-road pollutant gradients using path-integrated optical remote sensing.” Air & waste Management Association, 58, 879-890.

Toma, F.-L., Bertrand, G., Klein, D., Coddet, D. and Meunier, C. (2006). “Nanostructured photocatalytic titania coatings formed by suspension plasma spraying.” Journal of Thermal Spray Technology, 15(15), 587-592.

Toma, F.-L.; Berger, L.M.; Jacquet, D.; Wicky, D.; Villaluenga, I; Miguel, Y.R.; Lindelov, J.S. (2009). “Comparative study on the photocatalytic behavior of titanium oxide thermal sprayed coating from powders and suspensions.” Surface & Coatings Technology, 203(15), 2150-2156.

Treloar, G.J., P.E.D. Love, and R.H. Crawford, (2004). “Hybrid Life-Cycle Inventory for Road Construction and Use.” Journal of Construction Engineering and Management, 130(1), 43-49.

TSI Incorporated (TSI). (2010). “TSI knows Nano: Nano Instrumentation.” Shoreview, MN. <www.tsi.com> (June 7, 2011).

U.S. Census Bureau. (2009). American Housing Survey. <http://www.census.gov/hhes/www/housing/ahs/nationaldata.html> (June 7, 2011).

United State Environmental Protection Agency, (EPA). (1999). Atmospheric Sampling. ICES Ltd, North Carolina.

United State Environmental Protection Agency, (EPA). (2007). Air Pollution Control Orientation Course, <http:// www.epa.gov/air/oaqps/eog/course422/ce4b.html> (March 6, 2011).

United States Environmental Protection Agency (EPA[a]). (2010). Part II: Environmental Protection Agency Primary National Ambient Air Quality Standard for Sulfur Dioxide; Final Rule, 75(119), 35520-35603, June 22, 2010.

United States Environmental Protection Agency (EPA[b]). (2010). Proposal to Revise the National Ambient Air Quality Standards for Ground-level Ozone, <http://www.epa.gov/ozonepollution/pdfs/20100106present.pdf> (July 2, 2010).

Vallius, M., Ruuskanen, J., and Pekkanen, J. (2008). "Comparison of multivariate source apportionment of urban PM2.5 with chemical mass closure." Boreal Environment Research, 13, 347-358.

Valsaraj, K. (2009). "Heterogeneous Catalysis." Elements of Environmental Engineering, CRC Press, Boca Raton, FL, 228-234.

Vardoulakis, S., Fisher, B.E.A., Pericleous, K., Conzalez-Flesca, N. (2003). "Modelling air quality in street canyons: a review." Atmospheric Environment, 37, 155-182.

Vette A. (2010). "Near-Road Air Pollution." U.S. Environmental Protection Agency. Clean Air Research. <www.epa.gov/airscience> (June, 7 2007).

Wang, S., Ang, H.M.; and Tade, M. O. (2007). "Volatile organic compounds in indoor environment and photocatalytic oxidation: State of the art." Environment International, 33, 694-705.

Watts, M.J. and Cooper, A. (2008). "Photocatalysis of 4-chlorophenol mediated by TiO_2 fixed to concrete surfaces." Solar Energy, 82, 206-211.

Wiesner[a], M. R., G. V. Lowry, Alvarez, P, Dionysiou D, and Biswas, P. (2006). "Assessing the Risks of Manufactured Nanomaterials." Environmental Science & Technology 40(14), 4336-4345.

Wiesner[b], M. R., G. V. Lowry, Jones, K.L., Hochella, F.M., Di Giulio, R.T., Casman, and E., Bernhardt, E.S. (2009). "Decreasing Uncertainties in Assessing Environmental Exposure, Risk, and Ecological Implications of Nanomaterials." Environmental Science & Technology 43(17), 6458-6462.

Wigginton, N.S., Haus, K.L., and Hochella, M.F., (2007). "Aquatic environmental nanoparticles." Journal of Environmental Monitoring 9, 1306-1316.

Yu, J. C.-M.. (2003). Deactivation and Regeneration of Environmentally Exposed Titanium Dioxide (TiO_2) Based Products. Environmental Protection Department No. E183413, 1-21.

Yu, J. C.-M. (2002). Ambient Air Treatment by Titanium Dioxide (TiO_2) Based Photocatalyst in Hong

Zeng, F., Shi, G-L., Li, X., Feng, Y-C., Bi, X-H., Wu, J-H., and Xue, Y-H. (2010). "Application of a combined model to study the source apportionment of PM10 in Taiyuan, China." Aerosol and Air Quality Research, 10, 177-184.

Zhan, T, Stedman, D.H., Bishop, G.A, and A. Peddle. (2009). On-road motor vehicle emissions including NH_2, SO_2 and NO_2. California Air Resources Board, California Environmental Protection Agency. No. 07-319.

Zhang, H., G.A. Keoleian, and Lepech, M. D. (2008). "An integrated life cycle assessment and life cycle analysis model for pavement overlay systems." Proceedings of the First International Symposium of the International Association for Life Cycle Civil Engineering. Varenna, Lake Como, Italy.

Zhao, J. and Yang, X. (2003). "Photocatalytic oxidation of indoor air purification: a literature review." Building and Environment, 38, 645-654.

Zhu, X., Y. Chang, Y. and Chen, Y. (2010). "Toxicity and bioaccumulation of TiO_2 nanoparticle aggregates in Daphnia magna." Chemosphere, 78(3), 209-215.

Zorn, M.E., Tompkins, D.T, Zeltner, W.A.; and Anderson, M.A. (2000). "Catalytic and photocatalytic oxidation of ethylene on titania-based thin-films." Environmental Science and Technology, 34, 5206-5210

CHAPTER 3
FIELD EVALUATION OF PHOTOCATALYTIC CONCRETE PAVEMENTS' ABILITY TO REMOVE NITROGEN OXIDES[1]

3.1 INTRODUCTION

Negative health effects from vehicle pollution are associated with living, working and going to school near highways from long-term and short-term exposures. This includes respiratory effects (asthma, bronchitis), cardiovascular effects, premature mortality, cancer, and adverse birth outcomes and developmental effects (Baldauf et al. 2009, Kim et al. 2004, McConnell et al. 2010). Traditionally, zoning practices separated roadway microenvironments to limit exposure. As a result, the ambient air pollution concentrations and high short-term concentrations were of less concern. However, current urban development demand has led to residential development on infill sites of historical industrial or commercial urban zones (Bhatia and Rivard 2007). These zones are often near roads with heavy traffic, which led to increasing the exposure of roadway pollution along with its associated health effects (HEI 2010). In 2007, it was estimated by the American Housing Survey that more than 45 million people live within 300 feet of an airport, railroad, or major highway. According to the 2009 survey, this number is growing (Vette 2010, U.S. Census Bureau 2009).

The mobile nature of vehicle pollution sources significantly impacts how much emissions are emitted and the extent of the associated negative impact imposed on society. This makes the success of efficiently reducing traffic emissions difficult. Increasing fleet size persistently offsets the vehicle emission reductions. As a result, EPA expects that regulations will continually get stricter (EPA 2008). Some researchers argue that this practice of continually reducing the emissions from vehicles through improved technology may not be enough (Menz

[1] Reprinted with permission of the Transportation Research Board.
Published in the *Transportation Research Record: Journal of the Transportation Research Board*, No. 2290, pp. 154-160.

2002). Thus, a solution to reduce vehicle emissions once they are emitted into the atmosphere is needed.

Using heterogeneous photocatalysis, pollutants emitted into the atmosphere are decomposed to nonhazardous waste products with little energy requirements and little selectivity (Zhao and Yang 2003, Ballari et al. 2010). Photocatalytic pavements reduce pollutants such as nitrogen oxides (NO_x) by 40 to 85% once pollutants are emitted in the air (Beeldens 2006). In addition, photocatalytic pavements have the advantage that they may be a cost effective air pollution abatement technique since they may be applied only to target areas. As a result, many field studies are underway to demonstrate the potential of photocatalytic pavements under real world conditions. However, quantification of nitrogen oxides (NO_x) reduction in field studies is difficult and challenging due to the large number of environmental and operating variables (Maggos et al. 2008). This has limited current results of field studies. The objective of this paper is to identify evidence of photocatalytic reductions in the field and to determine the significant environmental and operating factors that impact efficiency. These factors are essential in order to make proper assessment of field photocatalytic efficiencies and to advance the success of future photocatalytic field studies.

3.2 BACKGROUND

To measure the pollution reduction of NO_x continuously in the field often presents a challenge, due to a large number of influencing parameters, time, and costs. Despite the amount of field studies, Hunger et al. 2010 highlight that none of the current field studies demonstrate a reduction in pollution exclusively resulting from the photocatalytic pavements (Hunger et al. 2010). Nonetheless, it is agreed that photocatalytic field studies are the next step to advance the use of photocatalytic pavements. Two techniques to measure photocatalytic degradation from

field studies have been explored. The first is to measure the reduction directly by measuring the ambient air pollution concentration and the second is to measure the reduction indirectly by measuring the byproducts created from the degradation process.

Of the many pollutants present in roadway microenvironments, nitrogen oxides are the most commonly used pollutant to evaluate the reduction of photocatalytic pavements. Nitrogen oxides, emitted from vehicle combustion, are easy to monitor in the air and the photocatalytic byproduct nitrates can also be measured. Further, roadway microenvironments contribute to 35% of NO_x emissions, which have detrimental effects on the outdoor environment by promoting acid rain and on indoor air quality, contributing to sick building syndrome (Kuhns et al. 2004). To directly measure NO_x reductions from photocatalytic roadways, the approved method of ambient air NO_x detection is chemiluminescence. Chemiluminescence occurs when light is emitted from a reaction, which in the case of NO_x is between nitrogen monoxide and ozone. The amount of light emitted is proportional to the NO concentration. For nitrogen dioxide, an indirect approach is taken, since a catalytic converter must first reduce the nitrogen dioxide to nitric oxide in order to be measured. After catalytic conversion, the total NO measured corresponds to the NO_x concentration. Therefore, the nitrogen dioxide concentration is the difference between the total NO_x and the NO (EPA 1999 and 2007). Another technique used to monitor ambient NO_x concentrations is to trap the gaseous pollutants onto a filter in which the concentrations are determined using laboratory colorimetric methods (Chen and Chu 2011).

Field studies have attempted to quantify NO_x reduction using chemiluminiescent ambient air monitoring techniques. Simultaneous measurements are preferred to compare photocatalytic pavement areas and non-photocatalytic pavement areas under similar environmental conditions. Li and Qian (2009) used this technique and measured NO_x reduction for 1 hour a day of each

month illustrating a photocatalytic reaction occurring in the field with reductions as high as 80% (Li and Qian 2009). Field studies using traps concluded up to 16% reductions (Chen and Chu 2011). However, long-term continuously monitored data has not been reported and is necessary to understand the full potential of photocatalytic pavement under various environmental conditions. These environmental conditions not only impact the photocatalytic reduction efficiency but also interfere with pollutants dispersion (Maggos et al. 2008).

Pilot studies have been used as an intermediate step between laboratory and full-scale tests in order to eliminate the additional factor of pollutants dispersion. A pilot study in France controlled the pollution source concentration and pollution distribution to evaluate the photocatalytic reductions from coated artificial street canyon walls under various environmental conditions. The first period measured the street canyon pollution from panels treated with a photocatalytic mortar and the second period was used to measure pollution from panels with no coating. The ambient air background concentrations were measured and subtracted from the total emissions measured. The difference between the coated and control average concentrations was then used to calculate photocatalytic degradation efficiency of NO_x (Maggos et al. 2008). Results concluded that NO_x could be reduced with an efficiency ranging from 36 to 82% dependent upon the pollution emissions, wind direction, and wind speed (Maggos et al. 2008). However, having a constant, uniform distribution of pollution is not likely in field applications where vehicle activity is variable.

The second technique is to use indirect techniques to measure photocatalytic reductions. For NO_x, the indirect method evaluates the photocatalytic degradation of NO_x by measuring the NO_3^- deposited on the surface. Nitrates are water-soluble and therefore washed from the surface with water to be quantified (Beeldens 2008). By knowing the amount of NO_3^- collected, the

amount of degradation is indirectly calculated, using the stoichiometry given in the following equations:

$$NO + \bullet OH \xrightarrow{hv,TiO_2} NO_2 + H^+ \quad (3.1)$$

$$NO_2 + \bullet OH \xrightarrow{hv,TiO_2} NO_3^- + H^+ \quad (3.2)$$

Beeldens (2008) used this technique to measure the photocatalytic degradation of NO_x from removable pavement blocks (Beeldens 2008). Results illustrated that 2 mmol NO_x/m^2 can be removed in 12 hours. However, results recorded in the field were unable to develop any photocatalytic reduction relationships due to the numerous impacting factors (i.e. traffic activity, wind, light, and humidity making comparisons difficult) and given that nitrate ions were not completely eluted (Beeldens 2008, Beeldens 2011). The objective of this study is to identify evidence of photocatalytic reductions and to identify the significant factors impacting photocatalytic reductions in efforts to advance the results of future field studies. To achieve this objective, a field study was conducted and the photocatalytic reduction was directly and indirectly measured for NO_x. In addition, the experimental program monitored significant environmental and operating factors during the test period.

3.3 EXPERIMENTAL PROGRAM

The field study consisted of a ¼-mile concrete pavement roadway located on Raphael Semmes Road in Louisiana State University's campus. This was the first field installation of TiO_2 photocatalytic pavement in the US. Because this is an already existing roadway, the photocatalytic coating was applied using the spray coat technique to the section highlighted in Figure 3.1. Test equipment is housed in a trailer, centrally located, such that NO_x concentrations can be measured for both the coated and uncoated areas (Figure 3.1). To characterize the field

study environmental conditions, NO_x ambient air pollution, weather and traffic data were collected directly from the field site. Background concentrations for NO_x, sulfur dioxide (SO_2), and ozone were also available from the Louisiana Department of Environmental Quality (DEQ) air monitoring station (DEQ 2006).

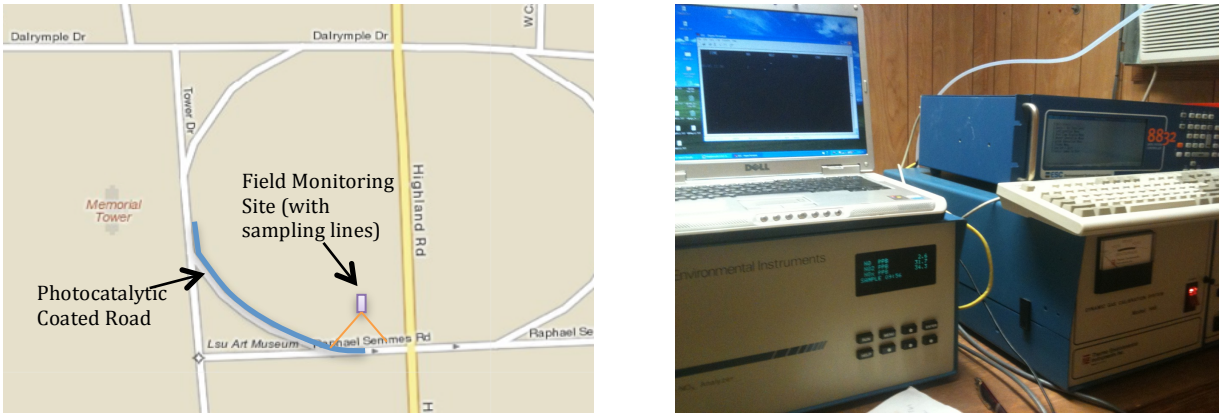

Figure 3.1 Field Site Location and Ambient Air Monitoring Equipment

3.3.1 FIELD PHOTOCATALYTIC SPRAY COAT APPLICATION

The photocatalytic spray coat used was a mixture of TiO_2 anatase nanoparticles with an average size of 6 nm suspended in an aqueous liquid at 2% by volume. Before application, the roadway was cleared of any debris. A primer was applied first before the photocatalytic coat. A computerized distributor truck was used for the application process. Mounted on the back of the truck, a spray bar fitted with nozzles distributed TiO_2 water-based solution at the specified application rate, 16.1 to 21.5 ml/m^2 (Figure 3.2). The application rate was adjusted by altering the truck speed and nozzle type and size. Further, the nozzles had electrostatic precipitators to separate the TiO_2 nanoparticles suspended in the aqueous solution and to ensure a more even coverage.

Figure 3.2 Illustration of TiO_2 Spray Coat Application

3.3.2 NO_X AMBIENT AIR DETECTION

NO_x concentrations were monitored for both the coated and uncoated sections simultaneously for three weeks during the spring season. NO, NO_2, and NO_x concentrations are measured using a Thermo NO_x analyzer and are stored as minute averages. The sample lines were located at the pavement level in order to measure the pollutant concentration released from car muffler that comes in contact with the pavement surface. The sample lines were made of 316 stainless steel and were covered with a protective bump as shown in Figure 3.3.

Figure 3.3 Air Sampling Line

3.3.3 ENVIRONMENTAL CONDITIONS DETECTION

Environmental conditions were recorded during the monitoring period. Both weather and traffic data were collected and stored in order to interpret different trends in the measurements. The weather station employed, Davis 6152 Wireless Vantage Pro shown in Figure 3.4, measured and stored ambient air temperature, relative humidity, wind speed, wind direction, barometric pressure, precipitation (rainfall and rain rate), and solar radiation per minute. The traffic counter employed is a portable Peek ADR-1000, capable of counting vehicles per 5-minute intervals.

Figure 3.4 Weather Station and Traffic Counter

3.3.4 NITRATE ANALYSIS

The concentration of nitrates was measured in six predefined locations, three in the coated area and three in the uncoated area. Measurements were collected for three consecutive days during the study to identify evidence of photocatalytic degradation of NO_x. Nitrates accumulated on the pavement surface were measured by dissolving them in deionized water. To collect the nitrate on the pavement surface, 40 mL of DI water was poured into a 100 mm x 150 mm rectangle opening in a wooden device sealed with plumber putty as shown in Figure 3.5. After five minutes, the solution was collected via a syringe and filtered through a 0.45 μm filter into a polyethylene jar. Three samples were collected from both the coated and uncoated areas and

transported to the laboratory for immediate analysis. An increase in nitrates on the coated pavement would demonstrate evidence of photocatalytic reduction of NO_x.

Figure 3.5 Dissolving Nitrates in Water

3.4 RESULTS AND ANALYSIS

3.4.1 Direct Measurements of NO_x Reduction

Measuring the pollution reduction of NO_x continuously in the field often presents a challenge, due to a large number of influencing parameters, time, and costs. In order to limit the variation due to environmental parameters, NO_x concentrations were measured simultaneously for the coated and uncoated section, eliminating variables such as humidity, temperature, wind direction, and wind speed. However, it should be noted that the traffic count during the 5 minute period was not always equal for the two locations since there was a time lag between the time the car passes the counter and either of the NO_x sample lines. In addition, vehicles may park or be idle any time after passing the counter. Nevertheless, the difference between the coated and the uncoated section concentrations theoretically should represent the photocatalytic NO_x reduction. Using this assumption, the daily total NO_x reduction is presented in Figure 3.6. From the figure, it is evident that the total daily NO_x reduction varies significantly during the day. This illustrates

the difficulty in understanding the photocatalytic reductions from field studies. Reduction presented in Figure 3.6 correlates to approximately 0.019-0.13 mmol NO/m^2 of photocatalytic pavement reduced per day assuming that the reduction measured was from 2.5 cm radius circle around the sampling point.

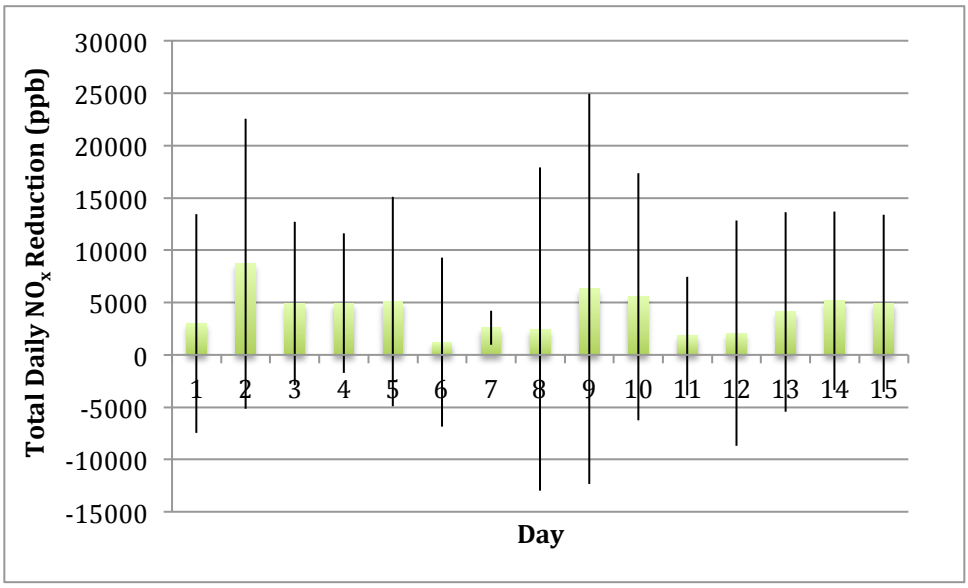

Figure 3.6 Daily NO_x Reduction

3.4.2 Indirect Evidence of NO_x Reduction Nitrate Analysis

For further evidence of a photocatalytic reduction, the nitrate accumulated on the pavement surface was measured for three locations in the coated area and three locations in the uncoated area. The increase of nitrates in the coated area is associated with photodegradation of NO_x. From the results shown in Figure 3.7, the first day had the most nitrates removed, due to a 4-week draught, in which the nitrates accumulated over time from the continuous photocatalytic degradation of NO_x. The second day, had slightly higher than the third day, since not all of the nitrates are eluted. Respectively, this equates to 0.204, 0.096, and 0.043 mmol NO/m^2 reduced.

These values are lower than what is calculated by the air since not all of the nitrates were eluted in the time allowed for the water sample collection.

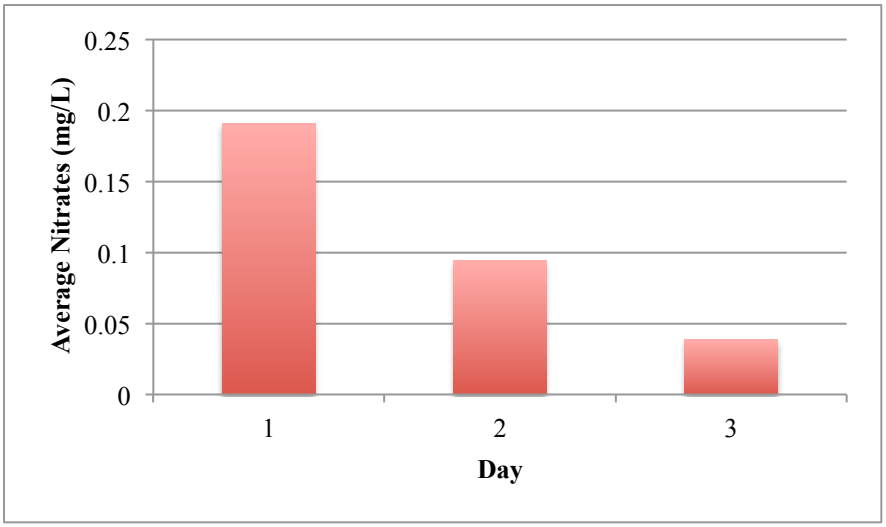

Figure 3.7 Average Nitrates Accumulated Due to Photocatalytic Degradation of NO_x

3.4.3 Variation of NO_x Reduction with Environmental and Operating Variables

To better understand field NO_x reductions, the effects of environmental parameters were investigated. To identify the influence of these parameters, photocatalytic degradation was plotted against each environmental factor including traffic. Figure 3.8 illustrates the average NO_x reduction observed over the three-week period plotted against its associated traffic count. The variation observed illustrates the influence of numerous factors including wind speed, vehicle type, humidity, and temperature on NO_x dispersion. Furthermore, it should be noted that the field site location had relatively low traffic concentrations explaining the low NO_x concentrations as well.

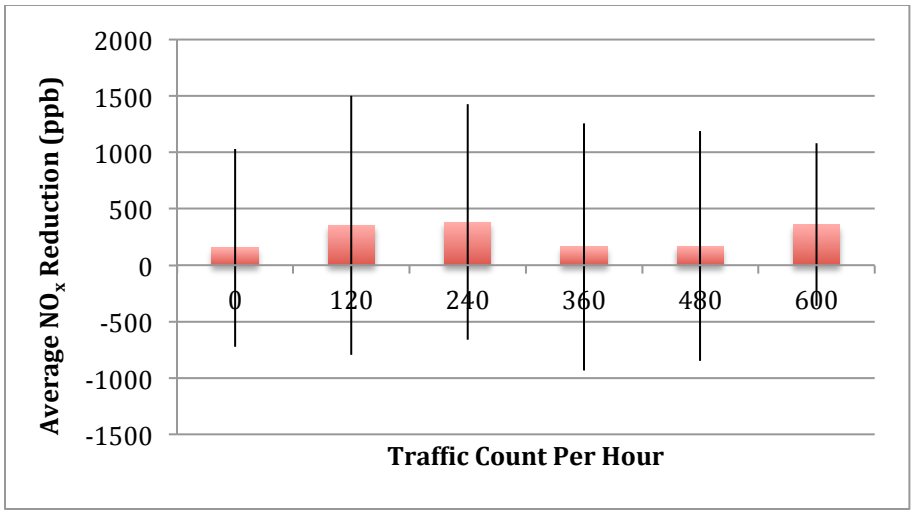

Figure 3.8 Variation of Average Hourly NO_x Reductions with Traffic Level

To evaluate the impact of various environmental parameters, the hourly average NO_x reduction was plotted against known environmental parameters; humidity, solar radiation, wind speed, and wind direction. Despite the impact of other variables, Figure 3.9 shows a clear trend, as the humidity increases, NO_x reduction decreases. Furthermore, this trend is consistent with previous laboratory studies results, which demonstrated the negative impact of relative humidity (Dylla et al. 2010).

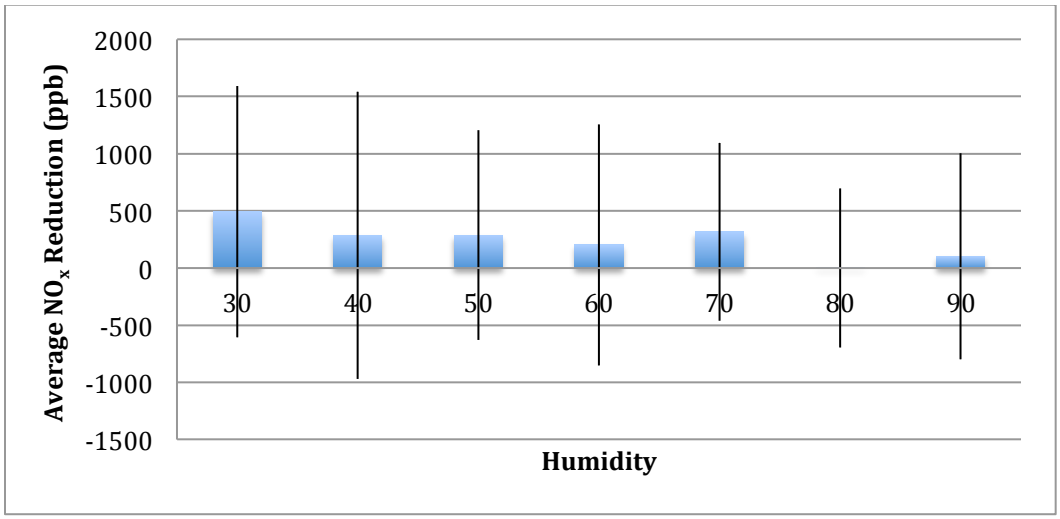

Figure 3.9 Variation of Average Hourly NO_x Reduction with Relative Humidity

Figure 3.10 illustrates the variation of the hourly average NO_x reduction with solar intensity. As shown in this figure, no clear trend is evident. However, by examining the impact of solar radiation hourly over a period of a day, where the relative humidity and wind speed was more stable, a correlation is evident, see Figure 3.11. As shown in Figure 3.11, as the solar radiation increases, the percent NO_x reduction also increases.

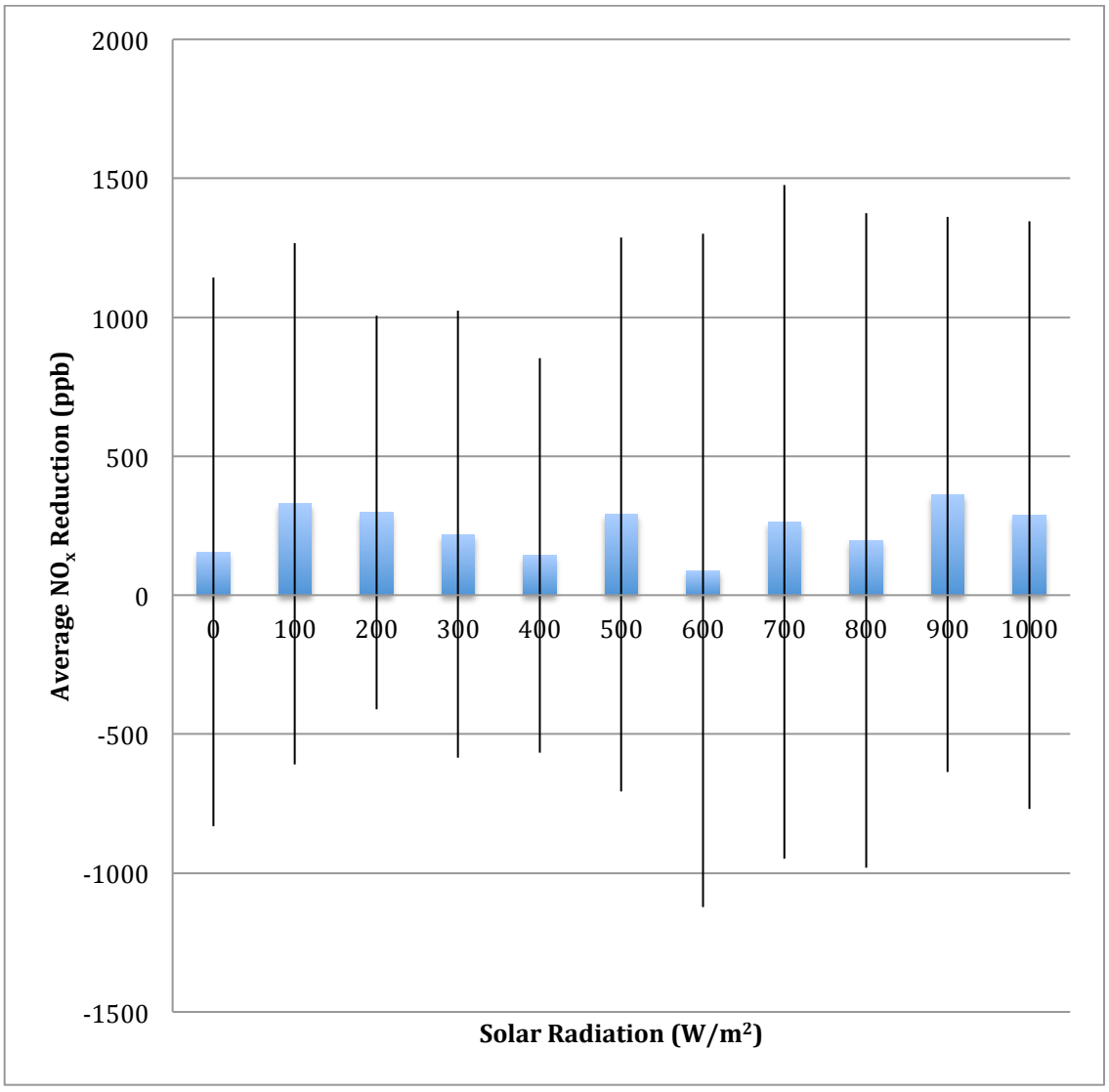

Figure 3.10 Variation of Average Hourly NO_x Reduction per Solar Radiation

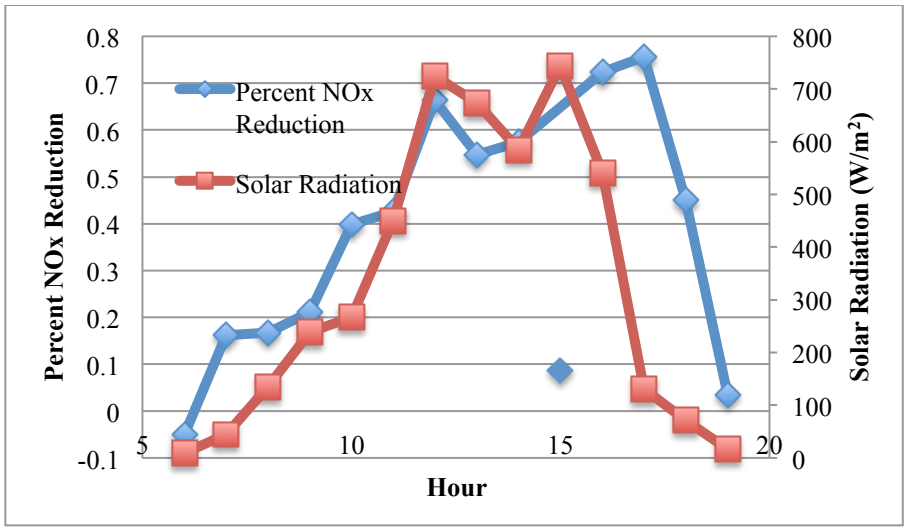

Figure 3.11 Daily Variation of Average NO_x Reduction Corresponding to Daily Variation of Solar Radiation

Figure 3.12 presents the influence of wind speed on the average NO_x reduction. As shown in this figure, a negative trend is associated with increasing wind speeds. As the wind speed increases, there is less pollutant contact time with the photocatalyst for a reaction to occur, thus, the photocatalytic reduction decreases (Dylla et al. 2010).

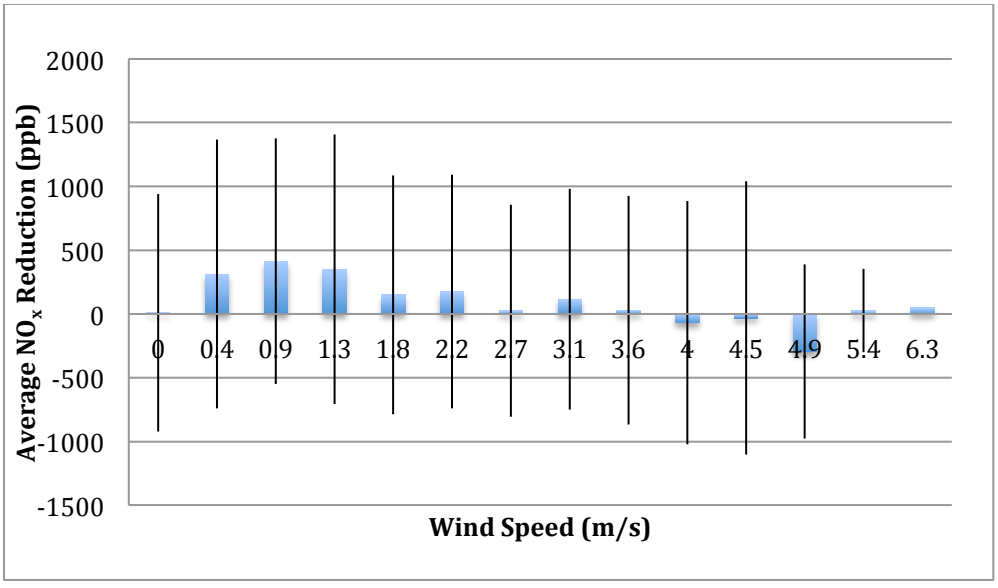

Figure 3.12 Variation of Average Hourly NO_x Reduction with Wind Speed

Figure 3.13 presents the influence of wind direction on photocatalytic efficiency. The wind direction influences the pollution concentration especially when the direction is downstream from the pollution point source. This may explain the large negative values in the Northeast direction. In addition, the wind direction changes the pollution dispersion characteristics especially as related to the contact time with the photocatalytic coating. For example, Northeast and Southwest wind directions are crosswinds compared to the road direction, and therefore, the pollutant contact time with the pavement is lower.

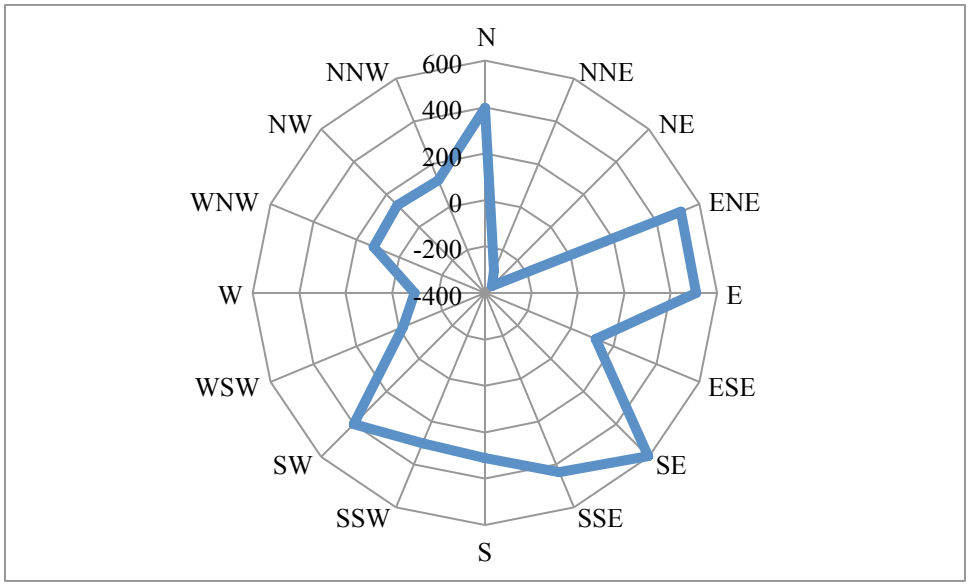

Figure 3.13 Variation of Average Hourly NO_x Reduction (ppb) with Wind Direction

3.5 SUMMARY AND CONCLUSIONS

The objective of this paper is to identify evidence of photocatalytic reductions in the field and to determine the significant environmental and operating factors that impact efficiency. A field study was conducted on a ¼-mile photocatalytic spray coated concrete road. Evidence of the photocatalytic reduction of NO_x was demonstrated by directly measuring NO_x reductions from

the air and by indirectly by measuring the nitrates deposited on the pavement surface. Based on the results of this study, the following conclusions were drawn:

- Results of the direct method and indirect methods of measuring photocatalytic degradation of NO_x show that there is evidence of a photocatalytic reaction occurring in the field.
- Environmental factors impacting photocatalytic efficiency are relative humidity, wind speed and direction, light intensity, and solar radiation. However, due to the variability demonstrated in the results, additional factors such as vehicle activity and vehicle classification need to be considered.

This study represents a step towards better evaluation of photocatalytic field studies and implementation of photocatalytic pavements as a feasible solution to mitigate near roadway air pollution problems. Based on the results presented in this study, further research is needed to identify additional significant factors including the impact of vehicle classification, and vehicle activity. In addition, the long-term effectiveness and durability of the photocatalytic coating in the field should be evaluated.

3.6 REFERENCES

Baldauf, R., Watkins, N., Heist, D., Bailey, C., Rowley, P., and Shores, R. (2009). "Near-road air quality monitoring: Factors affecting network design and interpretation of data." Air Qual Atmos Health, 2, 1-9.

Ballari, M.M., Hunger, M., Husken, G., and Brouwers, H.J.H.. (2010). "NO_x photocatalytic degradation employing concrete pavement containing titanium dioxide." Applied Catalysis B: Environmental, 95, 245-254.

Beeldens, A, Cassar, L and Murata, Y. (2011) "Applications of TiO_2 photocatalysis for Air Purification." RILEM, 23-35.

Beeldens, A. (2008). "Air purification by pavement blocks: final results of the research at the BRRC." Transport Research Arena Europe, Ljubljana.

Beeldens, A. (2006) "An environmental friendly solution for air purification and self-cleaning effect: the application of TiO_2 as photocatalyst in concrete." Belgian Road Research Centre. Proceedings of Transport Research Arena, Europe - TRA, Göteborg, Sweden, June, 2006.

Bhatia R. and Rivard T. (2007) "Assessment and Mitigation of Air Pollutant Health Effect from Intra-urban Roadways: Guidance for Land Use Planning and Environmental Review." Department of Public Health, San Francisco, 1-32.

Chen, M. and Chu, J.-W. (2011). "NO_x photocatalytic degradation on active concrete road surface - from experiment to real-scale application." Journal of Cleaner Production, 19, 1266-1272.

Dylla, H., Hassan, M. M., Mohammad, L., Rupnow T., and Wright, E. (2010). "Evaluation of the Environmental Effectiveness of Titanium Dioxide Photocatalyst coating for concrete pavements." Journal of the Transportation Research Record, 2164, 46-51.

Health Effects Institute (HEI). (2010) "Traffic-Related Air Pollution: A Critical Review of the Literature on Emissions, Exposure, and Health Effects." Special Report 17, 2010.

Hunger, M., Husken, G., and Brouwers, J. (2010). "Photocatalytic degradation of air pollutants – From modeling to large scale application." Cement and Concrete Research, 40, 313-320.

Kim, J.J., Smorodinsky, S., Lipsett, M., Singer, B. C., Hodgson, A.T., and Ostro, B. (2004). "Traffic-related air pollution near busy roads: the East Bay Children's Respiratory Health Study." American Journal Respiratory and Critical Care Medicine, 170, 520-536.

Kuhns, H.D., Mazzoleni, C., Moosmuller, H., Nikolic, D., Keislar, R.E., Barber, P.W., Li, Z., Etyemezian, V., and Watson, J.G. (2004). "Remote sensing of PM, NO, CO, HC emission factors for on-road gasoline and diesel engine vehicles in Las Vegas, NV." Science of the Total Environment, 322, 123-137.

Li, L. and Qian, C. (2009). "A lab study of photo-catalytic oxidation and removal of nitrogen oxides in vehicular emissions and its fieldwork on Nanjin No.3 bridge of Yangtze River." Journal of Pavement Resource Technology, 2(5), 218-222.

Louisiana Department of Environmental Quality (DEQ). (2006) "Ambient Air Data Sets," Ambient Air Monitoring Data and Reports, 2006. <http://www.deq.louisiana.gov/portal/DIVISIONS/Assessment/AirFieldServices/AmbientAirMonitoringProgram/AmbientAirMonitoringDataandReports.aspx> (March 6, 2011).

Maggos, T., Plassais, A., Bartzis, J.G., Vasilakos, C, Moussiopoulos, A. and Bonafous, L. (2008). "Photocatalytic degradation of NO_x in a pilot street canyon configuration using TiO_2-mortar panels." Environmental Monitoring Assessment, 136, 35-44.

McConnell, R., Islam, T., Shankardass, K., Jerrett, M., Lurmann, F., Gilliland, F., Gauderman, J., Avol, E., Kuenzli, N.,Yao, L., Peters, J., and Berhane, K.. (2010). "Childhood Incident Asthma and Traffic-Related Air Pollution at Home and School." National Institute of Environmental Health Sciences, 1-33.

Menz, F.C. (2002). "The US experience with controlling motor vehicle pollution: lessons for China." International Journal Environment and Pollution, 18(1), 1-21.

U.S. Census Bureau. (2009). "American Housing Survey," <http://www.census.gov/hhes/www/housing/ahs/nationaldata.html> (June 7, 2011).

United State Environmental Protection Agency (EPA). (2007) "Air Pollution Control Orientation Course." <http:// www.epa.gov/air/oaqps/eog/course422/ce4b.html> (March 6, 2011).

United State Environmental Protection Agency (EPA). (1999). Atmospheric Sampling. ICES Ltd, North Carolina.

United States Environmental Protection Agency (EPA). (2008). "Mobile Source Emissions- Past, Present, and Future." <http://www.epa.gov/otaq/invntory/overview/pollutants/index.htm> (May 5, 2011)

Vette A. (2010). "Near-Road Air Pollution." U.S. Environmental Protection Agency. Clean Air Research. <http://www.epa.gov/airscience> (June, 7 2007).

Zhao, J. and Yang, X. (2003). "Photocatalytic oxidation of indoor air purification: a literature review." Building and Environment, 38, 645-654.

CHAPTER 4
EFFECT OF VEHICLE CLASSIFICATION AND ACTIVITY ON FIELD EVALUATION OF PHOTOCATALYTIC CONCRETE PAVEMENTS' ABILITY TO REMOVE NITROGEN OXIDES

4.1 INTRODUCTION

Nitrogen oxide (NO_x) is a group of highly reactive gases, nitric oxide (NO) and nitrogen dioxide (NO_2), which have been correlated with adverse health and environmental impacts. Consequently, NO_2 is one of six criteria pollutants that the Environmental Protection Agency (EPA) is required to set National Ambient Air Quality Standards (NAAQS) under the Clean Air Act. The NAAQS for NO_2 has traditionally been an annual arithmetic average of 53 ppb; however, EPA developed an additional 1-hour standard due to the increasing scientific evidence of adverse health effects from NO_2 exposure as short as 30 minutes (EPA[a] 2012; EPA[b] 2012). This standard requires a 100 ppb daily hourly maximum averaged from the 98th percentile over 3 years (EPA[c] 2012). In addition to the new 2010 NO_2 1-hour standard, EPA requires ambient air monitoring and reporting for NO_2 from locations where maximum concentrations are expected. Near major roadways in urban areas is one of the expected locations. Although EPA found no area is violating the 2010 NAAQS for NO_2 according to the most recent survey from 2008-2010, this data does not include the new monitoring cites near roadways (EPA[d] 2012).

As a result, there has been an increasing interest in photocatalytic pavements to mitigate mobile emissions from roadway microenvironments. Photocatalytic pavements have a surface layer with titanium dioxide (TiO_2) nanoparticles, which when irradiated with ultraviolet light from the sun it decomposes pollutants to nonhazardous waste products (Zhao and Yang 2003; Ballari et al. 2010). Laboratory results show that photocatalytic pavements may reduce pollutants such as NO_x by 40% to 85% once pollutants are emitted in the air (Beeldens 2006). In

addition, photocatalytic pavements have the advantage of being a cost-effective air pollution abatement technique since they may be applied only to target areas.

In order to be cost-effective, knowledge of NO_x reduction efficiencies under various environments and operating conditions in larger scales must be understood. Several field studies have been conducted using various approaches in effort to study the photocatalytic reduction in real world settings (Maggos et al. 2008; Maggos et al. 2007; Beeldens 2008; Chen and Jiang-Wei 2011; Li and Qian 2009). Despite this, the understanding of large-scale photocatalytic efficacies is limited due to high experiment costs, the large number of significant parameters and no testing standards. Significant known parameters impacting the efficiency of NO_x reduction include humidity, concentration, temperature, light intensity, and wind speed (Sleiman et al. 2009; Hunger et al. 2010; Bengtsson and Castellote 2010). Previous field study results confirmed that relative humidity, wind speed and direction, light intensity, and solar radiation impact the NO_x reduction measured in the field; however, measurements were not able to identify a clear reduction (Dylla et al. 2012). The researchers suggested that unknown additional parameters such as vehicle activity and classification might significantly impact photocatalytic efficiency. Previous studies that showed reductions, also did not consider these potential factors: vehicle activity or classification (Beeldens 2006; Beeldens 2008; Li and Qian 2009; Chen and Jiang-Wei 2011).

Therefore, the objective of this study is to evaluate the effects of vehicle activity and classification on NO_x pollution emitted and its correlation to the NO_x reduction from photocatalytic pavements. The impact of vehicle activity and class on the concentration of NO_x emitted was investigated and how these two parameters, neglected from previous field studies, may impact interpretation of results from photocatalytic field studies. To achieve this objective,

an aqueous solution containing 2% nano-TiO_2 was applied on 6 meters of concrete pavement. NO_x concentrations were continuously monitored and recorded for the photocatalytic-coated area and for a control area simultaneously to quantify any photocatalytic reductions. The climatic conditions were monitored and a detailed traffic study was conducted to identify any correlations. Results of this study will assist the development of forthcoming photocatalytic field studies in the quest to understand larger scale efficiencies and where photocatalytic pavements may prove most useful.

4.2 BACKGROUND

Two techniques to measure photocatalytic degradation from field studies have been used. The first is to directly measure the pollutant reduction in the ambient air and the second is to indirectly quantify the reduction by measuring the byproducts created to calculate the reduction using stoichiometry. To directly measure the reduction of NO_x, the approved method of ambient air monitoring is chemiluminescence (EPA 2002). The indirect technique to measure photocatalytic reductions of NO_x is to measure nitrates (NO_3^-) and nitrites (NO_2^-) deposited on the pavement surface. Nitrates and nitrites are water-soluble and are easily washed from the surface (Beeldens 2008). EPA approved methods to measure nitrate and nitrite ions in water include cadmium reduction or ion chromatography (EPA 1993; EPA 1997).

Field studies have used both indirect and direct measuring techniques. Beeldens 2008 and Osborn et al. 2012 both used nitrates to estimate the photocatalytic reduction of NO_x. Using this method water samples are collected at least daily and analyzed for nitrates and nitrites (Osborn et al. 2012). Beeldens (2006) estimated that the overall reduction of NO_x over a year period is 20%. While the indirect method shows evidence of a photocatalytic reduction, because it cannot be continuously monitored, it does not capture the environmental variability essential

for understanding photocatalytic reduction of NO_x in real world environments. Therefore, the direct technique for measuring photocatalytic reductions using continuous emission monitors is preferred.

Few field studies directly measured the photocatalytic reduction using continuous emission monitors due to the significant investment in equipment required. In order to determine the photocatalytic reduction, simultaneous measurements are preferred to eliminate environmental variability. Therefore, at minimum, one NO_x analyzer is required to continuously measure the NO_x concentrations for a photocatalytic pavement area while a second is required to continuously measure the NO_x concentrations for a control area. Using this methodology, Beeldens (2008) reported that photocatalytic pavements have the potential to decrease emission spikes in air. Due to the limited time period of the study, no correlations to environmental conditions were made. In efforts to correlate NO_x reduction effectiveness to environmental conditions, previous work by the authors monitored the traffic and climatic conditions. Results confirmed that relative humidity, wind speed and direction, light intensity, and solar radiation all impact the NO_x reduction. Despite this, there was no clear evidence of a photocatalytic reduction due to additional unknown parameters such as differing vehicle activity and vehicle classification between the two areas (Dylla et al. 2012). Moreover, this parameter could have significantly impacted results and conclusions from similar field studies that have reported photocatalytic reductions from field settings. This includes the study by Beeldens (2006) that used an area with parking nearby and the study completed by Li and Qian (2009) that used a tollbooth area. Both of these areas have the potential to have been unknowingly impacted significantly by vehicle activity and classification.

Vehicle traffic emissions vary by both vehicle classification and by vehicle activity. While driving, vehicles cycle between stopping, starting, idle, cruising, accelerating, and decelerating. During this time, the NO emitted varies depending on the drive cycle (Frey et al. 2003). The EPA monitors these emissions and has developed a modeling system to predict emission factors per vehicle type and activity. The motor vehicle emission simulator (MOVES) is the latest version that was released in 2010 (Papson et al. 2012).

4.3 EXPERIMENTAL PROGRAM

The field study consisted of an 18.3-meter concrete pavement roadway located on Raphael Semmes Road on Louisiana State University's campus in Baton Rouge, LA. Because this is an already existing roadway, the photocatalytic coating was applied using the spray coat technique. The coated section was 3.7 meter wide being the width of the lane, by approximately 6 meters long. A control area of a similar size was separated from the photocatalytic coated area by approximately 6 meters; thus allowing for approximately 9 meters between the two sampling lines (Figure 4.1). The test equipment is housed in a trailer, centrally located, such that NO_x concentrations can be simultaneously measured from both the coated and uncoated areas. To characterize environmental conditions, NO_x ambient air pollution and climatic factors were collected directly from the field site. To address possible variation in the traffic from a nearby parking area; a traffic study was conducted to identify vehicle speed, activity, and vehicle classification for both areas. Results from the traffic study were used to understand the difference in NO_x emitted in the photocatalytic coated area versus the control area by estimating the emission rates using MOVES. Furthermore, a correlation study was conducted to determine the significance of the vehicle activity and class.

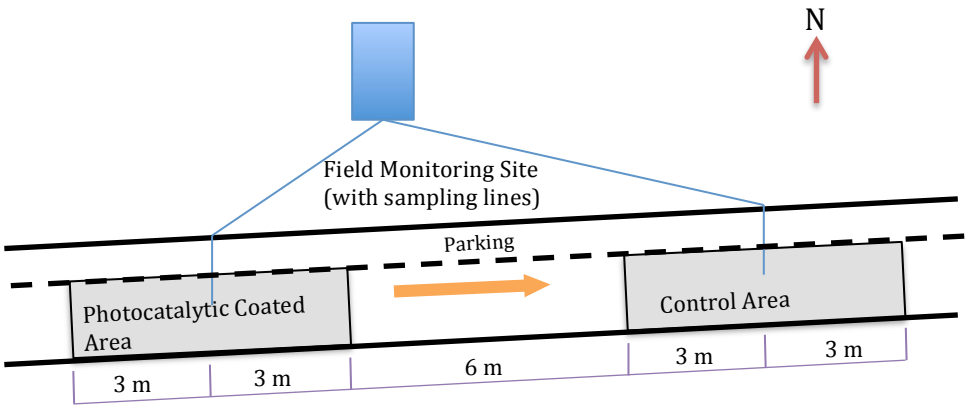

Figure 4.1 Field Site Location and Ambient Air Monitoring Equipment

4.3.1Field Photocatalytic Spray Coat Application

In preparation for TiO_2 spray application, the 3.7 by 6 meter area to be coated was divided into 0.6 m x 0.6 m grid. Before application, the roadway was cleared of any debris by sweeping. The spray coat consisted of anatase TiO_2 nanoparticles suspended in an aqueous binder at 2% by volume. The spray coat was applied using a hand spray gun (Figure 4.2) using a crosshatch formation at 100 ml/m^2. Therefore, 36 ml of sample was measured out for each 0.6 m x 0.6 m square of the grid. This equates to a 0.21 mg/cm^2 catalyst-loading rate. In real world applications, a distributer truck with nozzles with electrostatic precipitators, mitigating nanoparticle agglomeration, would apply the spray coat as presented elsewhere (Dylla et al. 2012).

4.3.2 Environmental Conditions Detection

Environmental conditions were recorded during the monitoring period. Weather data was collected and stored in order to interpret different trends in the measurements. The weather station utilized, Davis 6152 Wireless Vantage Pro, measured and stored ambient air temperature, relative humidity, wind speed, wind direction, barometric pressure, precipitation (rainfall and rain rate), and solar radiation per minute.

Figure 4.2 TiO_2 Spray Coat Application

4.3.3 Traffic Study

Due to the possible irregularity of the traffic in the field study area, a manual traffic study was conducted during the monitoring period to detect differences in vehicle classification, activity, and counts between the photocatalytic area and the control area. The traffic data was collected for the photocatalytic coated area and the control area separately per minute to align with the NO_x concentration measurements. Since the photocatalytic pavement requires sunlight, data was collected from dawn to sunset summing to a week. A tally sheet was used to classify the vehicle type and estimate vehicle speed.

The vehicle types were classified according to the EPA Motor Vehicle Emission Simulator (MOVES) source types. Only the transit bus and short haul trucks were used since it was difficult to differentiate between the various bus source types and between short and long haul trucks defined by MOVES. Therefore, the resulting MOVES source types identified for the traffic study are shown in Table 4.1 with the Highway Performance Monitoring System (HPMS) equivalents (EPA 2009). Vans and SUVs were considered as part of the passenger truck source type according to the HPMS other 2 axle-4 tire vehicle definition (FHWA 2010). Commercial

trucks and vans were considered as part of the light commercial truck source type. The speed limit of the roadway is 16 km/h. Therefore, the vehicle speed was separated according to the MOVES speed bins shown in Table 4.2 with the addition of idling.

Table 4.1. Vehicle Classification MOVES Correlated to HPMS

Source Type ID	Source Types	HPMS Vehicle Type ID	HPMS Vehicle Type
11	Motorcycle	10	Motorcycles
21	Passenger Car	20	Passenger Cars
31	Passenger Truck	30	Other 2 axle-4 tire vehicles
32	Light Commercial Truck	30	Other 2 axle-4 tire vehicles
42	Transit Bus	40	Buses
52	Single Unit Short-haul Truck	50	Single Unit Trucks
61	Combination Short-haul Truck	60	Combination Trucks

Table 4.2. MOVES Speed Bins

Bin	Average Speed (km/h)	Average Speed Range (km/h)
0	0	Idling
1	4.0	speed < 4.0 km/h
2	8.0	4.0 km/h <= speed < 12.0 km/h
3	16.0	12.0 km/h <= speed < 20.1 km/h

4.3.4 Moves Emission Calculations

To gain a better understanding of the NO_x emitted from the field site area, the field site weather and traffic data was used to create a project level database for MOVES to calculate the hourly emission rates. The project level consisted of two links, one being an urban unrestricted road and the second being the off network portion for the parking spaces. The off-network startup fraction, the number of startups per hour over the population of vehicles during the hour, were estimated by the parking meter data by assuming the end time of the parking meter was when the car started up. Since the traffic study was completed for the photocatalytic area and control area separately, the emission rates were calculated for both test areas separately. This allowed for considering the impact of the irregularity of the traffic over the two sections on the NO_x

pollution. MOVES default settings were used for the fuel formulation, fuel supply, age-distribution and operating mode, which was calculated by the average speed methodology. The average speed was assumed to be 16 km/h being the speed limit.

4.4.5 NO_x Ambient Air Detection

NO_x concentrations were monitored for both the coated and uncoated sections, simultaneously using Thermo NO_x analyzers. The NO_x analyzers meet the USEPA requirements for RFNA-1289-074 and were calibrated in accordance to EPA standards using the gas phase titration (GPT) method (EPA 2002; EPA[e] 2012). A zero-span check was conducted regularly for quality control as recommended by EPA to ensure proper calibration and operation of the equipment (EPA 2002). Equipment was recalibrated when the percent error was over 5%.

The sample lines were located at the pavement level centered in the photocatalytic area and control area as shown in Figure 4.1 and pictured in Figure 4.3. To withstand the traffic, the sample lines were made of 316 stainless steel, an approved material for NO_x sampling. NO, NO_2, and NO_x concentrations were continuously measured and were stored as minute averages. During events of heavy rain, sampling was discontinued to protect the equipment.

Figure 4.3 NO_x Air Sampling Line

4.4.6 Correlation Analysis

The recorded NO_x reduction was correlated with vehicle speed and vehicle classification, using the Pearson Correlation Coefficients. The Pearson Correlation Coefficient and the associated p-value were calculated using SAS.

4.5 RESULTS AND ANALYSIS

4.5.1 Traffic Study Vehicle Class

Results from the traffic study illustrate that there is minor variation between the hourly average traffic counts over the control section and the photocatalytic section. Figure 4.4 represents the total average vehicle count and distribution of the MOVES vehicle classes as defined in Table 4.1 per hour determined by the traffic study for both the control and photocatalytic test sections. As shown in Figure 4.4, the majority of the traffic is passenger cars and trucks. The vehicle classification does not change significantly from hour to hour. The peak traffic is around 13:00 reaching 143 total vehicles for the control area and 150 total vehicles for the photocatalytic pavement area. In general, the photocatalytic coated area had a slightly higher hourly vehicle count. This is reasonable due to the vehicles parking before reaching the control area.

Figure 4.5 illustrates the off-network portion average startup fraction estimated from the parking meter data. As expected, the photocatalytic section and the control section startup fractions are different complicating interpretation of NO photodegradation results.

To understand the significance of this variation, these results were incorporated into MOVES to characterize the difference in emissions rates. Figure 4.6 illustrates NO and NO_2 emission factors predicted for the photocatalytic and control sections from MOVES. As shown in this figure, the results show that the NO_x pollution emitted from the vehicles in this area is not significant. The highest amount of NO_x emitted in either the control or the photocatalytic area

due to the traffic was no more than 5 grams over an hour. However, it is clear that the photocatalytic section had higher predicted NO_x pollution emissions compared to the control section. The difference in NO_x concentrations emitted in the two areas could mislead the results. Higher concentrations being emitted in the photocatalytic section could be offsetting or reducing any NO_x reduction calculated.

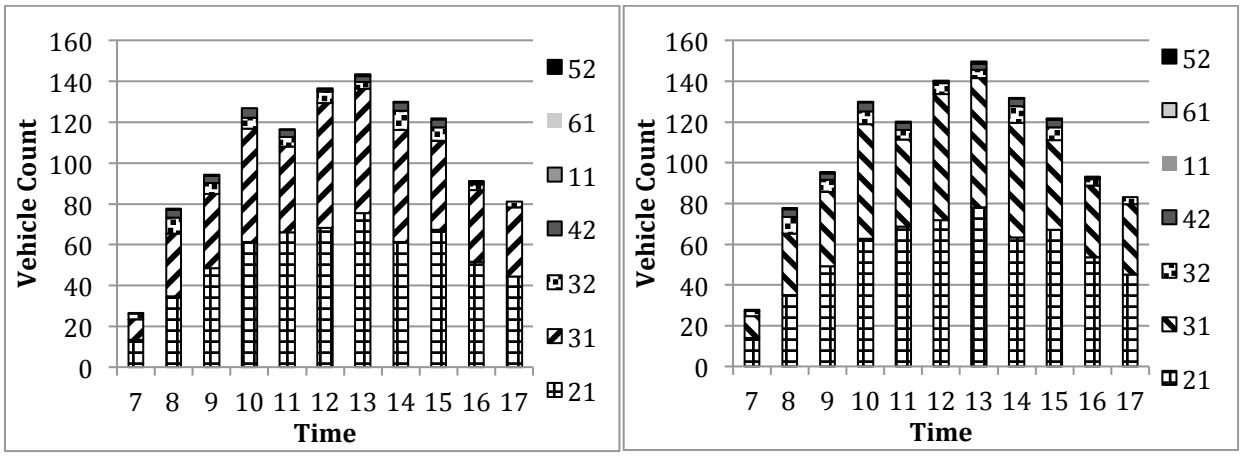

(a) (b)

Figure 4.4 Vehicle Classification per Hour as Defined in Table 4.1; (a) Control, (b) Photocatalytic

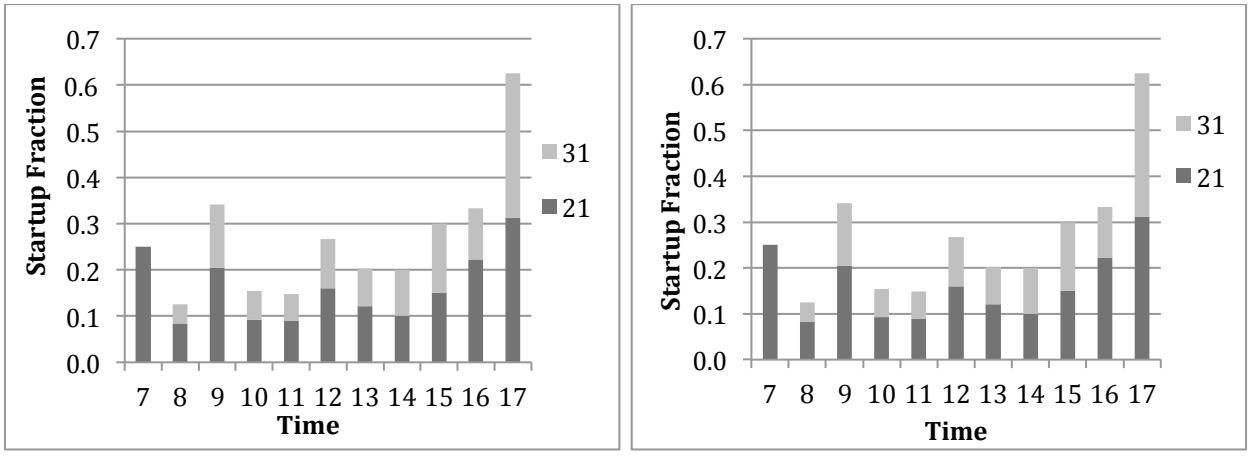

(a) (b)

Figure 4.5 Vehicle Startup Fractions per Vehicle Classification as Defined in Table 4.1; (a) Control, (b) Photocatalytic

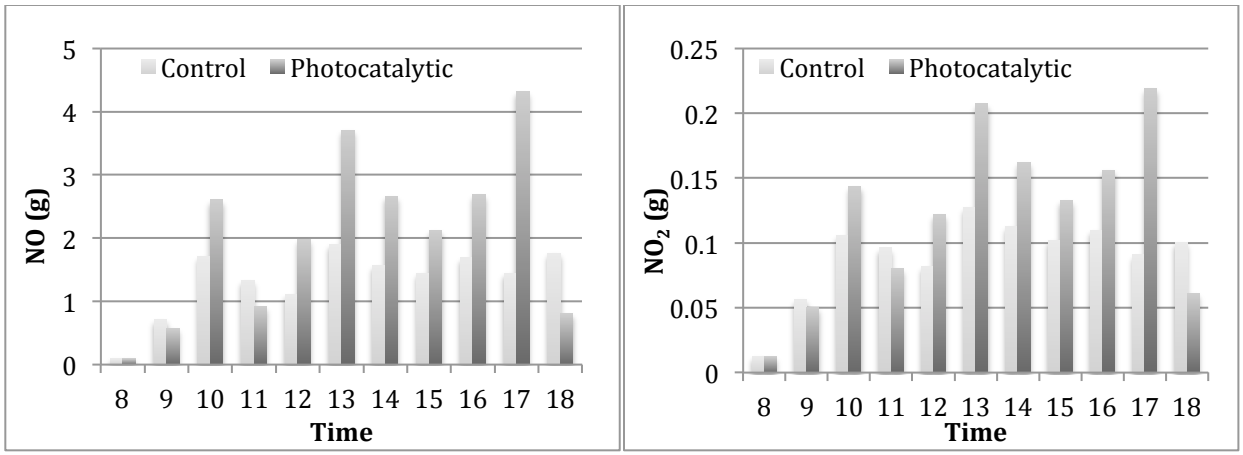

(a) (b)

Figure 4.6 MOVES Predicted Emission Factors; (a) NO, (b) NO_2

Figure 4.7 compares the difference of the vehicle counts previously discussed in relation to the difference of the predicted NO_x emissions for the photocatalytic area versus the control area. From this figure, it is evident that even though there is only a slight difference in the vehicle counts, there is a signficant difference in the predicted NO_x emitted especially when compared to the low total predicted NO_x emissions. However, not all of the differences seem to be related to the vehicle counts. As a result, Figure 4.8 compares the difference in startup fractions in relation to the difference in the predicted NO_x emissions for the photocatalytic section versus the control section. The startup fractions further explain the differences in hourly pollution emission rates predicted. For example at time 10 and 17, although there was more traffic on the photocatalytic section, there was more startups in the control section resulting in NO_x predicted higher emissions in the control section.

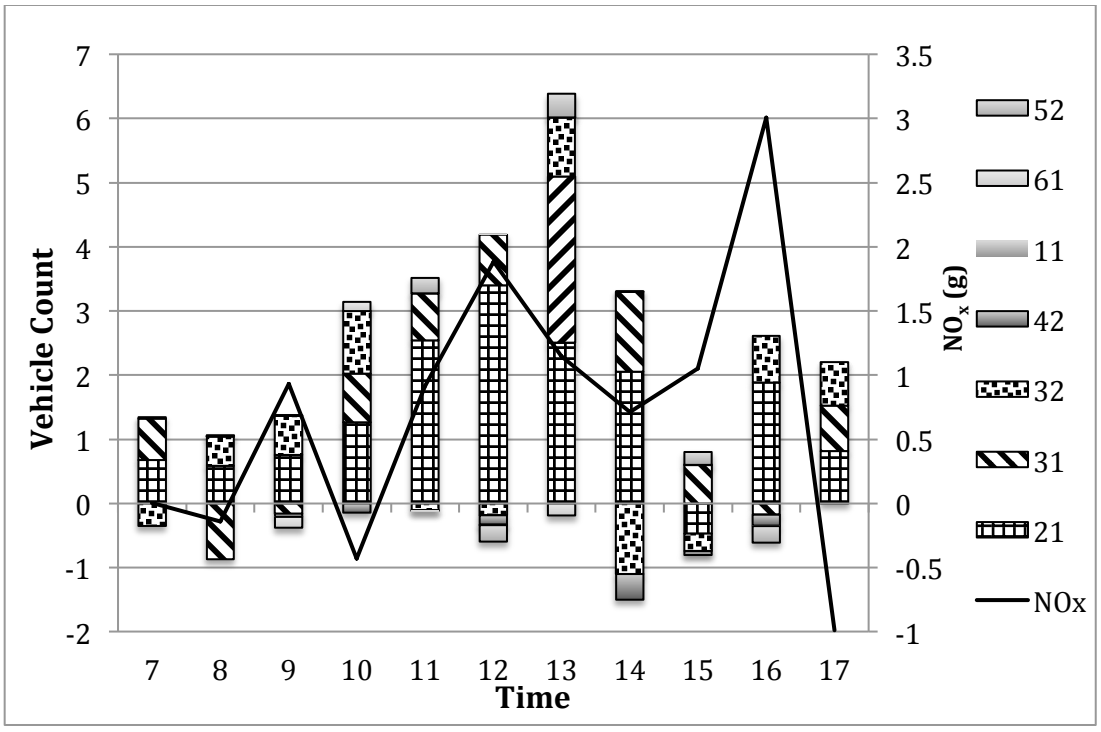

Figure 4.7 Difference Vehicle Count, Classification (Table 4.1) and MOVES Predicted NO_x Emissions in Photocatalytic Area from Control Area

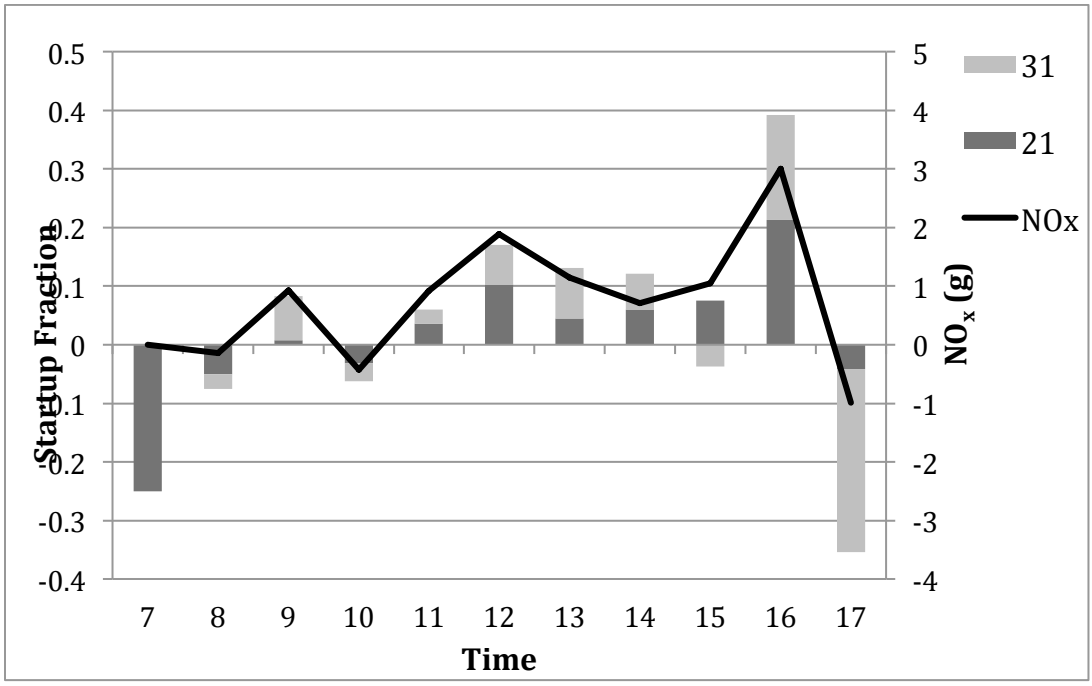

Figure 4.8 Difference Startup Fractions by Vehicle Classification (Table 4.1) and MOVES Predicted NO_x Emissions in Photocatalytic Area from Control Area

4.5.2 Hourly NO_x Reduction Recorded

With these results, it is not surprising that the average hourly NO_x reduction recorded in the field study is not easily comprehensible. Figure 4.9 details the average NO_x reduction recorded in the field compared to the difference in the predicted NO_x emissions. Only at time 10, 13, and 14, a significant NO_x reduction was recorded. During the remaining hours, the NO_x reduction could have been masked by the higher NO_x pollution in the photocatalytic coated section.

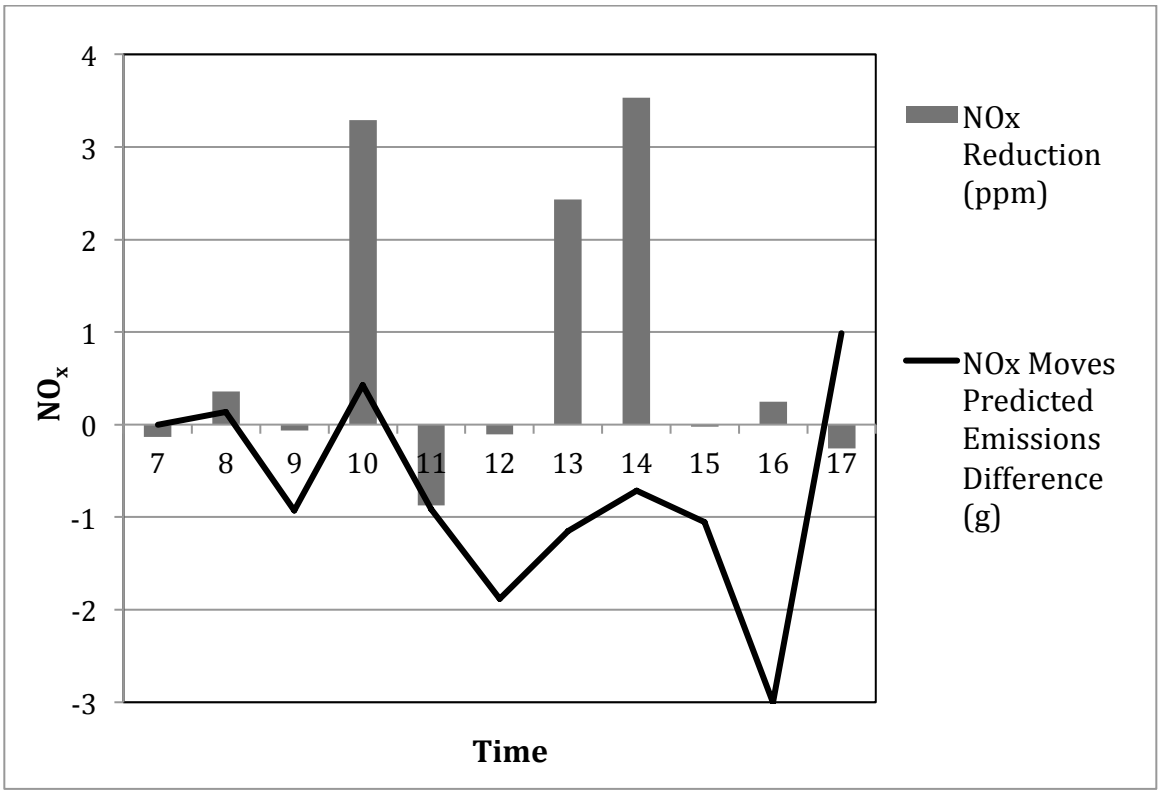

Figure 4.9 NO_x Reduction Compared to MOVES Predicted Emission

4.5.3 NO_x Reduction Correlation

The Pearson's coefficient of correlation was calculated to evaluate the degree of linear association between the NO_x reduction and the difference in vehicle class and vehicle speed recorded for the photocatalytic and control sections per minute. Thus, whether the difference in vehicle activity had a significant impact on the interpretation of the NO_x reduction recorded can

be evaluated. The coefficient of correlation was calculated for the vehicle class, vehicle speed, and combination of the two parameters. The results from the pairwise correlation for the vehicle class and vehicle speed are presented in Tables 4.3 and 4.4, where the coefficients of correlation and the p-values are provided. The lower is the p-value; the stronger is the linear association. For the Pearson's coefficient, numbers closer to 1 represent a positive linear relationship, -1 a negative linear relationship, and 0 no linear relationship.

Table 4.3. Pearson Correlation Coefficients for Vehicle Class

Source Type ID	Source Types	Pearson's Coefficient	P-value
11	Motorcycle	.	.
21	Passenger Car	0.0081	0.6553
31	Passenger Truck	-0.05516	0.0023
32	Light Commercial Truck	-0.00849	0.6397
42	Transit Bus	0.03379	0.0623
52	Single Unit Short-haul Truck	0.00029	0.9872
61	Combination Short-haul Truck	-0.00323	0.8586

Table 4.4. Pearson Correlation Coefficients for Speed Bins

Bin	Pearson's Coefficient	P-value
0	0.02282	0.2081
1	-0.02784	0.1246
2	-0.00077	0.9660
3	-0.00828	0.6477

In Table 4.3, none of the vehicle classes are significantly linearly associated with the NO_x reduction. Furthermore, vehicle classes, as a sole parameter, did not fully explain the NO_x reduction. From Table 4.3, the strongest linear correlation is a weak negative correlation between the NO_x reduction and MOVES source 31, the passenger truck, with a p-value of 0.0023. Therefore, when the control section had higher passenger trucks recorded compared to

the photocatalytic section the NO_x reduction was decreased. Unfortunately, this is not logical suggesting that there is another significant parameter that was not accounted in the model.

In Table 4.4, the correlation coefficients for the speed on the NO_x reduction are reported. None of the parameters are significantly linearly associated with the NO_x reduction. The results of the correlation between all of the parameters combined also showed no correlation. As a result, this suggests that the vehicle emissions are not the main source of pollution for this field study. This is further supported by the MOVES results, which predicted very low amounts of NO_x emitted.

4.6 CONCLUSIONS

The objective of this study was to evaluate the effects of vehicle activities and classification on NO_x pollution emitted and to correlate these factors to the NO_x reduction from photocatalytic pavements. To achieve this objective, a field study was conducted with 22.3 m^2 of photocatalytic spray coated area and 22.3 m^2 of uncoated control area. Evidence of the photocatalytic reduction of NO_x was evaluated by directly measuring NO_x reductions from the air. A traffic study was conducted for the photocatalytic control areas to characterize the variability in traffic classification and activity between the two areas and its effects on interpreting NO_x reduction. Based on the results of this study, the following conclusions were drawn:

- The highest amount of NO_x emitted in either the control or the photocatalytic sections due to traffic was predicted by MOVES to be no more than 5 grams over an hour period. Therefore, NO_x pollution emitted from the vehicles in this area is not a significant pollution source.
- Due to the low values of pollution emitted in the both the photocatalytic area and the control area, minor differences in traffic activity between these two areas resulted in

significant differences in the amount of pollution emitted between the photocatalytic and the control areas. This may complicate the interpretation of the NO_x reduction results.

- There was no significant linear correlation of vehicle class and speed and NO_x reduction.

This study provides valuable insight on conducting photocatalytic field studies during a time in which many state agencies are developing field studies of their own. While previous studies by researchers have shown evidence of the photocatalytic degradation of NO_x based on nitrate surface measurements, further research is still needed to identify relationships between environmental parameters in the field and their effects on NO_x photocatalytic degradation. In spite of the inconclusive results, valuable lessons were learned, which could improve future photocatalytic field studies. First, the field study area should be in an area where traffic pollution is determined as a major source of pollution. Second, the control area and photocatalytic area should be in an area that minimizes variability in traffic activity. In addition, the development of theoretical kinetic studies, which may provide an alternative avenue to understanding the significance of NO_x reduction in field studies through chemodynamic modeling, is needed.

4.7 REFERENCES

Ballari, M.M., Hunger, M., Husken, G., and Brouwers, H.J.H.. (2010). "NO_x photocatalytic degradation employing concrete pavement containing titanium dioxide." Applied Catalysis B: Environmental, 95, 245-254.

Beeldens, A. (2006) "An environmental friendly solution for air purification and self-cleaning effect: the application of TiO_2 as photocatalyst in concrete." Belgian Road Research Centre. Proceedings of Transport Research Arena, Europe - TRA, Göteborg, Sweden, June, 2006.

Beeldens, A. (2008). "Air purification by pavement blocks: final results of the research at the BRRC." Transport Research Arena Europe, Ljubljana.

Bengtsson, N. and Castellote, M. (2010). "Photocatalytic activity for NO degradation by construction materials: parametric study and multivariable correlations." Journal of Advance Oxidation Technologies, 13(3), 341-349.

Chen, M. and Chu, J.-W. (2011). "NO_x photocatalytic degradation on active concrete road surface - from experiment to real-scale application." Journal of Cleaner Production, 19, 1266-1272.

Dylla, H., Hassan, M. M., and Osborn, D. (2012). "Field Evaluation of Photocatalytic Concrete Pavements' Ability to Remove Nitrogen Oxides." Journal of the Transportation Research Record, 2290, 154-160.

Environmental Protection Agency (EPA[a]). (2012). "Nitrogen dioxide implementation – Programs and requirements for reducing oxides of nitrogen." Nitrogen Dioxide. <http://www.epa.gov/air/nitrogenoxides/implement.html.> (July 17, 2012).

Environmental Protection Agency (EPA[b]). (2012). "Nitrogen dioxide designations." <http://www.epa.gov/airquality/nitrogenoxides/designations/> (July 17, 2012).

Environmental Protection Agency (EPA[c]). (2012). "Nitrogen dioxide (NO_2) Standards – Table of Historical NO_2 NAAQS." National Ambient Air Quality Standards. <http://www.epa.gov/ttn/naaqs/standards/nox/s_nox_history.html> (July 17, 2012).

Environmental Protection Agency (EPA[d]). (2012). "Fact sheet – Air Quality Designations for the 2010 Primary Nitrogen Dioxide (NO_2) National Ambient Air Quality Standards." 20120120FS. <http://www.epa.gov/no2designations/pdfs/20120120FS.pdf> (July 17, 2012).

Environmental Protection Agency (EPA[e]). (2012). "List of Designated Reference and Equivalent Methods." <http://www.epa.gov/ttn/amtic/criteria.html> (November 6, 2012)

Environmental Protection Agency (EPA). (2009). Draft MOVES2009 Highway Vehicle Population and Activity Data. EPA-420-P-09-001.

Environmental Protection Agency (EPA). (2002). Draft Quality Assurance Guidance Document 2.3: Reference Method for the Determination of Nitrogen Dioxide in the Atmosphere (Chemiluminescence).

Environmental Protection Agency (EPA). (1993). Method 300.0: Determination of inorganic anions by ion chromatography. Revision 2.1.

Environmental Protection Agency (EPA). (1997). Method 353.2: Determination of nitrate-nitrite nitrogen by automated colorimetry. Revision 2.

Federal Highway Administration (FWHA), (2010). "Chapter 3: Summary of Data Requirements." Highway Performance Monitoring System (HPMS) Field Manual. <www.fhwa.dot.gov/ohim/hpmsmanl/chapt3.cfm> (July 17, 2012).

Frey, H.C., Unal, A., Rouphail, N., and Colyar. J.D. (2003). "On-road measurement of vehicle tailpipe emissions using a portable instrument." Journal of Air and Waste Management Association, 53, 992-1002.

Hunger, M., Husken, G., and Brouwers, J. (2010). "Photocatalytic degradation of air pollutants – From modeling to large scale application." Cement and Concrete Research, 40, 313-320.

Li, L. and Qian, C. (2009). "A lab study of photo-catalytic oxidation and removal of nitrogen oxides in vehicular emissions and its fieldwork on Nanjin No.3 bridge of Yangtze River." Journal of Pavement Resource Technology, 2(5), 218-222.

Maggos, T., Bartiz, J., Liakou, M., and Gobin, C. (2007). "Photocatalytic degradation of NO_x gases using TiO_2-containing paint: A real scale study." Journal of Hazardous Materials, 146, 668-673.

Maggos, T., Plassais, A., Bartzis, J.G., Vasilakos, C, Moussiopoulos, A. and Bonafous, L. (2008). "Photocatalytic degradation of NO_x in a pilot street canyon configuration using TiO_2-mortar panels." Environmental Monitoring Assessment, 136, 35-44.

Osborn, D., Hassan, M. M. and Dylla, H., (2012) "Quantification of Reduction of Nitrogen Oxides by Nitrate Accumulation on a Titanium Dioxide Photocatalytic Concrete Pavement." Journal of the Transportation Research Record, 2290, 147-153.

Papson, A., Hartley, S., and Kuo, K. (2012). "Analysis of emissions at congested and uncongested intersections using MOVES2010." 91st Annual Meeting Compendium of Papers. Transportation Research Board, Washington D.C, 12-0684,.

Sleiman, M., Conchon, P., Ferronato, C., and Chovelon, J.M. (2009). "Photocatalytic oxidation of toluene at indoor air levels (ppbv): Towards a better assessment of conversion, reaction intermediates and mineralization." Applied Catalysis B: Environmental, 86(3-4), 159-165.

U.S. Census Bureau. (2009). "American Housing Survey." <http://www.census.gov/hhes/www/housing/ahs/nationaldata.html> (June 7, 2011).

Vette A. (2010). Near-Road Air Pollution. U.S. Environmental Protection Agency, Clean Air Research, July 21, 2010 Presentation. <http://www.epa.gov/ncer/air40/videos/july2010/index.html> (June, 7 2011).

Zhao, J., and Yang, X. (2003). "Photocatalytic oxidation of indoor air purification: a literature review." Building and Environment, 38, 645-654.

CHAPTER 5
KINETIC STUDY OF PHOTOCATALYTIC DEGRADATION OF EMITTED NITROGEN MONOXIDE USING CONCRETE PAVEMENTS

5.1 INTRODUCTION

Negative health effects from vehicle pollution are associated with living, working and going to school near highways from long-term and short-term exposure (Kim et al. 2004, McConnell et al. 2010). Due to the scientific evidence of adverse health effects correlating to pollution, the Clean Air Act allows the US EPA to set National Ambient Air Quality Standards (NAAQS) (EPAa 2012). Nitrogen dioxide (NO_2), primarily emitted from combustion processes, is one of six criteria pollutants that is regulated and monitored according to the NAAQS. Traditionally the NAAQS for NO_2 has been for long-term exposure setting the annual arithmetic average of 53 ppb, however an additional standard to address short-term exposure has been developed. This standard requires a 1-hour 100 ppb daily hourly maximum averaged from the 98th percentile over 3 years (EPA[b] 2012).

Many technologies such as selective catalytic reduction and lean NO_x traps have been implemented and are continually being improved to reduce vehicle emissions (Xu and McCabe 2012, McCarthy et al. 2010). However, increasing urbanization, vehicle use, traffic congestion, and desire for larger cars, often offsets the reductions realized by these new vehicle emissions controls strategies (HEI 2010, Menz 2002). This has led to the practice of continually reducing vehicle emissions standards. Another technique of pollution abatement is photocatalytic pavements. Photocatalytic pavements use a semiconductor photocatalyst that when irradiated by sunlight can reduce air pollutants after they are emitted. Thus, they can decompose pollutants to nonhazardous waste products with little energy requirements and selectivity (Zhao and Yang 2003, Ballari et al. 2010).

For abatement of pollution in roadway microenvironments, pavements are an ideal substrate due to their close proximity to higher concentrations of pollution and large surface area (Beeldens 2006). Titanium dioxide (TiO_2) is the preferred photocatalyst used because of its high stability, super-hydrophilicity, relative cheapness, low toxicity, and commercial availability (Cassar 2004, Fujishima and Zhang 2006, Diamanti et al. 2008, Toma et al. 2009, Yu and Brouwers 2009). Previous laboratory results completed by the authors have illustrated that photocatalytic pavements may reduce pollutants such as NO_x by as much as 67% once pollutants are emitted in the air (Dylla[a] 2010). In addition, photocatalytic pavements may have the advantage that they could be a cost-effective air pollution abatement technique since they can be applied only to target areas. However, in order to grasp the widespread pollution reduction made possible from photocatalytic pavements, the next major step is to comprehend its behavior in the real world environment.

The current understanding of photocatalytic pavements in real world settings is still lacking. Lab studies have shown photocatalytic reduction of NO_x depends on many environmental factors impacting its efficiency including, humidity, concentration, intermediates, light intensity, and wind speed (Poon and Cheung 2007, Watts and Cooper 2008). Unfortunately, the quantification of NO_x reduction in field studies is difficult and challenging due to these environmental factors and many other unknown parameters that may exist in real world settings. An environmental model using the reaction kinetics is a promising alternative to evaluate the significance of pollution reduction that can be expected from photocatalytic pavements. Therefore, the objective of this study was to model the photocatalytic reaction kinetics of NO reduction under different environmental conditions to be used in future theoretical air pollution model simulations. Not only are these models important for

understanding the significance of the NO reduction expected, they could be included into State Implementation Plan (SIP) air quality calculations and models allowing photocatalytic pavements to be evaluated as a possible pollution reduction strategy (EPA[a] 2012).

5.2 BACKGROUND

5.1 Photocatalytic NO Oxidation Mechanism

Photocatalytic oxidation of NO is a heterogeneous reaction, such that the reaction occurs at the interfacial surface of a solid-gas or solid-liquid. The reaction follows a series of several steps (Figure 5.1). Diffusion, the first step, is rarely the mass transfer-limiting step, with the exception of diffusion through a solution. The following three steps: surface adsorption, reaction and product desorption, occur simultaneously and are difficult to differentiate. Thus, these three steps are considered together as a single reaction rate, which is often the mass transfer-limiting step (Valsaraj 2009).

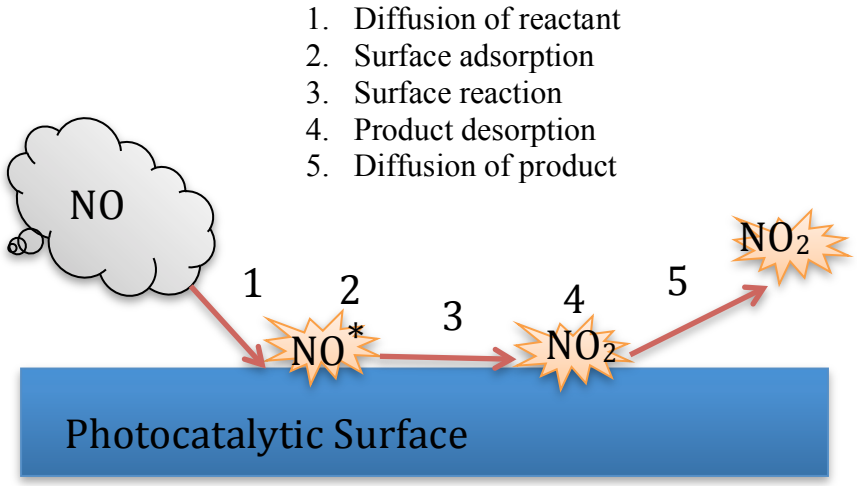

Figure 5.1 Heterogeneous Surface Reaction Schematic for NO (modified from Valsaraj 2009)

The photocatalytic oxidation of NO occurs when TiO_2 is exposed to energy, from photons, exceeding its band gap energy of 3.2 eV. When this occurs, an electron is expelled from the valence band to the conduction band, leaving a hole behind creating electron-hole pairs,

called excitons (Zhao and Yang 2003, Fujishima et al. 2000). For TiO_2, UV light initiates this process, where the exact wavelength required is determined by the electromagnetic radiation, *hv*, where *h* is Planck's constant and *v* is the frequency of light Equation 5.1.

$$TiO_2 + h\upsilon \rightarrow e^- + h^+ \quad (5.1)$$

In the presence of water and oxygen, the photogenerated holes, h^+, and electrons, e^-, create hydroxyl radicals and superoxides respectively, shown in Equations 5.2 and 5.3 (Fujishima et al. 2000).

$$OH^- + h^+ \rightarrow OH^* \quad (5.2)$$

$$O_2 + e^- \rightarrow O_2^- \quad (5.3)$$

The resulting hydroxyl radicals and superoxides are key for oxidation or reduction reactions allowing for degradation of pollutants such as the oxidation of NO_x to water soluble nitrates, as shown in Equations 5.4 and 5.5 below (Beeldens 2008):

$$NO + OH^* \xrightarrow{T_iO_2} NO_2 + H^* \quad (5.4)$$

$$NO_2 + OH^* \xrightarrow{T_iO_2} NO_3^- + H^* \quad (5.5)$$

As a result, it is evident from the reaction scheme that irradiation and the absorbed reactants (water, oxygen, NO) all play an important role in the photocatalytic oxidation as shown in Figure 5.1.

5.1 PHOTOCATALYTIC NO REACTION KINETIC MODELS

The theory behind heterogeneous reaction kinetics is well established by researchers in chemical engineering (Valsaraj 2009). As previously noted the NO reduction can be either diffusion mass-transfer controlled or reaction mass-transfer controlled, determined by whichever process

is slowest. Previous kinetic studies have shown that photocatalytic oxidation is reaction controlled (Hunger et al., 2010). The most widely used model for heterogeneous surface reactions is the Langmuir-Hinshelwood (L-H), where at high pressures a zero order reaction prevails and at low pressures a first order reaction prevails (Wang et al. 2007). Using this model, the NO photooxidation reaction rate is described as follows:

$$r_{NO} = \frac{k*KC_{NO}}{1+KC_{NO}} r_{NO} = \frac{k*KC_{NO}}{1+KC_{NO}} \quad (5.6)$$

where,

r_{NO} = NO photooxidation rate (mg/m^{3}s);
k = L-H reaction rate constant (mg/m^{3}s);
Kd = the L-H adsorption equilibrium constant (m^3/mg); and
C_{NO} = the concentration of NO in atmosphere (mg/m^3).

To account for the impact of humidity, competition between the two pollutants for adsorption exists, thus Equation 5.6 is modified as shown in Equation 5.7 (Hunger et al. 2010):

$$r_{NO} = \frac{kK_{NO}C_{NO}}{1+K_{NO}C_{NO}+K_{H2O}C_{H2O}} \quad (5.7)$$

where,

C_{H2O} = the concentration of H_2O; and
K_{H2O} = equilibrium constant for H_2O.

Despite this theory, Hunger et al. 2010 found that humidity did impact the NO photooxidation rate however the experimental results did not follow the proposed relationship described in Equation 5.7. As a result, many models use regression techniques to incorporate the impact of relative humidity (Hunger et al. 2010, Bengtsson and Castellote 2010).

Recently, kinetic studies have been incorporated in photocatalytic pavement studies. Hunger et al. modeled the kinetics of the photocatalytic degradation of NO_x using photocatalytic concrete paving stones. The impact of the UV-light intensity and humidity on the kinetic constants were modeled each separately at one humidity level and one UV-light intensity level, respectively (Hunger et al. 2010). To incorporate these parameters into one model, Bengtsson and Castellote (2010) used non-linear regression from a partial factorial study to model only the L-H reaction rate constant (Bengtsson and Castellote 2010). The present study expands on these works by completing a full factorial reaction kinetic study for 5 different humidity levels and 5 different UV light intensities for both the L-H reaction rate and adsorption equilibrium constants. As such, a global reaction rate model was created for NO photodegradation as a function of both humidity and irradiance.

5.3. MATERIALS AND METHODS

5.3.1 Photocatalyst

The titanium dioxide catalyst used in the photocatalytic concrete pavement was PC105 from Crystal Millennium. The specific surface area measured by the (BET) isotherm (ASAP 2000) by nitrogen physisorption was 73.2666 ± 0.9362 m^2/g. The X-ray diffraction (XRD) patterns obtained by a Rigaku, D/Max 2500 PC instrument using CuKα radiation characterized the TiO_2 crystal structure as 100% anatase (Search Match #4-447). The average primary particle size was 15 nm with agglomerates averaging 28 nm estimated by high-resolution transmission electron microscopy (HRTEM TECHNAI F20 FEI, 200kV).

5.3.2 Photocatalytic pavement sample preparation

The photocatalytic pavement samples were made of a concrete base and a thin photocatalytic mortar overlay. The sample size was 310 mm x 381mm x 40 mm for the base with an additional 10 mm in height for the photocatalytic overlay. The concrete base followed a typical concrete

pavement mix design with a compressive strength of 41 MPa. The photocatalytic cementitious mortar mix consisted of 5% ultrafine TiO_2 per cement weight, cement, aggregate filler with maximum nominal size of 1.18 mm, and water. The TiO_2 was added to the water; rather than mixed with the dry components, in efforts to limited nanoparticle exposure during construction and create a more even distribution of the nanoparticles. The photocatalytic layer was applied after the initial set, approximately 1 hour after the base layer pour. Three replicates were produced to account for variability.

5.3.3 Photoreactor and Experimental Setup

For the photocatalytic oxidation of NO, the experimental set-up specified by the Japanese Industrial Standard (JIS TR Z 0018 "Photocatalytic materials – air purification test procedure") was modified, as defined in Dylla[b] et al. 2010, to accommodate the larger sample sizes and to simulate various environmental conditions (JIS 2004). A zero air source, gas calibrator, humidifier, photoreactor, UV-lights, space heater/fan and a NO_x analyzer was used to measure the photocatalytic oxidation of NO_x under various levels of relative humidity, pollutant concentration, flow rate, and irradiance (Figure 5.2).

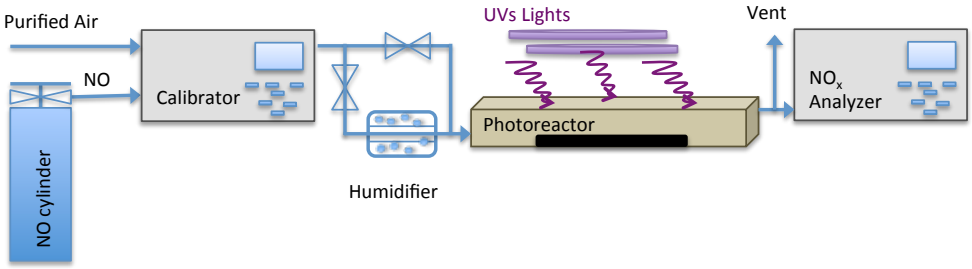

Figure 5.2 Experimental Setup

The sample was housed inside a single-pass plug flow photoreactor with an air space volume of 16.75 liters. A thermo scientific 146i calibrator supplied the appropriate NO

concentrations at 3 standard l/min to the photoreactor by blending 170 ppm of dry NO in a nitrogen balance with dry zero air. Twelve 20W fluorescent black lights (20W, Philips) emitting wavelengths within 300-400 nm (Zhao and Yang 2003) were used to illuminate the photocatalytic pavement. The distance between the sample surface and the photoreactor determined the UV irradiance measured at the pavement surface by UV-A intensity meter (OAI Model 306) at 365 nm. The UV profile was measured for each test condition and the average irradiance observed was calculated. The highest irradiance, 3.52 mW/cm^2, had the most variance due to the sample proximity to the lights in which this variance is illustrated in Figure 5.3. The average temperature during the testing period for each test condition was 26.5 ± 3.5°C. A hygrometer and temperature probe continuously monitored and recorded the temperature and relative humidity per minute.

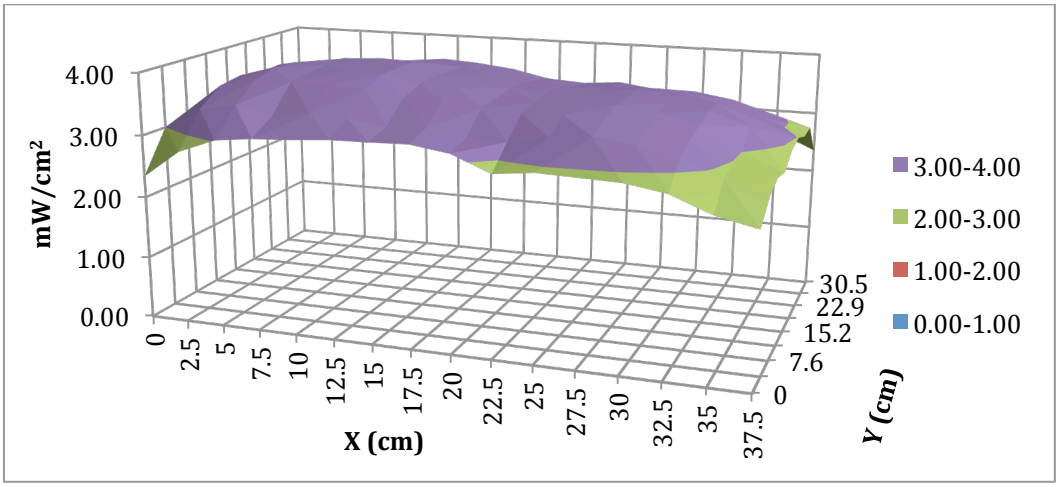

Figure 5.3 Profile of UV-A Irradiance Over Sample Surface (3.52 mW/cm^2)

5.3.4 Environmental Conditions

While in service, photocatalytic pavements will be exposed to a variety of environmental conditions including various humidity, irradiances, temperatures and pollutant concentrations, which all impact photocatalytic reaction kinetics of NO. Areas in the United States that have

reported high concentrations of NO pollution include California, Illinois, Massachusetts, New Jersey, New York, Texas and Utah. According to the 2011 EPA Air Quality System (AQS) NO data, these states have one or more counties that have recorded an hourly NO average concentration over 450 ppb in the year of 2011 (EPA[c] 2012). As a result, applying photocatalytic pavements in these areas may be most beneficial.

With this in mind, the typical meteorological year 2 (TMY-2) weather files correlating to the previously mentioned areas determined the ranges for the environmental conditions provided they were within the experimental setup capabilities. From the TMY-2 weather files the relative humidity varied from 4% to 100%, the temperature varied from -22.8°C to 39.4°C and the maximum irradiance was 3 mW/cm^2 (assuming that TiO_2 only uses 2.7% of the global horizontal radiation) (NREL 2009). As a result, the reaction kinetics was evaluated for five levels of humidity (27, 40, 51, 72, 81 ± 4%) and five levels of average irradiance (3.52, 2.7, 2.1, 1.3, 0.52 mW/cm^2). A full factorial experimental design was used resulting in the 25 combinations of environmental conditions found in Table 5.1.

5.3.5 Sampling and Kinetic Analysis

The photocatalytic oxidation (PCO) was conducted by following the JIS procedures. While JIS test procedure requires 5 hours of irradiation, it was noted that steady state equilibrium is achieved within the first half-hour of irradiation (JIS 2004). Therefore, the test procedure was shortened until equilibrium was achieved, defined by stability of NO_x concentration for 10 minutes. Thus, the photocatalytic oxidation test consisted of at least 40 minutes to reach non-irradiated equilibrium settings, 30 minutes of illumination and 20 minutes of non-irradiated and zero air to allow for NO_x desorption. To prevent deactivation by intermediates adsorbed on the TiO_2 active sites, samples were soaked periodically in Nanopure DI water for 2 hours replacing

the water hourly and dried for at least 48 hours before being retested. In order to test whether the photocatalytic degradation of NO was diffusion mass transfer limited or reaction rate mass transfer limited, the effect of the inlet concentration was varied. The NO inlet concentration was varied at 250, 550, 750, 1000, 2000, and 3000 ppb, while the flow rate, relative humidity and irradiance remained constant for each of the defined environmental conditions. This resulted in a total of 450 runs. An additional 83 runs, correlating to 18% of the total runs used to create the model were run at random environmental conditions and concentrations to test the validity of the model developed.

Table 5.1 Environmental Conditions Used to Determine L-H Constants

Run Scenario	Humidity (%)	Irradiance (mW/cm^2)
1	27	0.52
2	27	1.3
3	27	2.1
4	27	2.7
5	27	3.52
6	40	0.52
7	40	1.3
8	40	2.1
9	40	2.7
10	40	3.52
11	51	0.52
12	51	1.3
13	51	2.1
14	51	2.7
15	51	3.52
16	72	0.52
17	72	1.3
18	72	2.1
19	72	2.7
20	72	3.52
21	81	0.52
22	81	1.3
23	81	2.1
24	81	2.7
25	81	3.52

5.3.5.1. Diffusion Mass Transfer Limited

When diffusion controlled, the reaction is instantaneous. Thus, assuming instantaneous conversion, the mass balance can be written. Derivation of the NO mass balance equation for a plug flow reactor is described elsewhere (Hunger et al., 2010). Integrating the mass balance equation over the length of the photocatalytic surface the percent reduction can be calculated by the following equation:

$$1 - \frac{C_{NO,(in)}}{C_{NO(out)}} = e^{\frac{-ShDL}{2u_{air}h^2}} \quad (5.8)$$

where,

$C_{NO,in}$ = inlet concentration (mg/m^3);
$C_{NO,out}$ = outlet concentration (mg/m^3);
Sh = Sherwood number;
u_{air} = velocity of air (m/s);
h = height of air space in photoreactor (cm);
D = Diffusion Coefficient of NO (m^2/s); and
L = Length of sample (cm).

Using the variables defined in Table 5.2, if mass transferred is controlled; the percent reduction would be 80% regardless of the inlet concentration. Thus, if the NO reduction is dependent on pollutant concentrations, then the mass transfer is reaction controlled.

Table 5.2 Mass Transfer Variables

Variable	Symbol	Value
Sherwood Number	Sh	4.4
Length	L	38 cm
Height	h	4.8 cm
Diffusion Coefficient NO	D	1.51×10^{-5} m^2/s
Velocity of Air	u_{air}	0.003067 m/s

5.3.5.2. Reaction Rate Mass Transfer Limited

When the reaction rate controls, diffusion is instantaneous. Thus, for a single pass experimental setup, plug flow is assumed and the mass balance is written as follows:

$$r_{NO} = -u_{air} * \frac{dC_{NO}}{dx} = \frac{k*KdC_{NO}}{1+KdC_{NO}} \quad (5.9)$$

where,

$\frac{dC_{NO}}{dx}$= rate of change of concentration per horizontal distance (mg/m^2).

Integrating the mass balance Equation 5.9 over the length with the following boundary conditions shown in Equation 5.10 results in the following linear relationship, Equation 5.11.

$$C_{NO} = C_{NO,in} \quad (5.10)$$

$$\frac{\ln\left(\frac{C_{NO,in}}{C_{NO,out}}\right)}{C_{NO,in}-C_{NO,out}} = \frac{kKd\left(\frac{V}{Q}\right)}{C_{NO,in}-C_{NO,out}} - \frac{1}{k} \quad (5.11)$$

where,

Q = flow rate (m^3/s); and
V = volume of air space (m^3).

Thus, by graphing $\ln C_{NOin}/C_{NOout}/(C_{NOin}-C_{NOout})$ versus $(V/Q)/(C_{NOin}-C_{NOout})$ the k and Kd L-H parameters can be determined from the graph from linear regression analysis; where the k is the reciprocal of the y-intercept and Kd is 1/(mk), where m is the slope of the line. Furthermore, the linear relationship is evidence that the reaction is a gas-solid reaction following the L-H mechanism, rather than a gas-phase reaction (Sleiman et al., 2009).

5.4. RESULTS AND DISCUSSION

5.4.1 Validation of Reaction Kinetics Model

Figure 5.4 shows the NO reduction per initial concentration at 51% relative humidity and 2.1 mW/cm^2 light intensity. As the concentration increases, the percentage of NO degradation decreases, which was the trend for all the tested run scenarios listed in Table 5.1. Since NO reduction is dependent on the pollutant concentration, the mass transfer is the reaction rate controlled rather than diffusion controlled.

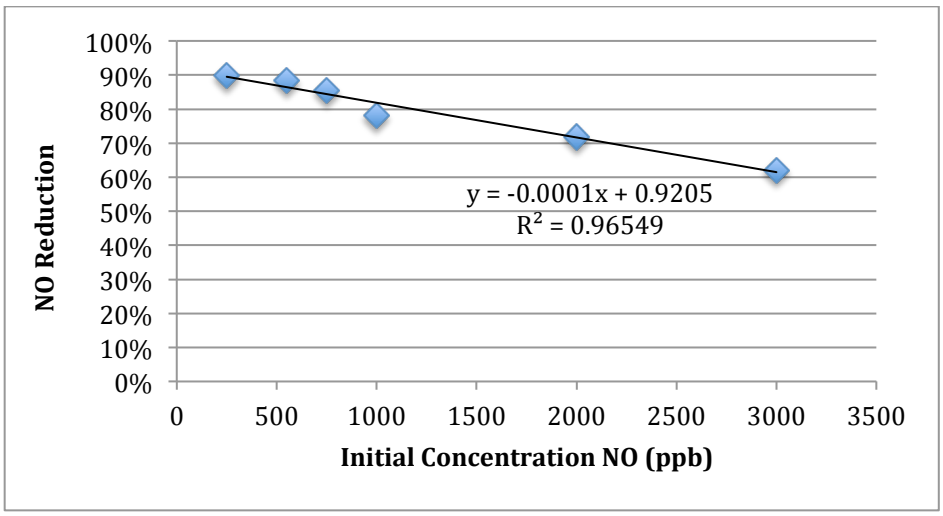

Figure 5.4 Influence of Initial Concentration on the Average NO Reduction (3 l/min flow, 51% relative humidity, 2.1 mW/cm^2 irradiance)

Furthermore, the $\ln C_{NOin}/C_{NOout}/(C_{NOin}-C_{NOout})$ and $(V/Q)/(C_{NOin}-C_{NOout})$ were calculated and plotted per sample. Figure 5.5 is a representation this plot for one of the three samples run at the same conditions described for Figure 5.3. As shown in this figure, there is a strong linearity thus further supporting that the mass transfer is reaction-rate limited and that Langmuir-Hinshelwood model is adequate. In addition, previous studies have shown that the percent degradation of NO is increased by increasing the amount of TiO_2 catalysis also suggesting reaction-controlled (Hassan et al, 2009, Diamanti et al. 2008).

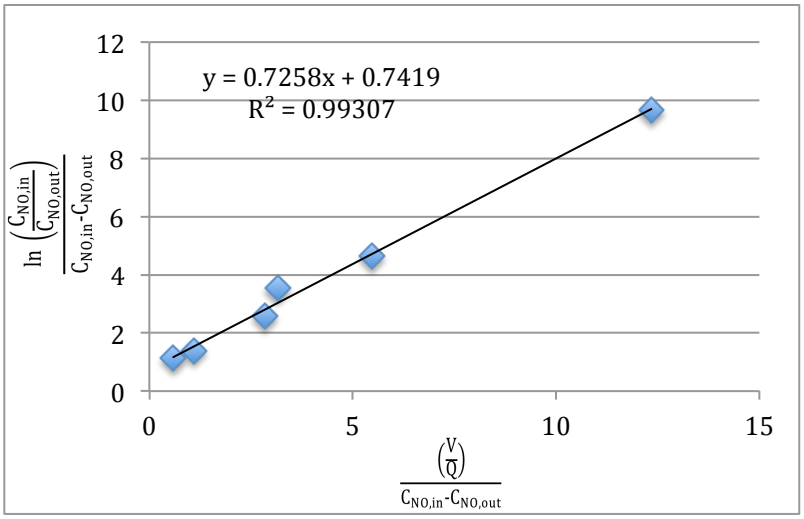

Figure 5.5 Determination of L-H Constants for Concrete Photocatalytic Pavement

From the regression results, the average Langmuir-Hinshelwood constants calculated for each environmental scenario are listed in Table 5.4. At 51% relative humidity and 2.1 mW/cm^2 irradiance, the environmental conditions described in Figure 5.4, the L-H constants were calculated as k=0.02 mg/m^{3}s and Kd=0.88 m^3/mg. At similar conditions, Hunger et al. 2010 evaluated the L-H reaction rate and adsorption equilibrium constants for photocatalytic paving stones as k=0.10 mg/m^{3}s and adsorption equilibrium of Kd=7.15 m^3/mg, respectively, whereby the inlet concentration of NO ranged from 100 to 1000 ppb (Hunger et al. 2010). Compared to these results, the reaction rate and the adsorption equilibrium constant are both significantly lower. The significantly lower reaction rate and adsorption equilibrium constants are most likely due to a lower number density of all active sites on the TiO_2 surface. As a result, rather than the apparent reaction rate the turnover frequency, calculated by dividing the apparent reaction rate by the number of active sites, is often used to relate reaction rates. The number of active sites on a surface is estimated by summing the total number of surface atoms. This is problematic for photocatalytic pavements where the TiO_2 nanoparticles were dispersed within a thin mortar

overlay and it is difficult to quantify the moles of TiO_2 on the surface. Table 5.4 summarizes the average regression fits and the resulting L-H constants calculated for each environmental scenario simulated.

Table 5.4 Summary of L-H Constants and Coefficient of Determination

Run Scenario	Slope (m)	Intercept (b)	Kd Avg. (m^3/mg)	Kd Stdev. (m^3/mg)	k Avg. (mg/m^3min)	k Stdev. (mg/m^3min)	Coefficient of Determination (r^2) Avg.
1	0.88	0.72	0.81	0.14	1.44	0.30	0.99
2	1.00	0.30	0.31	0.03	3.30	0.28	1.00
3	0.73	0.27	0.36	0.07	3.92	0.98	1.00
4	0.94	0.25	0.27	0.03	3.99	0.51	1.00
5	0.82	0.20	0.28	0.24	11.47	13.34	1.00
6	0.87	1.15	1.34	0.20	0.87	0.05	0.99
7	1.06	0.47	0.45	0.02	2.11	0.02	1.00
8	0.98	0.35	0.36	0.07	2.92	0.67	1.00
9	0.91	0.42	0.46	0.02	2.40	0.37	1.00
10	0.90	0.41	0.47	0.23	2.88	1.56	1.00
11	1.13	1.54	1.43	0.30	0.66	0.12	0.99
12	1.11	0.86	0.80	0.18	1.17	0.17	1.00
13	0.83	0.72	0.88	0.23	1.45	0.40	0.99
14	1.05	0.43	0.41	0.13	2.48	0.73	1.00
15	0.91	0.34	0.44	0.29	3.89	2.83	0.99
16	2.03	3.96	1.95	0.28	0.26	0.06	0.89
17	1.59	1.34	0.85	0.04	0.75	0.07	1.00
18	1.55	1.15	0.91	0.75	1.26	1.02	0.98
19	1.42	0.81	0.59	0.28	1.40	0.61	0.99
20	1.57	0.94	0.66	0.64	1.51	0.83	0.98
21	2.54	6.97	1.95	0.28	0.15	0.03	0.89
22	1.94	4.04	2.23	0.70	0.25	0.03	0.94
23	2.28	2.09	0.94	0.16	0.48	0.03	0.99
24	1.82	2.53	1.41	0.51	0.43	0.15	0.96
25	1.70	1.89	1.12	0.19	0.53	0.03	0.95

5.4.2 Parametric Study

5.4.2.1 Effect of Relative Humidity

From Figure 5.6, it is clear that relative humidity significantly impacts both the L-H adsorption equilibrium constant and the L-H reaction rate constant. The extent of the relative humidity's impact is largely dependent upon the substrate material. Titanium dioxide can be both hydrophobic and hydrophilic. Typically and during irradiation, TiO_2 undergoes a hydrophilic effect (Diamanti et al. 2008). This promotes a water monolayer that inhibits pollutants to adsorb

on the photocatalyst active sites (Hunger et al. 2010). However, water is also critical for the photocatalytic reduction of NO in the creation of the hydroxyl radicals, which are believed to be responsible for the NO oxidation to nitrates. This is evident from the previous described photocatalytic NO oxidation mechanism (section 5.2.1).

In Figure 5.6a, in general, as the relative humidity increases, the L-H adsorption equilibrium rate increases. In addition, due to the intersecting lines, there seems to be interaction between the impact of the relative humidity and irradiance on the adsorption equilibrium constant. This is different from previous research results from Hunger et al. 2010, which showed 40% relative humidity as an optimum level for the max adsorption equilibrium constant for an irradiance level of 10 mW/cm^2. And, this is contrary to the theory that the relative humidity solely competes with the NO adsorption for photocatalytic active sites, suggesting additional phenomena occur.

The additional phenomena occurring are hypothesized to be the diffusion and dissolution of the pollutants in the water clusters formed on the surface (Maudhuit et al. 2011). As a result, the L-H adsorption constants calculated may also include the phenomena of the diffusion and dissolution of the pollutant into the adsorbed water (Maudhuit et al. 2011). The extent of the impact is defined by the surface texture and characteristics, of the TiO_2 and photocatalytic medium, both of which impact the formation of a water layer film in humid conditions.

Under higher irradiance, the TiO_2 photocatalyst becomes more hydrophilic and a thin monolayers water film is created competing with pollutant adsorption. Thus, explaining the interaction between the relative humidity and irradiance as well as the lower adsorption equilibrium constants under higher irradiance. While under lower irradiances, there is less hydrophilic effect and several layers of water may form creating water clusters (Maudhuit et al.

2011, Diamanti et al. 2008). This reduces the competition between the water and NO for adsorption sites and increases the amount of NO adsorbed into the water. As a result, it is likely that the higher Kd observed, at higher humidity levels, is attributed to the phenomena of diffusion and dissolution of NO in the water. This is consistent with results from Maudhuit et al. (2011), which demonstrated that the adsorption phenomena for VOCs -toluene, acetone, and heptane- are significantly impacted by humidity and do not follow the classical adsorption models in humid conditions due to the addition of diffusion and dissolution in the adsorption mechanism.

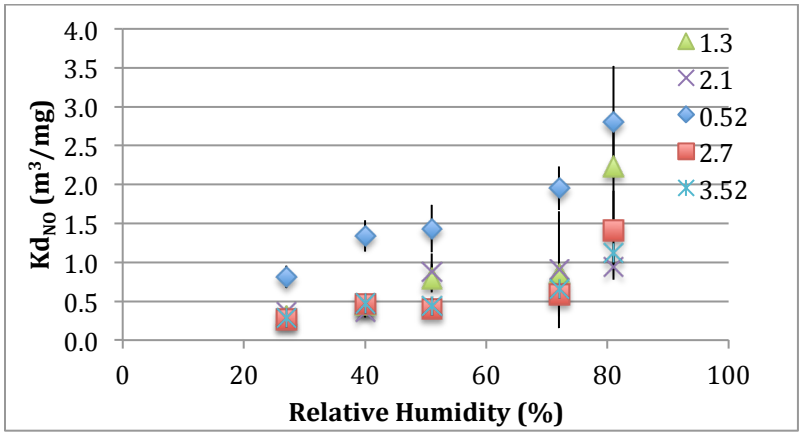

(a)

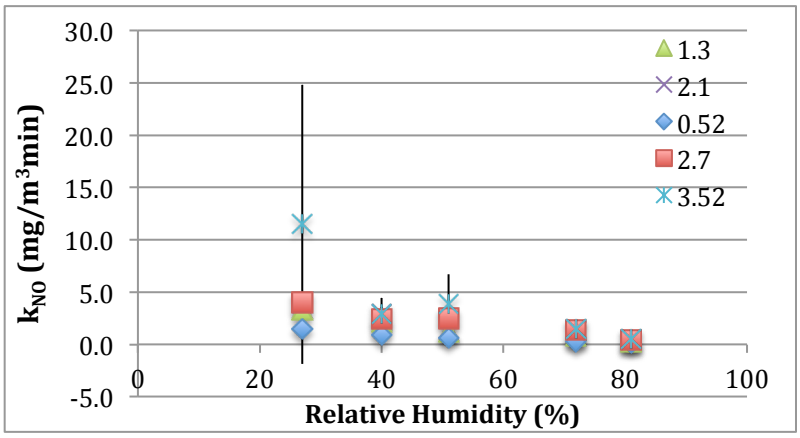

(b)

Figure 5.6 L-H Adsorption Equilibrium Constant (a) and L-H Reaction Rate (b) Versus Humidity at Irradiances 0.52, 1.3, 2.1, 2.7, 3.52 (mW/cm^2)

Figure 5.6b, illustrates at higher relative humidity levels the L-H reaction rates decreases. The lower reaction rates are explained by less active sites available on the TiO_2 photocatalyst thus reducing the reaction rate. In addition, due to the nonparallel trends illustrated in Figure 5.6b, there seems to be slight interaction between the relative humidity and light irradiance.

5.4.2.2 Effect of Irradiance on L-H Constants

As illustrated by the photocatalytic mechanism, the irradiance also plays an important role on the photocatalytic oxidation of NO. Both the wavelength and the photon flux determine the photocatalytic oxidation; where the wavelength is primarily responsible for whether the photocatalytic activity occurs and the irradiance or photon flux impacts the actual rate of degradation (Fujishima et al. 2000, Zhao and Yang 2003).

Figure 5.7 illustrates the UV irradiance impact on both the L-H adsorption equilibrium constant and the L-H reaction rate constant. Previous kinetic studies models assumed that Kd was unaffected by irradiance (Hunger et al. 2010, Bengtsson and Castellote 2010). However, at irradiances less than 3.5 W/m^2, typical of the real world environment and, thus, the levels used for this study, this does not seem to be case (Figure 5.7a). This is consistent with Hunger et al. results where at 50% relative humidity the L-H equilibrium adsorption constant significantly differed for various irradiances less than 4 W/m^2. Despite this, the model created excluded the impact of irradiance (Hunger et al. 2010). The impact of irradiance on Kd could be attributed to the change in the hydrophilic effect. At higher intensities the surface becomes more hydrophilic supporting a thin monolayer of water, which increases competition of adsorption on TiO_2 active sites between water and NO.

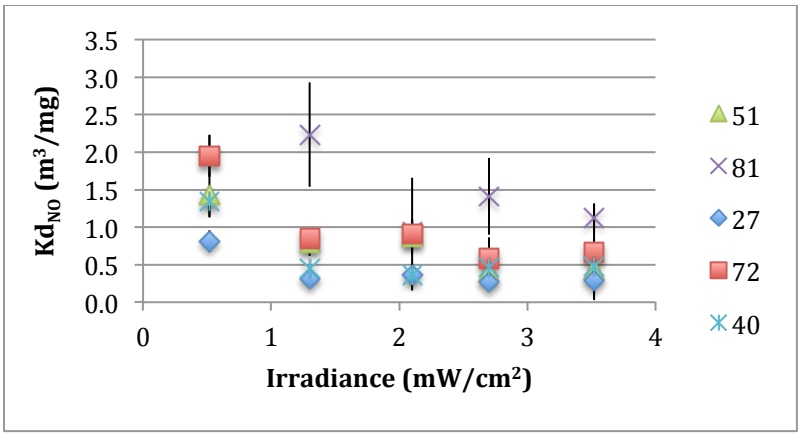

(a)

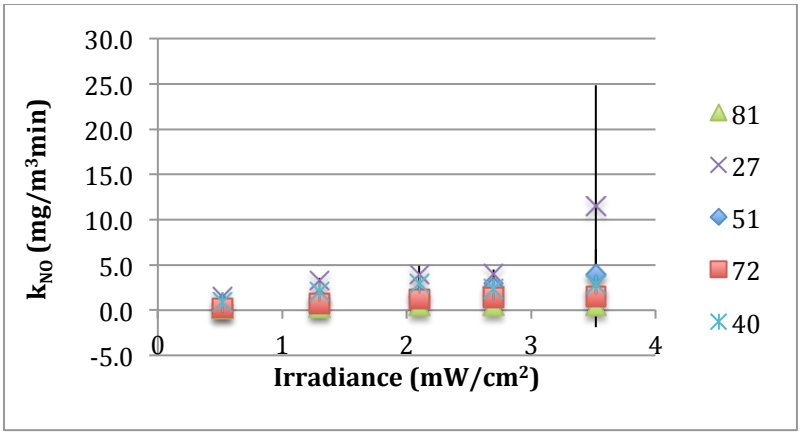

(b)

Figure 5.7 L-H Adsorption Equilibrium Constant (a) and L-H Reaction Rate (b) Versus Irradiance at Relative Humidity Levels 27%, 51%, 40%, 72% and 81%

The impact of the UV irradiance on the L-H reaction rate constants is as expected. The higher the photon flux, the more electron-hole pairs are created as illustrated by photocatalytic NO oxidation mechanism and thus a higher the reaction rate of NO is observed. Similarly to conclusions from Figure 5.6, both graphs in Figure 5.7 support evidence of an interaction effect between the relative humidity and irradiance factors on both the L-H constants.

5.4.3 Modeling

5.4.3.1 Multiple Parameter Kinetic Model for Photocatalytic Oxidation NO

Using multiple linear regression a model was created for the both the L-H equilibrium adsorption constant, Kd, and the L-H reaction rate constant, k, using the results presented in Table 5.4. A simple transformation was performed on the response variable to make linearity more appropriate. The square root transformation was used for both the Kd and the k response variables. Since the graphs above indicated that the effects of each predictor were not additive, interaction between the relative humidity variable and irradiance variable was investigated. As a result, the addition of a third variable, the product of the humidity and irradiance, was introduced into the models to account for possible interaction (Equations 5.12 and 5.13). Stepwise regression was the procedure used to determine the independent variables included into the model with an entry level of 0.15 and the variable stay level of 0.05. Table 5.5 displays the associated p-values for each of the parameters for Kd model while Table 5.6 displays the associated p-values for each of the parameters for the k model. The developed models are as follows:

$$\mathrm{Kd}(\mathrm{H},\mathrm{I}) = (0.01415 * \mathrm{H} - 0.00176 * \mathrm{H} * \mathrm{I} + 0.45672)\text{^}2 \qquad (5.12)$$

$$\mathrm{k}\,(\mathrm{H},\mathrm{I}) = (-0.007 * \mathrm{H} * \mathrm{I} + 0.69536 * \mathrm{I} + 1.19801)\text{^}2 \qquad (5.13)$$

where,

H = Humidity (%); and
I = Irradiance (W/m^2).

Table 5.5 Summary of Stepwise Selection for Kd Model

Step	Variable Entered	Variable Removed	Label	Number Vars In	Partial R-Square	Model R-Square	F Value	Pr > F
1	x1		Humidity	1	0.4753	0.4753	20.84	0.0001
2	x3		HI	2	0.3087	0.784	31.44	<.0001

Table 5.6 Summary of Stepwise Selection for k Model

Step	Variable Entered	Variable Removed	Label	Number Vars In	Partial R-Square	Model R-Square	F Value	Pr > F
1	x1		Humidity	1	0.5636	0.5636	29.71	<.0001
2	x2		Irradiance	2	0.263	0.8266	33.37	<.0001
3	x3		HI	3	0.0513	0.8779	8.81	0.0073
4		x1	Humidity	2	0.0206	0.8573	3.54	0.074

It is noted that the developed Kd and k models are only acceptable for the relative humidity and irradiance levels within the range of variation used to create the model as shown in Table 5.7.

Table 5.7 Parameters Investigated for Model and the Valid Input Ranges

Parameters	Range of Variation	
	Low Level	High Level
Humidity (%)	27	81
UV Irradiance (W/m^2)	0.52	3.52
Humidity*UV Irradiance	14	285

By substituting the models created for Kd and k, the apparent reaction rate model from Equation 5.6 can be modeled now as a function of humidity and irradiance.

$$r_{NO} = \frac{k(H,I) * Kd(H,I) C_{NO}}{1 + Kd(H,I) C_{NO}} \qquad (5.14)$$

5.4.3.2 Model Validation

The goodness of the fit of the Kd and k models was assessed through the coefficient of determination (R^2), the adjusted coefficient of determination (Adj R^2), which has been adjusted for the degrees of freedom and sample size, and the root mean square error (RMSE). These descriptive statistics for the developed Kd and k models are presented in Table 5.8. Furthermore, Figure 5.8 compares the predicted k and Kd values to the experimental calculated k and Kd values. Since the coefficient of determination for both models is less than 1, other variables not

included in the model still may exist. One such variable is the impact of intermediates created from the photodegradation process, which in this case would be the creation of NO_2. Another part of the error could be explained by the higher error present at higher humidity levels when calculating the L-H constants, exhibited in Table 5.4. This could suggest that the L-H model may not be adequate at the higher humidity levels (>70%) and other models need to be explored.

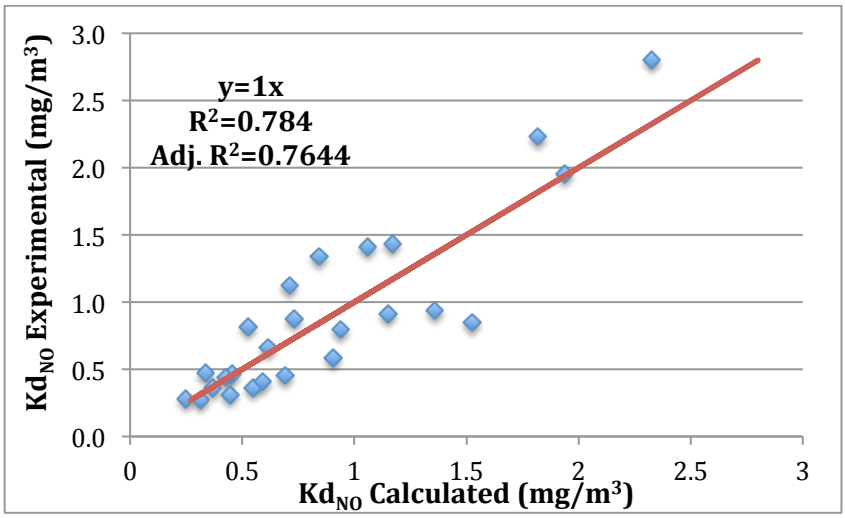

(a)

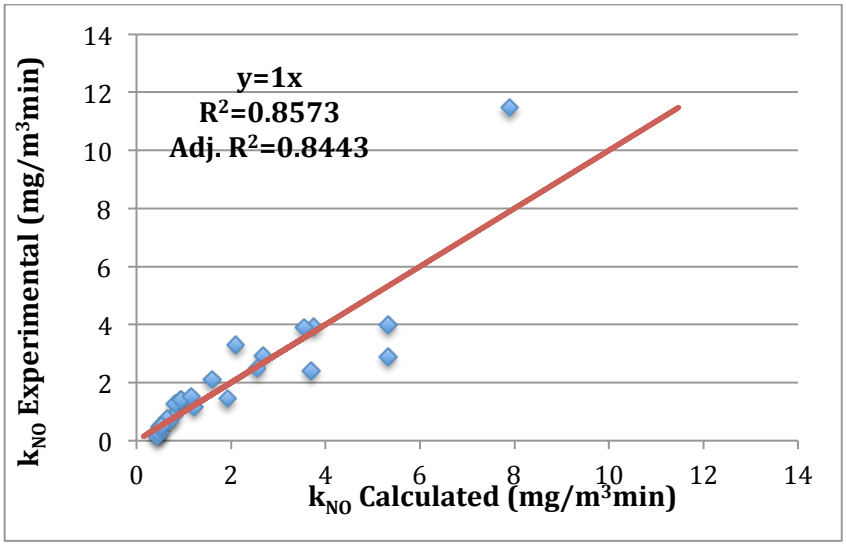

(b)

Figure 5.8 Comparison of Experimental L-H Reaction Constants to Predicted L-H Reaction Constants (a) L-H Equilibrium Adsorption Constant (b) L-H Reaction Rate Constant

Table 5.8 Descriptive Statistic of the Developed Models

Statistical parameters	Kd	K
Coefficient of Determination (R^2)	0.784	0.8573
Adjusted Coefficient of Determination (Adj. R^2)	0.7644	0.8443
Root Mean Square Error (RMSE)	0.26	0.15

The validity of the NO photooxidation rate model, r_{NO}, was evaluated by comparing predicted NO concentration out (CNO_{out}) results with the additional observed data, which was recorded but not used to build the models. An additional 83 runs were completed at random environmental conditions within the defined variable ranges. Using a mass balance for the experimental setup, the reaction rate model was used to predict the outlet concentration. The predicted outlet concentration was compared to the actual outlet concentration measured to evaluate accuracy of the photodegradation reaction rate model. The CNO_{out} was estimated using the Taylors Series Expansion of Equation 5.9, whereby Equations 5.12 and 5.13 predicted Kd and k, respectively. Figure 5.9 compares the resulting predicted CNO_{out} to the actual experimental CNO_{out}. From the results, the modified apparent reaction rate model explained about 87% of the total variance.

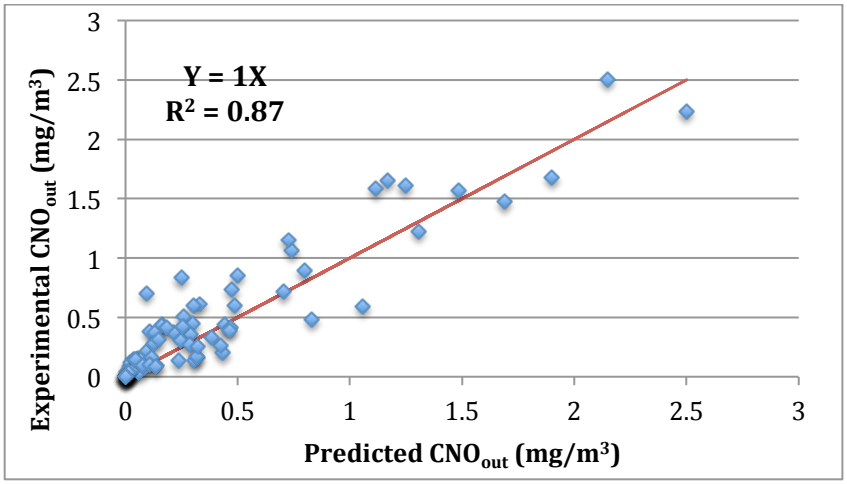

Figure 5.9 Comparison of Experimental NO Concentrations After Photocatalytic Reduction Compared to Predicted NO Concentrations.

5.4.3.3 Model Limitations

As recently stated, the model is only a function of relative humidity and irradiance and is limited to the ranges used to develop the model as previously noted in Table 5.7. The model was created for a 5 cm slit height with an air velocity of 0.003 m/s. The NO concentration was varied from 250 to 3000 ppb. The degradation of the intermediate, nitrogen dioxide, and its possible interaction was not investigated as part of this study and is part of future work.

5.5. CONCLUSION

The reaction kinetics of photocatalytic concrete pavements is essential for understanding the photocatalytic efficacies in real world environments. In this study, the NO reaction rate was modeled for photocatalytic pavement as a function of relative humidity and irradiance to be used in future theoretical air pollution model simulations. Using a plug flow photoreactor, laboratory experimental results supported that the photocatalytic oxidation of NO was indeed reaction controlled and could be adequately described by the Langmuir-Hinshelwood model. The results of the parametric study identified that the relative humidity and light intensity both had a significant impact on the L-H constants and there was an interaction effect between the relative humidity and light intensity. The impact of the relative humidity played a significant role on the L-H equilibrium constant, Kd. Contrary to theory, as the humidity increased the Kd increased, suggesting that additional phenomena to the typical competition of adsorption sites between water and the pollutant play a role in the Kd adsorption, including NO diffusion and dissolution in water. The impact of irradiance significantly impacts the reaction rate, k. With higher irradiance, more energy creates more active sites.

Using these findings, the L-H equilibrium adsorption constant and the L-H reaction rate were modeled using statistical techniques. Whereby, the resulting model for L-H equilibrium adsorption constant is a function of the humidity and the interaction variable (humidity

multiplied by irradiance), the L-H reaction rate model is a function of irradiance and the interaction variable. The resulting model for Kd explained 76% of the variance in the data, whereas the model for k explained 84% of the variance in the data. Substituting these two models into the apparent reaction rate model for heterogeneous reactions, a global NO photocatalytic reaction rate model was created in terms of humidity and irradiance. The NO photocatalytic reaction rate model was validated by comparing the predicted NO reduction to NO reductions measured from additional experimental runs that were not used in the model creation, determining that the global model describes 87% of the data variability. These results are important for future work to develop a NO reaction rate model for photocatalytic pavements to understand the significance of NO reductions in real world environments.

5.6 REFERENCES

Ballari, M.M., Hunger, M., Husken, G., and Brouwers, H.J.H.. (2010). "NO_x photocatalytic degradation employing concrete pavement containing titanium dioxide." Applied Catalysis B: Environmental, 95, 245-254.

Beeldens, A. (2006) "An environmental friendly solution for air purification and self-cleaning effect: the application of TiO_2 as photocatalyst in concrete." Belgian Road Research Centre. Proceedings of Transport Research Arena, Europe - TRA, Göteborg, Sweden, June, 2006.

Beeldens, A. (2008). "Air purification by pavement blocks: final results of the research at the BRRC." Transport Research Arena Europe, Ljubljana.

Bengtsson, N. and Castellote, M. (2010). "Photocatalytic activity for NO degradation by construction materials: parametric study and multivariable correlations." Journal of Advance Oxidation Technologies, 13(3), 341-349.

Cassar, L. (2004). "Photocatalysis of cementitious materials: clean buildings and clean air", MRS Bulletin, May 2004, 1-4.

Diamanti, M.V., Ormellese, M. and Pedeferri, M. (2008). "Characterization of photocatalytic and superhydrophilic properties of mortars containing titanium dioxide." Cement and Concrete Research, 38, 1349-1353.

Dylla[a], H., Hassan, M. M., Mohammad, L., Rupnow T., and Wright, E. (2010). "Evaluation of the Environmental Effectiveness of Titanium Dioxide Photocatalyst coating for concrete pavements." Journal of the Transportation Research Record, 2164, 46-51.

Dylla[b], H., Hassan, M., Schmitt, M., Rupnow, T. and Mohammad, L. (2010). "Laboratory investigation of mixed nitrogen dioxide (NO_2) and nitrogen oxide (NO) gasses on titanium dioxide photocatalytic efficiency in concrete pavements." Journal of Materials in Civil Engineering, 23(7) 1087-1093.

Environmental Protection Agency (EPA[a]). (2012). "Nitrogen dioxide implementation – Programs and requirements for reducing oxides of nitrogen." Nitrogen Dioxide. <http://www.epa.gov/air/nitrogenoxides/implement.html> (July 17, 2012).

Environmental Protection Agency (EPA[b]). (2012). "Nitrogen dioxide (NO_2) Standards – Table of Historical NO_2 NAAQS." National Ambient Air Quality Standards. <http://www.epa.gov/ttn/naaqs/standards/nox/s_nox_history.html> (July 17, 2012).

Environmental Protection Agency (EPA[c]). (2012). "Air Quality System (AQS)" <http://www.epa.gov/ttn/airs/airsaqs/detaildata/downloadaqsdata.htm> (April 14, 2013).

Fujishima, A., Rao, Tata N. and Tryk, Donald A. (2000). "Titanium dioxide photocatalysis." Journal of Photochemistry and Photobiology C: Photochemistry Reviews, 1, 1-21.

Fujishima, A., and Zhang, X. (2006). "Titanium dioxide photocatalysis: present situation and future approaches." Comptes Rendus Chimie. 9, 750-760.

Hassan, M.M., H. Dylla, L.N. Mohammad, and T. Rupnow. (2009). "Effect of Application Methods on the Effectiveness of Titanium Dioxide as a Photocatalyst Compound to Concrete Pavement." 89th Transportation Research Board Annual Meeting, 10-0963.

Health Effects Institute (HEI). (2010). "Traffic-Related Air Pollution: A Critical Review of the Literature on Emissions, Exposure, and Health Effects." Special Report 17.

Hunger, M., Husken, G., and Brouwers, Jos. (2010). "Photocatalytic degradation of air pollutants – From modeling to large scale application." Cement and Concrete Research, 40, 313-320.

Japanese Industrial Standard (JIS). (2004). "Fine ceramics (advanced ceramics, advanced technical ceramics) – Test method for air purification performance of photocatalytic materials- Part 1: Removal of nitric oxide", JIS R 1701-1,1-9.

Kim, J.J., Smorodinsky, S., Lipsett, M., Singer, B. C., Hodgson, A.T., and Ostro, B. (2004). "Traffic-related air pollution near busy roads: the East Bay Children's Respiratory Health Study." American Journal Respiratory and Critical Care Medicine, 170, 520-536.

Maudhuit, A., Raillard, C., Hequet, V., Le Coq, L., Sablayrolles, J., and Molins, L. (2011). "Adsorption phenomena in photocatalytic reactions: The case of toluene, acetone and heptane." Chemical Engineering Journal, 170, 464-470.

McCarthy, J.E., Dykes, E., and Ngan, E. (2010). "Aftertreatment system performance of a fuel reformer, LNT and SCR system meeting EPA 2010 emissions standards on heavy-duty vehicle." SAE International Journal of Commercial Vehicles, 3, 130-142.

McConnell, R., Islam, T., Shankardass, K., Jerrett, M., Lurmann, F., Gilliland, F., Gauderman, J., Avol, E., Kuenzli, N.,Yao, L., Peters, J., and Berhane, K.. (2010). "Childhood Incident Asthma and Traffic-Related Air Pollution at Home and School." National Institute of Environmental Health Sciences, 1-33.

Menz, F.C. (2002). "The US experience with controlling motor vehicle pollution: lessons for China." International Journal Environment and Pollution, 18(1), 1-21.

National Renewable Energy Laboratory (NREL). (2009). "National Solar Radiation Data Base: 1961-1990: Typical Meteorological Year 2. <http://rredc.nrel.gov/solar/old_data/nsrdb/1961-1990/tmy2/> (April 14, 2013).

Poon, C.S., and Cheung, E. (2007). NO Removal Efficiency of Photocatalytic Paving Blocks Prepared with Recycled Materials. Construction and Building Materials, Elsevier, Vol. 21, 1746-1753.

Sleiman, M., Conchon, P., Ferronato, C., and Chovelon, J.M. (2009). "Photocatalytic oxidation of toluene at indoor air levels (ppbv): Towards a better assessment of conversion, reaction intermediates and mineralization." Applied Catalysis B: Environmental, 86(3-4), 159-165.

Toma, F.-L., Berger, L.M., Jacquet, D., Wicky, D., Villaluenga, I, Miguel, Y.R., and Lindelov, J.S. (2009). "Comparative study on the photocatalytic behavior of titanium oxide thermal sprayed coating from powders and suspensions." Surface & Coatings Technology, 203(15), 2150-2156.

Valsaraj, K. (2009). "Heterogeneous Catalysis." Elements of Environmental Engineering, CRC Press, Boca Raton, FL, 228-234.

Wang, S., Ang, H.M., and Tade, M. O. (2007). "Volatile organic compounds in indoor environment and photocatalytic oxidation: State of the art." Environment International, 33, 694-705.

Watts, M. J., and Cooper, A. (2008). Photocatalysis of 4-chlorophenol mediated by TiO_2 fixed to concrete surfaces. Solar Energy, 82, 206-211.

Xu, L., and McCabe, R.W. (2012). "LNT + in situ SCR catalyst system for diesel emissions control." Catalysis Today, 184(1), 83-94.

Yu, Q.L., and Brouwers, H.J.H. (2009). “Indoor air purification using heterogeneous photocatalytic oxidation. Part I: Experimental study.” Applied Catalysis B: Environmental, 92, 454-461.

Zhao, J., and Yang, X. (2003). “Photocatalytic oxidation of indoor air purification: a literature review. Building and Environment, 38, 645-654

CHAPTER 6
EVALUATION OF THE PHOTODEGRADATION OF NITROGEN MONOXIDE FROM PHOTOCATALYTIC PAVEMENTS: A BOX MODELING APPROACH

6.1 INTRODUCTION

Heterogeneous photocatalysis has become a competitive technology for air and water environmental pollution remediation, evident by the growing number of photocatalytic products and research papers (Fujishima and Zhang 2006). Initial interest in environmental photocatalysis began in the 1970s, initiated by Fujishima and Honda's research in photoelectrochemical solar energy conversion (Fujishima and Honda 1972). Through biomimicy of plant photosynthesis, Fujishima attempted to replicate the photo-induced redox reactions, oxidizing water and reducing carbon dioxide, by using a semiconductor irradiated by UV light (Fujishima and Zhang 2006). To accomplish this, the semiconductor was used as an electrode connected to a counter electrode to generate electrical work to drive the redox chemical reactions (Fujishima and Honda 1972). By removing the electrode, environmental photocatalytic oxidation occurs completely decomposing both organic and inorganic compounds. Since then, interest in environmental photocatalysis has increased and TiO_2 photocatalysts have been applied to glass, tile, paper, and pavements for self-cleaning materials, water purification, air purification, sterilization, and oil spill remediation (Fujishima and Zhang 2006).

Recently, due to the growing concern of urban air pollution problems from traffic sources, significant interest has been given to photocatalytic pavements (Beeldens 2006, Ballari et al. 2010, Cassar 2004, Chen and Li 2007, Dylla et al. 2009, Hassan et al. 2009, and Poon and Cheung 2007). Several laboratory studies have investigated efficiencies of photocatalytic pavements using various photocatalytic pavement mix designs under different environmental conditions demonstrating its potential (Chen and Li 2007, Dylla et al. 2009, Hassan et al. 2009,

and Poon and Cheung 2007). Despite this, translating laboratory results to the field is a challenge and understanding the efficacies in real world environments remains a challenge (Berdahl and Akbari 2008). From these studies, it is evident that the efficiency depends on many environmental factors including the concentration of pollutants, relative humidity, temperature, irradiance and wind speed, all of which complicate the interpretation of field studies results (Sleiman et al. 2008, Bengtsson, and Castellote 2010, Dylla et al. 2010). Consequently, even though several field studies demonstrated reductions of nitrogen oxides, it is not clear whether these reductions are truly a result of photocatalytic oxidation (Beeldens 2008, Maggos et al. 2008, Li and Qian 2009, Hunger 2010).

A promising approach to understanding photocatalytic pavements in real world conditions is through air pollution modeling approaches, which incorporates the photocatalytic reaction kinetics. With this in mind, the present authors investigated the impact of relative humidity and irradiance on the reaction kinetics for the photocatalytic degradation of NO and developed a model for the apparent reaction rate as a function of these two parameters. Using a plug flow reactor, the reaction kinetics under various environmental conditions were investigated by varying the relative humidity between 27% to 81% and the irradiance between 0.52 W/m^2 to 3.52 W/m^2 (Chapter 5). The application of the Langmuir-Hinshelwood model for heterogeneous reactions has been studied by several researchers and has been used to model the degradation of volatile organic compounds (VOCs) and NO_x (Demeestere et al. 2004 Sleiman et al. 2008, Hunger et al. 2010). Thus, assuming the Langmuir-Hinshelwood model, the Langmuir reaction rate constant and Langmuir adsorption constant were calculated for each environmental condition (Chapter 5). Then using multiple linear regression statistical techniques, a model was created for k and Kd as a function of humidity and irradiance, which can be substituted into the

L-H apparent reaction rate model to allow for estimation of the photocatalytic oxidation of NO at different environmental conditions. Building on these findings, the objective of the present study is to develop a Lavoisier mass balance model for roadway microenvironments incorporating the chemical kinetics derived from previous studies. In doing so, the significance of the photocatalytic reduction of NO expected in outdoor environments will be compared to other mass transfer mechanisms.

6.2 BACKGROUND

There are several roadway microenvironments pollution dispersion models such as Gaussian plume dispersion model, computational fluid dynamics (CFD), atmospheric box model, and statistical models such as source apportionment (Lin and Yu 2008). Dispersions models are described as either, Lagrangian or Eulerian depending on the frame of reference of the transport equations. The Eulerian models relate the transport to coordinates working from a fixed grid while Lagrangian models follow a volume or parcel of air moving downwind, modeling the pollutant as it moves (Sharma et al. 2004). A brief description of these models and the associated advantages and disadvantages are presented in Table 6.1.

Table 6.1 Comparison of Air Dispersion Models

Model	Description	Advantages	Disadvantages
Gaussian Plume Dispersion Models	Models dispersion by bell-shaped normal standard distribution	Well developed, software available	Does not include reaction, unsuitable for urban conditions
Computational Fluid Dynamic Models	Models dispersion by fluid flow	Detailed, 3D fluid simulations, suitable for urban environments	Long processing time, requires expert knowledge, difficult to include reactions, uncertainties still exist
Statistical Models	Models concentration from receptor specific parameters	Simple, does not require expert knowledge,	Requires a large amount of historical data, receptor specific
Box Models	Models dispersion by mass balance	Simple for complex reactions	Assumes well mixed

For transportation pollution modeling, Gaussian plume models are the most common (Bhatt 2005). The Gaussian plume model assumes that the dispersion is modeled as a bell-shape normal standard distribution, which is a function of the horizontal and vertical dispersion (Lin and Yu 2008). The model is initially for a single puff point source; however, it is modified for continuous sources by the summation of a series of single puffs. For traffic pollution, the Gaussian line source model is used to predict pollutant concentrations for identified receptors. The most prominent models created for traffic pollution modeling is the CALINE series developed by the California Department of Transportation. There are several versions available including CAL3QHC, CALINE3, and the latest, CALINE4 (Chen et al. 2008). Input requirements included, traffic volume, emission factors, roadway geometry, wind speed and direction, ambient air temperature, mixing height, atmospheric stability class, and receptor coordinate (Benson 1984). Carbon dioxide, NO_2, and particulate matter all can be modeled, however NO_2 analysis requires additional inputs and reaction calculations (Chen et al. 2008, Benson 1984). Further background behind this model is described elsewhere (Benson 1984, Bhatt 2005).

Computational fluid dynamics (CFD) is a physical approach to model pollutant dispersion, predominantly used to understand the flow through complex systems (Sharma et al. 2004, Vardoulakis et al. 2003). For this reason, they are primarily used for modeling pollutant dispersion in street canyons of urban areas (Vardoulakis et al. 2003). Since they do not include photochemical reactions, simplified photochemical algorithms must be combined with CFD models. In addition, the computational power required to solve the fluid equations limit this modeling technique to micro-scale studies (Holmes and Morawska 2006, Vardoulakis et al. 2003). However, with improving technology, CFD techniques are becoming more popular, since

they provide detailed flow and concentration profiles for complex urban areas (Vardoulakis et al. 2003). ARIA Local, MISKAM, and MIMO are CFD models developed for local transportation air pollution modeling (Moussiopoulos et al. 2008, Holmes and Morawksa 2006). Yet, it is still uncertain the applicability and accuracy of results of CFD models for vehicular pollution dispersion models (Sharma et al. 2004).

Statistical approaches include regression, multiregression, and artificial neural networks. Estimates are calculated by the statistical relationship to various factors collected at a particular receptor (Sharma et al. 2004). Source apportionment models, which attempt to identify different sources contribution to the pollution at a particular receptor, use many of these statistical methods such as principal component analysis (PCA) and multilinear regression (Vallius et al. 2008). These models are important to identify sources contribution to human exposure for air pollution policy and regulation to mitigate associated risks (Zeng et al. 2010). These models are easy to use but they are receptor or location specific, require large amounts of historical data, and do not identify the significance of various physical and chemical processes (Sharma et al. 2004).

One drawback of the Gaussian plume models, and to some extent CFD and statistical models is that generally chemical and physical mechanisms are neglected or difficult to implement. To include more detailed chemical reaction schemes, box models are advantageous. Based on the fundamental theory of mass conservation for a defined a volume, various transport and transformation mechanisms are simple to incorporate into the model (Lin and Yu 2008, Holmes and Morawska 2006). The defined volume (the box) is assumed as a well-mixed uniform concentration (Holmes and Morawska 2006). This is the major drawback to box models; thus, they are not as effective for point sources or local environmental studies. Despite this, they are particularly effective for modeling area pollution sources and effective to identify

the significant transport and transformation mechanism (Holmes and Morawska 2006, Cheng et al. 2006). STREET-SRI, AURORA, and CPB are box models developed for transportation air pollution modeling (Cheng et al. 2006).

Few models exist to describe the performance of photocatalytic pavement materials reduction of NO under outdoor environmental settings. The only known model to incorporate the photocatalytic reduction of NO in an outdoor setting was a 3-D CFD model for the photocatalytic degradation of NO_x for a pilot street cannon containing TiO_2-mortar panels rather than photocatalytic pavements. This model used numerical modeling techniques using MIMO, an analytical microscale model, specific to air motion near building structures (Ehrhard et al 2000). The conservation of mass, momentum, energy and passive pollutants are numerically solved using the finite volume discretization method. However, rather than incorporating the reaction kinetics, the photocatalytic degradation of NO_x was simplified and incorporated as a "deposition" module to approximate removal flux (Moussiopoulos et al. 2008).

Extensive research has been conducted on TiO_2 photocatalytic reactor models, which have incorporated reaction kinetic modeling with pollutant dispersion models such as computational fluid dynamics (Duran et al. 2011, Salvado-Estivill et al. 2007). These models were useful to predict the concentration of pollutants and understand the significance of various transport mechanism when the reactor design is modified (Sharma et al. 2004). Despite this, to the authors' knowledge, no such model that incorporates reaction kinetic models into outdoor dispersion models for evaluating photocatalytic pavements exists.

6.3 MODEL DEVELOPMENT

The selected modeling approach was the box model because of its simple structure, ability to easily incorporate complex chemical reactions, and ability to compare the mass transfer

processes. The model created uses the principles of Lavoisier mass balance of NO for a defined system. The system boundaries were defined for a typical urban roadway microenvironment, where the height of the box was defined by the tree or building heights, the width was defined by the width of the road, and the length was defined as equal to the width. The system volume was assumed as well mixed, with a uniform concentration of NO, temperature, and pressure at steady-state. The transport and transformation processes for NO included the convection in and out of NO from the system sides, NO vehicle emissions, NO-Ozone reaction, photocatalytic degradation of NO, and turbulent diffusion out the system top and sides. For cross wind situations, as depicted in Figure 6.1, diffusion out of the sides can be neglected since advection dominates mass transfer. As a result, the chemical mass balance yields the following equation:

$$\mathrm{uhlC_{NO}^{in}} + \mathrm{W_{NO}^{in}} - \mathrm{r_{NO-Ozone}whl} - \mathrm{r_{NO}whl} - \mathrm{wlk_{NO}C_{NO}^{out}} - \mathrm{uhlC_{NO}^{out}} = \mathrm{whl}\frac{\mathrm{dC_{NO}}}{\mathrm{dt}} \qquad (6.1)$$

Where u is the wind velocity (m/s), h is the height of the box (m), l is the length of the box (m), C_{NO}^{in} is the ambient background concentration of NO ($\mu g/m^3$), W_{NO}^{in} is the vehicle emission mass transfer rate ($\mu g/s$), $r_{NO-ozone}$ is the reaction rate of NO and ozone ($\mu g/m^3 s$), w is the width of the box (m), r_{NO} is the photocatalytic reaction rate of NO ($\mu g/m^3 s$), k_{NO} is the vertical mass transfer coefficient for turbulent diffusion (m/s), C_{NO}^{out} is the concentration in the box ($\mu g/m^3$) and $\frac{dC_{NO}}{dt}$ is the change of NO concentration over time ($\mu g/m^3 s$).

At steady state, there is no change in concentration over time. Thus, the right side of the equation equals zero. All of the model inputs are known except for the steady state concentration in the box, C_{NO}^{out}, which was calculated for various environmental conditions. The percent of NO reduction is the mass transfer estimated for the photocatalytic degradation over the total inlet.

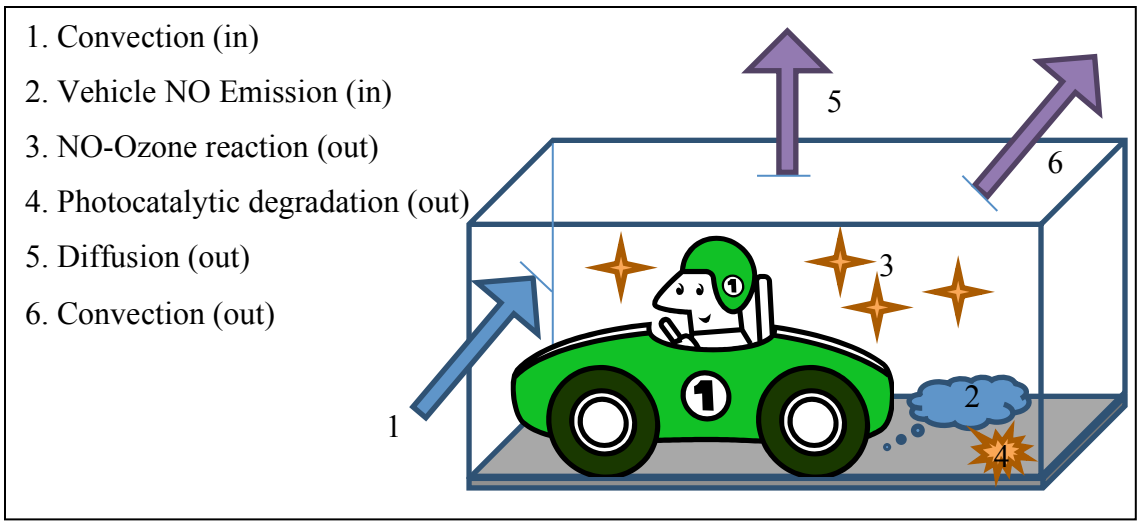

Figure 6.1 Mass Balance Box Model

6.3.1 Model Inputs

The model inputs were obtained from a variety of sources. Historical data were used to characterize the environmental conditions. Typical meteorological year (TMY-2) files defined possible meteorological inputs and the EPA 2011 Air Quality System (AQS) ambient air pollution records defined possible NO pollutant concentrations (NREL 2009, EPA 2012). Additional models were required to define the photocatalytic degradation rate, NO reaction rate with ozone, and NO vertical diffusion mass transport coefficient. Descriptions of the environmental conditions assumed and the models are described in the subsequent sections.

6.3.2 Environmental Conditions

Typical concentrations of NO and ozone were estimated from the Air Quality System (AQS). The Air Quality System (AQS) provides ambient air quality data for air toxics for over 10,000 monitors across the United States and parts of Mexico. These concentrations already include point pollution and mobile sources such that the vehicle emissions can be assumed as a part of these concentrations recorded. Areas in the United States that have reported high concentrations of NO pollution include California, Illinois, Massachusetts, New Jersey, New York, Texas and

Utah. According to the EPA AQS these states have one or more counties that have recorded an hourly NO average concentration over 450 ppb in the year of 2011 (EPA 2012). As a result, applying photocatalytic pavements in these areas may be most beneficial. Focusing on one of these areas, the model was applied for the city of Los Angeles (California) since it has reported high NO concentrations and it has a high solar potential (NREL 2012, NREL 2009).

With this in mind, the TMY-2 weather files for Los Angeles determined the ranges for the environmental conditions. From the TMY-2 weather files, the relative humidity varied from 6% to 100%, the temperature varied from 4.4°C to 35°C and the maximum irradiance was 2.77 mW/cm^2 (assuming that TiO_2 only uses 2.7% of the global horizontal radiation) (NREL 2009). Thus resulting environmental conditions are described in Table 6.2. The minimum and maximum values are also dependent upon the valid inputs ranges defined for the photocatalytic model. As noted, the relative humidity can be varied between 27%-81%, the irradiance can be varied between 0.52 mW/cm^2 -3.7 mW/cm^2, and the temperature must be 27°C.

The system boundaries were defined for a $13m^2$ typical urban roadway microenvironment area. The height of the box is defined by element heights. In a study completed by Burian et al. (2002), the average building heights are described and separated by the function of land use. The average element height for the transportation sector was 7.9 meters. The highest average element heights were downtown LA and the lowest are in residential areas, noted in the Table 6.2. The width of the system boundaries is 3.6 m defined by the width of a single lane and the length is defined as equal to the width (FHWA 2007).

Table 6.2 Environmental Characteristics

Parameters	Variable Notation	Min.	Max.	Avg.	Source
Humidity (%)	H	6[1]	100[1]	69	TMY-2
UV Irradiance (mW/cm^2)	I	0[1]	2.77	0.56	TMY-2
Wind Velocity (m/s)	u	0	22.6	3.6	TMY-2
Temperature (°C)[2]	T	4.4	35	16.7	TMY-2
Pavement Width (m)	w	3.6	30	-	FHWA
Element Heights (m)	h	4	45	-	Burian[b] et al. 2002
Concentration NO (µg/m^3)	C_{NO}	0	589	38	AQS
Concentration O_3 (µg/m^3)	C_{O3}	0	284	53	AQS

[1] Values used are determined by the valid input range for the photocatalytic NO reaction rate model (Table 6.3)
[2] Temperature is constant at 27°C limited by the photocatalytic NO reduction rate model

6.3.3 Multiple Parameter Kinetic Model for Photocatalytic Oxidation NO

The photocatalytic degradation of NO is most commonly reaction limited and modeled using the Langmuir-Hinshelwood model for heterogeneous surface reactions. Using this model, the NO photooxidation rate is described as follows:

$$r_{NO} = \frac{k^{*}KC_{NO}}{1+KC_{NO}} \tag{6.2}$$

where,

r_{NO} = NO photooxidation rate (mg/m^{3}s);
k = L-H reaction rate constant (mg/m^{3}s);
Kd = the L-H adsorption equilibrium constant (m^3/mg); and
C_{NO} = the concentration of NO (mg/m^3).

From previous research conducted by the authors, a multiple linear regression model was created for the both the L-H equilibrium adsorption constant, Kd and the L-H reaction rate constant, k as a function of humidity and irradiance. The resulting models are presented below:

$$\mathrm{Kd}(\mathrm{H},\mathrm{I}) = (0.01415 * \mathrm{H} - 0.00176 * \mathrm{H} * \mathrm{I} + 0.45672)\text{^}2 \tag{6.3}$$

$$\mathrm{k}\,(\mathrm{H},\mathrm{I}) = (-0.007 * \mathrm{H} * \mathrm{I} + 0.69536 * \mathrm{I} + 1.19801)\text{^}2 \tag{6.4}$$

where,

H = Humidity (%); and
I = Irradiance (mW/cm^2).

It is noted that the developed Kd and k models are only valid for the environmental conditions defined in Table 6.3. The resulting model for Kd explained 76% of the variance in the data, whereas the model for k explained 84% of the variance in the data.

Table 6.3 Valid Input Ranges

Parameters	**Range of variation**	
	Low Level	**High Level**
Humidity (%)	27	81
UV Irradiance (W/m^2)	0.52	3.52
Temperature °C	27	27

By substituting the models created for Kd and k into Equation 6.2, the apparent reaction rate for NO degradation is modeled as a function of humidity and irradiance as shown in Equation 6.5. An additional 83 runs were completed to test the validity of the overall NO photocatalytic apparent reaction rate model whereby 87% of the data variance was explained. Limitations to this model include competition with intermediates and other pollutants, catalyst poisoning, and durability of the photocatalytic pavements.

$$r_{NO} = \frac{k(H,I) * Kd(H,I) C_{NO}}{1 + Kd(H,I) C_{NO}} \quad (6.5)$$

6.3.4 Estimation of NO-Ozone reaction rate

Once NO is in the atmosphere it can be converted rapidly into NO_2 in a reaction with ozone through the following reaction (Shon 2008):

$$NO + O_3 \rightarrow NO_2 + O_2 \quad (6.6)$$

Several studies have measured the absolute rate coefficient and were summarized by Atkinson et al. (2004). The recommended rate coefficient, a function of temperature, is shown in Equation 6.7 (Atkinson et al. 2004):

$$k = 1.4x10^{-18}e^{\frac{-1310}{T}} \quad (6.7)$$

where,

k = m^3 $molecule^{-1}$ sec^{-1}; and
T = Temperature in K.

It is noted that the model is only valid for temperature between 195-308 K. Since the photocatalytic reaction model is only valid at 27°C (300 K), this reaction rate is actually constant at $1.8x10^{-20}$ m^3 $molecule^{-1}$ sec^{-1}. Using the rate law, the reaction rate, $r_{NO\text{-}Ozone}$ is as follows:

$$r_{NO-Ozone} = k[NO][O_3] \quad (6.8)$$

where,

$r_{NO\text{-}Ozone}$ = reaction rate of NO with Ozone (m/s);
NO = concentration of NO ($\mu g/m^3$); and
O_3 = concentration O_3 ($molecules/m^3$).

6.3.5 Estimation of NO Vertical Diffusion Mass Transport Coefficient

The vertical diffusion mass transfer coefficient was estimated by the theories developed for vegetation canopies. Using these theories, the turbulent mass transfer was estimated by bulk aerodynamic resistance, R_a, the quasilaminar sublayer resistance, R_b, as follows (Thibodeaux and Mackay 2011):

$$k_{NO} = \frac{1}{R_a + R_b} \quad (6.9)$$

The bulk aerodynamic resistance is primarily associated with the turbulent diffusion through the quasi laminar boundary layers. It is a function of wind speed, the roughness, and the atmospheric stability. Assuming neutral atmospheric stability, this is approximated as follows:

$$R_a = \frac{(\ln(z-d)/z_0)^2}{\kappa^2 u} \quad (6.10)$$

Where z is 10 meters the height above ground at which the wind speed is measured (m), u is the wind speed (m/h), d is the displacement height (m), z_0 is the surface roughness (m), and κ is the Karman constant which is 0.4. The surface roughness and displacement height for the transportation areas in Los Angeles was estimated by the average element heights using the Raupach (1994) equations as 0.05 and 1.41, respectively (Burian et al. 2002[a]).

The quasilaminar sublayer resistance, R_b, is primarily associated with the molecular diffusion through the quasi laminar boundary layers. For neutral atmospheric stability, it is estimated as follows:

$$R_b = \frac{2(\ln(z-d)/z_0)}{\kappa^2 u}\left(\frac{\nu}{D}\right)^{2/3} \quad (6.11)$$

Where ν is the kinematic viscosity (m^2/h), 1.51x10^{-5} m^2/s, and D is the molecular diffusion coefficient for NO (m^2/h). Since the kinematic viscosity of air estimates the molecular diffusion of NO, $\frac{\nu}{D}$ simplifies to 1 and Equation 6.11 can be re-written as follows:

$$R_b = \frac{2(\ln(z-d)/z_0)}{\kappa^2 u}(1)^{2/3} \quad (6.12)$$

6.4 RESULTS AND DISCUSSION

For a well-mixed system volume, with a uniform concentration of NO, temperature, and pressure at steady-state, the concentration of NO out of the box is calculated for the average conditions defined for Los Angeles. Figure 6.2 illustrates the proportions of each of the mass transfer fluxes

of NO out of the system boundaries. As shown, convection is the dominating mass transfer flux accounting for 97% of the concentration of NO out of the box. The percent of concentration of NO out due to the photocatalytic reaction is 2%, only 1% is accounted to the reaction between NO and O_3, and the diffusion of NO is insignificant.

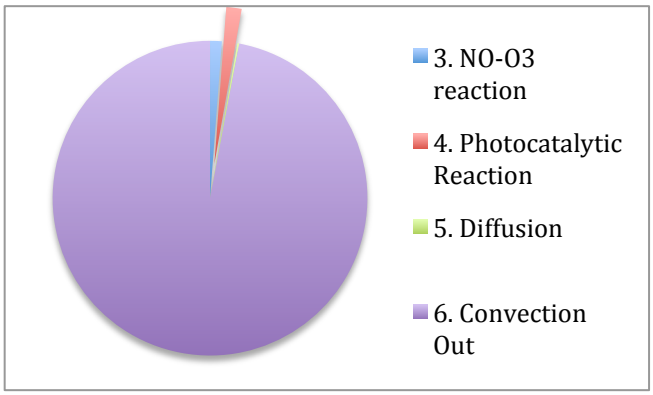

Figure 6.2 Percent of NO Out of System Boundaries per Mass Transfer Mechanism

6.4.2 Sensitivity Analysis

Due to the uncertainty of many of the parameters and to better understand the relationships between these parameters and the model output, the sensitivity of each of the inputs was evaluated. This includes, the inputs for the photocatalytic degradation reaction rate, NO convection mass transfer, NO diffusion and the reaction rate between NO and ozone. Figure 6.3 illustrates the relationship between the inputs and the mass transfer mechanism impacted for each mass transfer mechanism incorporated into the overall box model.

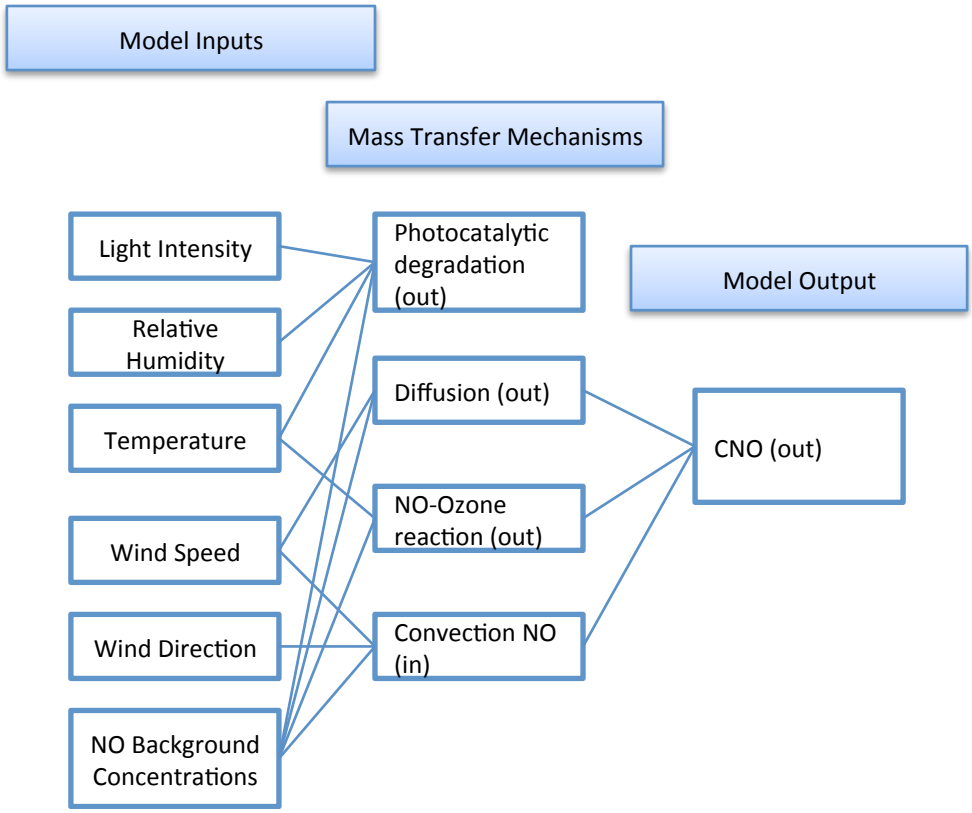

Figure 6.3 Model with Inputs, Mass Transfer Mechanism, and Outputs

Using these identified parameters, non-responsive variables were identified and the responsive variables ranked by using the sensitivity index. This index was calculated as a function of the output when the parameter is maximum, $Dmax$, and the output when the parameter is minimum, $Dmin$, shown in Equation 6.13. The concentration of NO out and the percent of NO reduced for the photocatalytic oxidation were both estimated for the minimum and maximum values of each parameter illustrated in Figure 6.3. Meanwhile, all other parameters were set at the average values.

$$\mathrm{SI} = \frac{(\mathrm{Dmax} - \mathrm{Dmin})}{\mathrm{Dmax}} \qquad (6.13)$$

The resulting sensitivity indexes are found in Table 6.4. As it can be seen, the most significant factor is the velocity of air, followed by the concentration of NO for both the

concentration out and the percent out due to the photocatalytic reduction of NO. The increasing air velocity significantly decreases the percent of NO reduced from the photocatalytic reaction as expected since the contact time is reduced. Consequently, with lower reductions of NO due to the photocatalytic reaction, the NO concentration out of the system boundaries is higher. The impact of the ozone concentration is the third largest impacting variable for the concentration of NO out. As higher concentrations of ozone are present more can react with the NO lowering the amount of NO out. However, this does not impact the percent of NO reduced from the photocatalytic reaction. Instead, the humidity is the third most influential variable on the photocatalytic reduction of NO out of the system boundaries and is followed by the UV irradiance.

Table 6.4 Environmental Characteristics

Parameters	Concentration NO out		% Photocatalytic Reduction of NO out	
	SI	Rank	SI	Rank
Humidity (%)	-0.0043	4	0.2641	3
UV Irradiance (W/m^2)	0.0006	5	-0.0394	4
Velocity of Air (m/s)	2.0391	1	-43.0000	1
Concentration NO ($\mu g/m^3$)	0.9569	2	-1.3951	2
Concentration O_3 ($\mu g/m^3$)	-0.0721	3	0.0000	5

The significant parameters identified by the sensitivity indices were further evaluated to identify the impacting trend. The parameter was varied between the minimum and maximum range, while all other parameters are held constant at the average. Figures 6.4-7 illustrate the resulting trends for the impact of the humidity, UV irradiance, velocity of air, and concentration of NO in the system boundaries on the concentration of NO out of the system boundaries and on the percent of the NO out due to photocatalytic reaction. With the exception of the wind velocity, the NO reduction due to the photocatalytic pavement is minor, with the maximum percentages less than 2%. Yet this is significantly low, use of photocatalytic pavements should

not be completely ruled out as a possible remediation technology. In Figure 6.6, when the velocity is low the amount of reduction due to the photocatalytic pavement is significant. One limitation of the proposed model is that it assumed that the velocity was uniform with increasing height. For example, in channels, which could be created by buildings in urban environments, the velocity is lower near the pavement surface. Despite this, caution should be used because the proposed model assumes that the photocatalytic pavement comes in contact with 100% of the inlet concentration of NO. As a result, this type of system would provide maximum reduction from the photocatalytic surface. This may be improved by creating a multiple box model, one box with a small height over the pavement surface and a second box above with height defined by average element heights.

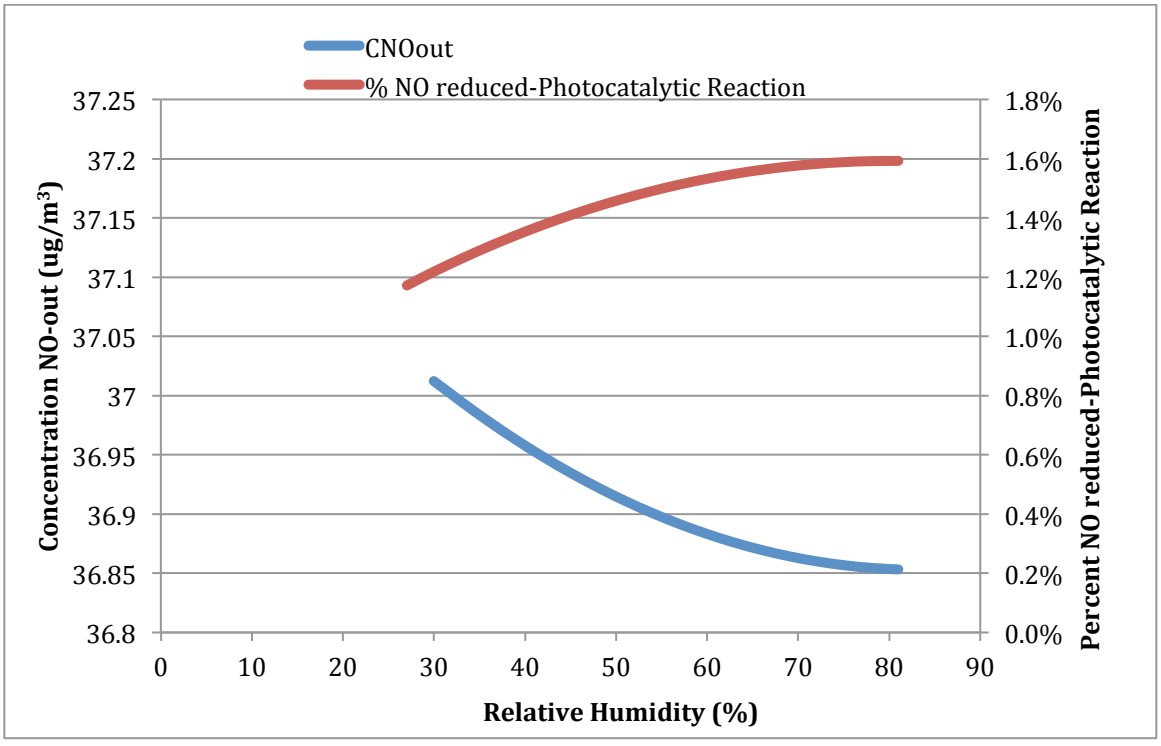

Figure 6.4 Impact of the Relative Humidity on the Concentration of NO Out and Percent of NO Reduced from the Photocatalytic Reaction

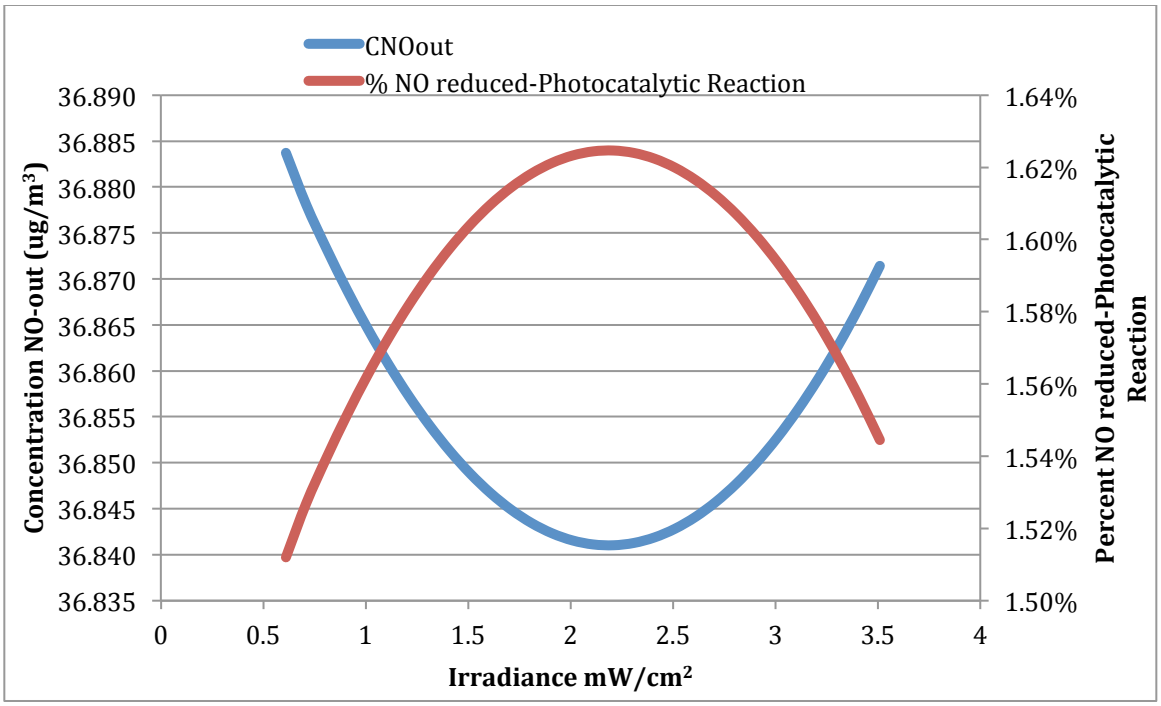

Figure 6.5 Impact of the Irradiance on the Concentration of NO Out and Percent of NO Reduced from the Photocatalytic Reaction

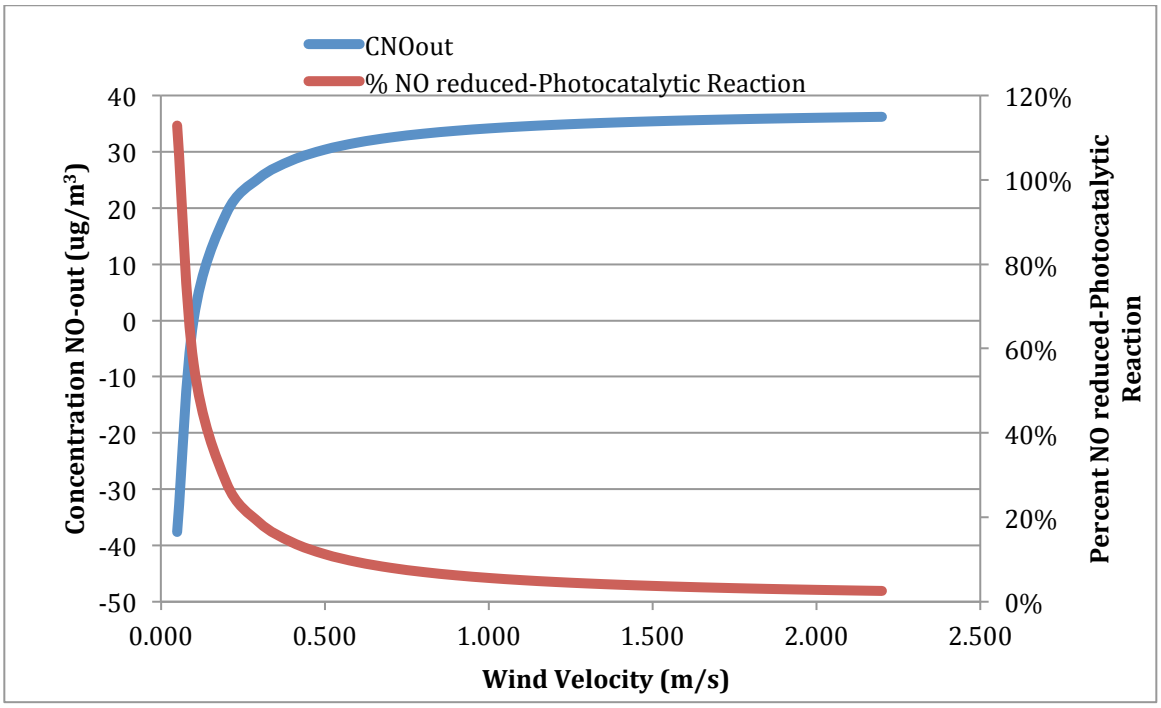

Figure 6.6 Impact of the Wind Velocity on the Concentration of NO Out and Percent of NO Reduced from the Photocatalytic Reaction

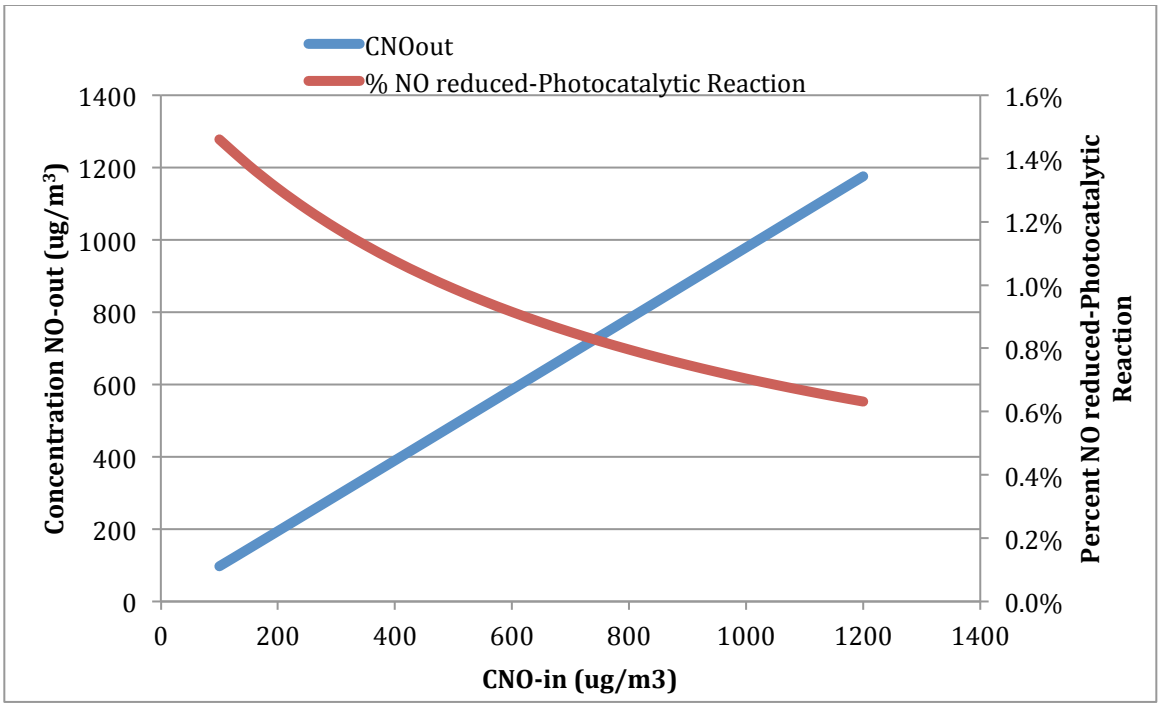

Figure 6.7 Impact of the Concentration of NO In the System on the Concentration of NO Out and Percent of NO Reduced from the Photocatalytic Reaction

6.4.2 Future Model Validation

One of the most overwhelming tasks is to validate these complex environmental models (Pederson et 2001). Future work is required to validate the model using observed data. In doing, so the vehicle emission rate should be estimated rather than assumed to be included in ambient pollution levels. To estimate the vehicle emission rate, the Motor Vehicle Emission Simulator MOVES developed by EPA should be used. This requires that the box model be separated into links, which are unique segments for each type of vehicle activity. For one lane of roadway, three vehicle links are required. One link would represent the free-flow vehicle travel. The second link would represent the queuing link, due to vehicle idling, while the final link would be an off-network link, representing vehicle start up activity. Project specific details are required for each activity link. These inputs and potential sources are identified and defined in Table 6.5 and should be specific to the intended field study. For each link, the vehicle age distribution,

vehicle classification, fuel supply, and inspection maintenance (I/M) program can be assumed the same. However, the vehicle average speed and count should be measured for each link separately. Traffic field studies should be conducted to estimate the amount of vehicle starts per hour and the distribution between queuing and free flow vehicles counted by a traffic counter.

Table 6.5 MOVES Emission Model Inputs

Inputs	Value	Source
Temperature	Degree Celsius	Determined by Field Site
Relative Humidity	%	Determined by Field Site
Vehicle Fleet Age Distribution	Fraction vehicle type by year	National defaults
Fuel Supply and Formulation	Fuel type and mix	National defaults
Inspection and Maintenance	Definition of I/M program	National defaults
Link Source type	Vehicle Class	National defaults
Traffic Count per vehicle activity: Free flow Idling Vehicle starts	Unit of vehicles per hour	Determined by Field Site
Average speed	m/s queuing (0 average speed)	Determined by Field Site
Road Grade	% (vertical distance/lateral distance, 100% is 45-degree slope)	Determined by Field Site
Length	m	Determined by Box Length

6.5 CONCLUSION

In order to better understand the significance NO_x reduction potentially realized in the field, a chemodynamic model is developed based on a Lavoisier mass balance model and the photocatalytic reaction kinetics. The model was applied to a $13m^2$ urban roadway microenvironment for Los Angeles, California, since it has reported some of the highest NO concentrations. Meteorological data estimated from historical TMY-2 files, NO and Ozone concentrations estimated from 2011 ambient air monitoring data sets, and NO-Ozone reaction rate constant, surface roughness, and displacement height, estimated from published literature

were used as the model inputs. The photocatalytic reaction rate model was estimated using a model developed from a previous study conducted by the researchers.

The concentration of NO out of the system volume was calculated as well as the percent of NO out due to the photocatalytic pavement assuming a well mixed, uniform concentration of NO, temperature, and pressure at steady-state. At average environmental conditions the model illustrated that the convection was the dominating mass transfer flux of NO out, accounting for 97% while the photocatalytic reduction of NO only accounted for 2%. Due to the uncertainty of many of the parameters, a sensitivity analysis was conducted indicating that the air velocity was the most significant factor impacting the percent of photocatalytic reduction of NO.

Despite the low photocatalytic reductions predicted, additional research is required to improve model limitations. Possible model modifications include creating a multi-box model to account for variance in velocity and concentrations at various heights. Further development of this model could be key for identifying key locations that would benefit most from photocatalytic pavements.

6.6 REFERENCES

Atkinson, R., Baulch, D.L., Cox, R.A., Crowley, J.N., Hampson, R.F., Hynes, R.G., Jenkin, M.E., Rossi, M.J., and J. Troe. (2004). "Evaluated kinetic and photochemical data for atmospheric chemistry: Volume I – gas phase reactions of Ox, HOx, NO_x, and SO_x species." Atmospheric Chemistry and Physics, 4, 1461-1738.

Ballari, M.M., Hunger, M., Husken, G., and Brouwers, H.J.H.. (2010). "NO_x photocatalytic degradation employing concrete pavement containing titanium dioxide." Applied Catalysis B: Environmental, 95, 245-254.

Beeldens, A. (2006) "An environmental friendly solution for air purification and self-cleaning effect: the application of TiO_2 as photocatalyst in concrete." Belgian Road Research Centre. Proceedings of Transport Research Arena, Europe - TRA, Göteborg, Sweden, June, 2006.

Beeldens, A. (2008). "Air purification by pavement blocks: final results of the research at the BRRC." Transport Research Arena Europe, Ljubljana.

Bengtsson, N. and Castellote, M. (2010). "Photocatalytic activity for NO degradation by construction materials: parametric study and multivariable correlations." Journal of Advance Oxidation Technologies, 13(3), 341-349.

Benson, P. (1984). "CALINE4 – A dispersion model for predicting air pollutant concentrations near roadways." 57328-604167. Office of Transportation Laboratory, California Department of Transportation, Sacramento, CA.

Berdahl, P. and Akbari, H. (2008). Evaluation of Titanium Dioxide as a Photocatalyst for Removing Air Pollutants. California Energy Commission, PIER Energy-Related Environmental Research Program. CEC-500-2007-112.

Bhatt, H. (2005). Determination of Safe Buffer Width of Roadway to Protect Human Health from Harmful NO_x Exposure. Master Thesis, University of Texas at Arlington.

Burian[a], S.J., Brown, M.J., and S.P. Velugubantia. (2002) "Roughness length and displacement height derived from building databases." AMS 4th Symposium on the Urban Environment, Norfolk, VA, May 2002.

Burian[b], S.J., Brown, M.J., and S.P. Linger. (2002). "Morphological analyses using 3D building databases: Los Angeles, California." LA-UR-02-781.

Cassar, L. (2004). "Photocatalysis of cementitious materials: clean buildings and clean air", MRS Bulletin, May 2004, 1-4.

Chen, D. H. and Li, K. (2007). Photocatalytic Coating on Road Pavements/Structures for NO_x Abatement. 26 January 2007. Texas Air Research Center, Lamar University, Beaumont, TX

Chen, H., Bai, S., Eisinger, D., Niemeier, D., and Claggett, M. (2008). "Modeling uncertainties and near-raod PM2.5: A comparison of CALINE4, CAL3QHC, and AERMOD." U.S. Federal Highway Administration, and U.C. Davis-Caltrans Air Quality Project.

Cheng, S., Li, J., Feng, B., Jin, Y. and Hao, R. (2006). "A Gaussian-box modeling approach for urban air quality management in a northern chinese city—I. model development." Water Air Soil Pollution, 178, 37-57.

Demeestere, K., Dewulf, J., De Witte, B., Beeldens, A. and Van Langenhove, H. (2008). "Heterogeneous photocatalytic removal of toluene from air on building materials enriched with TiO_2". Building and Environment, 43(4), 406-414.

Duran, E.J., Mohseni, M., and Taghipour, F. (2011). "Design improvement of immobilized photocatalytic reactors using a CFD-Taguchi combined method." Industrial and Engineering Chemistry Research, 50, 824-831.

Dylla, H., Hassan, M. M., Mohammad, L., Rupnow T., and Wright, E. (2010). "Evaluation of the Environmental Effectiveness of Titanium Dioxide Photocatalyst coating for concrete pavements." Journal of the Transportation Research Record, 2164, 46-51.

Ehrhard, J., Khatib, I.A., Winkler, C., Kunz, R, Moussiopoulos, N., and Ernst, G. (2000). "The microscale model MIMO: development and assessment." Journal of Wind Engineering and Industrial Aerodynamic, 85, 163-176.

Environmental Protection Agency (EPA). (2012). "Air Quality System (AQS)" <http://www.epa.gov/ttn/airs/airsaqs/detaildata/downloadaqsdata.htm> (April 14, 2013).

Federal Highway Administration (FHWA). (2007). "Chapter 3: The 13 Controlling Criteria, Lane Width" <http://safety.fhwa.dot.gov/geometric/pubs/mitigationstrategies/chapter3/3_lanewidth.htm> (April 14, 2013).

Fujishima, A., and K. Honda. (1972). "Electrochemical Photolysis of Water at a Semiconductor Electrode." Nature, 238, 37-38.

Fujishima, A., and Zhang, X.. (2006). "Titanium dioxide photocatalysis: present situation and future approaches." Comptes Rendus Chimie. 9, 750-760.

Hassan, M.M., H. Dylla, L.N. Mohammad, and T. Rupnow. (2009). "Effect of Application Methods on the Effectiveness of Titanium Dioxide as a Photocatalyst Compound to Concrete Pavement." 89th Transportation Research Board Annual Meeting, 10-0963.

Holmes, N.S. and Morawska, L. (2006). "A review of dispersion modeling and its application to the dispersion of particles: An overview of different dispersion models available." Atmospheric Environment, 40, 5902-5928.

Hunger, M., Husken, G., and Brouwers, J. (2010). "Photocatalytic degradation of air pollutants – From modeling to large scale application." Cement and Concrete Research, 40, 313-320.

Li, L. and Qian, C. (2009). "A lab study of photo-catalytic oxidation and removal of nitrogen oxides in vehicular emissions and its fieldwork on Nanjin No.3 bridge of Yangtze River." Journal of Pavement Resource Technology, 2(5), 218-222.

Lin, J. and Yu, D. (2008). "Traffic-related air quality assessment for open road tolling highway facility." Journal of Environmental Management, 88, 962-969.

Maggos, T., Plassais, A., Bartzis, J.G., Vasilakos, C, Moussiopoulos, A. and Bonafous, L. (2008). "Photocatalytic degradation of NO_x in a pilot street canyon configuration using TiO_2-mortar panels." Environmental Monitoring Assessment, 136, 35-44.

Moussiopoulos, N., Barmpas, P., Ossanlis, P. and Bartiz, J. (2008). "Comparison of Numerical and Experimental Results for the Evaluation of the Depollution Effectiveness of

Photocatalytic Coverings in Street Canyons." Environmental Modeling and Assessment, 13(3) 357-368.

National Renewable Energy Laboratory (NREL). (2009). “National Solar Radiation Data Base: 1961-1990: Typical Meteorological Year 2.” <http://rredc.nrel.gov/solar/old_data/nsrdb/1961-1990/tmy2/> (April 14, 2013).

National Renewable Energy Laboratory (NREL). (2012). “Solar Maps.” <http://www.nrel.gov/gis/solar.html> (April 14, 2013).

Poon, C.S., and Cheung, E. (2007). “NO removal efficiency of photocatalytic paving blocks prepared with recycled materials.” Construction and Building Materials, 21, 1746-1753.

Pederson, B.M., Thibodeaux, L.J., Valsaraj, K.T., and Reible, D.D. (2001). “Testing a multimedia compartmental model with monitoring data.” Enivornmental Toxicology and Chemistry, Vol. 20, No. 9, 2114-2121.

Salvado-Estivill, I., Hargreaves, D.M. and Puma, G.L., (2007). “Evaluation of the intrinsic photocatalytic oxidation kinetics of indoor air pollutants.” Environmental Science and Technology, 41, 2028-2035.

Sharma, N., Chaudhry, K.K., and Chalapati Rao, C.V. (2004). “Vehicular pollution prediction modeling: A review of highway dispersion models.” Transport Reviews, 24(4), 409-435.

Sleiman, M., Conchon, P., Ferronato, C., and Chovelon, J.M. (2009). “Photocatalytic oxidation of toluene at indoor air levels (ppbv): Towards a better assessment of conversion, reaction intermediates and mineralization.” Applied Catalysis B: Environmental, 86(3-4), 159-165.

Thibodeaux, L.J. and Mackay, D. (2011). “Dry Gaseous Deposition,” Handbook of chemical mass transport in the environment. CRC Press, Boca Raton, FL. 144-147.

Vallius, M., Ruuskanen, J., and Pekkanen, J. (2008). “Comparison of multivariate source apportionment of urban PM2.5 with chemical mass closure.” Boreal Environment Research, 13, 347-358.

Vardoulakis, S., Fisher, B.E.A., Pericleous, K., Conzalez-Flesca, N. (2003). “Modelling air quality in street canyons: a review.” Atmospheric Environment, 37, 155-182.

Zeng, F., Shi, G-L., Li, X., Feng, Y-C., Bi, X-H., Wu, J-H., and Xue, Y-H. (2010). “Application of a combined model to study the source apportionment of PM10 in Taiyuan, China.” Aerosol and Air Quality Research, 10, 177-184.

CHAPTER 7
POTENTIAL OF NANOPARTICLES AND NITRATES RELEASED TO WATER FROM PHOTOCATALYTIC PAVEMENTS

7.1 INTRODUCTION

Self-cleaning and air purifying materials, using heterogeneous photocatalysis, is a fast growing technology evident from the increasing number of products and publications available (Fujishima and Zhang 2006). Since the late 1980's applications of photocatalysts in construction materials began and a diverse range of nanocomposites varying from bathroom tiles, roofing materials, paints, facades, and pavements for self-cleaning and air purifying functions are now available (Folli et al. 2009, Fujishima and Zhang 2006). Heterogeneous photocatalysis uses a semiconductor (most commonly titanium dioxide (TiO_2) nanoparticles) to accelerate oxidation and reduction reactions decomposing organic and inorganic pollutants in the presence of sunlight. Furthermore, when irradiated the surface of TiO_2 become more hydrophilic enhancing the self-cleaning effect as the end products from the photocatalytic degradation can be easily adsorbed into water and washed off by rainwater (Diamanti et al. 2008).

As true of most materials, pros and cons exist. Much of the focus of recent research has been concentrated on understanding the photodegradation benefits. Few researchers have investigated the potential adverse effects due to application of photodegradation. In fact, researchers in a workshop on passive photocatalytic oxidation strategies in building materials, identified this as a key research need before deployment of the technology (Berdahl and Akbari 2008). Potential trade-offs include the adverse environmental impact from photodegradation intermediates, photodegradation end products, or TiO_2 nanoparticles released to the environment either into the atmosphere or the water (Berdahl and Akbari 2008). As a result, the adverse environmental consequences of photocatalytic pavements are the subject of this paper.

Potentially harmful compounds - TiO_2 nanoparticles and nitrates - released to water were evaluated for photocatalytic concrete pavements used to oxidize NO_x from mobile pollution sources.

7.2 BACKGROUND

Nitrogen oxides, 35% emitted from mobile sources, are one of the most common pollutants researched for photocatalytic removal potentials due to their association with acid rain, photochemical smog, and negative health impacts (Kuhns et al. 2004). Titanium dioxide has the ability to remove NO_x, following the oxidation reaction scheme presented in Equations 7.1 and 7.2 with the final product as nitrates (Yu 2003):

$$NO + OH^* \xrightarrow{Ti O_2} NO_2 + H^* \qquad (7.1)$$

$$NO_2 + OH^* \xrightarrow{Ti O_2} NO_3^- + H^* \qquad (7.2)$$

Yet nitrates are naturally found in the environment and an essential plant nutrient, in excess amounts they can cause serious water quality problems such as eutrophication. Eutrophication, overgrowth of aquatic plants, changes the environmental characteristics such as dissolved oxygen and temperature. As a result, changing both the animal and plant species that can survive in the environment are also impacted (EPA 2012[a]).

Few studies have mentioned the amount of nitrates being released to water, stating only that the amount released is 10 times inferior to the original pollutant level (PICADA 2001). One study shows that between 70-97% of the theoretical nitrates are removed from glass substrates after being immersed in deionized water for one hour (Martinez et al. 2011). For concrete substrates, researchers believe that NO_3^- is absorbed by concrete substrates, due to the alkalinity of concrete (Sleiman et al. 2009, Yu 2003). Furthermore it is theorized, but not confirmed, that

the nitrates adsorbed by the concrete can react with the calcium hydrate $Ca(OH)_2$ in the concrete cement, neutralizing to $Ca(NO_3)_2$ and H_2O (Li and Qian 2009).

In addition to nitrates, TiO_2 nanoparticles deployed from the photocatalytic layer may also be released. According to a model completed in Switzerland, the majority of the TiO_2 nanoparticles are likely to be released to water or soil rather than to the air (Mueller et al., 2008). Yet, nanoscale TiO_2 is one of the most manufactured and greatest used of all nanoparticles, few studies have shown the release of nano-TiO_2 into the natural environment (Kaegi et al. 2009). This absence of exposure data for current nanomaterial containing products has been widely reported as a significant research gap by nanoparticle toxicologists (Stern and McNeil 2008).

Uses of TiO_2 for photocatalyst cements for both building facades and pavements have the potential of releasing TiO_2 due to abrasion. For example the durability of TiO_2 used as a whitening agent in paints exhibits chalking effects exposing TiO_2 particles to the surface (Kaegi et al., 2009). Furthermore, a durability study on TiO_2 photocatalytic pavements illustrate the potential of TiO_2 particle loss due to abrasion from repeated traffic (Dylla et al., 2010). One study by Kaegi et al., illustrated the release of synthetic TiO_2 nanoparticles, 3.5×10^8 particles/L, from exterior applications to the aquatic environments. This study was the first time that showed significant amounts of manufactured TiO_2 released into the aquatic systems. TiO_2 was released first as agglomerates in direct façade storm water runoff and was disaggregated as it reached the inlet of the urban runoff storm water systems suggesting that the organic matrix was either dissolved or degraded during its transport (Kaegi et al. 2009).

The toxicity of TiO_2 nanoparticles is not completely understood. The toxicity of nanoparticles is dependent on several characteristics; particle size, surface area, metals/impurities, surface charge, morphology, crystallinity, and solubility in biological fluids,

some of which are even difficult to measure (Isaacs 2009). Furthermore, nanoparticles are ubiquitous formed naturally, incidentally or artificially. For example, natural TiO_2, nanoparticles were found in river water (Wigginton et al., 2007). Over the years, ecosystems have adapted to "cohabitate" with these nanoparticles however, many details are still unknown such as the relative exposure levels especially since the difference between these three types of nanoparticles are blurred (Wiesner et al. 2009). As a result, it is questionable whether one will be able to distinguish one type from the other two making it difficult to assess the risks of manufactured nanoparticles (Wiesner et al. 2009). Consequently, there is little understanding of the possible consequences when using manufactured photocatalytic nanoparticles. To avoid major negative implications, significant effort needs to be brought forward to quantify both the toxicity and exposure potential for these nanoparticles (Robichaud et al. 2009, Lee et al. 2009).

7.3 MATERIALS AND METHODS

This study was divided into two parts; (1) to quantify how much nitrates are eluted into water and (2) to quantify and characterize TiO_2 nanoparticles eluted into water. Part one of the study investigated the worse case scenario of how much nitrates were eluted into water from photocatalytic pavements. Water samples were analyzed from photocatalytic pavements and compared to water samples from concrete pavement controls before and after photocatalytic oxidation of NO. The nitrates were quantified using the automated cadmium reduction test in accordance to EPA Method 353.2 (EPA 1993). The difference in nitrates eluted from photocatalytic pavements and the concrete control is due to the photocatalytic oxidation of NO_x.

Part two of the study investigated whether engineered TiO_2 nanoparticles used in photocatalytic pavements entered into water. For this study water samples from two different types of photocatalytic concrete pavements (photocatalytic mortar overlays and photocatalytic

spray coats), were analyzed and compared to water samples from typical concrete pavement (control). The photocatalytic spray application was also included in this step to better understand its noted durability issues. These water samples were quantitatively analyzed with inductive coupled plasma atomic emission spectrometry (ICP-AES) in accordance to EPA Method 6010c and samples with Ti detected were to be qualitatively analyzed by transmission electron microscopy (TEM), respectively (EPA 2007).

7.3.1 Concrete Pavement Samples

Two different types of photocatalytic concrete pavements were investigated; photocatalytic mortar overlays, and photocatalytic spray coats (part 2 only). The photocatalytic coating was applied to a concrete base with a compressive strength of 41 MPa made from a typical concrete pavement mix design using Type I cement. The sample size was 310 mm x 381mm x 40 mm. Three replicates were produced for each to account for variability.

7.3.1.1 Photocatalytic Mortar Overlay

The photocatalytic mortar overlay, used for both parts of the study, was a 10 mm thick cementitious layer containing TiO_2 nanoparticles. The photocatalytic layer was applied after the initial set, approximately 1 hour after base layer pour. The photocatalytic cementitious mortar mix consisted of 5% ultrafine TiO_2 (anatase, Crystal Millennium PC105) per cement weight, cement, aggregate filler with maximum nominal size of 1.18 mm, and water. The TiO_2 nanoparticles were incorporated into the mortar mixture as aqueous suspended nanoparticles incorporated into the water requirements of the concrete mortar mix.

7.3.1.2 Photocatalytic Spray Coat

The photocatalytic concrete spray coat (used only for the second part of this study) employed a spray coat of TiO_2 nanoparticles suspended in an aqueous binder. After concrete curing, the

photocatalytic aqueous binder was spray coated onto the sample in a hatch formation. The photocatalytic solution contains suspended anatase TiO_2 nanoparticles, 2% by volume and was applied at a rate of 0.21 kg/m^2. The spray gun included an electrostatic precipitator to distribute the TiO_2 nanoparticles evenly.

7.3.1.3 Concrete Controls

Since nitrates may be absorbed to concrete pavements naturally through the nitrogen cycle, and Type I cement may contain a small percent of titanium, water samples were collected from control concrete pavements as well. The control samples used in the first part of the study were made following the same procedure for the photocatalytic motor overlay samples. Thus the concrete control samples were constructed of the same size and materials used for the concrete base and overlay without the addition of TiO_2 catalyst. The control samples for the second portion of the study were constructed of the same size and materials used for the concrete base typical of concrete pavements.

7.3.2 Part 1: Quantification of Nitrate Released to Water

The photocatalytic mortar overlay samples and the concrete with overlay control samples were initially soaked in Nanopure DI water for several hours to remove as many nitrate and nitrites absorbed on the surface as possible prior to the photocatalytic oxidation tests. The Nanopure DI water was replaced hourly. Water samples were collected in triplicates from the last hour soak to be later analyzed for nitrates to estimate a baseline amount of nitrates already on the concrete surface prior to photocatalytic oxidation of NO.

Similarly, after the pavement samples were subjected to the photocatalytic test, each sample was soaked in Nanopure DI water for two hours as recommended by the JIS standards

(JIS 2004). Again, the Nanopure DI water was replaced hourly and three samples were collected after each soak to be later analyzed for nitrate.

7.3.2.1 Sample Collection and Preparation

A polyethylene container of 450 mm X 320 mm X 130 mm was used to soak the samples in 2.5 L of Nanopure DI water which was the minimum amount required to completely saturate and cover the sample surface. All containers used were acid rinsed according to EPA Method B standards prior to each hourly soak (EPA 2012[c]). Before collecting the water samples, the effluent was agitated to ensure a more uniform concentration in the water. All samples were collected using a disposable polyethylene syringe and filtered through a 0.45 μm nylon membrane. For each pavement sample, three samples of approximately 20 ml of the effluent were collected and stored at temperature less than 4°C for no more than 14 days.

7.3.2.2 Nitrate Analysis

To analyze the nitrates, EPA Method 353.2 Determination of Nitrate-Nitrite Nitrogen by Automated Colorimetry was followed (EPA 1993). This procedure is a cadmium reduction test in which the nitrate is reduced to nitrite by passing through a copper-cadmium coil and reacted with sulfanilamide and N-(1-naphthyl)-ethylenediamine dihydrochloride. This reaction forms an azo dye that can be measured colorimetrically using Beer's law. Calibration standards for both methods were prepared by successive dilution of potassium nitrate (GR ACS grade) in DI water. To ensure quality control and assurance for every 20 samples, selected samples were spiked and duplicated. The recovery rate was calculated to evaluate the accuracy. In addition, samples of the Nanopure DI water used to soak the pavements and DI water used to make the reagents (blank samples) were also evaluated to detect any laboratory contamination during the soaking or reagent contamination during the analysis.

7.3.2.3 Environmental Conditions Expected to Result in Maximum Nitrates

The photocatalytic test was run at environmental conditions that were expected to provide the largest NO_x reduction equating to the worst-case scenario for nitrates released. Previous research has shown that humidity, irradiance, temperature and pollutant concentration all impact the amount of NO_x oxidized to nitrates. To determine these environmental settings previous research results, solar maps, weather database files, and EPA NO_x pollution files were used. From previous studies completed by researchers the irradiance, relative humidity, and temperature that provided the maximum NO reduction was 3.5 mW/cm^2, 25%, and 37°C, respectively. However, using, the TMY-2 files and National Renewable Energy Laboratory (NREL) solar maps, since TiO_2 only uses approximately 2.7% of the total global horizontal radiation, the maximum average hourly UV-irradiance can be estimated as 2.7 mW/cm^2 (NREL 2009, NREL 2012). Since the NO reduction is positively correlated with irradiance, 2.7 mW/cm^2 is a more reasonable than using 3.5 mW/cm^2. The higher the pollution concentration, the more NO is available to be photocatalytic oxidized to nitrates. According to the 2011 AQS NO files recorded by EPA, the maximum NO concentration reported was 940 ppb in North Baja California County, Mexico. However to make the study more applicable to other regions, including areas in California, Illinois, Massachusetts, New Jersey, New York, Texas and Utah, a high concentration of 480 ppb is more realistic (EPA[b] 2012).

7.3.2.4 Photocatalytic Oxidation of NO

For the photocatalytic oxidation (PCO) of NO, the experimental set-up specified by the Japanese Industrial Standard (JIS TR Z 0018 "Photocatalytic materials – air purification test procedure") was modified, as defined in Dylla et al. 2010, to accommodate the larger sample sizes and to simulate various environmental conditions (JIS 2004). A zero air source, gas calibrator, humidifier, photoreactor, UV-lights, space heater/fan and a NO_x analyzer was used to measure

the photocatalytic oxidation of NO_x under a set level of relative humidity, temperature, pollutant concentration, flow rate, and irradiance.

The photocatalytic oxidation test consisted of 45 minutes to reach equilibrium settings, 4.5 hours of illumination, which is the average daily number of hours of sunlight and 45 minutes of zero air to allow for NO_x desorption. A thermo scientific 146i calibrator supplied 480 ppb NO at 3 standard l/min to the photoreactor by blending 170 ppm of dry NO in a nitrogen balance with dry zero air. Twelve 20W fluorescent black lights were used to illuminate the photocatalytic pavement simulating UV-radiation from sunlight. The distance between the lights and the photoreactor bed was set to achieve an average irradiance of 2.7 mW/cm^2 measured at the pavement surface by a UV-A intensity meter OAI Model 306 at 365 nm. The humidity and temperature was set at 27±3% and 37±1°C, respectively. A hygrometer and temperature probe continuously monitored and recorded the temperature and relative humidity per minute.

7.3.3 Part 2: Quantification of TiO_2 Nanoparticles Released to Water

The experimental program for the water sample preparation and analysis procedures were based on a recent study completed by Kaegi et al. (2008). Each concrete pavement sample was soaked in Nanopure DI water for two hours, replacing the water hourly. Water samples were collected and filtered to remove all particles larger than 0.45 μm. The collected water samples were first analyzed by ICP-AES such that the quantity of Ti was estimated. Then only samples with Ti detected were to be centrifuged for TEM analysis.

7.3.3.1 Sample Collection and Analysis Procedures

The same polyethylene container, used in part 1 of the study, was used to soak the samples. The amount of water used was just enough to saturate the sample; 2.5 L for the samples with the photocatalytic overlay and 2.2 L for the control and spray coat samples. Before collecting the

water samples, the effluent was agitated to ensure a more uniform concentration of TiO_2 in the water. The samples were collected using a disposable polypropylene syringe and filtered through a 0.45 μm nylon membrane. For each concrete pavement sample, at least 150 mL of water sample was collected.

7.3.3.2 ICP-AES

ICP-AES, which measures the mass concentration of metals such as titanium up to 1 ppb, was used to quantify the mass concentration of TiO_2 in the water. Calibration standards and sample analysis were prepared in accordance to the U.S. EPA Method 6010C procedures (EPA 2007). Approximately 20 mL of each sample were analyzed by ICP-AES to identify if any of the samples were in the equipment detectable limits. The difference between the mass concentrations from the photocatalytic pavement samples and the concrete pavement control samples can be attributed to the engineered TiO_2 nanoparticles added in the pavement design.

7.4 RESULTS AND DISCUSSION

7.4.1 Results of Part 1: Quantification of Nitrate Released to Water

In Table 7.1 the average nitrate concentration measured for the water samples from the baseline soaks and the first and second hour soaks after 4.5 hours of NO photocatalytic oxidation are reported. As it can be seen, significantly higher amounts of nitrates were reported for the baseline of the concrete control samples compared to the baseline of the photocatalytic samples. Furthermore, as expected the nitrate concentration in the water samples from the second soak were typically lower than the concentrations reported for the first hour of soaks after PCO. The concentration of nitrates reported for the second hour soaks were comparable to the baseline soaks.

Figure 7.1 presents the average total nitrate theoretically on the sample surface and the average measured nitrate eluted for the photocatalytic mortar overlay samples and control

samples after 2 hours of soaking in 2.5 L of Nanopure DI water. The baseline nitrate concentrations were subtracted from the total nitrate concentration measured after PCO. As it can be seen in Figure 7.1, not all of the nitrates were eluted from the photocatalytic pavement samples, while the concrete samples more nitrates were eluted. This is possibly due to not all of the nitrates being removed from the sample surface prior to the PCO test. This is also evident in Table 7.1 where high concentrations of nitrates were recorded from the concrete control samples. Furthermore, the binding mechanism of nitrates on the TiO_2 could be responsible for why not all the nitrates were released.

Table 7.1 Average Concentration of Nitrates from Water Samples Collected from the Photocatalytic Mortar Overlay Samples and the Concrete Control Overlay Samples Soaked in 2.5 L of Nanopure Water

Sample	Baseline Nitrates (mg/L)		First Hour Nitrates (mg/L)		Second Hour Nitrates (mg/L)	
	Average	Std. Dev.	Average	Std. Dev.	Average	Std. Dev.
Concrete Control with Overlay 1	0.065	0.004	0.172	0.022	0.081	0.071
Concrete Control with Overlay 2	0.138	0.020	0.057	0.012	0.115	0.003
Concrete Control with Overlay 3	0.076	0.013	0.183	0.024	0.138	0.009
Photocatalytic Mortar Overlay 1	0.046	0.003	0.084	0.007	0.090	0.008
Photocatalytic Mortar Overlay 2	0.045	0.007	0.102	0.011	0.043	0.037
Photocatalytic Mortar Overlay 3	0.045	0.004	0.151	0.103	0.063	0.008

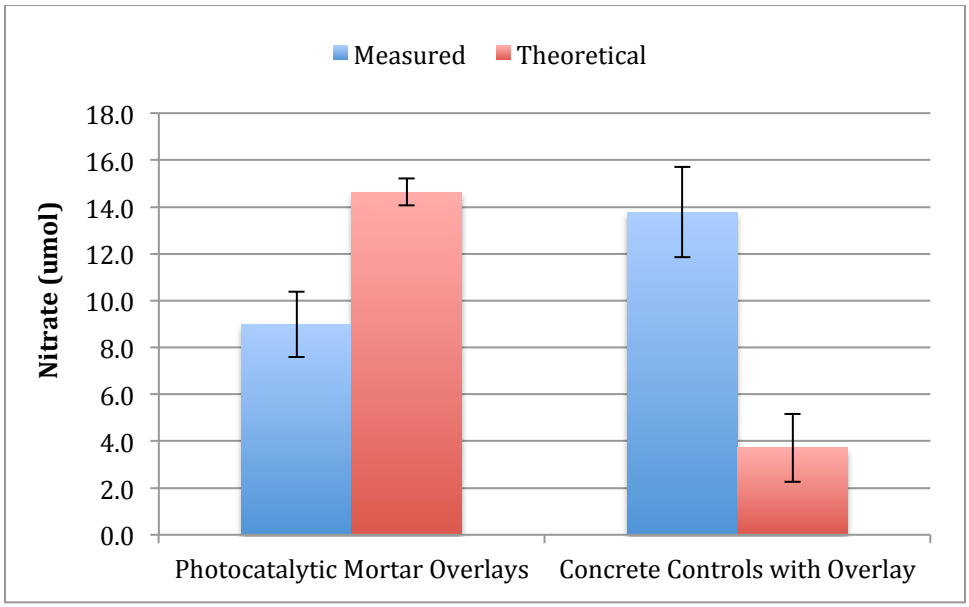

Figure 7.1 Nitrate Collected on the Photocatalytic Mortar Overlay Samples and the Concrete Control Overlay Samples

Furthermore, the percent eluted was calculated for each sample by comparing the amount of nitrates eluted to the amount of nitrates theoretically created based on the photodegradation results. These results are shown in Table 7.2.

Table 7.2 Comparison of Theoretical Amount of Nitrates Created to Estimated Total Amount of Nitrates Eluted to Water Measured after 4.5 Hours if Photocatalytic Oxidation of NO

Sample	% Reduction		Nitrates (µmol)		% Eluted
	NO	NO_x	Theoretical	Measured	
Concrete Control with Overlay 1	25.5%	24.3%	4.247	12.825	240%
Concrete Control with Overlay 2	16.5%	14.6%	2.057	12.511	338%
Concrete Control with Overlay 3	30.7%	27.8%	4.821	16.001	269%
Concrete Control with Overlay - Average	**24.2%**	**22.2%**	**3.708**	**13.779**	**282%**
Photocatalytic Mortar Overlay 1	94.0%	91.6%	15.225	8.858	46%
Photocatalytic Mortar Overlay 2	95.4%	92.5%	14.620	7.649	40%
Photocatalytic Mortar Overlay 3	94.9%	91.7%	14.065	10.446	61%
Photocatalytic Mortar Overlay - Average	**94.8%**	**91.9%**	**14.637**	**8.984**	**49%**

In general for an average of 95% NO reduced, only 49% of the nitrates created were eluted. It is also noted that there is high variability in the amount of nitrates eluted from each sample. For example the percent eluted varied from 40% to 61% for the photocatalytic samples.

7.4.2 Results of Part 2: Quantification of TiO_2 Nanoparticles Released to Water

The titanium (Ti) element was analyzed with ICP-AES to quantify if any TiO_2 was released to the water from photocatalytic pavement mortar overlays and photocatalytic spray coated pavements. The results of the analysis showed that no Ti was detected for the control sample, photocatalytic pavement mortar overlay, and even the photocatalytic spray coated samples, which are known to have a potential durability issue. Since no Ti was detected for any of the water samples, TEM analysis was not conducted. As a result, it is recommended that ICP-MS, a more sensitive technique with a detection limit of 1 ppt, be used instead of ICP-AES to quantify the amount of Ti. Samples with Ti detected and quantified using this more sensitive analysis should be characterized by TEM.

7.5 CONCLUSION

Potentially harmful compounds – nitrates and TiO_2 nanoparticles - released to water were evaluated for photocatalytic concrete pavements used to oxidize NO_x from mobile pollution sources. The amount of nitrates eluted to water were measured after 4.5 hours of photocatalytic oxidation of NO using the environmental settings which would provide the most NO reduced and nitrates created. On average after 4.5 hour of PCO of NO with 91.9% NO_x reduction efficiency, only 8.984 μmols of nitrates were released to water accounting for only 49% of the theoretical amount of nitrates created. Surprisingly the photocatalytic pavement eluted less nitrates than the concrete control samples. Further research is required to determine where the remaining nitrates created are disappearing and where the additional nitrates on the concrete controls are coming.

In addition, research is required to determine binding mechanisms of nitrates on concrete versus TiO_2. This could potentially explain why the photocatalytic pavements do not elute all of the nitrates created.

The second part of the study investigated whether engineered TiO_2 nanoparticles used in photocatalytic pavements entered into water. For this study water samples from two different types of photocatalytic concrete pavements (photocatalytic mortar overlays and photocatalytic spray coats), were analyzed and compared to water samples from typical concrete pavement (control). Using ICP-AES the Ti element was not detected in any of the water samples, including the water samples from the photocatalytic concrete spray coating, which has demonstrated a known durability issue. As a result, it is suggested that ICP-MS, with a detection limit of 1 ppt, is used to quantify the Ti in the water samples rather than ICP-AES. TEM can then be used to characterize the morphology of the particles, potentially identifying any engineered nanoparticles.

7.6 REFERENCES

Diamanti, M.V., Ormellese, M. and Pedeferri, M. (2008). "Characterization of photocatalytic and superhydrophilic properties of mortars containing titanium dioxide." Cement and Concrete Research, 38, 1349-1353.

Dylla, H., Hassan, M., Schmitt, M., Rupnow, T. and Mohammad, L. (2010). "Laboratory investigation of mixed nitrogen dioxide (NO_2) and nitrogen oxide (NO) gasses on titanium dioxide photocatalytic efficiency in concrete pavements." Journal of Materials in Civil Engineering, 23(7) 1087-1093.

Environmental Protection Agency (EPA). (1993). Determination of nitrate-nitrite nitrogen by automated colorimetry. Method 353.2.

Environmental Protection Agency (EPA). (2007). Inductively coupled plasma-atomic emission spectrometry. Method 6010C.

Environmental Protection Agency (EPA[a]). (2012). " 5.7 Nitrates" Water: Monitoring and Assessment. <http://water.epa.gov/type/rsl/monitoring/vms57.cfm> (April 14, 2013).

Environmental Protection Agency (EPA[b]). (2012). “Air Quality System (AQS)” <http://www.epa.gov/ttn/airs/airsaqs/detaildata/downloadaqsdata.htm> (April 14, 2013).

Environmental Protection Agency (EPA[c]). (2012). “Chapter 5 Water Quality Conditions” Water: Monitoring and Assessment < http://water.epa.gov/type/rsl/monitoring/vms50.cfm> (April 14, 2013).

Folli, A., Jakobsen, U.H., Guerrini, G.L., and Macphee, D.E. (2009). “Rhodamine B discolouration on TiO_2 in the cement environment: A look at fundamental aspects of the self-cleaning effect in concretes.” J. Adv. Oxid. Technol., Vol. 12 (1), 126-133.

Fujishima, A., and Zhang, X.. (2006). “Titanium dioxide photocatalysis: present situation and future approaches.” Comptes Rendus Chimie. 9, 750-760.

Hassan, M.M., Dylla, H., Mohammad, L., and Rupnow T. (2010). “Evaluation of the durability of titanium dioxide photocatalyst coating for concrete pavement.” Journal of Construction and Building Material, 28(8), 1456-1461.

Isaacs, J. (2009). “Considerations for LCA of Nanotechnologies” Presented at Nanotechnology and Life Cycle Analysis Workshop, Nov. 5-6, 2009, Chicago, IL.

Japanese Industrial Standard (JIS). (2004). “Fine ceramics (advanced ceramics, advanced technical ceramics) – Test method for air purification performance of photocatalytic materials- Part 1: Removal of nitric oxide”, JIS R 1701-1,1-9.

Kaegi, R., Ulrich, A., Sinnet, B., Vonbank, R., Wichser, A., Zuleeg, S., Simmier, H., Brunner, S., Vonmont, H., Burkhardt, M., and Boller, M. (2008). "Synthetic TiO_2 nanoparticle emission from exterior facades into the aquatic environment." Environmental Pollution 156(2), 233-239.

Kuhns, H.D., Mazzoleni, C., Moosmuller, H., Nikolic, D., Keislar, R.E., Barber, P.W., Li, Z., Etyemezian, V., and Watson, J.G. (2004). “Remote sensing of PM, NO, CO, HC emission factors for on-road gasoline and diesel engine vehicles in Las Vegas, NV.” Science of the Total Environment, 322, 123-137.

Lee, J., Mahendra, S., and Alvarez, P.J.J. (2009) “Potential environmental and human health impacts of nanomaterials used in the construction industry.” Nanotechnology in Construrction 3.

Li, L. and Qian, C. (2009). “A lab study of photo-catalytic oxidation and removal of nitrogen oxides in vehicular emissions and its fieldwork on Nanjin No.3 bridge of Yangtze River.” Journal of Pavement Resource Technology, 2(5), 218-222.

Martinez, T., Bertron, A. Ringot, E., and Escadeillas, G. (2011). “Degradation of NO using photocatalytic coatings applied to different substrates.” Building and Environment, 46, 1808-1816.

Mueller, N. C. and B. Nowack (2008). "Exposure Modeling of Engineered Nanoparticles in the Environment." Environmental Science & Technology, Vol. 42(12): 4447-4453.

National Renewable Energy Laboratory (NREL). (2009). “National Solar Radiation Data Base: 1961-1990: Typical Meteorological Year 2.” <http://rredc.nrel.gov/solar/old_data/nsrdb/1961-1990/tmy2/> (April 14, 2013).

National Renewable Energy Laboratory (NREL). (2012). “Solar Maps.” <http://www.nrel.gov/gis/solar.html> (April 14, 2013).

Photocatalytic Innovated Coverings Applications for Depollution Assessment (PICADA). (2001). “Guideline for end-users.” GROWTH Project GRD1-2001-40449, <http://www.picada-project.com> (June 7, 2011).

Rodichaud, CO, Uyar AE, Darby MR, Zucker LG, Wiesner, MR (2009) “Estimates of upper bounds and trends in nano-TiO_2 production as a basis for exposure assessment.” Environment Science and Technology, 43(12):4227-4233.

Sleiman, M., Conchon, P., Ferronato, C., and Chovelon, J.M. (2009). “Photocatalytic oxidation of toluene at indoor air levels (ppbv): Towards a better assessment of conversion, reaction intermediates and mineralization.” Applied Catalysis B: Environmental, 86(3-4), 159-165.

Stern, S.T. and McNeil, S.E. (2008). “Nanotechnology safety concerns revisited.” Toxicological Sciences, 101(1), 4-21.

Wiesner, M. R., G. V. Lowry, Jones, K.L., Hochella, F.M., Di Giulio, R.T., Casman, E., and Bernhardt, E.S. (2009). "Decreasing Uncertainties in Assessing Environmental Exposure, Risk, and Ecological Implications of Nanomaterials." Environmental Science & Technology, 43(17), 6458-6462.

Wigginton, N.S., Haus, K.L., and Hochella, M.F., (2007). “Aquatic environmental nanoparticles.” Journal of Environmental Monitoring, 9, 1306-1316.

Yu, J. C.-M.. (2003). Deactivation and Regeneration of Environmentally Exposed Titanium Dioxide (TiO_2) Based Products. Environmental Protection Department No. E183413, 1-21.

CHAPTER 8
CHARACTERIZATION OF NANOPARTICLES RELEASED DURING CONSTRUCTION OF PHOTOCATALYTIC PAVEMENTS USING ENGINEERED NANOPARTICLES[2]

8.1 INTRODUCTION

Self-cleaning materials using heterogeneous photocatalysis, is a fast growing technology. Heterogeneous photocatalysis employs semiconductors (most commonly titanium dioxide (TiO_2) nanoparticles) to oxidize and decompose organic and inorganic pollutants in the presence of sunlight. These nanoparticles are used in diverse range of nanocomposites varying from bathroom tiles, roofing materials, paints, facades, and pavements for self-cleaning and air purifying functions (Fujishima et al. 2006). As a result, titanium dioxide has seen a 283% growth since its discovery in the 1970s (Meyer et al. 2009). Yet, nanoparticles of TiO_2 currently only make up 2% percent of the titanium dioxide manufactured, this percent has the potential to increase to more than 10% by 2015 (Robichaud et al. 2009).

As the technology advances and spreads, human exposure to photocatalytic nanoparticles is inevitable, increasing concerns regarding their safety. The release of these particles into the environment will be throughout the life cycle of the photocatalytic material including manufacturing, construction, commercial material use, and end of life disposal (Wiesner et al. 2006, Meyer et al. 2009). Exposure to humans mostly likely follows one of three routes, inhalation, dermal, and ingestion (Hoerr 2009). Of these, inhalation is the most common with manufacturing and construction workers having the highest exposure potential (Tedja et al. 2011, Tsuji et al. 2006). With widespread use of photocatalytic materials and large scale

[2] Reprinted with permission of the Springer.
Published in the *Journal of Nanoparticle Research*, 2012, Vol. 14 (4), pp 1-15.

manufacturing of TiO_2 nanoparticles, TiO_2 nanoparticles exposure is expected to reach new quantities escalating the potential health risks (Wiesner et al. 2009).

The objective of this study is to evaluate nanoparticle emissions from photocatalytic pavement application through laboratory-simulated construction activities for photocatalytic pavement mortar overlays and an actual field study for photocatalytic pavement spray coatings. To achieve this objective and as recommended in the Nanotechnology Emission Assessment Technique (NEAT) procedure, the scanning mobility particle sizer measured the nanoparticles size distribution, surface area, mass and concentration. In addition, nanoparticles were collected for offline analysis in which transmission electron microscopy (TEM) characterized the nanoparticle shape, size, and surface morphology.

8.2 BACKGROUND

It is widely acknowledged that the risks of TiO_2 nanoparticles are mostly unknown (Tsuji et al. 2006). To avoid major negative implications, significant effort needs to be brought forward to quantify both the toxicity and exposure potential for these nanoparticles (Robichaud et al. 2009, Lee et al. 2009). Numerous studies have been initiated demonstrating that TiO_2 has the potential to be toxic. For example, initial toxicity studies of TiO_2 nanoparticles on rodents have shown that inhalation of nano-TiO_2 can cause pulmonary inflammation in rats and mice (Long et al. 2007; Zhu et al. 2010). Additional information on toxicity studies of nanoparticles is summarized in Hoet et al. (2004). However, it is not clear what nanoparticle characteristics (particle size, concentration, surface area, surface chemistry, etc.) most impact the toxicity, complicating exposure assessments (Tedja et al. 2011).

While several studies exist demonstrating that TiO_2 has a potential to be toxic, less information is available quantifying and characterizing the exposure of TiO_2 nanoparticles (Farre

et al. 2011). The challenge of obtaining nanoparticle exposure data is that nanoparticles are ubiquitous; formed naturally, incidentally or artificially also known as engineered. They are found in the atmosphere, oceans, soil, and on or in living organisms (Wiesner et al. 2009, Guzman et al. 2006). The differences between the three types of occurring nanoparticles are blurred and it is questionable whether the types are distinguishable from another (Wiesner et al. 2009). Regardless, in order to fully comprehend the toxicity reports to assess the potential risks, nanoparticle exposure must be fully understood (Colvin 2003). Therefore, research needs to quantify and characterize nanoparticle exposure as well as understand nanoparticle transport and transformation before results can be linked to the ongoing toxicity studies (Lee et al. 2009).

8.2.1 Method of Characterizing Nanoparticle Exposure

Currently, no known standard exists for measuring nanoparticles emissions to air further limiting the availability of nanoparticle exposure studies (Renn and Roco 2006). Various methodologies on studying potential exposure pathways have been proposed. A comprehensive technique is the NEAT developed by the National Institute for Occupational Safety and Health (NIOSH) for aerosol nanoparticle exposure studies (Methner[a] et al. 2010). Most investigations recommend that nanoparticles be characterized by particle size, surface area, particle count, elemental composition, and surface morphology (Brouwer et al. 2009; Methner[a] et al. 2010). In order to account for natural and incidental nanoparticles, nanoparticles released are identified if there is an increase of nanoparticles compared to background concentrations resulting from various activities (Bouwer et al. 2009; Methner[a] et al. 2010)

In the case of aerosolized nanomaterials, the scanning mobility particle sizer (SMPS) can provide real-time, on-line nanoparticles size distributions. Real-time size measurements can be made from 2.5 to 1000 nm. The SMPS system includes an electrostatic classifier, a differential

mobility analyzer (DMA), and a condensation particle counter (Sahu and Biswas 2010). The electrostatic classifier combined with the differential mobility analyzer collects and separates the particles by size before the sample is passed through the particle counter to give the size distribution. Recent studies employing SMPS equipment have been used by many disciplines to characterize incidental nanoparticles from processes such as combustion or welding and to characterize engineered nanoparticles released during synthesis/manufacturing, or nanocomposite abrasion (Brouwer et al. 2004; Hsu and Chein 2007; Methner[b] et al. 2010; Sahu and Biswas 2010). In addition, the nanoparticle sizes recorded can be used to calculate particle surface areas (Methner[a] et al. 2010).

For nanoparticle counting, both the condensation particle counter and the optical particle counter are recommended by NEAT to obtain accurate readings spanning the whole nanoparticle size ranges. The optical condensation particle counters provide precise counts of particles between 300 nm to 25 microns for various bin sizes. For sizes smaller than 300 nm, the particles are no longer detectable by optical scattering methodologies. Therefore, the condensation particle counter is used in which a fluid applied to the nanoparticles grows them to optical detectable sizes for real time counts. As a result, NEAT recommends that for nanoparticles less than 300 nm the condensation particle counter is used and for particles greater than 1 micron the optical particle counter. For particles between 300 nm and 1 micron, NEAT recommends the use of both methods (Methner [a] et al. 2010). In addition to NIOSH studies, this equipment have been used for studies related to nanoparticle fate and transport, vehicle and combustion emissions, tire pavement abrasion emissions, surface coating sanding, and nanoparticle synthesis (Dahl et al. 2006; Gohler et al. 2010; Methner[a] et al. 2010).

For morphology and shape characterization, nanoparticles must be collected for offline analysis. To conduct this characterization, an electrostatic precipitator nanoparticle sampler can be used. This ensures high collection efficiencies for various substrates such as TEM grids, or scanning electron microscopy (SEM) substrates (Dahl et al. 2006; Brouwer et al. 2009; Methner[a] et al. 2010). For more controlled particles size assurance, this equipment may be coupled downstream from an electrostatic classifier that filters samples by defined sizes between 2 nm to 1,000 nm (TSI 2010). Otherwise care needs to be taken to ensure grids are not overloaded (Methner[a] et al. 2010).

The majority of the exposure studies following these procedures, focused on the nanoparticles being released during manufacturing and use. Yet, as a result of increasing urban pollution problems relating to traffic pollution, recent photocatalytic material development is in photocatalytic pavements. Photocatalytic pavements have the advantage of mitigating traffic emissions due to its close proximity to higher pollution concentrations and its large surface area. However, pavement materials are often not manufactured in a controlled environment, increasing the risk of exposure. Thus, nanoparticle concentrations exposed to downstream workers such as construction workers need to be characterized. Currently, only one study has reviewed nanoparticle exposure to construction workers using nanoparticles (Broekhuizen et al. 2011). This study quantified the nanoparticle concentration exposed to construction workers fabrication of nanocomposites. While the nanoparticle exposure resulted in low concentrations not exceeding the warning level for 8 h-TWA exposures, research is needed to characterize the nanoparticles released, since it is not clear whether engineered nanoparticles were released (Broekhuizen et al. 2011). Furthermore, characterization of the nanoparticles collected is also

pertinent for relating to toxicity studies since it is still not clear what characteristics impact the toxicity of TiO_2 nanoparticles.

8.3 TEST MATERIALS AND METHODS

The exposure of nanoparticles released during application of two types of photocatalytic concrete pavements was analyzed: nanoparticle emissions from photocatalytic mortar overlays during laboratory-simulated construction activities and nanoparticle emissions from photocatalytic spray coating during actual construction activities in a field study. The average nanoparticle exposure concentrations separated by particle size from the background environment were subtracted from the photocatalytic pavement application activities, where a positive net nanoparticle count is the estimated nanoparticle exposure from the ongoing activity.

TiO_2 nanoparticles used in the photocatalytic mortar overlay and the photocatalytic spray coating were preliminary characterized for size and shape. High-resolution transmission electron microscopy (HRTEM TECNAI F20 FEI) operating at 200 kV was used. The particles were dispersed in DI water and were dripped on a carbon coated copper grid for characterization.

8.3.1 Photocatalytic Mortar Overlay – Laboratory-Simulated Construction Activities

For photocatalytic mortar overlays, TiO_2 nanoparticles (anatase, Crystal Millennium PC105) used were spherical with a primary particle size of 15 nm and agglomerates averaging of 28 nm (Figure 8.1). The nanoparticles were added directly to the mortar at 5% of the cement weight to produce the thin overlay, which was applied to a concrete pavement substrate. TiO_2 nanoparticles were incorporated into the mortar mixture in two forms: as aqueous suspended nanoparticles incorporated into the water requirements of the concrete mortar mix (aqueous TiO_2) or as nanoparticle powder added to the cement dry mix (powder TiO_2). In addition, in order to indicate if artificial nanoparticles were released, nanoparticle exposure was also

characterized for a control mortar mix where no TiO_2 nanoparticles were added (control). The control sample constructed was of the same size and materials used for the mortar overlay without the addition of nanoparticles. The activities for each mixture tested are summarized in Table 8.1.

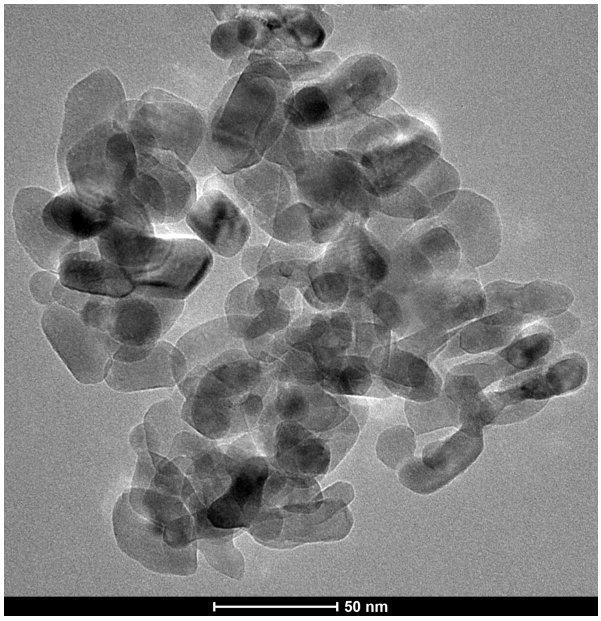

Figure 8.1 TEM images TiO_2 Used in Photocatalytic Pavement Mortar Overlay

Table 8.1 Photocatalytic Mortar Overlay - Lab Simulated Construction Activities

Application Name	Application Description	Task Name	Task Description
Powder TiO_2	Photocatalytic Mortar Overlay – powder TiO_2 nanoparticles	TiO_2-Weigh	Weigh 25 g of TiO_2 powder
		TiO_2-Dry Mix	Mix TiO_2 with cement and sand
		TiO_2-Wet Mix	Mix water with TiO_2 cement, sand, and TiO_2 aqueous solution
Aqueous TiO_2	Photocatalytic Mortar Overlay – aqueous suspended TiO_2 nanoparticles	Dry Mix	Mix cement with sand
		TiO_2-Weigh	Weigh 25 g of TiO_2 powder
		TiO_2-Water Mix	Mix TiO_2 with water
		TiO_2-Wet Mix	Mix water with TiO_2 cement, sand, and TiO_2 aqueous solution
Control	Concrete Control Mix	Dry Mix	Mix cement with sand
		Wet Mix	Mix water with dry mix

All activities were simulated in a laboratory environment to mitigate the interference from incidental and natural nanoparticles. The quantity of materials used was the amount required to make a 0.12-m^2 sample. The nanoparticles released were measured near the activity for each task as illustrated in Figures 8.2 and 8.3. Each activity was repeated to account for statistical variability. The results of the nanoparticles released during each task were compared to the background nanoparticle counts in the laboratory indicating that nanoparticles were released. Furthermore, comparison between the results provided for a better understanding if TiO_2 suspended in the water lessens the risks of exposure and if there is an increase in nanoparticle exposure when artificial nanoparticles are used.

Figure 8.2 Sampling Nanoparticle Exposure: Weighing TiO_2

Figure 8.3 Mixing Photocatalytic Mortar

8.3.2 Photocatalytic Spray Coat - Field Study Actual Construction Activities

For the spray coating photocatalytic application, TiO_2 nanoparticles used are suspended in an aqueous base coat and top coat. The base coat, which is used as a primer, has 2% by weight of anatase titanium dioxide (non photocatalytic grade) suspended nanoparticles. Whereas the top coat used, has 2% by weight of anatase titanium dioxide (photocatalytic grade) suspended nanorods. As shown in Figure 8.4, the TiO_2 nanoparticles used in the base coat are more spherical in shape with a primary particle size of 6.1 nm whereas in Figure 8.5, the TiO_2 particles used in the top coat are nanorods with an average 12 nm width by 75 nm length.

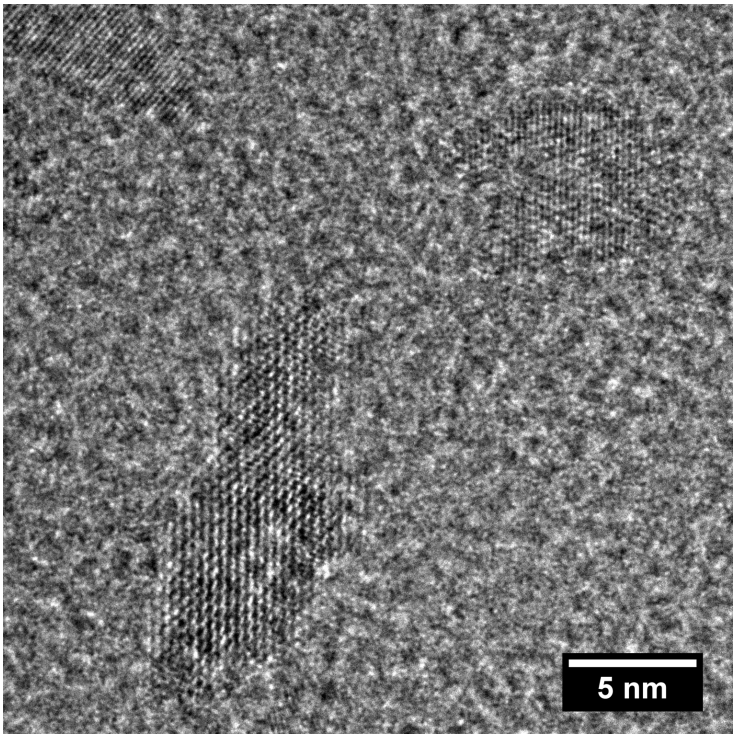

Figure 8.4 TEM image of TiO_2 Particles in Photocatalytic Spray Base Coat

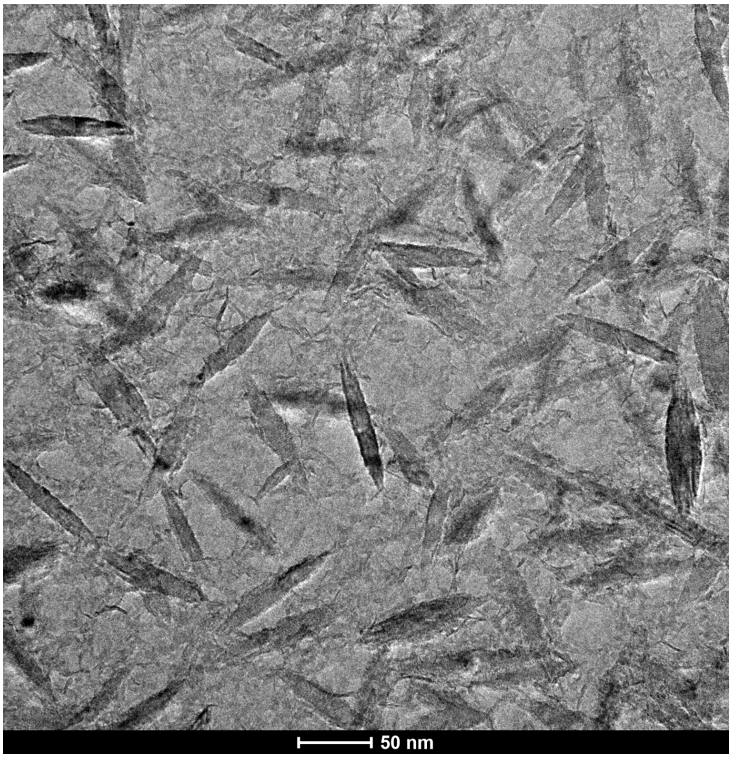

Figure 8.5 TEM images of TiO_2 Particles in Photocatalytic Spray Top Coat

The spray coat application was divided into two tasks: application of base coat and application of photocatalytic top coat. The nanoparticles released were measured from an actual field application of a photocatalytic spray coat for a ¼ mile of an existing concrete road. During the day of application, the average temperature was of 17.5°C and the average wind speed was 2.6 m/s. The coatings were sprayed on top of an existing pavement surface using a customized distributor truck. The truck speed and spray pressure remained constant to ensure that a TiO_2 surface layer of at least 10.76 ml/m^2 was applied. Mounted on the back of the truck, a spray bar fitted with nozzles distributed the TiO_2 aqueous solution (Figure 8.6). The nanoparticle sample line was attached to the distributor truck in order to be in proximity of the air near the spraying activity. Each sample recorded referred to approximately 5.6 m^2 of pavement coating. Since the spray coat is not an existing construction activity for non-nanocomposite pavement coatings, the results were only compared to background nanoparticle measurements. The background nanoparticle measurements recorded include measurements while the vehicle was moving in order to eliminate the incidental nanoparticles emitted from the vehicle exhaust during the spraying application.

8.3.3 Exposure Measurements

All exposure measurements were measured using the scanning mobility particle sizer (SMPS). The SMPS system consists of an electrostatic classifier (TSI Model 3080), a differential mobility analyzer (DMA, TSI 3081 and TSI 3085) and the condensation particle counter (CPC, TSI model 3776). Two differential mobility analyzers were used depending on the expected particle size determined by preliminary TiO_2 nanoparticle characterization. The long DMA (TSI 3081), suitable for 0.01 to 1 μm particles, was used for the photocatalytic mortar overlay application since the primary nanoparticles size was measured to be 16.7 nm. The associated particle size

distributions using the long DMA were measured from 10.2 nm to 224 nm over a span of 120 seconds. Whereas the nano DMA (TSI 3085), suitable for 0.002 to 0.15 μm particles, was used for the spray coat application since the primary nanoparticle size for the base coat was measured to be 6 nm and the width of the nanorods in the topcoat was 12 nm. The correlated particle size distributions measured using the nano DMA were from 2.02 nm to 63.8 nm over a span of 120 seconds. Regardless of the DMA column used, the system was operated at 1.5 lpm sheath flow rate and 1.5 lpm aerosol inlet flow rate. The Aerosol Instrument Manager software, capable of collecting data weighted by number concentration, diameter, surface area, volume, and mass, recorded the SMPS spectrometer data.

Figure 8.6 Sampling Nanoparticle Exposure: Photocatalytic Spray Coat Application

In addition, nanoparticles were collected for offline characterization of the particle size, shape, and morphology, using the Nano Aerosol Sampler (NAS, TSI 3089). Particles were

collected on silicon nitride grids with 100 nm square opening for offline characterization using TEM (Model JEOL 100CX). The nanoparticle sampler was set at 7000 V and collected continuously for the duration of the two application methodologies studied, photocatalytic mortar overlays and photocatalytic spray coatings.

8.4 EXPOSURE RESULTS PHOTOCATALYTIC MORTAR OVERLAY – LAB-SIMULATED CONSTRUCTION ACTIVITIES

8.4.1 Particle Number Concentrations

The results of the nanoparticle exposure for the aqueous photocatalytic pavement procedure, powder photocatalytic pavement procedure, and control are shown in the box plot in Figure 8.7, illustrating minimum, 25% percentile, median, 75% percentile, minimum and maximum nanoparticle number concentrations. As shown in Figure 8.7, both application methods investigated for photocatalytic mortar overlays released more nanoparticles compared nanoparticles released during a normal mortar mix. The aqueous TiO_2 average concentration was $1.18x10^6$ #/cm^3 and the powder TiO_2 average concentration was $1.06x10^6$ #/cm^3. Furthermore, the addition of TiO_2 nanoparticles to water rather than the cement did not decrease the total amount of nanoparticles released.

Nanoparticles released could be from incidental sources such as the electric mixer, cement, and aggregate components of the mortar, or from artificial sources such as TiO_2 nanoparticles added to the mix. While it is likely that a large percentage of the nanoparticles released are not actually artificial nanoparticles, there is an increase of nanoparticles released when engineered nanoparticles are introduced into the mix design.

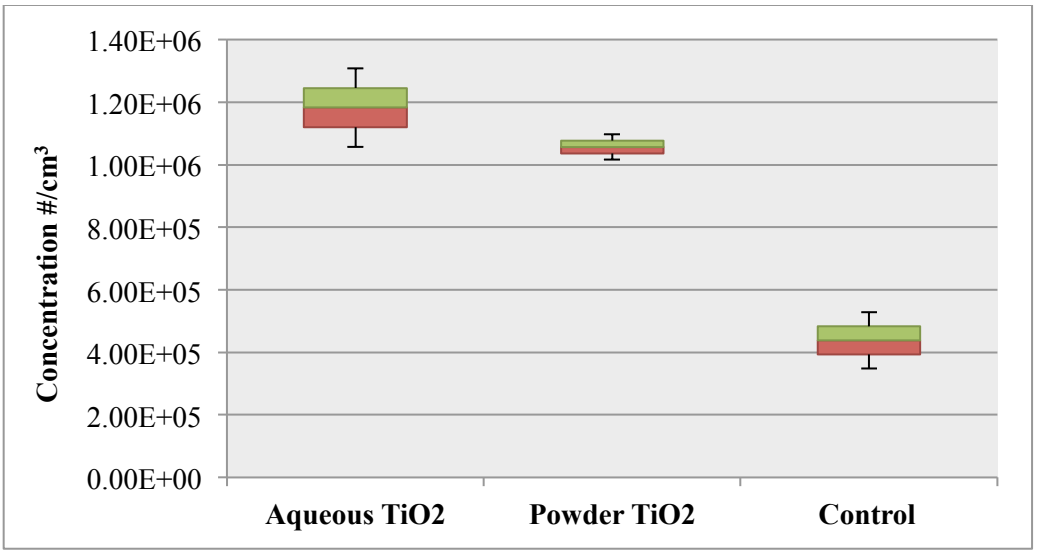

Figure 8.7 Lab Simulated Construction Activities Number Concentration for Photocatalytic Mortars Compared to Control

Figure 8.8 is a box plot of the concentrations of nanoparticles released for each simulated construction activity. It is evident that nanoparticles are released regardless of the construction activity. It is noted, that the increase in nanoparticles released for the aqueous photocatalytic mix is most likely attributed to the addition of the weighing step, which released an additional $1.94x10^5$ #/cm^3 number concentration and the mixing with water step, which released an additional $2.62x10^5$ #/cm^3 number concentration. As for the powder mix technique, the increase of nanoparticles released is due to the additional step of weighing the nanoparticles and the dry mixing step, which showed an elevated concentration compared to the dry mix step without nanoparticles. Although the concentration of the nanoparticles released from the powder mix in total is lower than the aqueous mix, if the nanoparticles were already suspended in water, thus eliminating the weighing and mixing in water steps, the amount released during construction would be less than when the nanoparticles are added to the cement. The theory that water may mitigate nanoparticle exposure is further supported in that there is not a significant difference

between the nanoparticle counts released during the wet mix with TiO_2 nanoparticles and wet mix without the addition of TiO_2 nanoparticles. On the contrary, there is a significant difference released between the dry mix with TiO_2 and dry mix without the addition of TiO_2 nanoparticles.

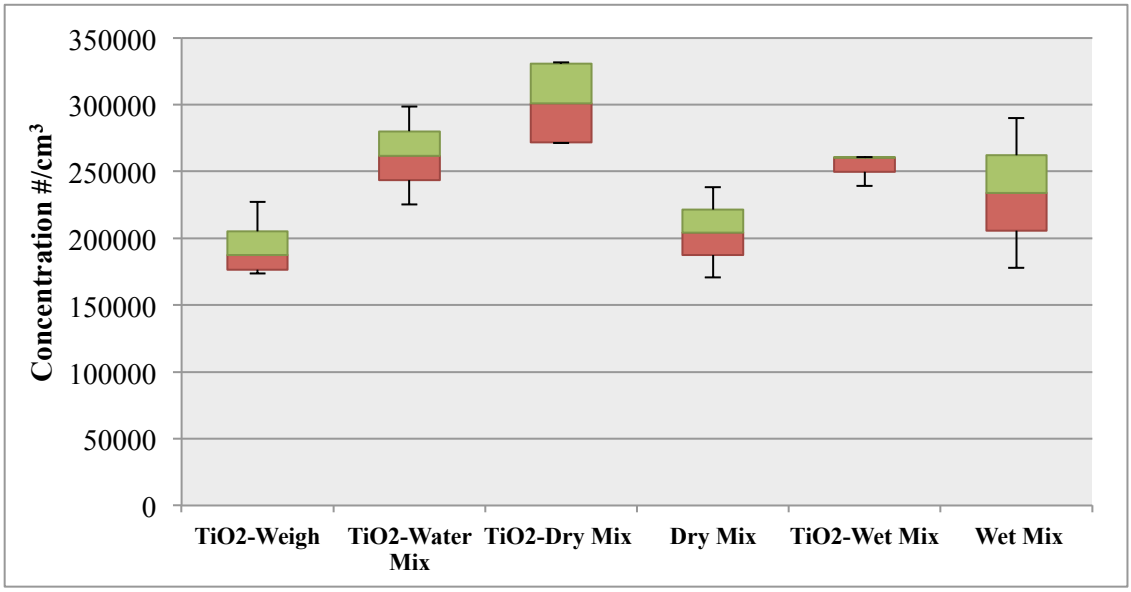

Figure 8.8 Nanoparticles Concentrations Released for Simulated Construction Activities Required for Photocatalytic Mortar Overlays

8.4.2 Particle Distributions

The average particle size, number concentration, surface area and mass concentration for each activity with the background subtracted are presented in Table 8.2. The average nanoparticle concentration, for the background environment in the laboratory, measured before the construction activities began is also presented. The background particles, particles emitted during weighing the TiO_2 and mixing the TiO_2 with water, were smaller compared to those released during wet and dry mixing activities. Since no other machinery was operating during the weighing task, it is likely that all of the nanoparticles released were engineered nanoparticles. The similarity of the average particle size released to the agglomerate average particle size of the TiO_2 nanoparticles used could be a result of nanoparticle agglomerates released. When mixing

the TiO_2 with water or cement, the average particle size increases. Furthermore, the average particle size of the control activities is larger than the activities with TiO_2 nanoparticles in the mix. The difference in average particle sizes could result from several influencing factors: the release of smaller artificial nanoparticles, the agglomeration of particles already in the air from previous activities, the addition of incidental nanoparticles released from the electric mixer, water contributing to particle agglomeration and the addition cement particles released in the case of the dry mixing step.

Table 8.2 Photocatalytic Mortar Overlay Laboratory-Simulated Construction Activities Mean Exposure Measurements

Task	Particle Diameter (nm)	Number Concentration (#/cm³)	Surface Area Concentration (nm²/cm³)	Mass Concentration (µg/m³)
Background Lab	30.95	2.65E+05	1.68E+09	3.36
TiO_2-Weigh[a]	29.58	1.94E+05	1.96E+09	3.93
TiO_2-Water Mix[a]	29.18	2.62E+05	4.14E+09	8.27
TiO_2-Wet Mix[a]	45.22	2.53E+05	4.59E+09	9.18
TiO_2-Dry Mix[a]	44.36	3.01E+05	5.42E+09	10.84
Wet Mix[a]	53.79	2.34E+05	4.29E+09	8.59
Dry Mix[a]	52.40	2.04E+05	3.54E+09	7.08

[a] *Background Lab Concentration Subtracted*

8.4.3 Background Lab Concentration Subtracted

Figure 8.9 shows the size distribution of particles emitted for each of the simulated construction tasks. It can be illustrated from this figure that all of the activities including TiO_2 nanoparticles had a concentration peak of particles emitted around 15-20 nm in diameter. However, for the mixes without TiO_2 nanoparticles added to the mix, there is no such peak. The higher concentrations emitted around 15 nanometers for the activities with TiO_2 could be explained by TiO_2 nanoparticles being released. Therefore, while the quantities of engineered nanoparticles are low, results suggest that they may be released into the environment. However, distinction

between the incidental nanoparticles released possibly due to electrical motor during mixing activities and engineered nanoparticles added to the mix cannot be made. Thus, further chemical analysis is required to prove that this smaller average is indeed related to the emission of engineered nanoparticles.

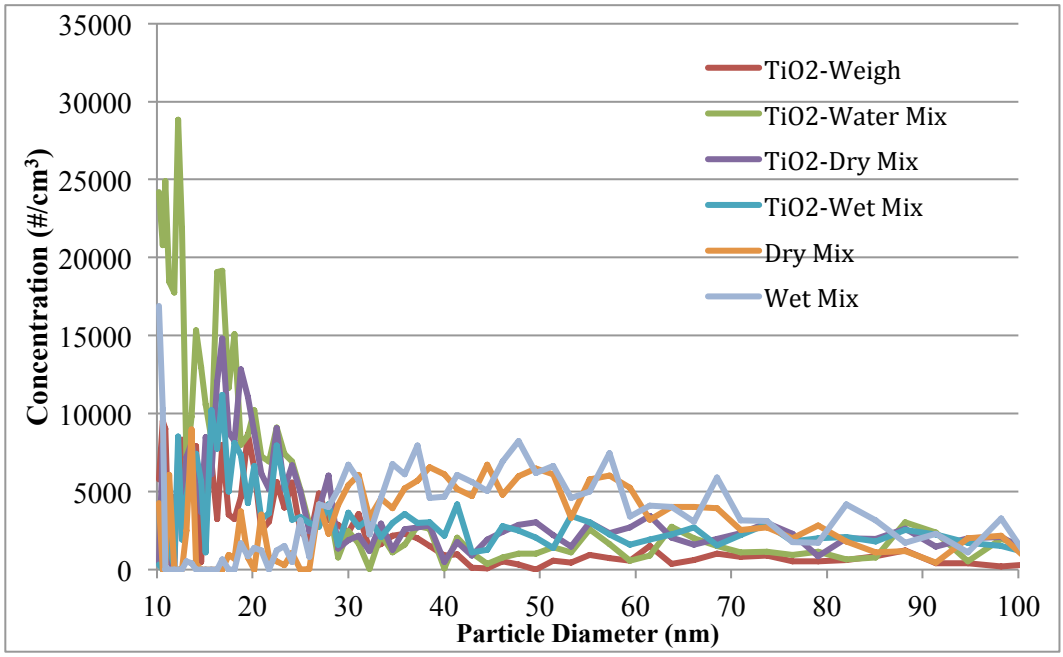

Figure 8.9 Size Distribution for Nanoparticles Released During the Simulated Construction Activities Required for Photocatalytic Mortar Overlays

8.4.4 Particle Morphology

A representative TEM image of the nanoparticles collected during the laboratory-simulated construction activities for the photocatalytic concrete overlay is shown in Figure 8.10. In general, the particles collected seem to be spherical; however, the particle boundary layer was difficult to define possibly indicating that the particles were not solidified. Due to the instability, high-resolution images were not possible inhibiting chemical identification. Nevertheless, the particle sizes, obtained by digital image processing, were estimated to be in average 50 nm in size. The particle sizes obtained from the samples are within what is expected according to the

SMPS data results, where the majority of the particles from the photocatalytic mortar overlay were within 10-50 nm in size. Furthermore, this discrepancy in particle size estimated by the TEM images compared to the SMPS results has been previously noted (Dahl et al. 2006). This could be explained by the different physical measurement techniques between the TEM and SMPS systems. While the TEM diameters are estimated by a projected equivalent diameter, the SMPS estimates the diameter by the electrical mobility.

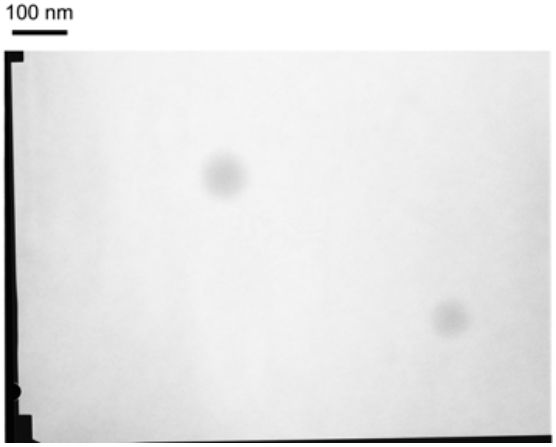

Figure 8.10 TEM Image of Nanoparticles Captured during Lab Simulation Construction Activities for Photocatalytic Mortar Overlay

8.5 PHOTOCATALYTIC SPRAY COAT - FIELD STUDY ACTUAL CONSTRUCTION ACTIVITIES

8.5.1 Particle Number Concentrations

Figure 8.11 is a box plot illustrating the increase in nanoparticle concentrations for the two activities of the spray coat application. The photocatalytic spray coating nanoparticle emissions totaled $2.3x10^8$ #/cm^3, significantly higher than the emissions measured from the laboratory-simulated construction activities. These results may be due to the difference in application size between the two studies and the natural nanoparticles that may already exist in the environment. Nanoparticles measured could be from vehicle combustion along with the spray coat application.

From the box plot, it is evident that there is larger variation in the concentrations recorded. An explanation for this observation is the variation of wind speed and direction throughout the application processes, which could not be controlled. The larger nanoparticle counts and variation in the real world environment could be a result of the passing traffic and more turbulence disturbing settled nanoparticles, similar to findings of Broekhuizen et al. (2011). Furthermore, it is noted that some of the photocatalytic coat samples did not increase the nanoparticles concentration in the atmosphere.

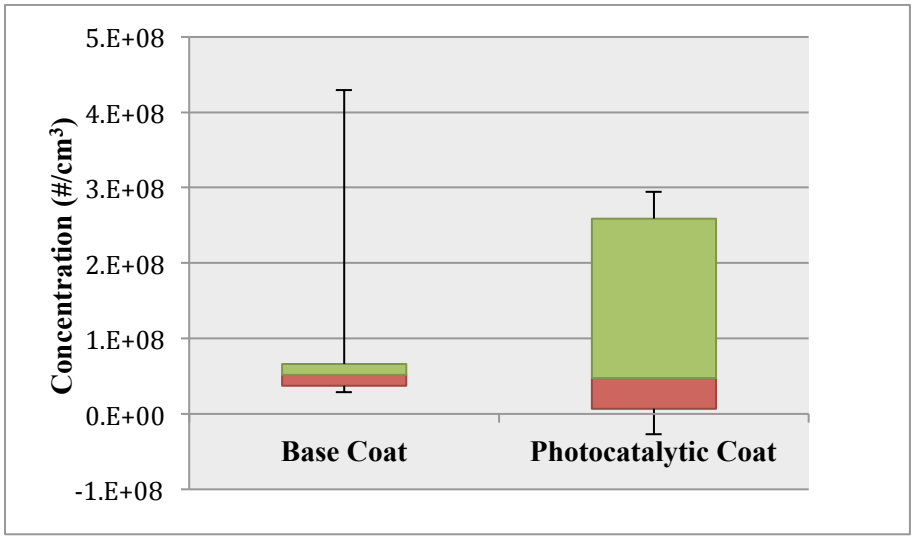

Figure 8.11 Concentration of Nanoparticles Released during the Construction of Photocatalytic Spray Coatings

8.5.2 Particle Distributions

The average particle size, number concentration, surface area and mass concentration for each activity with the background subtracted are presented in Table 8.3. In comparison of the nanoparticle sizes, the average particle size is smaller for the base spray activities compared to the particle size in the background environment. The smaller average particle size could be a

result of the smaller artificial nanoparticles being released into the environment due to the base coat spraying activity.

Table 8.3 Photocatalytic Spray Coat Construction Activities Mean Exposure Measurements

Task	Particle Diameter (nm)	Number Concentration (#/cm³)	Surface Area Concentration (nm²/cm³)	Mass Concentration (µg/m³)
Background Outside	33.94	2.23E+08	9.19E+11	7804.42
Base Coat[b]	23.28	5.19E+07	1.06E+11	678.25
Photocatalytic Coat[b]	37.35	1.78E+08	8.65E+11	7746.53

[b] *Background Outside Concentration Subtracted*

Figure 8.12 shows the size distribution of the nanoparticles released for both of the spray activities. The size distributions of the particles in the air are significantly different for the two applications. This was expected due to the differences in particles sizes determined by the preliminary nanoparticle characterization. The base coat, which had particles around 6 nm, only released particles up to 42 nm in diameter. On the contrary, the photocatalytic coat, which was applied approximately 5 minutes after, shows exposure of particles up to 62 nm in size peaking at particles 42 nm in size correlating to the preliminary characterization results, which had larger particles, 12 nm wide by 75 nm long.

8.5.3 Particle Morphology

A representative TEM image of the nanoparticles collected during the construction activities for the photocatalytic spray coating is shown in Figures 8.13 and 8.14. In general, there were more nanoparticles collected from the photocatalytic spray coating compared to the laboratory-simulated application of the concrete photocatalytic overlay demonstrated by the zoomed out picture on Figure 8.13. The higher number of nanoparticles collected agrees with the significantly higher number concentration recorded for the spray coat application. In general, the

particles collected seem to be spherical with some agglomeration. None of the particles collected matched the distinct shape of the nanorods used in the spray coat application. The particles sizes range from 20-70 nm, which is within what is expected according to the SMPS data results, where the majority of the particles from the spray coat application were within 10-60 nm in size.

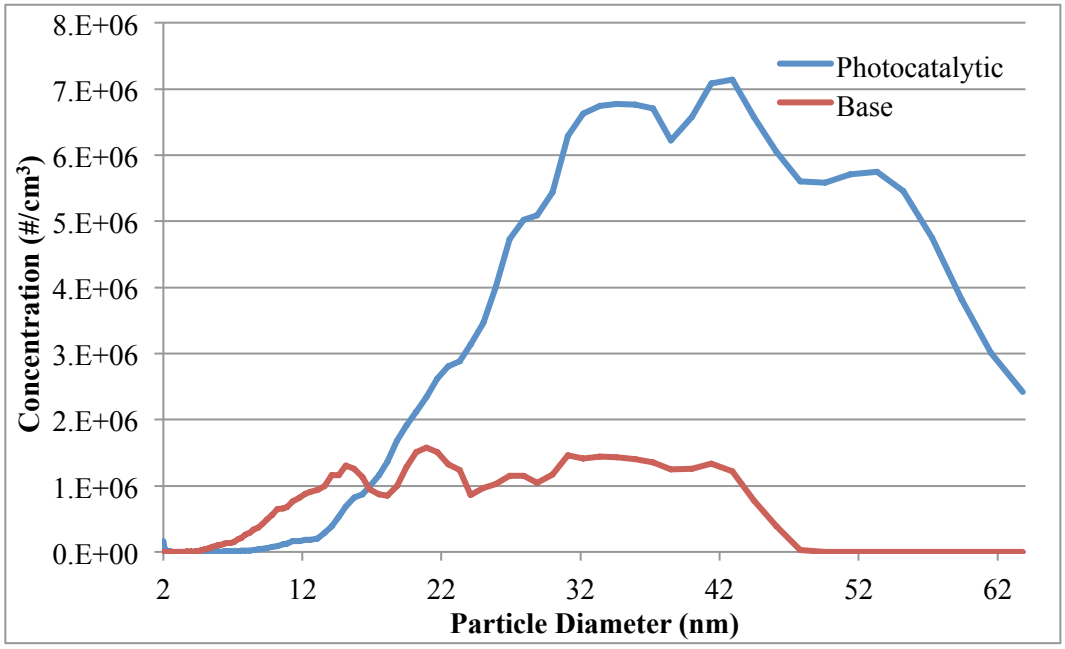

Figure 8.12 Size Distribution of the Concentration of Nanoparticles Released during the Construction of Photocatalytic Spray Coatings

It is also noted that when the electron beam was focused on the particles, the particles disappeared or diminished slowly while focusing. An explanation for this is that these particles are actually not TiO_2 nanoparticles but volatile particles and are actually evaporating. The cluster of particles shown in Figure 8.14 illustrates evidence of these particles. This suggests that these nanoparticles are actually incidental nanoparticles from the vehicle exhaust rather than from the TiO_2 application process. Previous research characterizing nanoparticles from vehicle exhaust has also reported particle evaporation. In fact, a study of the evaporation of volatile

particles collected from vehicle exhaust was also completed (Mathis et al. 2004). In addition, this inhibited chemical identification through high-resolution images; thus, further sampling is required to identify chemical compositions of the nanoparticles exposed.

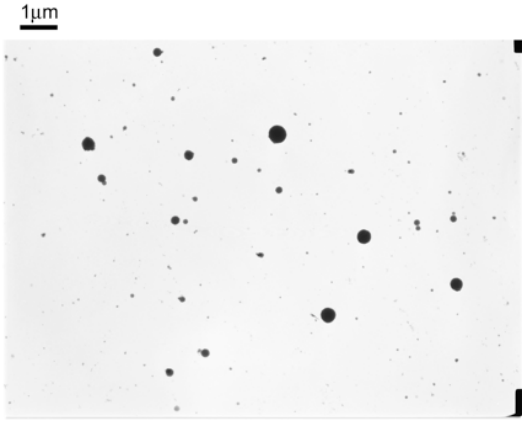

Figure 8.13 TEM image of Nanoparticles Captured during Application of Photocatalytic Spray Coating

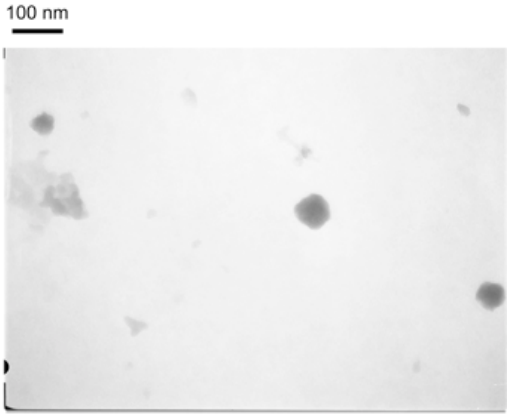

Figure 8.14 TEM Image of Nanoparticles Captured during Application of Photocatalytic Spray Coating (zoomed)

8.6 CONCLUSIONS AND RECOMMENDATIONS

The particles released during the application of photocatalytic pavements using TiO_2 nanoparticles were characterized. Two different photocatalytic concrete pavement applications were investigated; a photocatalytic mortar - using laboratory simulated construction activities,

and a photocatalytic spray coating - using field construction activities. The average nanoparticle exposure concentrations separated by particle size from the background environment were subtracted from the photocatalytic pavement application activities, where a positive net nanoparticle count is the estimated nanoparticle exposure of the ongoing activity. Engineered nanoparticles used were characterized using TEM and were compared to TEM images of the nanoparticles collected for further evidence of emission source.

The laboratory simulated construction activities for mortar applications showed that when engineered nanoparticles are added to the mix there is an increase in nanoparticle exposure; aqueous TiO_2 average concentration of $1.18x10^6$ #/cm^3 and powder TiO_2 average concentration of $1.06x10^6$ #/cm^3. Of these released, $1.94x10^5$ #/cm^3 released during weighing are likely all TiO_2 nanoparticles since there were no sources of incidental nanoparticles during this activity. The particles collected and analyzed using TEM were spherical in shape. However, due to the low quantity collected and the particle instability, high-resolution images were not obtained in efforts for chemical identification. As a result, further research is needed in order to identify the nanoparticle composition and sources.

The actual construction activities for spray-coat application resulted in higher nanoparticle concentrations compared to the laboratory-simulated construction activities totaling $2.3x10^8$ #/cm^3 released. The base coat released significantly smaller nanoparticles compared to the top coat. Both nanoparticle distributions correlated to the corresponding nanoparticle sizes comprised in each solution. The nanoparticles collected were spherical with some agglomerating and none matching the shape of the photocatalytic nanorods in the top coat solution. Thus, further research is needed to identify the nanoparticle source.

The nanoparticle released from photocatalytic pavements should also be investigated for the whole life cycle. This should include nanoparticles released due traffic abrasion and weathering. Furthermore, nanoparticles that are not aerosolized may be released to other mediums such as water runoff impacting aquatic ecosystems.

8.7 REFERENCES

Broekhuizen, P., Broekhuizen, F., Cornelissen, R., and Reijnders, L. (2011) "Use of nanomaterials in the European construction industry and some occupational health aspects thereof." Journal of Nanoparticle Research.

Brouwer, D.H., Gijsbers, J.H.J., Lurvink, M.W.M. (2004) "Personal exposure to ultrafine particles in the workplace: Exploring sampling techniques and strategies." Ann Occup Hyg 48(5), 439-453.

Brouwer, D., Duuren-Stuurman, B., Berges, M., Jankowska, E., Bard, D., and Mark, D. (2009) "From workplace air measurement results toward estimates of exposure? Development of a strategy to assess exposure to manufactured nano-objects." Journal of Nanopartical Research, 11,1867-1881.

Colvin, V. (2003) "The potential environmental impact of engineered nanomaterials." Nat Biotechnol, 21(10), 1166-1170.

Dahl, A., Gharibi, A., Swietlicki, E., Gudmundsson, A., Bohgard, M., Ljungman, A., Blomqvist, G., and Gustafsson, M. (2006) T"raffic-generated emissions of ultrafine particles from pavement-tire interface." Atmos Environ, 40, 1314-1323.

Farre, M., Sanchis, J., and Barcelo, D. (2011) "Analysis and assessment of the occurrence, the fate and the behavior of nanomaterials in the environment." Trends Anal Chem 30(3):517-527.

Fujishima, A., and Zhang, X. (2006) "Titanium dioxide photocatalysis: present situation and future approaches." C R Chim, 9:750-760.

Gohler, D., Stintz, M. Hillemann, L. and Vorbau, M. (2010). "Characterization of nanoparticle release from surface coatings by the simulation of a sanding process." Annals of Occupational Hygiene, 1-10.

Guzman, K. A., Taylor, M. R., and Banfield, J.F. (2006). "Environmental Risks of Nanotechnology: National Nanotechnology Initiative Funding, 2000−2004." Environmental Science & Technology, 40(5), 1401-1407.

Hoerr, R.A., Gupta, A., and Matuszewski, M.J. (2009) “Developing practices for safe handling of nanoparticles and nanomaterials in a development state enterprise: A practical guide for research and development organizations.” Safety Nanopart, Nanostruct Sci Technol.

Hoet, P.H.M., Bruske-Hohlfeld, I., and Salata, O.V. (2004) “Nanoparticles-known and unknown health risks.” J Nanobiotechnology, 2(12).

Hsu, L.Y., and Chein, H.M. (2007) “Evaluation of nanoparticle emission for TiO_2 nanopowder coating materials.” Nanopart Occup Health 9:157-163. doi:10.1007/s11051-006-9185-3

Lee J., Mahendra, S., and Alvarez, P.J.J. (2009) “Potential environmental and human health impacts of nanomaterials used in the construction industry.” Nanotechnology in Construction 3.

Long TC, Saleh N, Tilton RD, Lowry GV, Veronesi B (2006) Titanium Dioxide (P25) Produces Reactive Oxygen Species in Immortalized Brain Microglia (BV2): Implications for Nanoparticle Neurotoxicity. Environ Sci Technol 40(14):4346-4352. doi:10.1021/es060589n

Mathis, R., Kaegi, R., Mohr, M., and Zenobi, R. (2004) “TEM analysis of volatile nanoparticles from particle trap equipped diesel and direct-injection spark-ignition vehicles.” Atmos Environ, 38, 4347-4355.

Methner[a], M., L. Hodson, Dames, A., and Geraci, C. (2010). "Nanoparticle emission assessment technique (NEAT) for the identification and measurement of potential inhalation exposure to engineered nanomaterials--Part A." Journal of Occupational & Environmental Hygiene, 7(3), 127-132.

Methner[b], M., L. Hodson, A. Dames, and C. Geraci. (2010). “Nanoparticle emission assessment technique (NEAT) for the identification and measurement of potential inhalation exposure to engineered nanomaterials --Part b: Results from 12 field studies.” Journal of Occupational and Environmental Hygiene, 7, 163-176.

Meyer, D.E., Curran, M.A., Gonzalez, M.A. (2009) “An Examination of Existing Data for the Industrial Manufacture and Use of Nanocomponents and Their Role in the Life Cycle Impact of Nanoproducts.” Environment Science and Technology, 43(5),1256-1263.

Renn, O., and Roco, M.C. (2006). “Nanotechnology and the need for risk governance.” Journal of Nanoparticle Research, 8, 153-191.

Robichaud, C.O., Uyar, A.E., Darby, M.R., Zucker, L.G., and Wiesner, M.R. (2009) “Estimates of upper bounds and trends in nano-TiO_2 production as a basis for exposure assessment.” Environment Science and Technology, 43(12), 4227-4233.

Sahu, M and Biswas, P. (2010). “Size distributions of aerosols in an indoor environment with engineered nanoparticle synthesis reactors operating under different scenarios.” Journal Nanoparticle Research, 12, 1055-1064.

Tedja, R., Marquis, C., Lim, M., and Amal, R. (2011) “Biological impacts of TiO_2 on human lung cell lines A549 and H1299: particle size distribution effects.” Journal of Nanoparticle Resesarch, 13, 3801-3813.

TSI (2011) TSI Knows Nanoparticle Measurement <http://tsi.com/en-1033/applications/nanoparticle_measurements.aspx.> (28 November 2011)

Tsuji, J.S., Maynard, A.D., Howard, P.C., James, J.T., Lam, C., Warheit, D.B., and Santamaria A.B. (2006) “Research strategies for safety evaluation of nanomaterials, Part IV: Risk assessment of nanoparticles.” J Toxicol Sci, 89(1), 42-50.

Wiesner, M.R., Lowry, G.V., Alvarez, P., Dionysiou, D., and Biswas, P. (2006) “Assessing the Risks of Manufactured Nanomaterials.” Environment Science and Technology, 40(14), 4336-4345.

Wiesner, M. R., G. V. Lowry, Jones, K.L., Hochella, F.M., Di Giulio, R.T., Casman, E., and Bernhardt, E.S. (2009). "Decreasing Uncertainties in Assessing Environmental Exposure, Risk, and Ecological Implications of Nanomaterials." Environmental Science & Technology, 43(17), 6458-6462.

Zhu, X., Chang, Y., and Chen, Y. (2010) “Toxicity and bioaccumulation of TiO_2 nanoparticle aggregates in Daphnia magna.” Chemosphere, 78(3):209-215.

CHAPTER 9
SUMMARY AND CONCLUSIONS

Photocatalytic concrete pavements are a promising technology for mobile source air pollution remediation. Although this technology has the potential to support environmentally friendly road infrastructure, widespread application has not been realized due to several unanswered questions: 1. How significant is the NO_x reduction from photocatalytic pavement in roadway microenvironments? 2. Are nitrates released at harmful quantities potentially creating a water problem? 3. Are nanoparticles released during photocatalytic pavement life cycle?

In response to these questions, the goal of this study was to increase the understanding of the environmental impact of photocatalytic concrete pavement highways, following a life cycle approach. To achieve this goal, the objectives of this study are to (A) construct a model that evaluates the NO_x reduction from photocatalytic pavements, (B) quantify the nitrates released from the photocatalytic degradation of NO_x, and (C) identify and characterize pathways for TiO_2 nanoparticle exposure. To achieve this, the project was split into three phases: Model Development, Potential Hazards to Water, and Potential Nanoparticle Exposure to Air.

9.1 MODEL DEVELOPMENT

The first phase was to develop a model that quantifies the significance of NO_x reduction from photocatalytic pavements under various environmental conditions, meeting objective (A). To achieve this, two model approaches were used; a statistical model, based on field study data and a mathematical model, based on the conservation of mass.

The field study consisted of a ¼-mile concrete roadway sprayed with a photocatalytic coating in Baton Rouge, LA. This was the first field installation of the spray TiO_2 photocatalytic pavement coating in the US. NO_x concentrations were monitored for both the coated and

uncoated sections simultaneously for three weeks during the spring season to directly measure photocatalytic degradation. Further, nitrates were collected from the coated and uncoated areas for evidence of photocatalytic NO_x reduction. Results from both approaches show evidences of photocatalytic NO_x reduction. Environmental factors with significant impacts on photocatalytic efficiency include relative humidity, solar intensity, and wind speed and direction.

Despite evidence of a photocatalytic reduction, the amount reduced was significantly low with high variability suggesting additional factors, such as vehicle activity and vehicle classification, may need to be considered. Therefore, a second field study was preformed to evaluate the effect of these two possible significant factors, vehicle activity and classification, on the NO_x concentration emitted and the evaluation of NO_x reduction from photocatalytic pavements.

The second field study was conducted with 22.3 m^2 of photocatalytic spray coated area and 22.3 m^2 of uncoated control area using a TiO_2 spray coat with improved durability. Similarly, to the first field study, the photocatalytic reduction of NO_x was evaluated by directly measuring NO_x reductions from the ambient air. Expanding from the previous field study, a traffic study was conducted for the photocatalytic control areas to characterize the variability in traffic classification and activity between the two areas and its effects on interpreting NO_x reduction. Results showed that the amount of NO_x emitted in the area predicted to be from traffic sources is no more than 5 grams per hour. Due to the low values of pollution emitted in the both the photocatalytic area and the control area, minor differences in traffic activity between these two areas resulted in significant differences in the amount of pollution emitted. This may have complicated the interpretation of the NO_x reduction results. Furthermore, there was no significant linear correlation of vehicle class and speed and NO_x reduction. As a result, creating

a statistical model for the photocatalytic reduction using the field study data was not feasible. Despite this, conclusions arising from this study are important for planning of future photocatalytic pavement field studies.

For the mathematical model, based on the conservation of mass, first the reaction rate was modeled using the Langmuir Hinshelwood model for the degradation of nitrogen monoxide (NO) at various humidity and irradiance levels for photocatalytic concrete pavement. Due to durability issues with the spray coating, the concrete samples were prepared using a two layer concrete system. Using a plug flow photoreactor, laboratory experimental results support that the photocatalytic oxidation of NO was reaction controlled and adequately described by the Langmuir-Hinshelwood model. Simulating 5 different levels of relative humidity and 5 different levels of irradiance, the L-H reaction rate constant, k, and the adsorption equilibrium constant, Kd, was calculated for 25 unique environmental conditions. Graphical representation of the irradiance and humidity effect on the L-H constants indicated variable interaction was present. Using multiple linear regression statistical techniques, a model was created for k with the irradiance and interaction variable of humidity and irradiance significant. Similarly, a model was created for Kd with the humidity and interaction variable of humidity and irradiance significant. The models for k and Kd were incorporated into the L-H apparent reaction rate model allowing for determination of the photocatalytic oxidation of NO at different environmental conditions. The resulting model was validated by additional laboratory runs not used to create the model, determining that 87% of model explains the data variability.

Using the photocatalytic reaction kinetic results, a Lavoisier mass balance model for roadway microenvironments was created to better understand the potential NO reductions in a real world setting. In doing so, the amount of NO reduced due to the photocatalytic pavement

can be compared to other mass transfer mechanisms. The transport processes for NO included convection in and out, the reaction between NO and ozone, turbulent diffusion out of the system top and the photocatalytic degradation of NO. The model was applied to a 13 m^2 urban roadway microenvironment in Los Angeles, California, since it has reported some of the highest NO concentrations. Meteorological data estimated from historical TMY-2 files, NO and Ozone concentrations estimated from 2011 ambient air monitoring data sets, and NO-Ozone reaction rate constant, surface roughness, and displacement height, estimated from published literature were used as the model inputs. The concentration of NO out of the system volume was calculated as well as the percent of NO out due to the photocatalytic pavement assuming a well mixed, uniform concentration of NO, temperature, and pressure at steady-state. At average environmental conditions the model illustrated that the convection was the dominating mass transfer flux of NO out, accounting of 97% while the photocatalytic reduction of NO only accounted for 2%. Due to the uncertainty of many of the parameters, a sensitivity analysis was conducted indicating that the air velocity was the most significant factor impacting the percent of photocatalytic reduction of NO.

9.2 POTENTIAL HAZARDS TO WATER

The second phase was to evaluate potentially harmful compounds – nitrates and TiO_2 nanoparticles - released to water for photocatalytic concrete pavements used to oxidize NO_x from mobile pollution sources. The amount of nitrates eluted to water were measured after 4.5 hours of photocatalytic oxidation of NO using the environmental settings which would provide the most NO reduced and nitrates created. On average after 4.5 hour of photocatalytic oxidation (PCO) of NO with 91.9% NO_x reduction efficiency, only 8.984 μmols of nitrates were released

to water accounting for only 49% of the theoretical amount of nitrates created. Surprisingly the photocatalytic pavement eluted less nitrates than the concrete control samples.

The second part of the study investigated whether engineered TiO_2 nanoparticles used in photocatalytic pavements entered into water. For this study water samples from two different types of photocatalytic concrete pavements (photocatalytic mortar overlays and photocatalytic spray coats), were analyzed and compared to water samples from typical concrete pavement (control). ICP-AES did not detect any titanium in any of the water samples, including the water samples from the photocatalytic concrete spray coating, which has demonstrated a known durability issue. As a result, it is suggested that ICP-MS, with a detection limit of 1 ppt, is used to quantify the Ti in the water samples rather than ICP-AES.

9.3 POTENTIAL NANOPARTICLE EXPOSURE TO AIR

With the increasing use of titanium dioxide (TiO_2) nanoparticles in self-cleaning materials such as photocatalytic concrete pavements, the release of nanoparticles into the environment is inevitable. As a result, to ensure that there are no unintended environmental consequences, the third phase was to evaluate the potential of TiO_2 nanoparticle exposure to air. Nanoparticle concentration, particle size, surface area, elemental composition, and surface morphology are pertinent to determine the associated risks. The potential of exposure to synthetic nanoparticles released during construction activities for application of photocatalytic pavements was measured during laboratory-simulated construction activities of photocatalytic mortar overlays and in an actual field application of photocatalytic spray coat. A scanning mobility particle sizer system measured the size distribution of nanoparticles released during laboratory and field activities. Since incidental nanoparticles are released during construction activities, nanoparticle emissions were compared to those from similar activities without nano-

TiO_2. Nanoparticle counts and size distribution suggest that synthetic nanoparticles are released during application of photocatalytic pavements. In order to identify the nanoparticle source, nanoparticles were also collected for offline characterization using transmission electron microscopy. Despite this, positive identification of synthetic nanoparticles was not possible due to difficulties in obtaining high-resolution images. Thus, further research is required to obtain chemical composition and positive identification of nanoparticle sources.

9.4 Future Work

The results of the work opened up many topics for future research including:

- Identification nanoparticle composition and sources for nanoparticles released to air during construction activities with and without engineered nanoparticles
- Are nanoparticles released to water at lower concentrations?
- What happens to the nitrates that are not eluted from photocatalytic pavements?
- How much nitrates exist on concrete pavement samples?
- What reduction efficiencies are realized in real world environments for other pollutants and how significant are they compared to the pollution problem?
- What locations would be optimal for photocatalytic pavements?
- How much pollutants actually come in contact with the pavement surface?
- What is the durability of the layer?
- What is the shear strength of the layer?
- What is the impact of mixed gas environments?
- Are other pollutants reduced?
- Did the proposed photocatalytic layer mix design impact the surface friction?
- What is the overall environmental impact?

APPENDIX A
COPYRIGHT PERMISSION

Dear Ms. Dylla:

The Transportation Research Board grants permission to use your paper, "Field Evaluation of Ability of Photocatalytic Concrete Pavements to Remove Nitrogen Oxides," by H. Dylla, M. Hassan, and D. Osborn, in your doctorate dissertation, as identified in your request of March 21, 2013, subject to the following conditions:

1. Please cite the paper's publication in *Transportation Research Record: Journal of the Transportation Research Board, No. 2290,* pp. 154-160.

2. Please acknowledge that the material is reproduced with permission of the Transportation Research Board.

3. None of this material may be presented to imply endorsement by TRB of a product, method, practice, or policy.

Every success with your doctorate dissertation. Please let me know if you have any questions.

Sincerely,

Javy Awan
Director of Publications
Transportation Research Board

SPRINGER LICENSE
TERMS AND CONDITIONS

Mar 21, 2013

This is a License Agreement between Heather Dylla ("You") and Springer ("Springer") provided by Copyright Clearance Center ("CCC"). The license consists of your order details, the terms and conditions provided by Springer, and the payment terms and conditions.

All payments must be made in full to CCC. For payment instructions, please see information listed at the bottom of this form.

License Number	3113750354548
License date	Mar 21, 2013
Licensed content publisher	Springer
Licensed content publication	Journal of Nanoparticle Research
Licensed content title	Characterization of nanoparticles released during construction of photocatalytic pavements using engineered nanoparticles
Licensed content author	Heather Dylla
Licensed content date	Jan 1, 2012
Volume number	14
Issue number	4
Type of Use	Thesis/Dissertation
Portion	Full text
Number of copies	1
Author of this Springer article	Yes and you are the sole author of the new work
Order reference number	
Title of your thesis / dissertation	QUANTIFICATION OF THE ENVIRONMENTAL IMPACT OF TITANIUM DIOXIDE PHOTOCATALYTIC PAVEMENTS FOR AIR POLLUTION REMEDIATION
Expected completion date	May 2013
Estimated size(pages)	200
Total	0.00 USD
Terms and Conditions	

Introduction
The publisher for this copyrighted material is Springer Science + Business Media. By clicking "accept" in connection with completing this licensing transaction, you agree that the following terms and conditions apply to this transaction (along with the Billing and Payment terms and conditions established by Copyright Clearance Center, Inc. ("CCC"), at the time that you opened your Rightslink account and that are available at any time at http://myaccount.copyright.com).

Limited License
With reference to your request to reprint in your thesis material on which Springer Science and Business Media control the copyright, permission is granted, free of charge, for the use indicated in your enquiry.

Licenses are for one-time use only with a maximum distribution equal to the number that you identified in the licensing process.

This License includes use in an electronic form, provided its password protected or on the university's intranet or repository, including UMI (according to the definition at the Sherpa website: http://www.sherpa.ac.uk/romeo/). For any other electronic use, please contact

Springer at (permissions.dordrecht@springer.com or permissions.heidelberg@springer.com).

The material can only be used for the purpose of defending your thesis, and with a maximum of 100 extra copies in paper.

Although Springer holds copyright to the material and is entitled to negotiate on rights, this license is only valid, provided permission is also obtained from the (co) author (address is given with the article/chapter) and provided it concerns original material which does not carry references to other sources (if material in question appears with credit to another source, authorization from that source is required as well).

Permission free of charge on this occasion does not prejudice any rights we might have to charge for reproduction of our copyrighted material in the future.

Altering/Modifying Material: Not Permitted
You may not alter or modify the material in any manner. Abbreviations, additions, deletions and/or any other alterations shall be made only with prior written authorization of the author(s) and/or Springer Science + Business Media. (Please contact Springer at (permissions.dordrecht@springer.com or permissions.heidelberg@springer.com)

Reservation of Rights
Springer Science + Business Media reserves all rights not specifically granted in the combination of (i) the license details provided by you and accepted in the course of this licensing transaction, (ii) these terms and conditions and (iii) CCC's Billing and Payment terms and conditions.

Copyright Notice:Disclaimer
You must include the following copyright and permission notice in connection with any reproduction of the licensed material: "Springer and the original publisher /journal title, volume, year of publication, page, chapter/article title, name(s) of author(s), figure number(s), original copyright notice) is given to the publication in which the material was originally published, by adding; with kind permission from Springer Science and Business Media"

Warranties: None

Example 1: Springer Science + Business Media makes no representations or warranties with respect to the licensed material.

Example 2: Springer Science + Business Media makes no representations or warranties with respect to the licensed material and adopts on its own behalf the limitations and disclaimers established by CCC on its behalf in its Billing and Payment terms and conditions for this licensing transaction.

Indemnity
You hereby indemnify and agree to hold harmless Springer Science + Business Media and CCC, and their respective officers, directors, employees and agents, from and against any and all claims arising out of your use of the licensed material other than as specifically authorized pursuant to this license.

No Transfer of License
This license is personal to you and may not be sublicensed, assigned, or transferred by you to any other person without Springer Science + Business Media's written permission.

No Amendment Except in Writing
This license may not be amended except in a writing signed by both parties (or, in the case of Springer Science + Business Media, by CCC on Springer Science + Business Media's behalf).

Objection to Contrary Terms
Springer Science + Business Media hereby objects to any terms contained in any purchase order, acknowledgment, check endorsement or other writing prepared by you, which terms

are inconsistent with these terms and conditions or CCC's Billing and Payment terms and conditions. These terms and conditions, together with CCC's Billing and Payment terms and conditions (which are incorporated herein), comprise the entire agreement between you and Springer Science + Business Media (and CCC) concerning this licensing transaction. In the event of any conflict between your obligations established by these terms and conditions and those established by CCC's Billing and Payment terms and conditions, these terms and conditions shall control.

Jurisdiction
All disputes that may arise in connection with this present License, or the breach thereof, shall be settled exclusively by arbitration, to be held in The Netherlands, in accordance with Dutch law, and to be conducted under the Rules of the 'Netherlands Arbitrage Instituut' (Netherlands Institute of Arbitration).***OR:***

All disputes that may arise in connection with this present License, or the breach thereof, shall be settled exclusively by arbitration, to be held in the Federal Republic of Germany, in accordance with German law.

Other terms and conditions:

v1.3

If you would like to pay for this license now, please remit this license along with your payment made payable to "COPYRIGHT CLEARANCE CENTER" otherwise you will be invoiced within 48 hours of the license date. Payment should be in the form of a check or money order referencing your account number and this invoice number RLNK500982648.
Once you receive your invoice for this order, you may pay your invoice by credit card. Please follow instructions provided at that time.

Make Payment To:
Copyright Clearance Center
Dept 001
P.O. Box 843006
Boston, MA 02284-3006

For suggestions or comments regarding this order, contact RightsLink Customer Support: customercare@copyright.com or +1-877-622-5543 (toll free in the US) or +1-978-646-2777.

Gratis licenses (referencing $0 in the Total field) are free. Please retain this printable license for your reference. No payment is required.

APPENDIX B
CHAPTER 3 CALCULATIONS

$$NO_x\ Reduction\ Per\ 1\ Min = NO_x\ Conc.Control - NO_x\ \ Conc.Photocatalytic\ Area$$

$$NO_x\ Reduction\ Per\ 1\ Hour = NO_x\ Reduction\ Per\ 1\ Min * 60$$

Table B.1 Calculation for Average Daily NO_x Reductions

Traffic Count		NO_x Reduction (ppb)			
Day	Hour	Per 1 Min		Per 1 Hour	
		Avg.	Stdev.	Avg.	Stdev.
	6	-3.00	2.68	-180	161
	7	-3.25	7.31	-195	439
	8	0.583	6.80	35	408
	9	4.42	1.78	265	107
	10	3.25	1.71	195	103
	11	5.55	8.09	333	485
	12	7.92	10.7	475	643
	13	8.58	7.65	515	459
	14	5.83	8.24	350	495
	15	19.9	25.0	1195	1498
	16	7.80	12.2	468	729
	17	8.58	7.84	515	471
	18	11.8	18.3	710	1100
	19	4.13	11.8	248	707
3			**Total**	**4928**	**7805**
	6	-0.200	0.447	-12	27
	7	0.833	1.27	50	76
	8	0.917	0.793	55	48
	9	1.08	1.00	65	60
	10	2.42	0.515	145	31
	11	5.75	9.65	345	579
	12	19.5	24.2	1173	1450
	13	5.00	1.65	300	99
	14	5.75	1.06	345	63
	15	2.00	13.7	120	823
	16	9.67	13.2	580	792
	17	23.2	28.4	1390	1701
	18	2.75	1.14	165	68
	19	3.25	14.1	195	845
4			**Total**	**4916**	**6662**

Traffic Count		NO_x Reduction (ppb)			
Day	Hour	Per 1 Min		Per 1 Hour	
		Avg.	Stdev.	Avg.	Stdev.
	6	-0.429	1.62	-26	97
	7	2.50	3.92	150	235
	8	8.00	12.8	480	767
	9	10.2	7.65	611	459
	10	-3.50	2.94	-210	176
	11	8.64	11.2	518	674
	12	6.17	3.54	370	212
	13	20.1	26.6	1205	1598
	14	2.09	24.0	125	1437
	15	7.09	36.1	425	2163
	16	3.82	9.15	229	549
	17	7.00	11.6	420	696
	18	7.60	6.54	456	392
	19	5.50	8.80	330	528
5			**Total**	**5085**	**9984**
	7	-0.250	0.452	-15	27
	8	-0.667	2.42	-40	145
	9	-0.700	9.03	-42	542
	10	5.92	10.3	355	620
	11	0.083	2.84	5	171
	12	11.7	33.2	700	1991
	13	-0.750	23.7	-45	1424
	14	-3.67	23.6	-220	1416
	15	4.91	12.1	295	728
	16	1.91	4.93	115	296
	17	0.083	1.62	5	97
	18	0.417	3.20	25	192
	19	1.30	6.93	78	416
6			**Total**	**1215**	**8065**
	6	4.14	1.07	249	64
	7	2.58	2.84	155	171
	8	17.7	13.7	1060	822
	9	18.7	9.51	1120	571
7			**Total**	**2584**	**1628**
8	6	-50.83	21.8	-3050	1310
	7	-5.33	20.4	-320	1226

Traffic Count		NO_x Reduction (ppb)			
Day	Hour	Per 1 Min		Per 1 Hour	
		Avg.	Stdev.	Avg.	Stdev.
	8	-1.17	8.01	-70	481
	9	-2.25	23.7	-135	1420
	10	18.4	22.4	1105	1346
	11	9.75	9.51	585	570
	12	16.4	18.2	985	1089
	13	7.42	5.71	445	343
	14	13.6	11.4	815	685
	15	4.45	27.5	267	1651
	16	1.33	19.4	80	1166
	17	0.727	19.2	44	1152
	18	7.55	17.6	453	1058
	19	20.8	32.5	1245	1950
8			**Total**	**2449**	**15446**
	6	-7.35	1.84	-441	110
	7	-10.20	18.6	-612	1118
	8	23.5	17.2	1412	1033
	9	29.9	9.87	1796	592
	10	26.7	23.4	1599	1403
	11	22.5	20.7	1349	1242
	12	8.75	22.3	525	1337
	13	19.5	29.4	1172	1763
	14	8.25	23.0	495	1380
	15	-1.96	28.0	-118	1683
	16	-7.35	26.1	-441	1566
	17	5.18	28.2	311	1691
	18	-0.247	28.4	-15	1701
	19	-12.04	33.7	-723	2020
9			**Total**	**6310**	**18639**
	6	-3.75	1.52	-225	91
	7	-3.46	9.49	-207	569
	8	6.50	12.3	390	740
	9	20.8	16.2	1251	971
	10	12.0	3.86	723	232
	11	5.32	20.0	319	1198
	12	13.6	17.6	818	1053
	13	12.4	11.1	744	667
	14	18.7	19.3	1125	1156
	15	3.44	14.0	207	841
	16	4.94	5.53	297	332
10	17	7.16	32.1	430	1926

Traffic Count		NO_x Reduction (ppb)			
Day	Hour	Per 1 Min		Per 1 Hour	
		Avg.	Stdev.	Avg.	Stdev.
	18	4.51	6.02	270	361
	19	-10.00	27.9	-600	1677
10			**Total**	**5541**	**11814**
	6	-1.55	1.42	-93	85
	7	-1.26	1.14	-75	68
	8	-1.84	1.29	-110	77
	9	-1.25	1.59	-75	96
	10	11.9	7.73	713	464
	11	-1.50	9.58	-90	575
	12	-3.19	20.4	-191	1226
	13	7.39	11.3	443	680
	14	4.63	4.70	278	282
	15	3.56	1.12	214	67
	16	4.31	2.24	259	134
	17	-0.577	13.6	-35	817
	18	3.01	4.85	180	291
	19	6.48	13.3	389	795
11			**Total**	**1807**	**5658**
	6	0.171	1.38	10	83
	7	-0.395	1.89	-24	114
	8	1.52	26.4	91	1587
	9	-2.31	13.0	-139	782
	10	7.70	9.18	462	551
	11	6.79	3.69	408	221
	12	3.50	6.96	210	418
	13	8.10	19.9	486	1196
	14	2.36	10.5	141	632
	15	6.01	4.79	360	287
	16	-1.79	22.4	-107	1345
	17	-5.44	25.6	-327	1537
	18	2.60	26.1	156	1565
	19	5.64	7.23	338	434
12			**Total**	**2067**	**10752**
	6	-8.51	18.3	-511	1096
	7	4.20	16.3	252	979
	8	4.98	11.9	299	713
	9	22.1	24.8	1324	1486
	10	19.6	20.8	1174	1250
	11	6.02	9.02	361	541
13	12	4.58	3.27	275	196

Traffic Count		NO_x Reduction (ppb)			
Day	Hour	Per 1 Min		Per 1 Hour	
		Avg.	Stdev.	Avg.	Stdev.
	13	2.21	15.9	133	957
	14	5.28	N/A	317	N/A
	16	2.22	4.13	133	248
	17	1.62	13.3	97	797
	18	5.41	10.6	325	637
	19	-1.21	10.5	-72	631
13			**Total**	**4106**	**9530**
	6	-0.586	5.00	-35	300
	7	11.7	21.1	701	1267
	8	4.30	6.36	258	381
	9	4.38	4.99	263	299
	10	9.71	4.15	582	249
	11	8.06	16.5	483	991
	12	7.14	2.59	428	155
	13	8.61	25.1	516	1508
	14	0.991	17.9	59	1074
	15	8.96	12.8	538	770
	16	6.21	4.84	373	291
	17	8.88	10.6	533	638
	18	7.27	2.57	436	154
	19	0.559	7.19	34	431
14			**Total**	**5169**	**8509**
	6	-1.32	7.84	-79	470
	7	-0.396	3.38	-24	203
	8	8.35	18.0	501	1082
	9	5.56	3.29	333	198
	12	-0.177	17.2	-11	1033
	13	13.7	12.6	820	754
	14	6.74	16.8	404	1008
	15	3.53	24.8	212	1485
	16	16.7	16.3	1004	977
	17	16.3	11.5	977	691
	18	5.25	5.25	315	315
	19	7.57	3.85	454	231
15			**Total**	**4907**	**8446**

Table B.2 Example Calculation for Average NO_x Reductions per Traffic Count

Traffic Count		NO_x Reduction (ppb)			
Per 1 Min	Per 1 Hour	Per 1 Min		Per 1 Hour	
		Avg.	Stdev.	Avg.	Stdev.
0	0	2.55	14.6	153	877
10	120	5.90	19.2	354	1149
20	240	6.38	17.4	383	1043
30	360	2.70	18.3	162	1096
40	480	2.82	17.0	169	1018
50	600	5.98	12.0	359	721

Table B.3 Calculations for Average NO_x Reductions per Humidity

	NO_x Reduction (ppb)			
	Per 1 Min		Per 1 Hour	
Humidity	Avg.	Stdev.	Avg.	Stdev.
30	8.24	18.3	1100	494
40	4.77	20.9	1256	286
50	4.79	15.3	916	288
60	3.38	17.6	1055	203
70	5.27	12.9	777	316
80	0.00	11.6	695	0
90	1.73	15.0	902	104

Table B.4 Example Calculation for Average NO_x Reductions per Solar Radiation

Solar Radiation (W/m^2)	NO_x Reduction (ppb)			
	Per 1 Min		Per 1 Hour	
	Avg.	Stdev.	Avg.	Stdev.
0	2.59	16.4	155	987
100	5.48	15.6	329	938
200	4.97	11.8	298	709
300	3.65	13.4	219	804
400	2.37	11.8	142	710
500	4.83	16.6	290	996
600	1.48	20.2	89	1211
700	4.40	20.2	264	1212
800	3.28	19.6	197	1178
900	6.03	16.6	362	998
1000	4.80	17.6	288	1058
1100	-18.0	N/A	-1079	N/A

Table B.5 Example Calculation for Average NO_x Reductions per Wind Speed

Wind Speed (m/s)	NO_x Reduction (ppb)			
	Per 1 Min		Per 1 Hour	
	Avg.	Stdev.	Avg.	Stdev.
0	0.17	15.5	10.2	932
0.4	5.22	17.5	313	1053
0.9	6.89	16.0	414	963
1.3	5.83	17.6	350	1057
1.8	2.48	15.6	149	936
2.2	2.92	15.2	175	915
2.7	0.41	13.8	24.7	830
3.1	1.92	14.4	115	865
3.6	0.49	14.9	29.6	896
4	-1.15	15.9	-69.1	953
4.5	-0.53	17.9	-31.7	1073
4.9	-4.93	11.4	-296	683
5.4	0.42	5.4	25.0	326
6.3	0.80	N/A	47.8	N/A

Table B.6 Example Calculation for Average NO_x Reductions per Wind Direction

Wind Speed (m/s)	NO_x Reduction (ppb)			
	Per 1 Min		Per 1 Hour	
	Avg.	Stdev.	Avg.	Stdev.
N	6.63	15.4	398	922
NNE	-4.94	33.6	-296	2017
NE	-5.93	27.5	-356	1650
ENE	8.57	12.5	514	749
E	8.49	19.6	510	1178
ESE	1.94	7.86	116	472
SE	9.90	13.9	594	836
SSE	7.28	14.3	437	856
S	5.21	16.3	312	978
SSW	5.03	17.0	302	1018
SW	6.68	15.9	401	955
WSW	-0.31	5.65	-18.8	339
W	-1.63	1.48	-97.7	89
WNW	2.00	9.07	120	544
NW	2.21	17.0	133	1020
NNW	2.08	12.6	125	754

APPENDIX C
CHAPTER 4 CALCULATIONS

MOVES INPUT FILES – PHOTOCATALYTIC COATED AREA

Hour 7

Table C.1 Links – Photocatalytic Coated Area Hour 7

linkID	countyID	zoneID	roadTypeID	linkLength	linkVolume	linkAvgSpeed	linkDescription	linkAvgGrade
1	22033	220330	1	0.004	1	0	parking	0
2	22033	220330	5	0.004	28	10	road	0

Table C.2 Links Source – Photocatalytic Coated Area Hour 7

linkID	sourceTypeID	sourceTypeHourFraction
2	11	0
2	21	0.508297258
2	31	0.387085137
2	32	0.082611833
2	42	0.022005772
2	52	0
2	61	0

Table C.3 Meteorology – Photocatalytic Coated Area Hour 7

monthID	zoneID	hourID	temperature	relHumidity
2	220330	8	13.01233333	81.822

Table C.4 Off Network – Photocatalytic Coated Area Hour 7

sourceTypeID	vehiclePopulation	startFraction	extendedIdleFraction	parkedVehicleFraction
11	0	0	0	1
21	1	0	0	1
31	0	0	0	1
32	0	0	0	1
42	0	0	0	1
52	0	0	0	1
61	0	0	0	1

Hour 8

Table C.5 Links – Photocatalytic Coated Area Hour 8

linkID	countyID	zoneID	roadTypeID	linkLength	linkVolume	linkAvgSpeed	linkDescription	linkAvgGrade
1	22033	220330	1	0.004	3	0	parking	0
2	22033	220330	5	0.004	78	10	road	0

Table C.6 Links Source – Photocatalytic Coated Area Hour 8

linkID	sourceTypeID	sourceTypeHourFraction
2	11	0
2	21	0.452275
2	31	0.386848
2	32	0.103984
2	42	0.047399
2	52	0.009494
2	61	0

Table C.7 Meteorology – Photocatalytic Coated Area Hour 8

monthID	zoneID	hourID	temperature	relHumidity
2	220330	9	13.71413	79.23667

Table C.8 Off Network – Photocatalytic Coated Area Hour 8

sourceTypeID	vehiclePopulation	startFraction	extendedIdleFraction	parkedVehicleFraction
11	0	0	0	1
21	2	0.033	0	1
31	1	0.017	0	1
32	0	0	0	1
42	0	0	0	1
52	0	0	0	1
61	0	0	0	1

Hour 9

Table C.9 Links – Photocatalytic Coated Area Hour 9

linkID	countyID	zoneID	roadTypeID	linkLength	linkVolume	linkAvgSpeed	linkDescription	linkAvgGrade
1	22033	220330	1	0.004	4	0	parking	0
2	22033	220330	5	0.004	95	10	road	0

Table C.10 Links Source – Photocatalytic Coated Area Hour 9

linkID	sourceTypeID	sourceTypeHourFraction
2	11	0
2	21	0.516013
2	31	0.380655
2	32	0.061734
2	42	0.035806
2	52	0.004053
2	61	0.001739

Table C.11 Meteorology – Photocatalytic Coated Area Hour 9

monthID	zoneID	hourID	temperature	relHumidity
2	220330	10	14.63456	75.27355

Table C.12 Off Network – Photocatalytic Coated Area Hour 9

sourceTypeID	vehiclePopulation	startFraction	extendedIdleFraction	parkedVehicleFraction
11	0	0	0	1
21	2	0.213	0	1
31	2	0.213	0	1
32	0	0	0	1
42	0	0	0	1
52	0	0	0	1
61	0	0	0	1

Hour 10

Table C.13 Links – Photocatalytic Coated Area Hour 10

linkID	countyID	zoneID	roadTypeID	linkLength	linkVolume	linkAvgSpeed	linkDescription	linkAvgGrade
1	22033	220330	1	0.004	3	0	parking	0
2	22033	220330	5	0.004	130	10	road	0

Table C.14 Links Source – Photocatalytic Coated Area Hour 10

linkID	sourceTypeID	sourceTypeHourFraction
2	11	0
2	21	0.4821
2	31	0.434327
2	32	0.048591
2	42	0.033877
2	52	0
2	61	0.001105

Table C.15 Meteorology – Photocatalytic Coated Area Hour 10

monthID	zoneID	hourID	temperature	relHumidity
2	220330	11	15.88268	71.73085

Table C.16 Off Network – Photocatalytic Coated Area Hour 10

sourceTypeID	vehiclePopulation	startFraction	extendedIdleFraction	parkedVehicleFraction
11	0	0	0	1
21	2	0.061	0	1
31	1	0.031	0	1
32	0	0	0	1
42	0	0	0	1
52	0	0	0	1
61	0	0	0	1

Hour 11

Table C.17 Links – Photocatalytic Coated Area Hour 11

linkID	countyID	zoneID	roadTypeID	linkLength	linkVolume	linkAvgSpeed	linkDescription	linkAvgGrade
1	22033	220330	1	0.004	5	0	parking	0
2	22033	220330	5	0.004	120	10	road	0

Table C.18 Links Source – Photocatalytic Coated Area Hour 11

linkID	sourceTypeID	sourceTypeHourFraction
2	11	0.002
2	21	0.570921
2	31	0.356897
2	32	0.039046
2	42	0.029137
2	52	0.002
2	61	0

Table C.19 Meteorology – Photocatalytic Coated Area Hour 11

monthID	zoneID	hourID	temperature	relHumidity
2	220330	12	16.98238	68.64834

Table C.20 Off Network – Photocatalytic Coated Area Hour 11

sourceTypeID	vehiclePopulation	startFraction	extendedIdleFraction	parkedVehicleFraction
11	0	0	0	1
21	3	0.125	0	1
31	2	0.083	0	1
32	0	0	0	1
42	0	0	0	1
52	0	0	0	1
61	0	0	0	1

Hour 12

Table C.21 Links – Photocatalytic Coated Area Hour 12

linkID	countyID	zoneID	roadTypeID	linkLength	linkVolume	linkAvgSpeed	linkDescription	linkAvgGrade
1	22033	220330	1	0.004	5	0	parking	0
2	22033	220330	5	0.004	140	10	road	0

Table C.22 Links Source – Photocatalytic Coated Area Hour 12

linkID	sourceTypeID	sourceTypeHourFraction
2	11	0.00221
2	21	0.512081
2	31	0.441745
2	32	0.03713
2	42	0.002429
2	52	0.002817
2	61	0.001587

Table C.23 Meteorology – Photocatalytic Coated Area Hour 12

monthID	zoneID	hourID	temperature	relHumidity
2	220330	13	18.02015	65.56288

Table C.24 Off Network – Photocatalytic Coated Area Hour 12

sourceTypeID	vehiclePopulation	startFraction	extendedIdleFraction	parkedVehicleFraction
11	0	0	0	1
21	3	0.263	0	1
31	2	0.175	0	1
32	0	0	0	1
42	0	0	0	1
52	0	0	0	1
61	0	0	0	1

Hour 13

Table C.25 Links – Photocatalytic Coated Area Hour 13

linkID	countyID	zoneID	roadTypeID	linkLength	linkVolume	linkAvgSpeed	linkDescription	linkAvgGrade
1	22033	220330	1	0.004	4	0	parking	0
2	22033	220330	5	0.004	150	10	road	0

Table C.26 Links Source – Photocatalytic Coated Area Hour 13

linkID	sourceTypeID	sourceTypeHourFraction
2	11	0
2	21	0.521967
2	31	0.424059
2	32	0.027403
2	42	0.019032
2	52	0.007539
2	61	0

Table C.27 Meteorology – Photocatalytic Coated Area Hour 13

monthID	zoneID	hourID	temperature	relHumidity
2	220330	14	18.68788	63.36908

Table C.28 Off Network – Photocatalytic Coated Area Hour 13

sourceTypeID	vehiclePopulation	startFraction	extendedIdleFraction	parkedVehicleFraction
11	0	0	0	1
21	2	0.167	0	1
31	2	0.167	0	1
32	0	0	0	1
42	0	0	0	1
52	0	0	0	1
61	0	0	0	1

Hour 14

Table C.29 Links – Photocatalytic Coated Area Hour 14

linkID	countyID	zoneID	roadTypeID	linkLength	linkVolume	linkAvgSpeed	linkDescription	linkAvgGrade
1	22033	220330	1	0.004	4	0	parking	0
2	22033	220330	5	0.004	132	10	road	0

Table C.30 Links Source – Photocatalytic Coated Area Hour 14

linkID	sourceTypeID	sourceTypeHourFraction
2	11	0
2	21	0.480824
2	31	0.428387
2	32	0.061662
2	42	0.027624
2	52	0.001504
2	61	0

Table C.31 Meteorology – Photocatalytic Coated Area Hour 14

monthID	zoneID	hourID	temperature	relHumidity
2	220330	15	19.17484	61.52955

Table C.32 Off Network – Photocatalytic Coated Area Hour 14

sourceTypeID	vehiclePopulation	startFraction	extendedIdleFraction	parkedVehicleFraction
11	0	0	0	1
21	2	0.16	0	1
31	2	0.16	0	1
32	0	0	0	1
42	0	0	0	1
52	0	0	0	1
61	0	0	0	1

Hour 15

Table C.33 Links – Photocatalytic Coated Area Hour 15

linkID	countyID	zoneID	roadTypeID	linkLength	linkVolume	linkAvgSpeed	linkDescription	linkAvgGrade
1	22033	220330	1	0.004	6	0	parking	0
2	22033	220330	5	0.004	122	10	road	0

Table C.34 Links Source – Photocatalytic Coated Area Hour 15

linkID	sourceTypeID	sourceTypeHourFraction
2	11	0
2	21	0.549488
2	31	0.363227
2	32	0.051474
2	42	0.029628
2	52	0.004745
2	61	0.001439

Table C.35 Meteorology – Photocatalytic Coated Area Hour 15

monthID	zoneID	hourID	temperature	relHumidity
2	220330	16	19.11867	60.43833

Table C.36 Off Network – Photocatalytic Coated Area Hour 15

sourceTypeID	vehiclePopulation	startFraction	extendedIdleFraction	parkedVehicleFraction
11	0	0	0	1
21	4	0.225	0	1
31	2	0.113	0	1
32	0	0	0	1
42	0	0	0	1
52	0	0	0	1
61	0	0	0	1

Hour 16

Table C.37 Links – Photocatalytic Coated Area Hour 16

linkID	countyID	zoneID	roadTypeID	linkLength	linkVolume	linkAvgSpeed	linkDescription	linkAvgGrade
1	22033	220330	1	0.004	5	0	parking	0
2	22033	220330	5	0.004	93	10	road	0

Table C.38 Links Source – Photocatalytic Coated Area Hour 16

linkID	sourceTypeID	sourceTypeHourFraction
2	11	0.002597
2	21	0.574035
2	31	0.376739
2	32	0.036644
2	42	0.007388
2	52	0.002597
2	61	0

Table C.39 Meteorology – Photocatalytic Coated Area Hour 16

monthID	zoneID	hourID	temperature	relHumidity
2	220330	17	18.31273	62.55926

Table C.40 Off Network – Photocatalytic Coated Area Hour 16

sourceTypeID	vehiclePopulation	startFraction	extendedIdleFraction	parkedVehicleFraction
11	0	0	0	1
21	3	0.435	0	1
31	2	0.29	0	1
32	0	0	0	1
42	0	0	0	1
52	0	0	0	1
61	0	0	0	1

Hour 17

Table C.41 Links – Photocatalytic Coated Area Hour 17

linkID	countyID	zoneID	roadTypeID	linkLength	linkVolume	linkAvgSpeed	linkDescription	linkAvgGrade
1	22033	220330	1	0.004	1	0	parking	0
2	22033	220330	5	0.004	83	10	road	0

Table C.42 Links Source – Photocatalytic Coated Area Hour 17

linkID	sourceTypeID	sourceTypeHourFraction
2	11	0
2	21	0.542172
2	31	0.416691
2	32	0.041137
2	42	0
2	52	0
2	61	0

Table C.43 Meteorology – Photocatalytic Coated Area Hour 17

monthID	zoneID	hourID	temperature	relHumidity
2	220330	18	17.19032	65.32166

Table C.44 Off Network – Photocatalytic Coated Area Hour 17

sourceTypeID	vehiclePopulation	startFraction	extendedIdleFraction	parkedVehicleFraction
11	0	0	0	1
21	1	0.271	0	1
31	0	0	0	1
32	0	0	0	1
42	0	0	0	1
52	0	0	0	1
61	0	0	0	1

MOVES INPUT FILES – CONTROL AREA

Hour 7

Table C.45 Links – Control Area Hour 7

linkID	countyID	zoneID	roadTypeID	linkLength	linkVolume	linkAvgSpeed	linkDescription	linkAvgGrade
1	22033	220330	1	0.004	1	0	parking	0
2	22033	220330	5	0.004	27	10	road	0

Table C.46 Links Source – Control Area Hour 7

linkID	sourceTypeID	sourceTypeHourFraction
2	11	0
2	21	0.501947
2	31	0.377477
2	32	0.098665
2	42	0.021911
2	52	0
2	61	0

Table C.47 Meteorology – Control Area Hour 7

monthID	zoneID	hourID	temperature	relHumidity
2	220330	8	13.01233333	81.822

Table C.48 Off Network – Control Area Hour 7

sourceTypeID	vehiclePopulation	startFraction	extendedIdleFraction	parkedVehicleFraction
11	0	0	0	1
21	1	0.25	0	1
31	0	0	0	1
32	0	0	0	1
42	0	0	0	1
52	0	0	0	1
61	0	0	0	1

Hour 8

Table C.49 Links – Control Area Hour 8

linkID	countyID	zoneID	roadTypeID	linkLength	linkVolume	linkAvgSpeed	linkDescription	linkAvgGrade
1	22033	220330	1	0.004	3	0	parking	0
2	22033	220330	5	0.004	78	10	road	0

Table C.50 Links Source – Control Area Hour 8

linkID	sourceTypeID	sourceTypeHourFraction
2	11	0
2	21	0.445819
2	31	0.39898
2	32	0.098439
2	42	0.047502
2	52	0.00926
2	61	0

Table C.51 Meteorology – Control Area Hour 8

monthID	zoneID	hourID	temperature	relHumidity
2	220330	9	13.71413	79.23667

Table C.52 Off Network – Control Area Hour 8

sourceTypeID	vehiclePopulation	startFraction	extendedIdleFraction	parkedVehicleFraction
11	0	0	0	1
21	2	0.083	0	1
31	1	0.042	0	1
32	0	0	0	1
42	0	0	0	1
52	0	0	0	1
61	0	0	0	1

Hour 9

Table C.53 Links – Control Area Hour 9

linkID	countyID	zoneID	roadTypeID	linkLength	linkVolume	linkAvgSpeed	linkDescription	linkAvgGrade
1	22033	220330	1	0.004	5	0	parking	0
2	22033	220330	5	0.004	94	10	road	0

Table C.54 Links Source – Control Area Hour 9

linkID	sourceTypeID	sourceTypeHourFraction
2	11	0
2	21	0.513495
2	31	0.386364
2	32	0.055904
2	42	0.03672
2	52	0.003977
2	61	0.00354

Table C.55 Meteorology – Control Area Hour 9

monthID	zoneID	hourID	temperature	relHumidity
2	220330	10	14.63456	75.27355

Table C.56 Off Network – Control Area Hour 9

sourceTypeID	vehiclePopulation	startFraction	extendedIdleFraction	parkedVehicleFraction
11	0	0	0	1
21	3	0.205	0	1
31	2	0.137	0	1
32	0	0	0	1
42	0	0	0	1
52	0	0	0	1
61	0	0	0	1

Hour 10

Table C.57 Links – Control Area Hour 10

linkID	countyID	zoneID	roadTypeID	linkLength	linkVolume	linkAvgSpeed	linkDescription	linkAvgGrade
1	22033	220330	1	0.004	5	0	parking	0
2	22033	220330	5	0.004	127	10	road	0

Table C.58 Links Source – Control Area Hour 10

linkID	sourceTypeID	sourceTypeHourFraction
2	11	0
2	21	0.483551
2	31	0.438585
2	32	0.042064
2	42	0.035801
2	52	0
2	61	0

Table C.59 Meteorology – Control Area Hour 10

monthID	zoneID	hourID	temperature	relHumidity
2	220330	11	15.88268	71.73085

Table C.60 Off Network – Control Area Hour 10

sourceTypeID	vehiclePopulation	startFraction	extendedIdleFraction	parkedVehicleFraction
11	0	0	0	1
21	3	0.093	0	1
31	2	0.062	0	1
32	0	0	0	1
42	0	0	0	1
52	0	0	0	1
61	0	0	0	1

Hour 11

Table C.61 Links – Control Area Hour 11

linkID	countyID	zoneID	roadTypeID	linkLength	linkVolume	linkAvgSpeed	linkDescription	linkAvgGrade
1	22033	220330	1	0.004	5	0	parking	0
2	22033	220330	5	0.004	117	10	road	0

Table C.62 Links Source – Control Area Hour 11

linkID	sourceTypeID	sourceTypeHourFraction
2	11	0.002062
2	21	0.565776
2	31	0.361004
2	32	0.041052
2	42	0.030106
2	52	0
2	61	0

Table C.63 Meteorology – Control Area Hour 11

monthID	zoneID	hourID	temperature	relHumidity
2	220330	12	16.98238	68.64834

Table C.64 Off Network – Control Area Hour 11

sourceTypeID	vehiclePopulation	startFraction	extendedIdleFraction	parkedVehicleFraction
11	0	0	0	1
21	3	0.089	0	1
31	2	0.059	0	1
32	0	0	0	1
42	0	0	0	1
52	0	0	0	1
61	0	0	0	1

Hour 12

Table C.65 Links – Control Area Hour 12

linkID	countyID	zoneID	roadTypeID	linkLength	linkVolume	linkAvgSpeed	linkDescription	linkAvgGrade
1	22033	220330	1	0.004	5	0	parking	0
2	22033	220330	5	0.004	137	10	road	0

Table C.66 Links Source – Control Area Hour 12

linkID	sourceTypeID	sourceTypeHourFraction
2	11	0.002222
2	21	0.500692
2	31	0.447618
2	32	0.039453
2	42	0.003556
2	52	0.004765
2	61	0.001695

Table C.67 Meteorology – Control Area Hour 12

monthID	zoneID	hourID	temperature	relHumidity
2	220330	13	18.02015	65.56288

Table C.68 Off Network – Control Area Hour 12

sourceTypeID	vehiclePopulation	startFraction	extendedIdleFraction	parkedVehicleFraction
11	0	0	0	1
21	3	0.16	0	1
31	2	0.107	0	1
32	0	0	0	1
42	0	0	0	1
52	0	0	0	1
61	0	0	0	1

Hour 13

Table C.69 Links – Control Area Hour 13

linkID	countyID	zoneID	roadTypeID	linkLength	linkVolume	linkAvgSpeed	linkDescription	linkAvgGrade
1	22033	220330	1	0.004	5	0	parking	0
2	22033	220330	5	0.004	143	10	road	0

Table C.70 Links Source – Control Area Hour 13

linkID	sourceTypeID	sourceTypeHourFraction
2	11	0
2	21	0.52705
2	31	0.424344
2	32	0.022181
2	42	0.019836
2	52	0.005291
2	61	0.001299

Table C.71 Meteorology – Control Area Hour 13

monthID	zoneID	hourID	temperature	relHumidity
2	220330	14	18.68788	63.36908

Table C.72 Off Network – Control Area Hour 13

sourceTypeID	vehiclePopulation	startFraction	extendedIdleFraction	parkedVehicleFraction
11	0	0	0	1
21	3	0.121	0	1
31	2	0.081	0	1
32	0	0	0	1
42	0	0	0	1
52	0	0	0	1
61	0	0	0	1

Hour 14

Table C.73 Links – Control Area Hour 14

linkID	countyID	zoneID	roadTypeID	linkLength	linkVolume	linkAvgSpeed	linkDescription	linkAvgGrade
1	22033	220330	1	0.004	4	0	parking	0
2	22033	220330	5	0.004	130	10	road	0

Table C.74 Links Source – Control Area Hour 14

linkID	sourceTypeID	sourceTypeHourFraction
2	11	0
2	21	0.471665
2	31	0.424746
2	32	0.070986
2	42	0.031089
2	52	0.001515
2	61	0

Table C.75 Meteorology – Control Area Hour 14

monthID	zoneID	hourID	temperature	relHumidity
2	220330	15	19.17484	61.52955

Table C.76 Off Network – Control Area Hour 14

sourceTypeID	vehiclePopulation	startFraction	extendedIdleFraction	parkedVehicleFraction
11	0	0	0	1
21	2	0.1	0	1
31	2	0.1	0	1
32	0	0	0	1
42	0	0	0	1
52	0	0	0	1
61	0	0	0	1

Hour 15

Table C.77 Links – Control Area Hour 15

linkID	countyID	zoneID	roadTypeID	linkLength	linkVolume	linkAvgSpeed	linkDescription	linkAvgGrade
1	22033	220330	1	0.004	4	0	parking	0
2	22033	220330	5	0.004	122	10	road	0

Table C.78 Links Source – Control Area Hour 15

linkID	sourceTypeID	sourceTypeHourFraction
2	11	0
2	21	0.553368
2	31	0.358295
2	32	0.053699
2	42	0.030114
2	52	0.003095
2	61	0.001429

Table C.79 Meteorology – Control Area Hour 15

monthID	zoneID	hourID	temperature	relHumidity
2	220330	16	19.11867	60.43833

Table C.80 Off Network – Control Area Hour 15

sourceTypeID	vehiclePopulation	startFraction	extendedIdleFraction	parkedVehicleFraction
11	0	0	0	1
21	2	0.15	0	1
31	2	0.15	0	1
32	0	0	0	1
42	0	0	0	1
52	0	0	0	1
61	0	0	0	1

Hour 16

Table C.81 Links – Control Area Hour 16

linkID	countyID	zoneID	roadTypeID	linkLength	linkVolume	linkAvgSpeed	linkDescription	linkAvgGrade
1	22033	220330	1	0.004	3	0	parking	0
2	22033	220330	5	0.004	91	10	road	0

Table C.82 Links Source – Control Area Hour 16

linkID	sourceTypeID	sourceTypeHourFraction
2	11	0.00274
2	21	0.565993
2	31	0.386917
2	32	0.029459
2	42	0.009412
2	52	0.005479
2	61	0

Table C.83 Meteorology – Control Area Hour 16

monthID	zoneID	hourID	temperature	relHumidity
2	220330	17	18.31273	62.55926

Table C.84 Off Network – Control Area Hour 16

sourceTypeID	vehiclePopulation	startFraction	extendedIdleFraction	parkedVehicleFraction
11	0	0	0	1
21	2	0.222	0	1
31	1	0.111	0	1
32	0	0	0	1
42	0	0	0	1
52	0	0	0	1
61	0	0	0	1

Hour 17

Table C.85 Links – Control Area Hour 17

linkID	countyID	zoneID	roadTypeID	linkLength	linkVolume	linkAvgSpeed	linkDescription	linkAvgGrade
1	22033	220330	1	0.004	2	0	parking	0
2	22033	220330	5	0.004	81	10	road	0

Table C.86 Links Source – Control Area Hour 17

linkID	sourceTypeID	sourceTypeHourFraction
2	11	0
2	21	0.546845
2	31	0.419209
2	32	0.033947
2	42	0
2	52	0
2	61	0

Table C.87 Meteorology – Control Area Hour 17

monthID	zoneID	hourID	temperature	relHumidity
2	220330	18	17.19032	65.32166

Table C.88 Off Network – Control Area Hour 17

sourceTypeID	vehiclePopulation	startFraction	extendedIdleFraction	parkedVehicleFraction
11	0	0	0	1
21	1	0.313	0	1
31	1	0.313	0	1
32	0	0	0	1
42	0	0	0	1
52	0	0	0	1
61	0	0	0	1

APPENDIX D
CHAPTER 5 CALCULATIONS

SAS INPUTS

Langmuir-Hinshelwood Reaction Rate Constant Linear Regression SAS Code

```
data one;
input   time x1-x2 y ;
x3=x1*x2;
label x1 ='Humidity'
      x2 ='Intensity'
       x3='HI'
      y='k';
cards;
1    27   0.52 1.20
2    40   0.52 0.94
3    51   0.52 0.81
4    72   0.52 0.51
5    81   0.52 0.38
6    27   1.3  1.82
7    40   1.3  1.45
8    51   1.3  1.08
9    72   1.3  0.87
10   81   1.3  0.50
11   27   2.1  1.98
12   40   2.1  1.71
13   51   2.1  1.21
14   72   2.1  1.12
15   81   2.1  0.69
16   27   2.7  2.00
17   40   2.7  1.55
18   51   2.7  1.58
19   72   2.7  1.18
20   81   2.7  0.66
21   27   3.52 3.39
22   40   3.52 1.70
23   51   3.52 1.97
24   72   3.52 1.23
25   81   3.52 0.73
;
ods rtf;

/*Pairwise correlation coefficients*/proc corr data=one; var y
x1-x3;
run;
```

```
/*VIF, Type I & II SS*/proc reg data=one;
model y=x1-x3/ vif ss1 ss2;
run;

proc reg data=one;
model y=x1-x3/ selection=stepwise details SLENTRY=0.15
SLSTAY=0.05;
run;

ods rtf close;
```

Langmuir-Hinshelwood Adsorption Equilibrium Constant Linear Regression SAS Code

```
data one;
input   time x1-x2 y ;
x3=x1*x2;
label x1 ='Humidity'
      x2 ='Intensity'
       x3='HI'
      y='Kd';
cards;
1    27   0.52 0.90
2    40   0.52 1.16
3    51   0.52 1.20
4    72   0.52 1.40
5    81   0.52 1.67
6    27   1.3  0.56
7    40   1.3  0.67
8    51   1.3  0.89
9    72   1.3  0.92
10   81   1.3  1.49
11   27   2.1  0.60
12   40   2.1  0.60
13   51   2.1  0.94
14   72   2.1  0.95
15   81   2.1  0.97
16   27   2.7  0.52
17   40   2.7  0.68
18   51   2.7  0.64
19   72   2.7  0.77
20   81   2.7  1.19
21   27   3.52 0.53
22   40   3.52 0.69
23   51   3.52 0.66
24   72   3.52 0.82
25   81   3.52 1.06;
```

```
ods rtf;

/*Pairwise correlation coefficients*/proc corr data=one; var y
x1-x3;
run;

/*VIF, Type I & II SS*/proc reg data=one;
model y=x1-x3/ vif ss1 ss2;
run;

proc reg data=one;
model y=x1-x3/ selection=stepwise details SLENTRY=0.15
SLSTAY=0.05;
run;

ods rtf close;
```

SAS OUTPUTS

Langmuir-Hinshelwood Reaction Rate Constant Linear Regression SAS Results

The SAS System

The CORR Procedure

4 Variables:	y x1 x2 x3

Simple Statistics

Variable	N	Mean	Std Dev	Sum	Minimum	Maximum	Label
y	25	1.29040	0.65888	32.26000	0.38000	3.39000	k
x1	25	54.20000	20.34494	1355	27.00000	81.00000	Humidity
x2	25	2.02800	1.06916	50.70000	0.52000	3.52000	Intensity
x3	25	109.91760	74.26027	2748	14.04000	285.12000	HI

Pearson Correlation Coefficients, N = 25
Prob > |r| under H0: Rho=0

	y	x1	x2	x3
y k	1.00000	-0.75076 <.0001	0.51281 0.0088	-0.08193 0.6970
x1 Humidity	-0.75076 <.0001	1.00000	0.00000 1.0000	0.55561 0.0039
x2 Intensity	0.51281 0.0088	0.00000 1.0000	1.00000	0.78034 <.0001
x3 HI	-0.08193 0.6970	0.55561 0.0039	0.78034 <.0001	1.00000

The SAS System

The REG Procedure
Model: MODEL1
Dependent Variable: y k

Number of Observations Read	25
Number of Observations Used	25

Analysis of Variance					
Source	**DF**	**Sum of Squares**	**Mean Square**	**F Value**	**Pr > F**
Model	3	9.14642	3.04881	50.32	<.0001
Error	21	1.27248	0.06059		
Corrected Total	24	10.41890			

Root MSE	0.24616	**R-Square**	0.8779
Dependent Mean	1.29040	**Adj R-Sq**	0.8604
Coeff Var	19.07619		

Parameter Estimates									
Variable	**Label**	**DF**	**Parameter Estimate**	**Standard Error**	**t Value**	**Pr > |t|**	**Type I SS**	**Type II SS**	**Variance Inflation**
Intercept	Intercept	1	1.19801	0.31078	3.85	0.0009	41.62830	0.90044	0
x1	Humidity	1	-0.01012	0.00538	-1.88	0.0740	5.87253	0.21429	4.74783
x2	Intensity	1	0.69536	0.13615	5.11	<.0001	2.73990	1.58053	8.39289
x3	HI	1	-0.00700	0.00236	-2.97	0.0073	0.53399	0.53399	12.14073

The SAS System

The REG Procedure
Model: MODEL1
Dependent Variable: y k

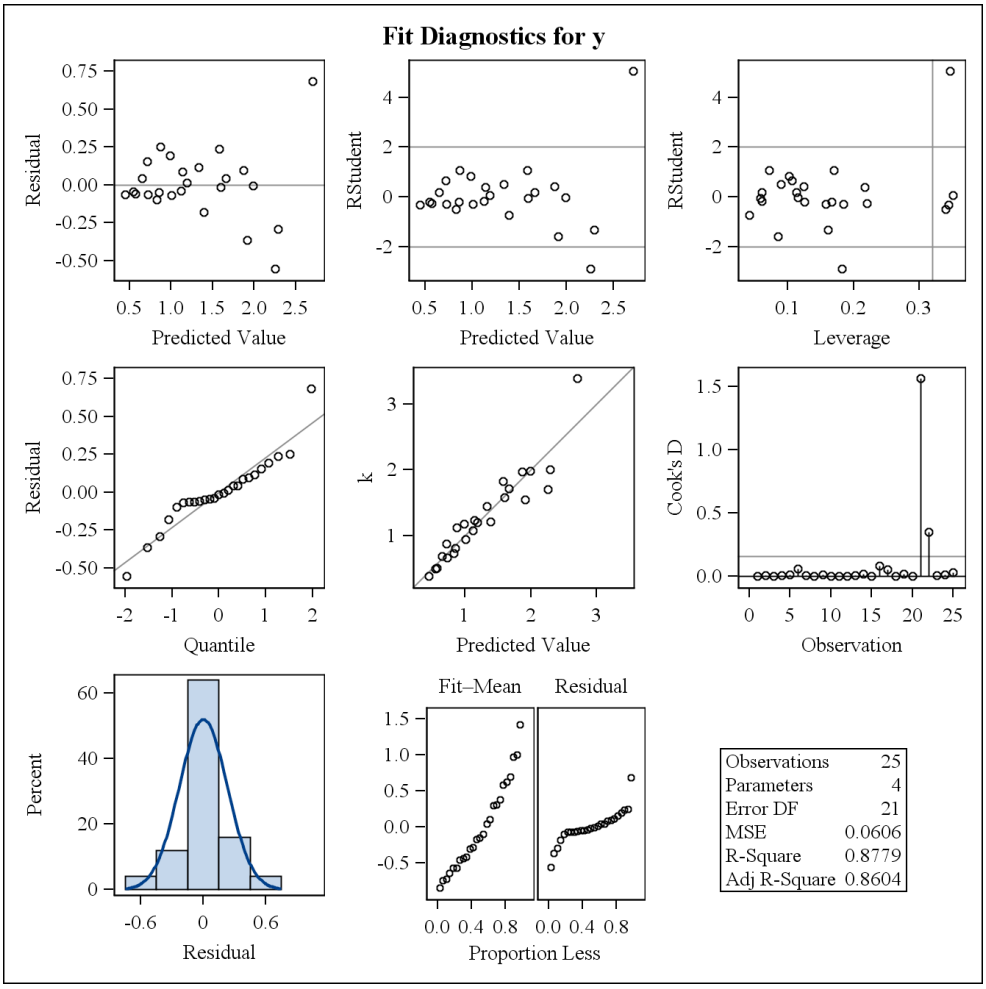

The SAS System

The REG Procedure
Model: MODEL1
Dependent Variable: y k

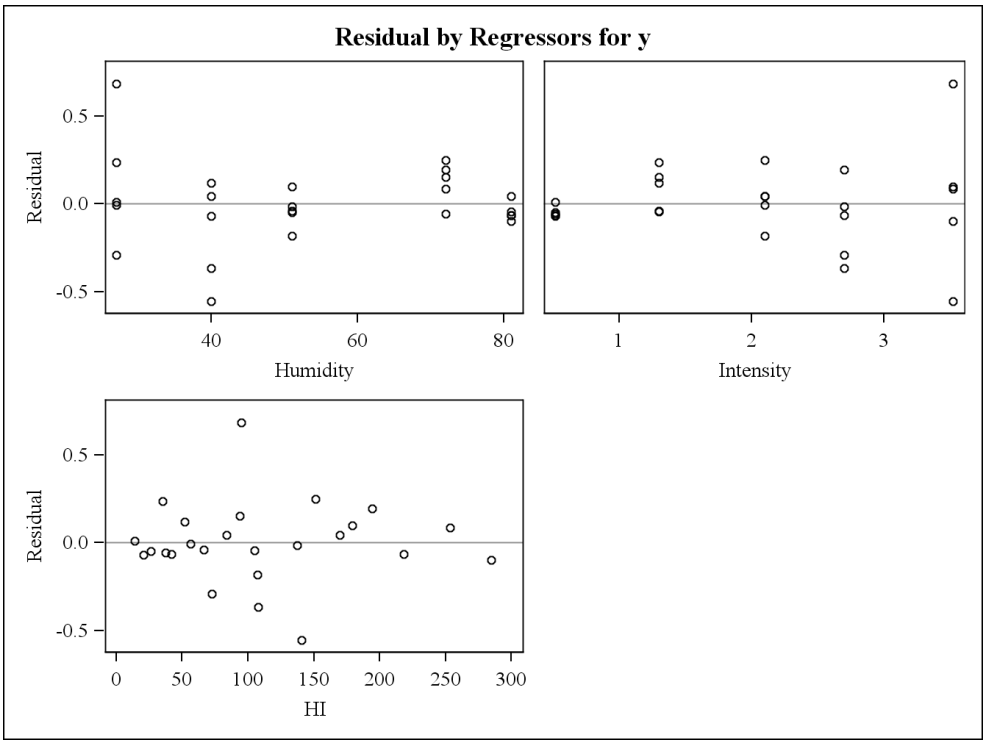

The SAS System

The REG Procedure
Model: MODEL1
Dependent Variable: y k

Number of Observations Read	25
Number of Observations Used	25

Stepwise Selection: Step 1

Statistics for Entry DF = 1,23				
Variable	**Tolerance**	**Model R-Square**	**F Value**	**Pr > F**
x1	1.000000	0.5636	29.71	<.0001
x2	1.000000	0.2630	8.21	0.0088
x3	1.000000	0.0067	0.16	0.6970

Variable x1 Entered: R-Square = 0.5636 and C(p) = 54.0296

Analysis of Variance					
Source	**DF**	**Sum of Squares**	**Mean Square**	**F Value**	**Pr > F**
Model	1	5.87253	5.87253	29.71	<.0001
Error	23	4.54637	0.19767		
Corrected Total	24	10.41890			

Variable	**Parameter Estimate**	**Standard Error**	**Type II SS**	**F Value**	**Pr > F**
Intercept	2.60820	0.25760	20.26331	102.51	<.0001
x1	-0.02431	0.00446	5.87253	29.71	<.0001

Bounds on condition number: 1, 1

The SAS System

The REG Procedure
Model: MODEL1
Dependent Variable: y k

Stepwise Selection: Step 1

Stepwise Selection: Step 2

Statistics for Entry DF = 1,22				
Variable	**Tolerance**	**Model R-Square**	**F Value**	**Pr > F**
x2	1.000000	0.8266	33.37	<.0001
x3	0.691301	0.7262	13.06	0.0015

Variable x2 Entered: R-Square = 0.8266 and C(p) = 10.8125

Analysis of Variance					
Source	**DF**	**Sum of Squares**	**Mean Square**	**F Value**	**Pr > F**
Model	2	8.61243	4.30621	52.44	<.0001
Error	22	1.80647	0.08211		
Corrected Total	24	10.41890			

Variable	**Parameter Estimate**	**Standard Error**	**Type II SS**	**F Value**	**Pr > F**
Intercept	1.96730	0.19969	7.96964	97.06	<.0001
x1	-0.02431	0.00288	5.87253	71.52	<.0001
x2	0.31602	0.05471	2.73990	33.37	<.0001

Bounds on condition number: 1, 4

Stepwise Selection: Step 3

The SAS System

The REG Procedure
Model: MODEL1
Dependent Variable: y k

Stepwise Selection: Step 3

Statistics for Removal DF = 1,22				
Variable	**Partial R-Square**	**Model R-Square**	**F Value**	**Pr > F**
x1	0.5636	0.2630	71.52	<.0001
x2	0.2630	0.5636	33.37	<.0001

Statistics for Entry DF = 1,21				
Variable	**Tolerance**	**Model R-Square**	**F Value**	**Pr > F**
x3	0.082367	0.8779	8.81	0.0073

Variable x3 Entered: R-Square = 0.8779 and C(p) = 4.0000

Analysis of Variance					
Source	**DF**	**Sum of Squares**	**Mean Square**	**F Value**	**Pr > F**
Model	3	9.14642	3.04881	50.32	<.0001
Error	21	1.27248	0.06059		
Corrected Total	24	10.41890			

Variable	**Parameter Estimate**	**Standard Error**	**Type II SS**	**F Value**	**Pr > F**
Intercept	1.19801	0.31078	0.90044	14.86	0.0009
x1	-0.01012	0.00538	0.21429	3.54	0.0740
x2	0.69536	0.13615	1.58053	26.08	<.0001
x3	-0.00700	0.00236	0.53399	8.81	0.0073

Bounds on condition number: 12.141, 75.844

The SAS System

The REG Procedure
Model: MODEL1
Dependent Variable: y k

Stepwise Selection: Step 3

Stepwise Selection: Step 4

Statistics for Removal DF = 1,21				
Variable	**Partial R-Square**	**Model R-Square**	**F Value**	**Pr > F**
x1	0.0206	0.8573	3.54	0.0740
x2	0.1517	0.7262	26.08	<.0001
x3	0.0513	0.8266	8.81	0.0073

Variable x1 Removed: R-Square = 0.8573 and C(p) = 5.5364

Analysis of Variance					
Source	**DF**	**Sum of Squares**	**Mean Square**	**F Value**	**Pr > F**
Model	2	8.93213	4.46606	66.09	<.0001
Error	22	1.48677	0.06758		
Corrected Total	24	10.41890			

Variable	**Parameter Estimate**	**Standard Error**	**Type II SS**	**F Value**	**Pr > F**
Intercept	0.64950	0.11329	2.22130	32.87	<.0001
x2	0.90886	0.07937	8.86219	131.14	<.0001
x3	-0.01094	0.00114	6.19223	91.63	<.0001

Bounds on condition number: 2.5571, 10.228

The SAS System

The REG Procedure
Model: MODEL1
Dependent Variable: y k

Stepwise Selection: Step 4

Stepwise Selection: Step 5

Statistics for Removal DF = 1,22				
Variable	**Partial R-Square**	**Model R-Square**	**F Value**	**Pr > F**
x2	0.8506	0.0067	131.14	<.0001
x3	0.5943	0.2630	91.63	<.0001

Statistics for Entry DF = 1,21				
Variable	**Tolerance**	**Model R-Square**	**F Value**	**Pr > F**
x1	0.210622	0.8779	3.54	0.0740

All variables left in the model are significant at the 0.0500 level.

The stepwise method terminated because the next variable to be entered was just removed.

Summary of Stepwise Selection									
Step	**Variable Entered**	**Variable Removed**	**Label**	**Number Vars In**	**Partial R-Square**	**Model R-Square**	**C(p)**	**F Value**	**Pr > F**
1	x1		Humidity	1	0.5636	0.5636	54.0296	29.71	<.0001
2	x2		Intensity	2	0.2630	0.8266	10.8125	33.37	<.0001
3	x3		HI	3	0.0513	0.8779	4.0000	8.81	0.0073
4		x1	Humidity	2	0.0206	0.8573	5.5364	3.54	0.0740

The SAS System

The REG Procedure
Model: MODEL1
Dependent Variable: y k

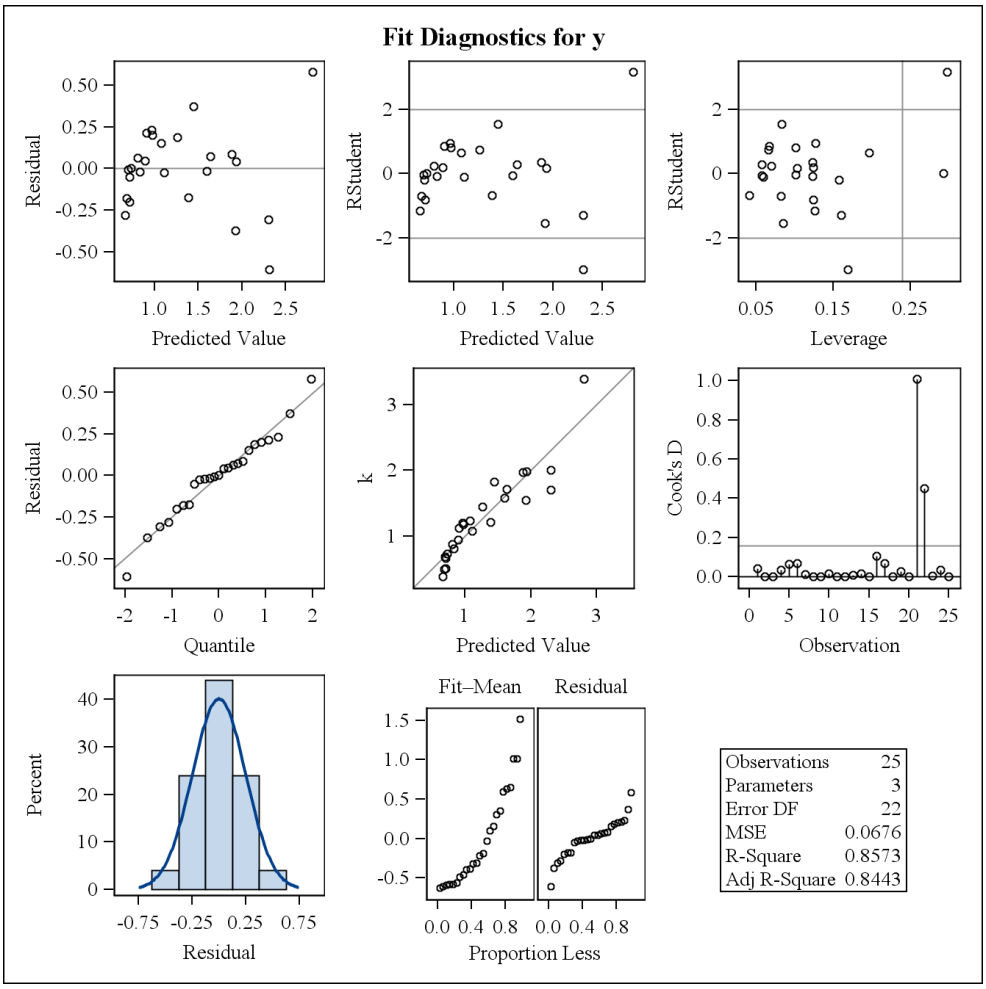

The SAS System

The REG Procedure
Model: MODEL1
Dependent Variable: y k

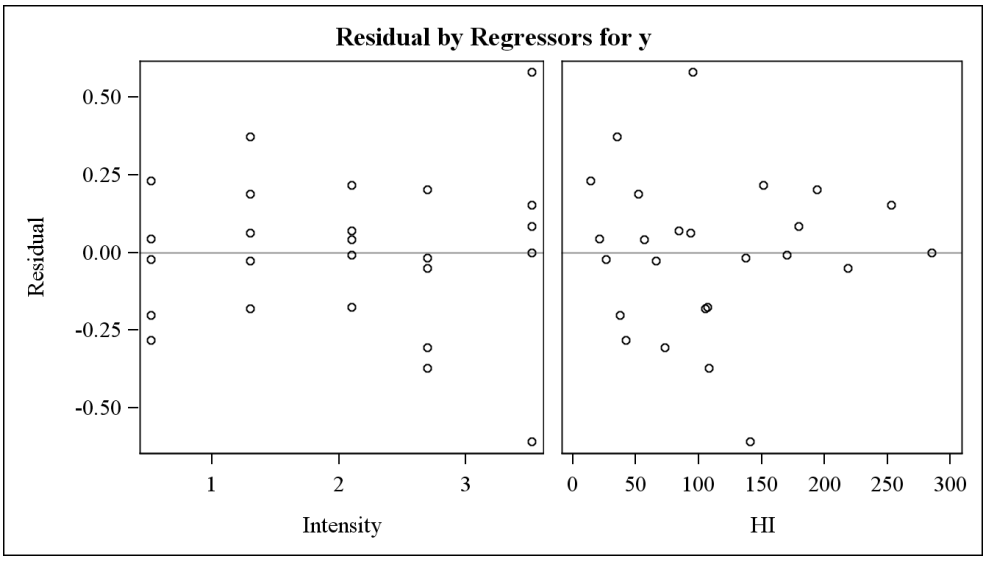

Langmuir-Hinshelwood Adsorption Equilibrium Constant Linear Regression SAS Results

The SAS System

The CORR Procedure

4 Variables:	y x1 x2 x3

Simple Statistics							
Variable	**N**	**Mean**	**Std Dev**	**Sum**	**Minimum**	**Maximum**	**Label**
y	25	0.89920	0.31216	22.48000	0.52000	1.67000	Kd
x1	25	54.20000	20.34494	1355	27.00000	81.00000	Humidity
x2	25	2.02800	1.06916	50.70000	0.52000	3.52000	Intensity
x3	25	109.91760	74.26027	2748	14.04000	285.12000	HI

Pearson Correlation Coefficients, N = 25 Prob > |r| under H0: Rho=0				
	y	**x1**	**x2**	**x3**
y Kd	1.00000	0.68944 0.0001	-0.54778 0.0046	-0.07889 0.7078
x1 Humidity	0.68944 0.0001	1.00000	0.00000 1.0000	0.55561 0.0039
x2 Intensity	-0.54778 0.0046	0.00000 1.0000	1.00000	0.78034 <.0001
x3 HI	-0.07889 0.7078	0.55561 0.0039	0.78034 <.0001	1.00000

The SAS System

The REG Procedure
Model: MODEL1
Dependent Variable: y Kd

Number of Observations Read	25
Number of Observations Used	25

Analysis of Variance					
Source	**DF**	**Sum of Squares**	**Mean Square**	**F Value**	**Pr > F**
Model	3	1.84710	0.61570	26.31	<.0001
Error	21	0.49148	0.02340		
Corrected Total	24	2.33858			

Root MSE	0.15298	**R-Square**	0.7898
Dependent Mean	0.89920	**Adj R-Sq**	0.7598
Coeff Var	17.01325		

Parameter Estimates									
Variable	**Label**	**DF**	**Parameter Estimate**	**Standard Error**	**t Value**	**Pr > |t|**	**Type I SS**	**Type II SS**	**Variance Inflation**
Intercept	Intercept	1	0.45672	0.19314	2.36	0.0278	20.21402	0.13087	0
x1	Humidity	1	0.01415	0.00334	4.23	0.0004	1.11160	0.41881	4.74783
x2	Intensity	1	-0.06453	0.08462	-0.76	0.4542	0.70172	0.01361	8.39289
x3	HI	1	-0.00176	0.00147	-1.20	0.2430	0.03378	0.03378	12.14073

The REG Procedure
Model: MODEL1
Dependent Variable: y Kd

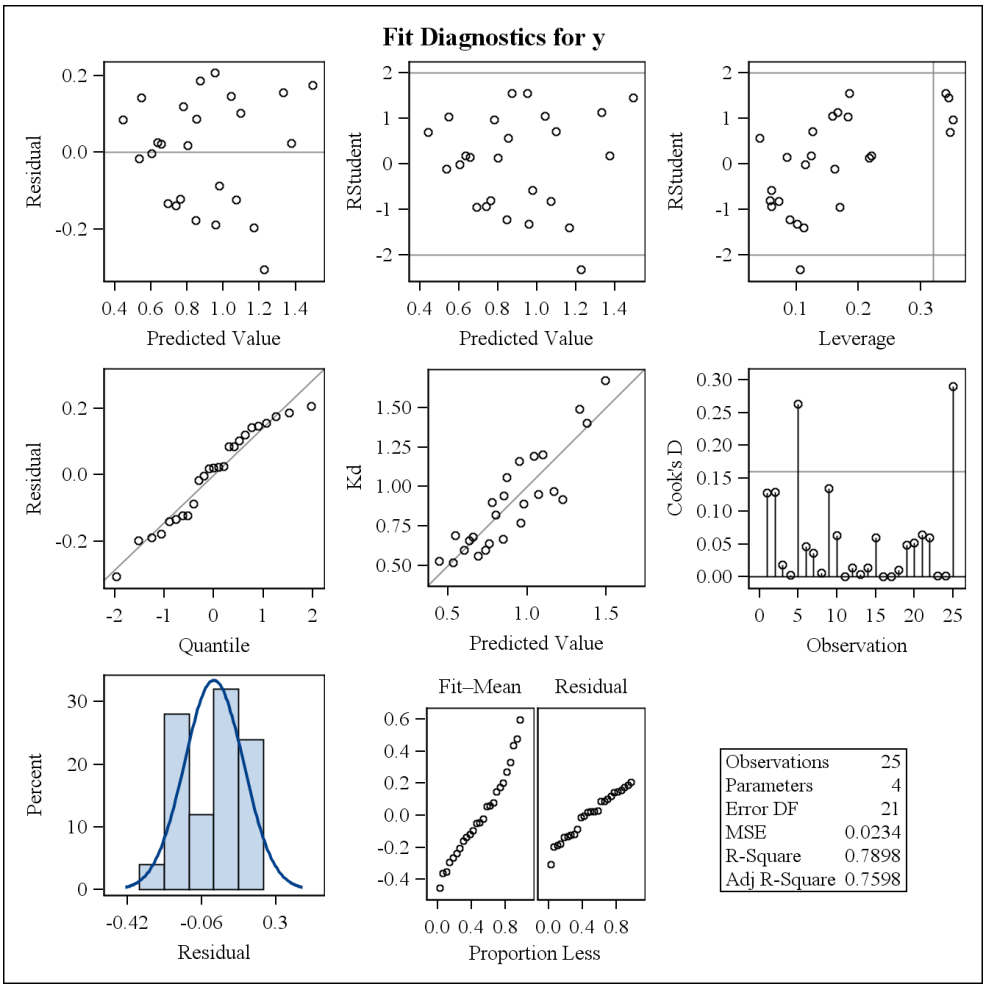

The REG Procedure
Model: MODEL1
Dependent Variable: y Kd

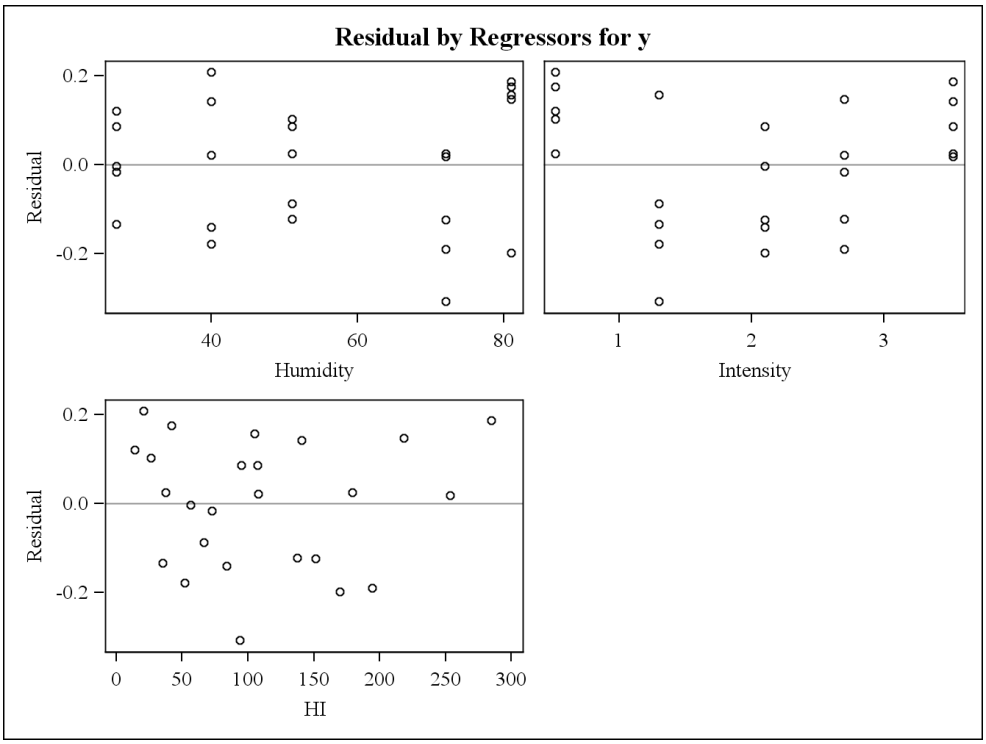

The SAS System

The REG Procedure
Model: MODEL1
Dependent Variable: y Kd

Number of Observations Read	25
Number of Observations Used	25

Stepwise Selection: Step 1

Statistics for Entry DF = 1,23				
Variable	**Tolerance**	**Model R-Square**	**F Value**	**Pr > F**
x1	1.000000	0.4753	20.84	0.0001
x2	1.000000	0.3001	9.86	0.0046
x3	1.000000	0.0062	0.14	0.7078

Variable x1 Entered: R-Square = 0.4753 and C(p) = 31.4265

Analysis of Variance					
Source	**DF**	**Sum of Squares**	**Mean Square**	**F Value**	**Pr > F**
Model	1	1.11160	1.11160	20.84	0.0001
Error	23	1.22698	0.05335		
Corrected Total	24	2.33858			

Variable	**Parameter Estimate**	**Standard Error**	**Type II SS**	**F Value**	**Pr > F**
Intercept	0.32586	0.13383	0.31629	5.93	0.0231
x1	0.01058	0.00232	1.11160	20.84	0.0001

Bounds on condition number: 1, 1

The SAS System

The REG Procedure
Model: MODEL1
Dependent Variable: y Kd

Stepwise Selection: Step 1

Stepwise Selection: Step 2

Statistics for Entry DF = 1,22				
Variable	**Tolerance**	**Model R-Square**	**F Value**	**Pr > F**
x2	1.000000	0.7754	29.39	<.0001
x3	0.691301	0.7840	31.44	<.0001

Variable x3 Entered: R-Square = 0.7840 and C(p) = 2.5815

Analysis of Variance					
Source	**DF**	**Sum of Squares**	**Mean Square**	**F Value**	**Pr > F**
Model	2	1.83349	0.91675	39.93	<.0001
Error	22	0.50509	0.02296		
Corrected Total	24	2.33858			

Variable	**Parameter Estimate**	**Standard Error**	**Type II SS**	**F Value**	**Pr > F**
Intercept	0.32586	0.08779	0.31629	13.78	0.0012
x1	0.01627	0.00183	1.81894	79.23	<.0001
x3	-0.00281	0.00050093	0.72189	31.44	<.0001

Bounds on condition number: 1.4465, 5.7862

Stepwise Selection: Step 3

The SAS System

The REG Procedure
Model: MODEL1
Dependent Variable: y Kd

Stepwise Selection: Step 3

Statistics for Removal DF = 1,22				
Variable	Partial R-Square	Model R-Square	F Value	Pr > F
x1	0.7778	0.0062	79.23	<.0001
x3	0.3087	0.4753	31.44	<.0001

Statistics for Entry DF = 1,21				
Variable	Tolerance	Model R-Square	F Value	Pr > F
x2	0.119148	0.7898	0.58	0.4542

All variables left in the model are significant at the 0.0500 level.

No other variable met the 0.1500 significance level for entry into the model.

Summary of Stepwise Selection									
Step	Variable Entered	Variable Removed	Label	Number Vars In	Partial R-Square	Model R-Square	C(p)	F Value	Pr > F
1	x1		Humidity	1	0.4753	0.4753	31.4265	20.84	0.0001
2	x3		HI	2	0.3087	0.7840	2.5815	31.44	<.0001

The SAS System

The REG Procedure
Model: MODEL1
Dependent Variable: y Kd

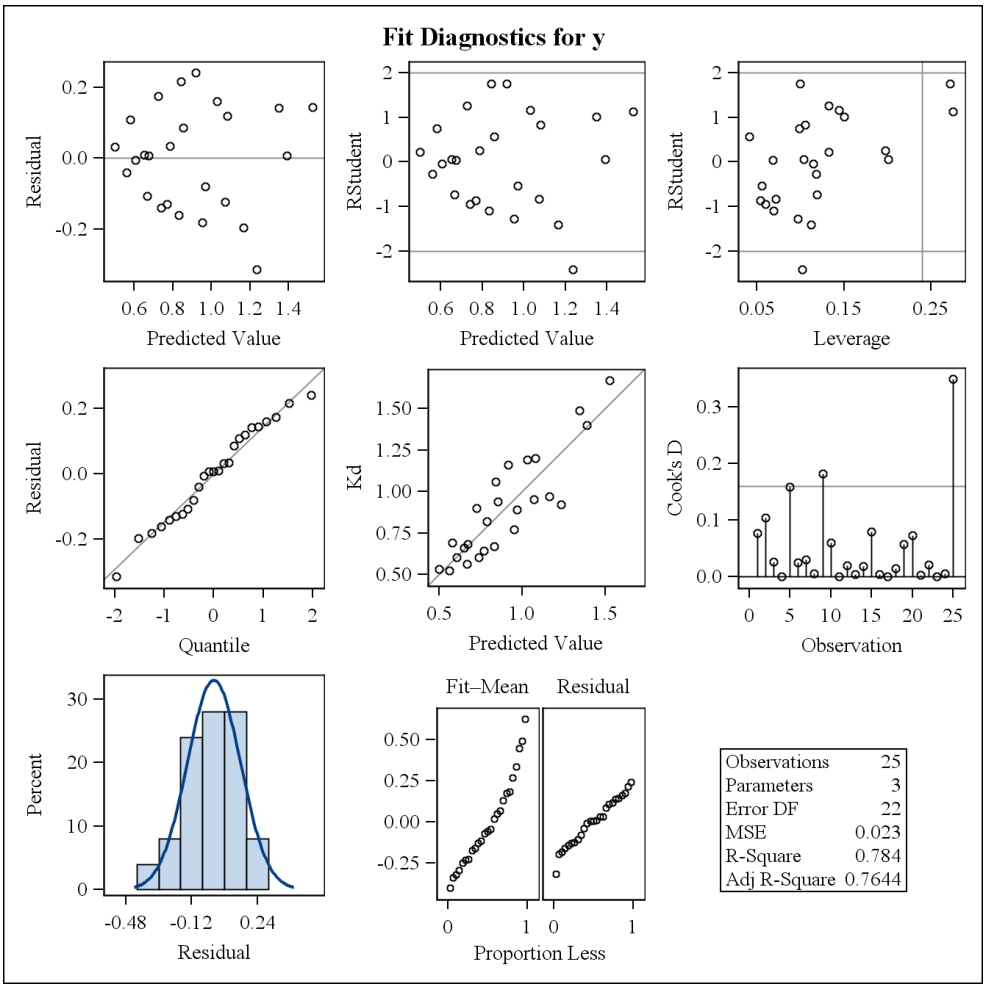

The SAS System

The REG Procedure
Model: MODEL1
Dependent Variable: y Kd

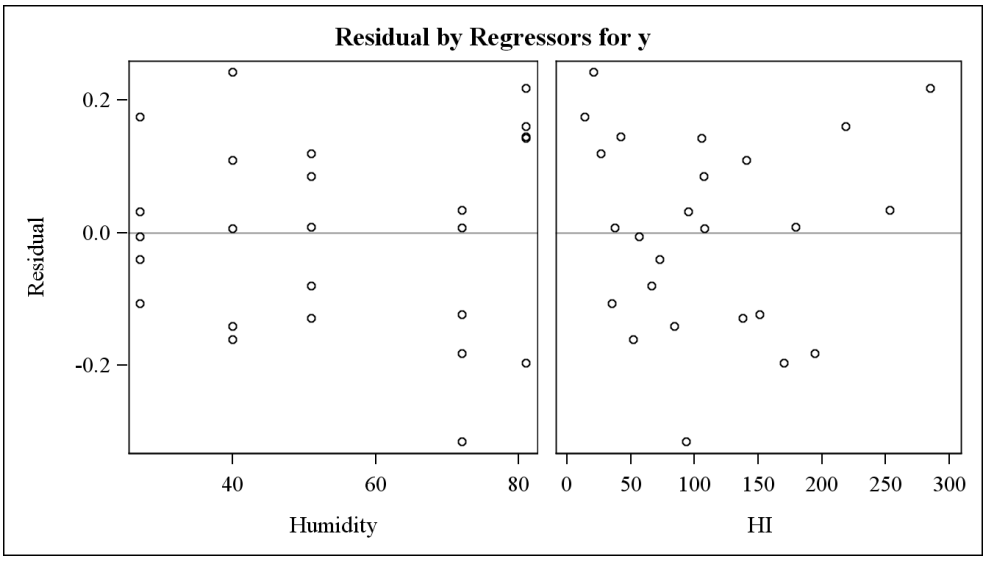

APPENDIX E
CHAPTER 6 CALCULATIONS

MASS TRANSFER MECHANISMS FOR BOX MODEL

$$uhlC_{NO}^{in} - r_{NO-Ozone}whl - r_{NO}whl - wlk_{NO}C_{NO}^{out} - uhlC_{NO}^{out} = 0$$

$$1 - 2 - 3 - 4 - 5 = 0$$

Where,
1. Convection (in)
2. NO-Ozone reaction (out)
3. Photocatalytic degradation (out)
4. Diffusion (out)
5. Convection (out)

1. Estimate Convection In Mass Transfer

$$\boldsymbol{uhlC_{NO}^{in} = 3911\ \mu g/s}$$

Table E.1 Convection In Mass Transfer Calculation Inputs

Variable	Symbol	Units	Value
Air Velocity	*u*	m/s	3.5
Height	*h*	m	8
Length	l	m	3.6
Concentration of NO	[NO]	µg/m^3	38

2. Estimate NO-Ozone Reaction Mass Transfer

$$r_{NO-Ozone}whl = 47.27\ \mu g/s$$

$$r_{\mathrm{NO-Ozone}} = k[NO][O_3] = 0.456\ \mu g/m^3 s$$

$$k = 1.4x10^{-18}e^{\frac{-1310}{T}} = 1.8x10^{-20}\ \mathrm{m^3\ molecule^{-1}\ sec^{-1}}$$

Table E.2 NO-Ozone Reaction Mass Transfer Calculation Inputs

Variable	Symbol	Units	Value
Temperature	T	K	300
Rate Coefficient for NO-O_3 Reaction	k	m^3 $molecule^{-1}$ sec^{-1}	$1.8x10^{-20}$
Concentration of NO	[NO]	$\mu g/m^3$	38
Concentration of O_3	[O_3]	$\mu g/m^3$	52.9
Width	w	m	3.6
Length	l	m	3.6

3. Estimate Photocatalytic Reaction Mass Transfer

$$r_{NO}whl = 61.7\ \mu g/s$$

$$\mathrm{Kd(H,I)} = (0.01415 * \mathrm{H} - 0.00176 * \mathrm{H} * \mathrm{I} + 0.45672)^2 = 0.00144\ m^3/\mu g$$

$$\mathrm{k\ (H,I)} = (-0.007 * \mathrm{H} * \mathrm{I} + 0.69536 * \mathrm{I} + 1.19801)^2 = 11.1\ \mu g/m^3 s$$

$$\mathrm{r_{NO}} = \frac{\mathrm{kKdC_{NO}}}{1 + \mathrm{KdC_{NO}}} = 0.57\ \mu g/m^3 s$$

Table E.3 Photocatalytic Reaction Mass Transfer Calculation Inputs

Variable	Symbol	Units	Value
Irradiance	I	mW/cm^2	0.56
Humidity	H	%	70
Concentration of NO	[NO]	$\mu g/m^3$	38
Width	w	m	3.6
Length	l	m	3.6
Height	h	m	8

4. Estimate Diffusion Mass Transfer Coefficient

$$k_{NO} = \frac{1}{R_a + R_b} = 0.0156\ m/s$$

$$R_a = \frac{(\ln(z-d)/z_0)^2}{\kappa^2 u} = 46.3\ m/s$$

$$R_b = \frac{2(\ln(z-d)/z_0)}{\kappa^2 u}\left(\frac{\nu}{D}\right)^{2/3} = 18.0\ m/s$$

Table E.4 Diffusion Mass Transfer Coefficent Calculation Inputs

Variable	Symbol	Units	Value
Height at which wind speed is measured	z	m	10
Surface Roughness	z_0	m	0.05
Displacement Height	d	m	1.41
Karman Constant	κ	-	0.4
Velocity of Air	*u*	m/s	3.6
Diffusion Coefficient NO	D	m^2/s	$1.51x10^{-5}$
Kinematic viscosity of air	*v*	m^2/s	$1.51x10^{-5}$
Width	*w*	m	3.6
Length	*l*	m	3.6

5. Calculate Concentration Out

$$C_{NO}^{out} = \frac{uhlC_{NO}^{in} - r_{NO-Ozone}whl - r_{NO}whl}{wlk_{NO} + uhl} = 36.9\ \mu g/m^3$$

Table E.5 Concentration Out Calculation Inputs

Variable	Symbol	Units	Value
Width	*w*	m	3.6
Length	*l*	m	3.6
Height	*h*	m	8
Velocity of Air	*u*	m/s	3.6
Concentration of NO	[NO]	$\mu g/m^3$	38

6. Calculate Convection Out

$$uhlC_{NO}^{out} = 3795\ \mu g/s$$

Table E.6 Convection Out Mass Transfer Calculation Inputs

Variable	Symbol	Units	Value
Length	*l*	m	3.6
Height	*h*	m	8
Velocity of Air	*u*	m/s	3.6
Concentration of NO	[NO]	$\mu g/m^3$	38

7. Calculate Diffusion Out

$$\boldsymbol{wlk_{NO}C_{NO}^{out} = 7.4\,\mu g/s}$$

Table E.7 Diffusion Out Mass Transfer Inupts

Variable	Symbol	Units	Value
Length	*l*	m	3.6
width	*w*	m	3.6

VITA

Heather Dylla was born and grew up in Minnesota. In 2006, she finished her Bachelor of Science in Civil Engineering from Bradley University. Heather worked two years for Black and Veatch for the Project Controls team on a design build for coal power plant projects. She joined Louisiana State University in August 2008 and to pursue a Master of Science in Engineering Science degree. Her interests include sustainable engineering, nanotechnology in construction materials, and environmental chemodynamics.